

“Numerical investigation of new geometries of photonic crystal fiber for enhancement of optical properties”

Doctoral Thesis

Submitted by

Ashish Kumar Ghunawat

*Research Scholar & Assistant Professor, Dept. of ECE, MNIT Jaipur
(ID-2013REC9549)*

Under Supervision of

Dr. Ghanshyam Singh

Associate Professor, Dept. of ECE, MNIT Jaipur



Department of Electronics and Communication Engineering

Malaviya National Institute of Technology Jaipur

November 2017

“Numerical investigation of new geometries of photonic crystal fiber for enhancement of optical properties”

Submitted by

Ashish Kumar Ghunawat

*Assistant Professor, Dept. of ECE, MNIT Jaipur & Research Scholar
ID-2013REC9549*

Under Supervision of

Dr. Ghanshyam Singh

Associate Professor, Dept. of ECE, MNIT Jaipur

Submitted in fulfillment of the requirements of the degree of Doctor of Philosophy
to the



**Department of Electronics and Communication Engineering
Malaviya National Institute of Technology Jaipur
November 2017**

Dedicated to My Parent and Wife

Certificate

This is to certify that the thesis entitled “**Numerical investigation of new geometries of photonic crystal fiber for enhancement of optical properties**”, being submitted by **Ashish Kumar Ghunawat** to the Department of Electronics and Communication Engineering, Malaviya National Institute of Technology, Jaipur, for the award of the degree of **Doctor of Philosophy**, is a bonafide research work carried out by him under my supervision and guidance. The results obtained in this thesis have not been submitted to any other university or institute for the award of any other Degree.

(Dr. Ghanshyam Singh)

Associate Professor

Department of Electronics and Communication Engineering

Malaviya National Institute of Technology Jaipur

Jaipur-302017, Rajasthan (India).

Declaration of Authorship

I, Ashish Kumar Ghunawat, declare that this thesis titled, ‘**Numerical investigation of new geometries of photonic crystal fiber for enhancement of optical properties**’ and the work presented in it are my own. I confirm that:

- This work was done wholly or mainly while in candidature for a Ph.D. degree at MNIT.
- Where any part of this thesis has previously been submitted for a degree or any other qualification at MNIT Jaipur or any other institution, this has been clearly stated.
- Where I have consulted the published work of others, this is always clearly attributed.
- Where I have quoted from the work of others, the source is always given. With the exception of such quotations, this thesis is entirely my own work.
- I have acknowledged all main sources of help.
- Where the thesis is based on work done by myself jointly with others, I have made clear exactly what was done by others and what I have contributed myself.

Signed: _____

Date: _____

Acknowledgement

The satisfaction and euphoria that accompany the successful completion of any work, will be incomplete unless a profound thanks is conveyed to all those whose kind encouragement and valuable guidance made this work a grand success.

I express my sincere gratitude to Dr. Ghanshyam Singh, Associate Professor, Department of Electronics & Communication Engineering, for his valuable supervision, support and inspiration during my PhD work His constantly energetic attitude, optimism and result oriented outlook have been helpful to me during the work and in writing of the thesis. Without his continuous and strong support, my PhD. would not have started and finished smoothly.

I am also grateful to Prof. K. K. Sharma, Head, Dept. of ECE, my respected DREC committee members Dr. Vijay Janyani, Dr. Ritu Sharma and Dr. Ravi Maddila for their valuable suggestion during my research work and presentations at the end of each semester. I would also like to add few heartfelt words for the faculty members of ECE Department who gave me unending support right from the beginning.

During the work on my thesis, I was fortunate to collaborate and generate knowledge sharing technical platform with a number of researchers from other academic institutions. I very much appreciate knowledge received from Prof. Manish Tiwari from Manipal University Jaipur and Dr. Rim Cheriff, University of Carthage, Tunisia; I extend my sincere thanks for their kindness and support.

Last, but not the least I wish to thank my parents, wife, brother and other family members for their everlasting support, love, understanding, and patience, during the research work.

(Ashish Kumar Ghunawat)

Department of Electronics and Communication Engineering
Malaviya National Institute of Technology Jaipur
Rajasthan (India)

Abstract

Recently incredible growth in technology is driven by increasing demand of high bandwidth application, mainly video and data. By utilizing the tremendous large bandwidth and ultra fast response time of photonic materials, fiber optics has emerged as a promising technology. Recently, photonic crystal fibers have captivated significant attention because of its flexibility in the design, outstanding optical properties, and various applications. PCFs are mainly known for smartly tuning transmission properties like dispersion, nonlinearity, and birefringence. Consequently, PCFs are finding various applications at present in different areas of optical communication systems. PCFs are very suitable because they offer surplus design parameters such as air-hole diameter d , air-hole rings, hole-to-hole spacing, and pitch Λ , and higher degree design freedom of transmission characteristics to attain the requirements of several applications. For high data rate optical communication systems, polarization maintaining fibers plays a major role in utilizing differential group delay between the two Eigen polarization modes of the first order polarization mode dispersion (PMD) compensation techniques. A large differential group delay or high birefringence is required to augment the figure of merit in PMD compensation.

High birefringence in the PCFs can be ensured because of its design flexibility and high index contrast. PCFs with high birefringence can find essential applications in the field of coherent optical fiber communications, fiber filters, fiber sensors, fiber lasers, electro-optical modulation and signal processing systems, etc. Moreover, with birefringence, a large attention is being grasped by the nonlinearity in PCFs. The small mode areas that lead to high nonlinearity in the PCF structures is an ongoing challenge, but highly birefringent PCFs with nonlinear properties have been receiving high attention due to its application in telecommunication field. One of the main reason to enhance nonlinearity is that the power-consumption of the optical device can be reduced. Nonlinear PCFs can be extensively used for various useful applications like supercontinuum generation, optical parametric amplification, all optical wavelength conversion, distributed in-fiber amplification and pulse regeneration, optical monitoring, multiplexing and demultiplexing and switching, etc.

Another crucial parameter of optical fibers is the dispersion, as it has the ability of strongly affecting the functioning of optical communication systems and

nonlinear fiber-optic devices, by distorting or delaying the signal. The speed dependency of the light on its wavelength is considered as dispersion. The chromatic dispersion, over a wide range of wavelength division multiplex communication systems, can be compensated by the generation of negative broadband dispersion in PCFs. However, due to the trade off between the high birefringence and large negative dispersion with low confinement loss in traditional PCF, it is not easy to control the light polarization and dispersion. By setting up large air holes in the cladding, the modal birefringence can be increased. By having large refractive index contrast between core and cladding in PCF, low confinement loss can be achieved. But this result in very large chromatic dispersion and dispersion compensating fiber has to be used to nullify the chromatic dispersion. High birefringence, dispersion compensation, large nonlinearity and low confinement loss over wide optical communication bands are an essential requirement for many applications, and this is why PCFs has to be optimally designed. Along with fiber parameters, the optical properties of photonic crystal fibers are also dependent on the material. Preferred materials are not only compatible with existing fiber structures, easily available, cost effective but also having a high nonlinear refractive index like Silicon, Silica, silicon nanocrystals.

Many approaches have been used to enhance nonlinearity, birefringence with flattened negative dispersion. Here a novel high index elliptical spiral photonic crystal fiber structure is designed that is providing a ultra-flattened negative dispersion, high nonlinearity, and high birefringence. Finite element method is used to simulate the design. This design provides negative dispersion that is ultra-flattened within the wavelength range from 1.385 μm to 1.99 μm with a deviation of ± 1.5 ps/nm/km. Dispersion value of -93.577 ps/nm/km at 1.55 μm wavelength is achieved. This highly negative flattened dispersion fiber can be utilized as residual dispersion compensation fiber (RDCF). The numerical results also indicate the birefringence up to order of 10^{-2} and nonlinear coefficient of (678.264, 763.485) $\text{W}^{-1}\text{km}^{-1}$ at 1.55 μm wavelength for fundamental X and Y polarized modes. High nonlinearity makes it useful for numerous optical applications.

To further enhance the optical characteristics, a silicon photonic crystal fiber with a nano dimensional slot having low index materials is embedded in the core, is designed and finite element method is used to study its characteristics. Here light is trapped in the low index material due to electric field discontinuity at the interface.

Strong confinement of one of the mode leads to enhance nonlinearity. Simulation results show that nonlinear coefficient at 1.55 μm wavelength for quasi-TM mode and the quasi-TE mode are 1348 $\text{W}^{-1}\text{m}^{-1}$ and 638 $\text{W}^{-1}\text{m}^{-1}$, respectively. This design also offers high birefringence up to 0.2503 at the 1.55 μm wavelength. In addition to this, the dispersion is also evaluated having a very large negative dispersion value of -1288 ps/nm/km. To further improve the characteristics, certain parameters are modified, and the simulation results show that nonlinear coefficient at 1.55 μm wavelength for quasi-TM mode and the quasi-TE mode is 2951 $\text{W}^{-1}\text{m}^{-1}$ and 1379 $\text{W}^{-1}\text{m}^{-1}$, respectively. This design also offers high birefringence up to 0.292219 at 1.55 μm wavelength. Dispersion is also examined and observed that ultra high negative flattened dispersion is achieved. In addition to this, confinement factor, effective area, and confinement loss are also reported and discussed. Now, rectangle slot, which has the same material as of elliptical slot, i.e., silicon nanocrystal, is analyzed. Also, both the slots are defined by the same area to compare the optical properties. Numerical analysis of the designed slot is attained by finite element method. By optimizing the fiber geometrical parameters of the rectangle slot, the nonlinearity coefficient of the fundamental modes and birefringence at 1.55 μm wavelength are achieved as high as 1614 $\text{W}^{-1}\text{m}^{-1}$ and 0.2589, respectively.

Now it can be concluded that although all proposed designs provide better results but low index slotted structures provide superior properties compared to high index PCF structures. The proposed research work can be used to realize a coherent digital optical transmission technology, polarization maintaining all optical signal processing devices at small scale.

Table of Contents

	Page no.
Certificate	i
Declaration of Authorship	ii
Acknowledgements	iii
Abstract	iv
Table of Contents	vii
List of Figures	ix
List of tables	xii
Abbreviations	xiii
Chapter 1: Introduction	
1.1 Introduction	1
1.2 Motivation of Research	3
1.3 Research Contribution	4
1.4 Thesis Outline	5
Chapter 2: Photonic Crystal Fibers: Properties and Applications	
2.1 Introduction	7
2.2 Light Guiding Mechanism in PCF	9
2.2.1 <i>Modified total internal reflection</i>	9
2.2.2 <i>Photonic bandgap effect</i>	10
2.2.3 <i>Electric field discontinuity</i>	10
2.3 Fiber Modes	11
2.4 Optical Properties of Fiber	17
2.4.1 <i>Birefringence</i>	17
2.4.2 <i>Dispersion</i>	19
2.4.3 <i>Nonlinearity</i>	22
2.5 Losses in PCFs	30
2.6 Fabrication Techniques of PCF	32
2.6.1 <i>Stack and Draw Technique</i>	32
2.6.2 <i>Extrusion Method</i>	33
2.6.3 <i>Die-cast Process</i>	33
2.6.4 <i>Sol-gel Technique</i>	34
2.7 Applications	36
2.7.1 <i>Polarization maintaining Fiber</i>	36
2.7.2 <i>Dispersion Compensation Fiber</i>	37
2.7.3 <i>Supercontinuum Generation</i>	38
2.7.4 <i>Coherent optical fiber communication</i>	42
2.8 Summary	43
Chapter 3: Research at a Glance	
3.1 Introduction	44
3.2 Research contribution in past	44
3.3 Summary	54

Chapter 4: Numerical Investigation of High Index Elliptical Spiral Photonic Crystal Fiber

4.1 Introduction	55
4.2 Structure and Design of Elliptical Spiral PCF	57
4.3 Research Outcomes and Discussion	60
4.4 Elliptical Spiral PCF as Residual Dispersion Compensation Fiber	67
4.5 Conclusion	68
4.6 Summary	68

Chapter 5: Numerical Investigation of Low Index Slotted Spiral Silicon Photonic Crystal Fibers

5.1 Introduction	69
5.2 Material Properties	70
5.2.1 Silicon	70
5.2.2 Silicon nanocrystals	72
5.3 Research Background	72
5.4 Highly Nonlinear Polarization Maintaining Dispersion Compensation Slotted Spiral PCF	75
5.4.1 Structure and Design of Slotted Spiral PCF	75
5.4.2 Characterization and optical properties of slot spiral PCF	77
5.4.3 Research Outcomes and Discussion	79
5.5 Ultrahigh Nonlinear Polarization Maintaining PCF with Flat Negative Dispersion	86
5.5.1 Design of Elliptical Slot Spiral PCF	87
5.5.2 Research Outcomes and Discussion	88
5.6 Ultrahigh Nonlinear Polarization Maintaining Rectangle Slotted PCF with Negative Dispersion	96
5.6.1 Rectangle Slotted PCF Structure	97
5.6.2 Research Outcomes and Discussion	99
5.7 Slot Spiral PCF Application: Nonlinear Optical Signal Processing	105
5.8 Conclusion	110
5.9 Summary	110

Chapter 6: Conclusion and Future Scope

6.1 Conclusion	111
6.2 Future Scope	114

References	115
-------------------	-----

Appendix A: Numerical Method for Design Analysis	137
Finite Element Method	137
References (Appendix A)	147

Appendix B: List of publications	148
---	-----

Appendix C: Profile Summary	150
------------------------------------	-----

List of Figures

Fig. No.	Caption
2.1	: Classification of photonic crystals
2.2	: Classification of Photonic Crystal fiber
2.3	: Transmission effects in optical fiber
2.4	: Chromatic Dispersion in optical fiber
2.5	: Self Phase Modulation
2.6	: Four wave mixing
2.7	: Scattering phenomenon in optical fiber
2.8	: Setup of PCF preform fabrication in Die-Cast Process
2.9	: Three types of conventional PMF
2.10	: Dispersion compensation fiber
2.11	: Display of SCG by Soliton radiation and Non Soliton radiation
4.1	: Cross sectional view of elliptical spiral PCF
4.2	: Fundamental modal field distribution for X and Y polarization
4.3	: Dispersion Vs wavelength curve for different ellipticity ratio for wavelength range 1.33 μm -1.99 μm
4.4	: Flat dispersion curve for wavelength range of 1.385 μm -1.99 μm
4.5	: Dispersion variation for $\pm 1\%$ and $\pm 2\%$ variation of ellipticity ratio around optimum value.
4.6	: Effective area Vs wavelength curves for various ellipticity ratios
4.7	: Nonlinearity of PCF for wavelength range 1.33 μm -1.99 μm

- 4.8 : Birefringence Vs wavelength for different ellipticity ratios
- 4.9 : Birefringence variation for $\pm 1\%$ and $\pm 2\%$ variation of ellipticity ratio around optimum value.
- 5.1 : Cross sectional view of Ellipse slotted spiral PCF (design 1)
- 5.2 : Field distribution of fundamental modes (a) Quasi TE-mode and (b) Quasi TM-mode at $1.55 \mu\text{m}$ for vertically aligned Si-NC slot
- 5.3 : Birefringence Vs wavelength for vertical aligned slot in core with variation in (a) Semi Minor axis 'a' for $b = 220 \text{ nm}$ and (b) Semi Major axis 'b' for $a = 32 \text{ nm}$.
- 5.4 : Electric Field intensity distribution of fundamental modes for (a) Quasi-TM Mode and (b) Quasi-TE Mode at $1.55 \mu\text{m}$ for horizontally aligned slot
- 5.5 : Birefringence Vs wavelength for horizontally aligned slot in core with variation in (a) Semi Minor axis 'a' for ' $b = 220 \text{ nm}$ ' and (b) Semi Major axis 'b' for $a = 32 \text{ nm}$.
- 5.6 : Nonlinearity variation of fundamental mode of vertical slot at $1.55 \mu\text{m}$ wavelength with variation in (a) Semi Minor axis 'a' and (b) Semi Major axis 'b'
- 5.7 : Dispersion Vs wavelength for vertically aligned slot with variation in (a) Semi Minor axis 'a' and (b) Semi Major axis b.
- 5.8 : Field distribution of fundamental modes for (a) quasi TE mode and (b) quasi TM mode at $1.55 \mu\text{m}$ for vertically aligned Si-NC slot.
- 5.9 : Birefringence Vs wavelength for vertical aligned slot in core with variation in (a) Semi Major axis 'b' for ' $a = 30 \text{ nm}$ ' and (b) Semi Minor axis 'a' for ' $b = 200 \text{ nm}$ '.
- 5.10 : Field distribution of fundamental modes for (a) quasi-TM mode and (b) quasi-TE mode at $1.55 \mu\text{m}$ for horizontally aligned Si-NC slot

- 5.11 : Birefringence Vs wavelength for horizontally aligned slot in core with variation in (a) Semi Major axis 'b' for 'a' = 30 nm and (b) Semi Minor axis 'a' for 'b' = 200 nm.
- 5.12 : Effective area vs. wavelength for variation in (a) semi minor axis 'a' and (b) semi major axis 'b'
- 5.13 : Nonlinearity variation of fundamental mode at 1.55 μm wavelength with variation in (a) Semi Minor axis 'a' and (b) Semi Major axis 'b'
- 5.14 : Confinement factor variation at 1.55 μm wavelength with variation in (a) Semi Minor axis 'a' and (b) Semi Major axis 'b'
- 5.15 : Effective index variation with wavelength for quasi TE mode at semi minor axis 'a' = 30 nm and semi major axis 'b' = 200 nm.
- 5.16 : Dispersion for quasi TE mode at semi minor axis 'a' = 30 nm and semi major axis 'b' = 200 nm.
- 5.17 : Cross sectional view of rectangle slotted PCF (third design)
- 5.18 : Electric field distribution of fundamental quasi modes at 1.55 μm wavelength (a) quasi-TE mode (b) quasi-TM mode
- 5.19 : Birefringence as a function of wavelength when slot height 'a' and slot width 'b' are varied
- 5.20 : (a) Effective area and Nonlinearity variation with variation in slot height (b) Effective area and Nonlinearity variation with variation in slot width
- 5.21 : Dispersion characteristics as a function of wavelength for the PCF with variation in (a) slot height 'a' (b) slot width 'b'
- 5.22 : Nonlinearities and optical wave parameters used for data encoding and signal processing.

List of Tables

Table No.	Caption
4.1	: Designing parameters of PCF
5.1	: Proposed PCF structures reported in recent
5.2	: Ellipse Slotted PCF (design 1) parameters values for vertically aligned Slot
5.3	: Ellipse Slotted PCF (design 1) parameters values for horizontally aligned slot
5.4	: Ellipse Slotted PCF (design 2) parameters values for vertically aligned slot
5.5	: Ellipse Slotted PCF (design 2) parameters values for horizontally aligned slot
5.6	: Comparison of design 1 and design 2 at 1.55 μm wavelength
5.7	: Rectangle Slotted PCF (design 3) parameter values for vertically aligned slot
5.8	: Comparison between different designs (design 1 and design 3)

List of Abbreviation

2D	: Two Dimensional
ADR	: Anomalous Dispersion Regime
DCF	: Dispersion Compensation Fiber
DFG	: Difference Frequency Generation
ESM	: Endlessly Single Mode
FM	: Fundamental Mode
FSM	: Fundamental Space-filling Mode
FEM	: Finite Element Method
FWM	: Four Wave Mixing
GVD	: Group Velocity Dispersion
Hi-Bi Fiber	: High-Birefringence Fiber
HNLF	: Highly Nonlinear Fiber
IC	: Integrated Circuit
MCVD	: Modified Chemical Vapour Deposition
MOF	: Microstructured Optical Fiber
M-TIR	: Modified Total Internal Reflection
NDR	: Normal Dispersion Regime
PBG	: Photonic band-gap
PC	: Photonic Crystal
PCF	: Photonic Crystal Fiber
PMF	: Polarization Maintaining Fiber
PIC	: Photonic Integrated Circuits
PMD	: Polarisation Mode Dispersion
RDCF	: Residual Dispersion Compensation Fiber
SCG	: Supercontinuum Generation
SOP	: State Of Polarization
SRS	: Stimulated Raman Scattering
SBS	: Stimulated Brillion Scattering
SPM	: Self Phase Modulation
SMF	: Single Mode Fiber

SPSM	: Single Polarization Single Mode
SOI	: Silicon-on-Insulator
SFG	: Sum Frequency Generation
SHG	: Second Harmonic Generation
TIR	: Total Internal Reflection
TE	: Transverse Electric
TM	: Transverse Magnetic
UFD	: Ultra Flattened Dispersion
WDM	: Wavelength Division Multiplexing
XPM	: Cross Phase Modulation
ZDW	: Zero Dispersion Wavelength

Chapter 1: Introduction

1.1 Introduction

Fibre optics is an eminent field of research brimming with enthusiastic fervor and remarkable advancements. Newer technologies are facilitating both development and understanding of new application areas in the nonlinear physics, as well as visually and rationally appealing new research outcomes. The development of new types of optical fibers has been one of the most stimulating areas. The optical fiber is the best-known data transmission medium due to its tremendous features like larger bandwidth, less losses, immunity to electromagnetic interference, data security, etc. The efficiency of the transmission medium is governed by its characteristics. Important characteristics like dispersion, birefringence, confinement losses, etc. have been used to maintain desired propagation of light signals in optical fibers and to enhance performance and applications of optical fibers with the controlled mechanism. These characteristics are controlled by variation in parameters of the optical fiber. Unfortunately, traditional optical fibers don't have the flexibility to tailor the fiber parameters. To overcome these limitations, in 1991, a concept was propounded that have an index material in the center with an arrangement of microscopic air holes along its length [1]. Microstructured optical fibers (MOF's) were developed on the basic motive of finding a dielectric waveguide to transmit light through 2-D Photonic band gap (PBG) effect [2]. The basic idea of MOF was presented for the very first time by Yeh and Yariv in 1978 in the form of Bragg fibers. In such fibers, Bragg grating core similar to 1D photonic crystal (PC) is defined to carry the light signals [3]. First intensive research towards PCs was initiated by E. Yablonovitch and S. John in 1987 [4,5], popularly known as founders of PCs in photonics. In 1991, an idea emerged that light traveling through a fiber can be stopped by using stop bands, that paved the way for the development of 2D and 3D PBG materials worldwide [6,7]. In 1992 Philip Russell invented a new two-dimensional Photonic Crystal fiber (2D-PCF) also known as MOF, having its core made up of air [8]. Since then various attempts are made in the direction of the structuring of PCFs involving variations in fiber material, core diameter, size of air holes and their geometry. In these MOFs light can be trapped inside core by two mechanisms- total internal reflection (TIR) [9,10] and PBG [11,12]. Even though one light guiding

mechanism in some respect similar to traditional TIR phenomenon, but it proves to be a case of some exclusive, interesting features that makes it different from conventional step-index fiber operating features. Nowadays, a modified structure of PCF that have nano dimension slot inside the fiber core is gaining tremendous attention [13-15]. In this PCF structure, a low index material is embedded in the slot and light inside the slot region is guided due to the electric field discontinuity at the interface of two dielectric mediums [16-18]. Due to this, electric field intensity in the low index material is more intense as compared to high index material. PCFs are having freedom of design flexibility that provides the ability to engineer the optical properties of fiber such as endlessly single mode (ESM) fiber [9], large mode area[19], dispersion[20,21], birefringence [22], nonlinearity [23], confinement loss, etc. Large nonlinearity coefficients in MOFs can be achieved by reducing the effective mode area of the core or using materials with high nonlinear refractive index values. These highly nonlinear fibers (HNLFs) can be utilized in various applications including optical parametric amplification [24], optical wavelength conversion [25] and supercontinuum generation (SCG) [26,27], etc.

Control of dispersion is very important for high speed long-haul optical communication systems because it significantly impacts the data carrying capacity of the optical fibers. The conventional single mode fiber (SMF) has nonzero dispersion typically ranging from 10 to 20 ps/nm/km [28]. With the rapidly increasing data traffic over a wavelength division multiplexed (WDM) communication systems, a transformed interest in dispersion compensating fiber (DCF) have been taken place over the last decade. It may also be concluded that more efficient DCF with very high negative dispersion values can be developed through PCFs. For multichannel WDM system, DCF over a wide wavelength bands is essential [29]. Such type of PCF may replace existing DCF in high capacity DWDM system for long distance communication systems. After using DCF, some positive dispersion still remains that will lead to severe limitations on the transmission data rates. Therefore, the insightful study of flattened negative dispersion becomes indispensable.

Polarization is one more crucial feature of PCFs, which needs to maintain necessarily for long distance communication. Polarization maintenance can be attained by using fibers with high birefringence. Birefringence can be induced either

by structural disturbances or by stress. High birefringent PCFs can be employed as single-polarization mode fibers or polarization maintaining fibers (PMFs) [30], optical sensing [31], etc.

Because of these intrinsic characteristic features, PCF supports numerous appealing applications which are responsible for the boom in the domain of optical signal processing. The term “Optical Signal Processing” encompasses the wide range of applications that function on optical data signals. This can incorporate broadly used systems, such as, optical pulse shapers, optical multiplexing, wavelength converters and optical switches, de-multiplexing, equalizers, optical memories [32-33], and diverse/several regions of microwave photonics [34-35].

1.2 Motivation of Research

The research of past few years reveals that PCF is a major topic of research because of its properties such as ESM operation, better control on dispersion, large mode area, more birefringence, small mode area, high nonlinearity and lesser confinement losses, etc. Photonic crystal structures in fiber optic communication have led to many new advancements in various field of optical fiber applications which are unattainable in conventional optical fibers. Every possible application takes benefit of tailoring the geometrical parameters of microstructures. Because of these properties, PCF has applications in fiber lasers, communications, nonlinear devices, generation of slow light, etc.

Researchers have proposed different PCFs structures as per the need of numerous applications. Presently, index guiding PCFs have been comprehensively studied because of their effective optical characteristics in different fields of optical systems that seem to be inconceivable in conventional SMF. Most of the researchers are working on high index PCF designs to improve the optical properties. High index PCFs structures have the ability to provide enhanced application oriented properties but to realize applications efficiently at small scale, low index slot effect induced PCF can be utilized. Low index slotted PCF design has the better capability to trap the light efficiently inside the fiber core as compared to traditional regular PCFs structures such as hexagonal, octagonal, decagonal, etc. Benefitting from slot effect which provides

better light confinement in nanometer sized low index region, improved characteristics such as high nonlinearity, high birefringence, and large negative flat dispersion is achieved[13-15]. Such extraordinary PCFs, inducing high performance characteristics, are prominent devices for use in on-chip applications, integrated optical signal processing and green photonics. The material of fiber also plays a key role in meeting the requirements. Silicon and silicon nanocrystals are found to be more applicable than other materials because Silicon based devices have not only met the requirement of operation but also Silicon has the potential for direct chip level integration.

1.3 Research Contribution

In this proposed work, different geometries of PCFs are investigated to improve the optical properties of the fiber. The primary aim of the work is to improve the birefringence, nonlinearity and dispersion properties. Effective mode area is also analyzed, and it is analytically shown that small effective mode area provides large nonlinearity with high birefringence. Investigation of properties is done by using index guiding PCF structures. Firstly, high index guiding elliptical spiral PCF structures are investigated by finite element method (FEM) for obtaining different optical properties. In one of the structure, soft glass SF57 is utilized as the high index material and in another design, silicon is used as the fiber material. Next, to gain better results of optical characteristics, low index slotted spiral PCF structures are investigated numerically.

Proposed PCF designs, which are numerically investigated, provide ultrahigh nonlinearity which has numerous application like optical parametric amplification, wavelength conversion, optical lasers, multiplexer and demultiplexer, optical switches, soliton formation, SCG, etc. Another studied feature is birefringence which can be used for maintenance of polarization in fiber and sensing applications. Maximum birefringence of the order of 10^{-1} is obtained which can reduce beat length up to μm . Designs are also providing a large negative dispersion which is essential to compensate the dispersion incurred during the propagation of light through the fiber. Thus, PCF designs proposed in the research work can be used to exploit numerous applications in optical domain within ultra-compact devices.

1.4 Thesis Outline

The thesis is organised into six chapters. The arrangement of the thesis is as follows:

Chapter 2 is intended to provide a brief idea about the concept of the PCF. Particular concentration has been paid to the optical properties and guidance characteristics of the PCF. This study also consists of the details of the fiber mode theory. Other than that, the fabrication techniques and optical losses that are induced during fabrication or light propagation are also reviewed. Moreover, some of the applications that are being utilized in almost all the technological areas of the present generation have been described.

The prime objective of this thesis is to enhance the optical characteristics of the PCF. The fundamental characteristics of PCF like dispersion, birefringence, effective mode area, nonlinearity, confinement loss are discussed. Although these characteristics have various applications, few important applications such as SCG, DCF, and PMF are briefly described.

Chapter 3 narrates the recent research work progress in the field of PCF geometries and respective applications. Challenges associated with modeling of different structures are also addressed. Review of the previous research work helped us in establishing a theoretical framework for our research.

In Chapter 4, a novel high index elliptical spiral PCF structure is proposed, particularly for DCF with PMF and nonlinear signal processing. Elliptical shaped air holes in the first ring of the spiral structure are introduced to generate large asymmetry in the design that results in large birefringence of the order of 10^{-2} and negative flattened dispersion in E+S+C+L+U bands. Additionally, high nonlinearity is also achieved which makes it favorable for various applications like parametric amplification, wavelength conversion, regeneration, multicasting, SCG, tunable delays, etc. With variation in the ellipticity of elliptical air holes, the fiber characteristics show no significant variation, which confirms the robustness of the design. FEM is utilized to analyze the results. Optical properties of material used in designed PCF and design fabrication possibilities are also discussed. Among the various applications of this design, a residual dispersion compensation (RDCF)

application is briefly discussed. Finally, all the observed simulation results are reviewed with concluding remarks.

Chapter 5 deals with the theoretical and numerical investigation of optical characteristics in low index slot spiral PCF structure. Nowadays, low index PCF design are getting much attention due to its high light confinement ability. Here three slot spiral PCF designs are discussed. First and second design are having low index elliptical slot in core region whereas third design has low index rectangle slot in the core region. By varying the pitch size (center to center distance between air hole) and diameter of air holes, all the structures are optimized. FEM is used to analyze the designs. Materials also make a significant impact on characteristics of the optical fiber. So properties and applicability of the materials used in the proposed design are also elaborated in details.

The proposed designs have large asymmetry in the structure that induces large birefringence up to the order of 10^{-1} , which makes it useful as PMF and in sensing applications. Large air holes size also provides better light confinement that would result in ultra high nonlinearity in fiber. HNLF has numerous applications in the optical domain such as SCG, parametric amplification, wavelength conversion, nonlinear signal processing, etc. Although all designs provide large negative dispersion but flat dispersion is achieved in the second design. Due to large negative dispersion, proposed designs can be a perfect candidate for DCF.

Obtained results of slotted spiral Silicon PCF designs are analytically discussed with variation in slot dimensions. Fabrication possibilities of proposed designs are also explained. Owing to its excellent performance, all optical signal processing can be realized by the ultra compact devices. Further, one major application of designs is also discussed. Finally, a conclusion and review of obtained results are presented.

All the results obtained are discussed and reviewed along with the scope of future possibilities in Chapter 6.

Chapter 2: Photonic Crystal Fibers: Properties and Applications

The primary focus of this chapter is to provide a detailed study about the PCFs. The optical properties and guidance characteristics of the PCFs have been a primary focus of this study. The fiber mode theory is explained with the help of Maxwell's equations in this chapter. Furthermore, the fabrication techniques are described and the optical losses that induce during light propagation are reviewed. Moreover, few applications are also discussed that have utmost importance in all areas of the optical domain.

2.1 Introduction

Photonic crystals are an innovative kind of optical medium that can be represented by the natural structures reliant on the modulation of refractive index of medium. In fact, optical properties of PC are determined by the modulation of the permittivity or the refractive index. The PCs grabbed a huge attention first time when the possibility of using it for controlling light was explained in 1887. Then almost after 100 years, the possibility to use PCs for the spontaneous emission control was introduced by V.P. Bykov in 1972. However, the real progress of PCs was initiated with the revolutionary work of E. Yablonovitch and S. John in 1987 [36].

The PCs are often compared to the solid state physics due to the similarity they obtain, such as, the lattice formed by variation of the refractive index is similar in both. Also photons characteristics in PCs is equivalent to the electrons and holes of the atomic lattice. Band gap is induced by both the solid state and PCs due to the lattice periodicity and determination of the Eigen functions in a PCs is very analogous to computation of solid-state particle wave functions, which is suitable for achieving photonic band structure [37]. In addition to that, geometric conformations of PCs are considered as a term, 'lattice'. In 1-D PCs there are very less number of variations that can be made due to the layered structure it consist of, only the refractive index, the number of layers within the period and layer's thickness can be varied. The consideration of lattice starts with the 2-D case. More types of lattices can be engineered with the 3-D case. The number of possible types of lattice helps in determining the transmittance, band structure and reflectance spectrum [38].

PCF is known for its low loss and confined transmission of signals. These fibers with different dielectric constant help in maintaining the confinement of light [39]. In addition, PCFs structural parameters can be tailored in order to achieve the required outcome. The PCF can be classified in different kind of fibers on the basis of structure and light propagation dimensions [37]. On the basis of structure, the PCFs are such as solid core PCF, PBG effect PCF and Bragg fibers. On the basis of light propagation dimension, it can be classified as 1-D PCF, 2-D PCF and 3-D PCF [1] as shown in Fig.2.1.

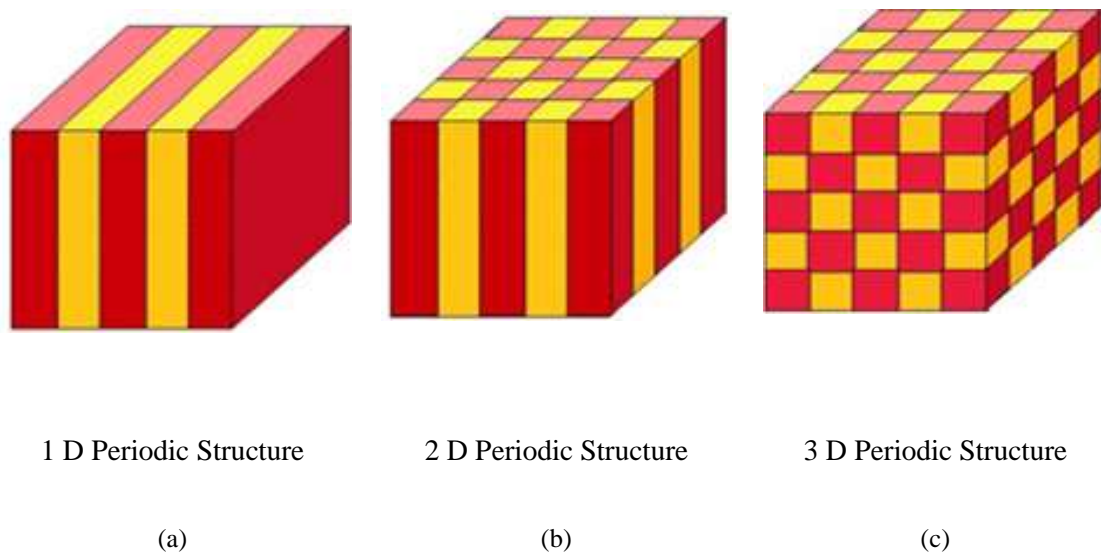


Fig.2.1 Classification of photonic crystals

Moreover, the PCF's light propagation depends on the multilayer dielectric mirror. This mirror consists of multiple layers of material having different dielectric constant. If the periodicity of dielectrics is in one direction then the PCF can be considered as one-dimensional, if in two directions then it will be two-dimensional PCF and like this the PCF can be also be three-dimensional based on the periodicity of dielectrics [40]. Furthermore, the Bragg fiber mainly follows the 1-D PCF principle. The concentric rings of more than one film form the Bragg fiber and it is broadly used as the distributed reflector in vertical cavity surface emitting lasers. Presently, air core Bragg fibers are based on a combination of polymer and soft glass. The holey fibers mainly follow the 2-D PCF concept where cladding consists of the air holes having smaller refractive index than the solid core. Another kind of 2-D PCF is hollow core

PCF having lower attenuation than solid core PCF and core can be filled with air and gas [41].

Commercial index guiding PCFs are also available. First is the ESM fiber that is based on the principle of confining light mode strictly within the core region and the higher modes will be able to infringe the core weakening the confinement. Second is the large mode area fiber (LMA-PCF) that is suitable for higher power levels without any material damages and nonlinear effect [42]. Similarly like LMA-PCF, there is a single mode double cladding fiber that has the same features like LMA-PCF but has a double cladding and actively doped core. Third is the HNLF that is very much suitable for achieving high nonlinear coefficient and small effective area even less than $1 \mu\text{m}$ with the help of large index core-cladding contrast. Another fiber is the PMF that actively maintains the polarization of the light [43].

2.2 Light Guiding Mechanism in PCF

For the purpose of guiding light, into the core and not in the cladding, along the fiber axis, the light should be introduced with the value of β i.e. the propagation constant. The higher and smaller value of β , both are allowed and are dependent on the relation, $\beta = nk_0$, where k_0 is the free-space propagation constant. The 2-D PCF is characterized by a maximum value of β that can transmit. Moreover, the propagation constant at particular wavelength corresponds to the effective refractive index of the material [44].

PCFs can be broadly classified into two broad categories, namely solid core index guiding PCF [45,46] and hollow core or band gap PCF [11,12], are shown in Fig. 2.2. Solid core PCFs can be further categorised into two types namely high index PCF and low index PCF. In high index guiding PCF, the wave guiding phenomena is modified TIR that is alike to wave guiding phenomena in optical fibers. In low index guiding PCF, the light propagation mechanism is based on electric field discontinuity at core cladding interface. In hollow core PCFs, light guiding mechanism exhibits a PBG effect at operating wavelength to guide light.

2.2.1 Modified total internal reflection

High index guiding fibers are the fibers which propagate light through them using the

phenomena of modified total internal reflection (M-TIR) [10]. The basic principle and mechanism of M-TIR is analogous to TIR mechanism as followed in standard fibers. That is the refractive index of the cladding is lower than the core refractive index. Due to the presence of periodic patterns of air holes in cladding region, the cladding effective refractive index becomes lower than core region. M-TIR provide an effective way of developing a type of PCF which contain many different properties not possible with standard technology thereby introducing PCF in many new applications. High index guiding fibers allows us to obtain a design which allows only a single mode to propagate through it irrespective of the range of wavelength used [46].

2.2.2 Photonic Bandgap Effect

PBG effect is a physical mechanism in which defined regular arrangement of air holes in the cladding region induces so called photonic band gap [11,12]. The areas which block the propagation of light through it are called as PBG. Only a certain amount of light with a few wavelengths are blocked and not allowed propagation through the region. A PBG fiber is created by deforming the air core by generating a new air hole in the core structure. This property of light guidance in hollow core or air guiding fibers show many propitious uses for example one can transmit high power through these fibers without the peril of damaging the fiber structure. Also when light is propagated through vacuum one can observe highly low confinement loss.

2.2.3 Electric field discontinuity

A slot waveguide configuration [16] comprises of high index material cladding in which has embedded a sub-micrometer size low refractive index material (i.e. slot) in core region. This structure operates on the principle of having continuity of the electric flux density at the interface of large index contrast (junction of high index material and the low index slot region). Maxwell's equation for a high index contrast interface says that to have continuity of electric flux density D the normal component of the electric field corresponding to that must have large discontinuity and for that it will have large amplitude of electric field intensity in low index region. Provided that the slot width is of same order to the decay field length. The electric field across the slot region remains high as compared to the high index region which in turn results in higher power density across the slot region than that in the high index region [16-18].

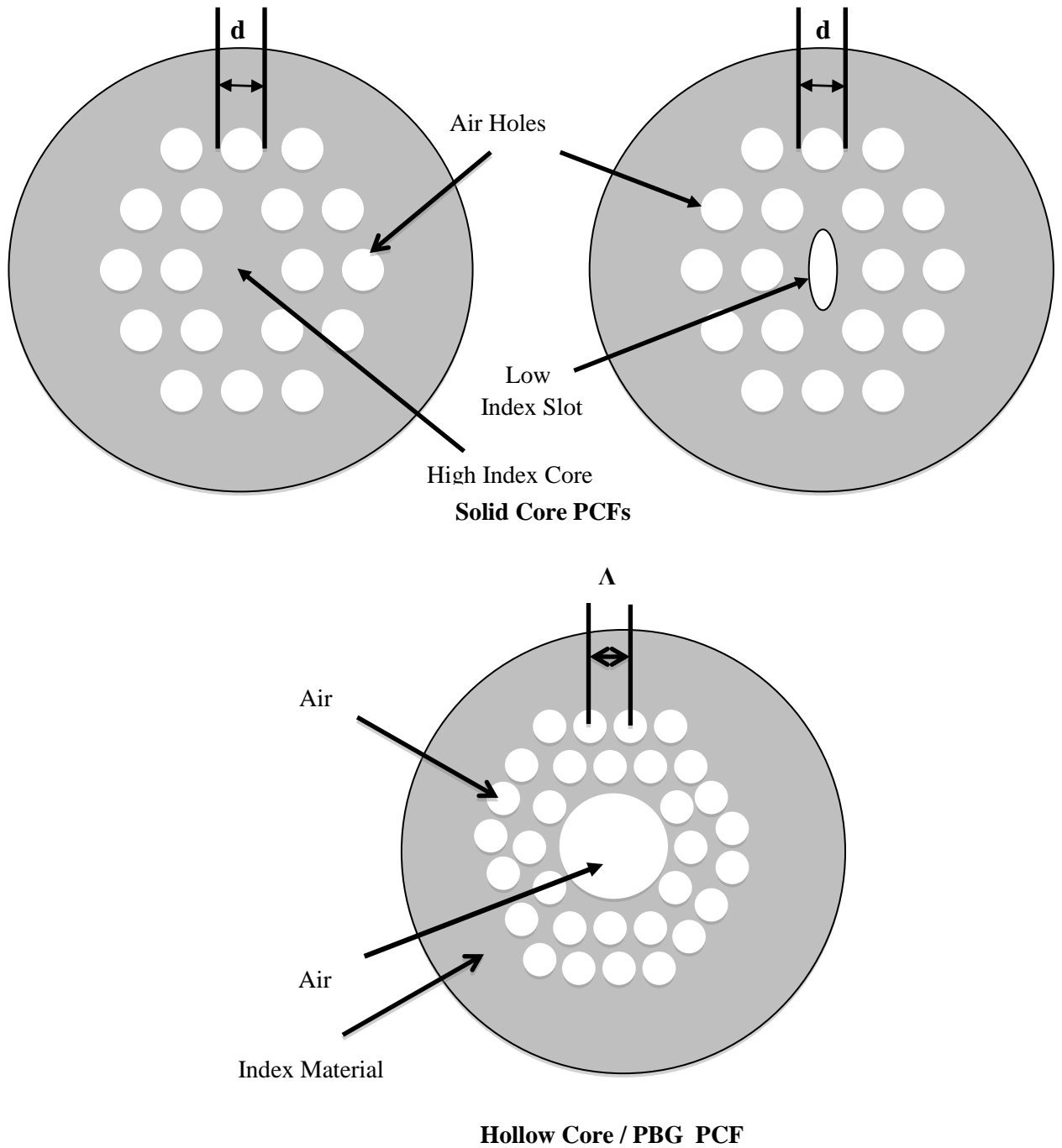


Fig.2.2 Classification of Photonic Crystal fiber

2.3 Fiber Modes

Light or electromagnetic wave propagates through different modes in an optical fiber. Maxwell's equations are used to determine the eigenvalue equation for defining these modes [47-49]. Maxwell's equations for a source-free medium (i.e., the charge density and the conduction current densities in the medium are zero) are given as,

$$\nabla \cdot D = 0 \quad (2.1)$$

$$\nabla \cdot B = 0 \quad (2.2)$$

$$\nabla \times E = -\frac{\partial B}{\partial t} \quad (2.3)$$

$$\nabla \times H = -\frac{\partial D}{\partial t} \quad (2.4)$$

We have two more equations, called the constitutive relations, as

$$B = \mu_0 H + M \quad (2.5)$$

$$D = \epsilon_0 E + P \quad (2.6)$$

where μ is the permeability of the medium, ϵ is the permittivity of the medium, and P and M are the induced electric and magnetic polarizations, respectively. Due to the non-magnetic nature of optical fibers, magnetic polarization is zero.

Now, we take curl of equation (2.3) as

$$\nabla \times \nabla \times E = -\nabla \times \frac{\partial B}{\partial t}$$

Substituting for $B = \mu H$ and interchanging the space and time derivatives, we get

$$\begin{aligned} \nabla \times \nabla \times E &= -\frac{\partial}{\partial t} \nabla \times (\mu_0 H) \\ &= -\mu_0 \frac{\partial}{\partial t} (\nabla \times H) \end{aligned}$$

Now substituting from eqn.(2.4) we get

$$\begin{aligned} \nabla \times \nabla \times E &= -\mu_0 \frac{\partial}{\partial t} \left\langle \frac{\partial D}{\partial t} \right\rangle \\ \nabla \times \nabla \times E &= -\mu_0 \epsilon \frac{\partial^2 E}{\partial t^2} - \mu_0 \frac{\partial^2 P}{\partial t^2} \end{aligned} \quad (2.7)$$

Polarization is related to the electric field by the following equation,

$$P(r, t) = \epsilon_0 \int_{-\infty}^{\infty} \chi(r, t - t') E(r, t') dt' \quad (2.8)$$

Where χ represents the susceptibility.

Fourier transform of $E(r, t)$ is

$$\tilde{E}(r, \omega) = \int_{-\infty}^{\infty} E(r, t) \exp(i\omega t) dt \quad (2.9)$$

Similarly, by taking the Fourier transform of $P(r, t)$ and by using eqn (2.8), equation (2.7) can be expressed in the frequency domain as follows,

$$\nabla \times \nabla \times \tilde{E} = -\epsilon(r, \omega) \frac{\omega^2}{c^2} \tilde{E}(r, \omega) \quad (2.10)$$

Because of the low optical losses in fibers, we can replace $\varepsilon(r, \omega)$ by $n^2(\omega)$.

From vector algebra we have the identity

$$\nabla \times \nabla \times \tilde{E} = \nabla(\nabla \cdot \tilde{E}) - \nabla^2 \tilde{E}$$

so the above equation can be simplified to

$$\nabla(\nabla \cdot \tilde{E}) - \nabla^2 \tilde{E} = -\nabla^2 \tilde{E} \quad (2.11)$$

By using eqn. (2.11) in eqn. (2.10), we can write

$$\nabla^2 \tilde{E} + n^2(\omega)k_0^2 \tilde{E} = 0 \quad (2.12)$$

To specifically solve the wave equation that meets the boundary conditions, a finite number of optical modes are maintained by the fiber. The modes inside the optical fiber can be classified into three categories namely, guided modes, leaky modes and radiation modes [48]. Information transmission through the optical fiber mainly takes place in guided modes. So the following discussion is entirely related to the guided mode of optical fiber. Because of the cylindrical shape of the optical fiber, equation, (2.12) can be expressed in cylindrical coordinates as follows

$$\frac{\partial^2 \tilde{E}}{\partial \rho^2} + \frac{1}{\rho} \frac{\partial \tilde{E}}{\partial \rho} + \frac{1}{\rho^2} \frac{\partial^2 \tilde{E}}{\partial \phi^2} + \frac{\partial^2 \tilde{E}}{\partial z^2} + n^2 k_0^2 \tilde{E} = 0 \quad (2.13)$$

Traditionally E_z and H_z are chosen as the independent components and E_ρ , E_ϕ , H_ρ and H_ϕ are calculated in terms of E_z and H_z . The method of separation of variables is used through which eqn. (2.13) can be written as follows

$$\tilde{E}_z(r, \omega) = A(\omega)F(\rho)\exp(im\phi)\exp(i\beta z) \quad (2.14)$$

Here A depends on ω , β is optical propagation constant, m is bound to take integer values because field must have period of 2π and $F(\rho)$ is the solution of following equation

$$\frac{d^2 F}{d\rho^2} + \frac{1}{\rho} \frac{dF}{d\rho} + \left(n^2 k_0^2 - \beta^2 - \frac{m^2}{\rho^2} \right) F = 0 \quad (2.15)$$

The above equation is the well known differential equation of Bessel functions. The solution of this equation for core and cladding part of fiber can be expressed as

$$F(\rho) = \begin{cases} AJ_m(p\rho) + BK_m(p\rho); & \rho \leq a, \\ CL_m(q\rho) + DM_m(q\rho); & \rho > a \end{cases} \quad (2.16)$$

Where A, B, C and D are constants and J_m, K_m, L_m and M_m are different types of Bessel functions.

Where p and q are defined as

$$p^2 = n_1^2 k_0^2 - \beta^2 \quad (2.17)$$

$$q^2 = \beta^2 - n_2^2 k_0^2 \quad (2.18)$$

At the boundary conditions, the optical field must be finite for a guided mode at $\rho = 0$ and declines to zero at $\rho = \infty$. As $K_m(p\rho)$ has a singularity at $\rho = 0$, so $F(0)$ can remain finite only if $B = 0$. Similarly $F(\rho)$ disappears at infinity only if $D = 0$. Thus

$$F(\rho) = AJ_m(p\rho) \quad \rho \leq a \quad (2.19)$$

Similarly in the cladding region solution of $F(\rho)$ must decline exponentially. Modified Bessel function $L_m(q\rho)$ illustrate such a solution. Thus,

$$F(\rho) = CL_m(q\rho) \quad \rho > a \quad (2.20)$$

Same method can be followed to calculate the magnetic field component. By using boundary condition that the tangential component of E and H be continuous at the core cladding interface requires that $\tilde{E}_z, \check{H}_z, \tilde{E}_\phi$ and \check{H}_ϕ should be same.

Tangential component of electric field is

$$n \times (E_1 - E_2) = 0 \quad \Rightarrow E_{t_1} = E_{t_2} \quad (2.21)$$

Tangential component of magnetic field is

$$n \times (H_1 - H_2) = 0 \quad \Rightarrow H_{t_1} = H_{t_2} \quad (2.22)$$

Normal component of electric flux density is

$$n \cdot (D_1 - D_2) = 0 \quad \Rightarrow D_{n_1} = D_{n_2} \quad (2.23)$$

$$\varepsilon_1 E_{n_1} = \varepsilon_2 E_{n_2} \quad \Rightarrow E_{n_1} \neq E_{n_2} \quad (2.24)$$

Where medium 1 and medium 2 have the permittivity ε_1 and ε_2 respectively, here $\varepsilon_1 \neq \varepsilon_2$. Normal component of magnetic flux density is

$$n \cdot (H_1 - H_2) = 0 \quad \Rightarrow B_{n_1} = B_{n_2} \quad (2.25)$$

$$\mu_1 H_1 = \mu_2 H_2 \quad \Rightarrow H_1 \neq H_2 \quad (2.26)$$

Where the permeability of medium 1 and medium 2 is μ_1 and μ_2 respectively. Here $\mu_1 = \mu_2 = 1$, hence

$$H_{n_1} = H_{n_2}. \quad (2.27)$$

The symmetricity of normal component of magnetic field at boundary is expressed by above equation.

In some conditions, out of two medium one is considered as perfect electric or magnetic conductor. The transform boundary condition is expressed as follows,

$$n \times E = 0 \quad \text{or} \quad n \cdot H = 0 \quad (2.28)$$

From the condition it can be concluded that electric field E displays continuity whereas the magnetic field H disappears at surface boundary.

In another condition, if one of the medium is perfect electric conductor, the transform boundary condition can be expressed as follows

$$n \times H = 0 \quad \text{or} \quad n \cdot E = 0 \quad (2.29)$$

In this case, continuity at the boundary both electric field and magnetic field vanish. These fields components at $\rho = a$ are equal, leading to an eigenvalue equation whose solution determine the propagation constant β for the fiber modes.

$$\begin{aligned} & \left[\frac{J'_m(pa)}{pJ_m(pa)} + \frac{L'_m(qa)}{qL_m(qa)} \right] \left[\frac{J'_m(pa)}{pJ_m(pa)} + \frac{n_2^2 L'_m(qa)}{n_1^2 qL_m(qa)} \right] \\ &= \left(\frac{m\beta k_0(n_1^2 - n_2^2)}{an_1 p^2 q^2} \right)^2 \end{aligned} \quad (2.30)$$

where a prime refers differentiation with respect to the argument.

For a given set of parameters k_0 , n_1 , n_2 and a , the eigenvalue equation has several solutions of β for each integer m . Conventionally these solutions are presented by β_{mn} where both m and n have integer values. There are basically two modes of fiber, such as, HE_{mn} and EH_{mn} and each value of β_{mn} corresponds to one particular mode of the fiber. This concept can be classified as when $m=0$, these modes are symmetric to the transverse-electric (TE) and transverse-magnetic (TM) modes of a planar waveguide as the axial component of the electric field or the magnetic field diminishes. On the other side, when $m > 0$, both the modes of fiber become hybrid, that is, all six components of the electromagnetic field are nonzero [49]. In optical fibers, Eigen values are mainly used for calculating effective refractive index and for

full vector analysis of the fiber structure. In addition to that, it is known that number of modes supported by the optical fiber depends on the structural parameters of the fiber such as the refractive index difference and the core radius. One additional parameter is also considered important that is normalized frequency, V . It is the parameter where different modes have a cut-off frequency and it is defined as

$$V = \left(\frac{2\pi a}{\lambda}\right) \sqrt{n_1^2 - n_2^2} \quad (2.31)$$

Because of the inverse relation with wavelength, this parameter is called normalized frequency parameter. In conventional optical fibers, to enable the single mode, the V parameter has to be less than 2.405 and when the V is slightly nearer to value of 2, it becomes a good fit for telecommunication fibers [50].

V-parameter of PCF:

V-parameter of a PCF is defined as follows [50,51]:

$$V_{PCF} = \frac{2\pi}{\lambda} \Delta (n_{core}^2(\lambda) - n_{FSM}^2(\lambda))^{1/2} \quad (2.32)$$

Although the mathematical expression for both standard step index fibers and PCF remains the same. In Eq. (2.32), $n_{FM}(\lambda)$ is the effective index of the fundamental mode (FM) in core region that is a function of wavelength and $n_{FSM}(\lambda)$ is the corresponding effective refractive index of the first cladding mode in the infinite periodic cladding structure which often expressed as the fundamental space filling mode (FSM) [50,51].

The PCF has a unique advantage of design flexibility that restricts it to become multi-mode in any experiment for any given wavelength of light. The guided mode always has a strong electric field inside the core. For this purpose, so as to maintain the ESM condition, ratio of hole diameter and pitch ($\frac{d}{\lambda}$) should be less than 0.4 [46].

The holes play an important part as they act as the “wire mesh”. It doesn’t let the light to intrude in the cladding area because the distance between the holes is very small. In other words, the light gets more trapped inside the core as the relative hole size $\frac{d}{\lambda}$ becomes larger. Hence, an appropriate arrangement of holes ensures that only the FM is to be guided.

2.4 Optical Properties of Fiber

Inculcating properties of both PCs and optical fibers as shown in Fig. 2.3, PCFs have such properties which allow it to control the modal behaviour in better way that is found not conceivable to achieve with conventional fiber technology. The development of these fibers was one of the major scientific advancements of the twentieth century and these fibers have proved to be beneficial in almost all important fiber applications. Important properties with the PCF technology has been developed significantly over the last two decades, and now researchers are working for characteristics improvement for meeting the new trend applications. Out of various characteristics of PCFs, control of dispersion, birefringence, and nonlinearity paves the way for tremendous applications. This section deals with the basic phenomenon of these characteristics.

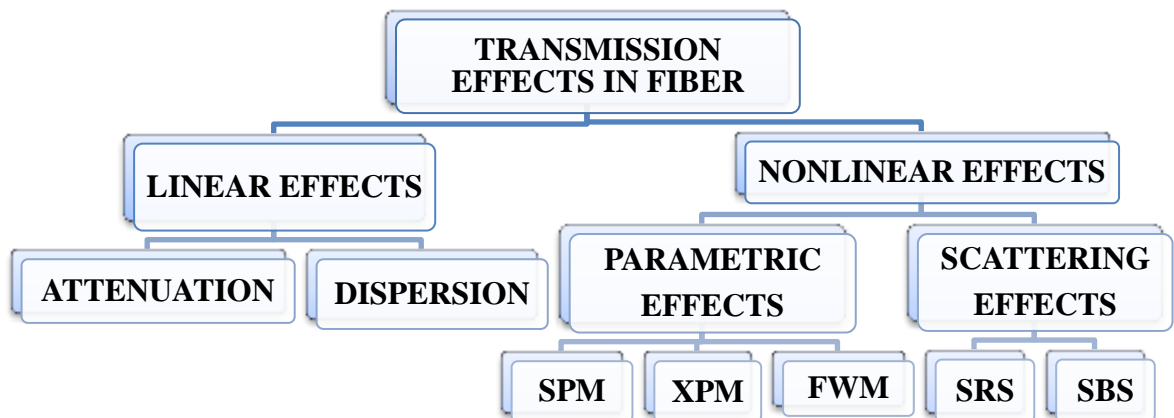


Fig 2.3 Transmission effects in optical fiber

2.4.1 Birefringence

The SMF carry two orthogonally polarized modes at the same time [44]. These two orthogonal modes normally have same phase velocity in an ideal circular core during the propagation. However, practically, fibers are not perfectly circular, and so the two modes have different phase and group velocities during the propagation. Additionally, the factors such as bend, anisotropic stress, and twist also induce birefringence in the fiber[22]. The magnitude and direction of birefringence keep varying with time because of the external factors such as temperature. These factors also influence the coupling of energy from one mode to another mode. Due to the fluctuation of

birefringence, the state of polarization (SOP) also changes frequently with time, which becomes an issue for several applications like coherent communication systems, the coupling between optical fibers and integrated optic devices, fiber optic sensors; as the basic need of such applications is the stability of output SOP [52].

The high birefringence fibers are considered as very useful as it maintains the SOP of the input signal for long distance communication and is also called as PMFs [53]. Such fibers can be realized by introducing very high birefringence in the fibers at the time of fabrication process.

Moreover, the birefringence can be termed as the optical property of the material in which the refractive index has a dependency on the propagation direction and polarization of light.

Types of birefringence

Birefringence is classified into two categories, intrinsic and stress-induced birefringence

1. Intrinsic birefringence – The anisotropy present in the crystal is responsible for this type of birefringence. The atomic arrangement of the crystal itself is the source of birefringence. The birefringence is also dependent on the refractive index of the material and the space between the atoms in the arrangement [54]. Examples are calcite, quartz, etc.
2. Stress-induced birefringence – This type of birefringence is caused by the stress imposed on the material. Higher the stress, higher will be the birefringence. In the long-distance transmission, the large length of optical fiber does generate birefringence due to the stress [55]. Glass, plastic are the prime examples of this type of birefringence.

Birefringence is used for various applications such as to provide a single mode polarization and also make the fiber insensitive to the temperature. The birefringence is defined as the difference of the refractive index of two mode indices of the polarization. The birefringence can be numerically shown as [56]:

$$B = |\text{Re}(n_{eff}^x) - \text{Re}(n_{eff}^y)| \quad (2.33)$$

Where n_{eff}^x and n_{eff}^y are the effective refractive index of both the polarization components.

Geometrical birefringence (B_g) is dependent on the aspect ratio a/b of the core and also on the difference between refractive index Δn between the core and cladding. For a fiber having small aspect ratio of core ($a/b < 1.2$), the birefringence is given by

$$B_g = (\beta_x - \beta_y) = 0.2k_0\left(\frac{a}{b} - 1\right)(\Delta n)^2$$

It is introduced by bringing a defect in the fiber like by adding the two rods or big size holes nearer to the core in the opposite side or by having an elliptical core. These deformities help in introducing the birefringence. Also, the birefringence can be suppressed by decreasing the hole size and increasing the pitch; it also depends on the hole position as closer the holes, less will be the birefringence. Additionally, for the same degree of irregularity, the position-dependent birefringence is larger than the size-dependent birefringence [57-61].

2.4.2 Dispersion

The phenomenon chromatic dispersion takes place when the interaction occurs between an electromagnetic wave and the charge carriers of a dielectric; the medium response, which is related to the frequency of the wave ω . In other words, the chromatic dispersion depends on the resonance frequencies at which medium absorb the radiation when oscillations of bound electrons occur [47,49]. It is evident that chromatic dispersion is produced due to the refractive index $n(\omega)$ being dependent on the frequency. The relation between refractive index and frequency can be approximated by Sellmeier equation [62]

$$n^2(\lambda) = 1 + \sum_{j=1}^m \frac{B_j \lambda_j^2}{\lambda_j^2 - \lambda^2} \quad (2.34)$$

When short optical pulses propagate in the fiber, fiber dispersion becomes an important parameter because different frequency components present in the pulse are having different speeds which are expressed as $c/n(\omega)$. So the dispersion leads to broadening of the pulse which is harmful to optical pulse propagating through a channel. If we are considering nonlinear effects, the combined effect of dispersion and nonlinearity produces a phenomenon, that is, Soliton dynamics, which ensures stable wave propagation without any distortion. The propagation constant (β) which explains dispersion can be expressed in Taylor series about the center frequency ω_0 of the pulse:

$$\beta(\omega) = n(\omega) \frac{\omega}{c} = \beta_0 + (\omega - \omega_0) + \frac{1}{2}\beta_2(\omega - \omega_0)^2 + \dots \quad (2.35)$$

Where $\beta_m = \left(\frac{d^m \beta}{d\omega^m} \right)_{\omega=\omega_0}$ ($m = 0, 1, 2, \dots$)

the relation between parameters β_1 and β_2 with refractive index n and its derivative is given by

$$\beta_1 = \frac{1}{v_g} = \frac{n_g}{c} = \frac{1}{c} \left(n + \omega \frac{dn}{d\omega} \right), \quad (2.36)$$

$$\beta_2 = \frac{1}{c} \left(2 \frac{dn}{d\omega} + \omega \frac{d^2 n}{d\omega^2} \right), \quad (2.37)$$

where n_g and v_g represents the group index and group velocity respectively.

Physically, the group velocity denotes the speed at which the envelope of the pulse propagates, and β_2 (GVD coefficient) represents the dispersion of the group velocity due to which broadening of pulse takes place [63]. For fused silica, it was observed that β_2 vanishes at 1.27 μm and for higher wavelengths β_2 is negative. This wavelength is called as the wavelength of zero-dispersion and is represented by λ_D . But in reality, the dispersion is not zero at λ_D because the cubic term present in the Taylor series of β is non-zero. Moreover, β_3 coefficient in eq. (2) can be termed as the third order dispersion [64]. Optical pulses can be affected, both in the linear and nonlinear region by higher order effects. The contribution of high order effects is important for ultrashort optical pulses or when the pump wavelength is closer to the zero dispersion wavelength (ZDW) within a few nanometers [65].

Mainly, there are two reasons due to which the chromatic dispersion takes place, is shown in Fig. 2.4 also. First, is the material dispersion which is present because the fiber core may have some unwanted dopants like GeO_2 and P_2O_3 . Second, being the waveguide contribution. So the total chromatic dispersion is the result of material as well as waveguide contribution [62], [66,67].

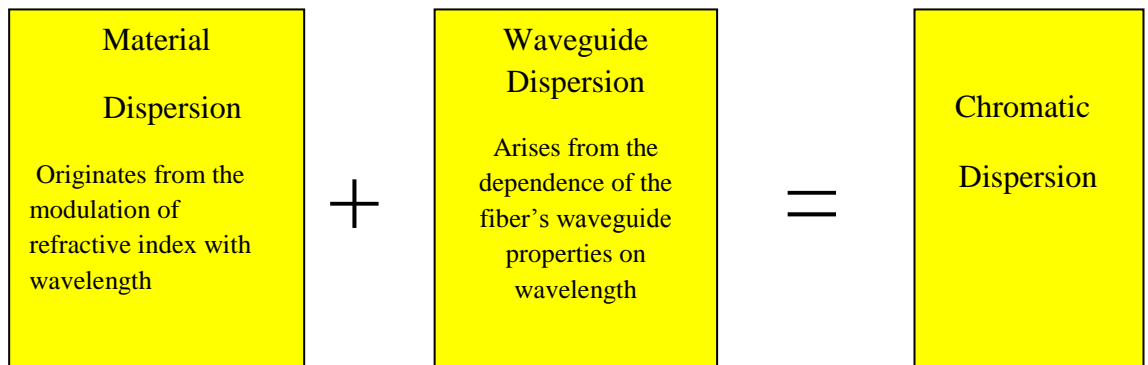


Fig. 2.4 Chromatic Dispersion in optical fiber

The dispersion parameter D is the commonly used quantity instead of β_2 and it is related to β_2 in the following manner:

$$D = \frac{d\beta_1}{d\lambda} = -\frac{2\pi c}{\lambda^2} \beta_2 \approx -\frac{\lambda}{c} \frac{d^2 n}{d\lambda^2} \quad (2.38)$$

An interesting thing about the waveguide dispersion is that its effect relies on the design parameters of the fiber such as the core radius a and core-cladding index difference Δ . So by using this fact, the wavelength of zero-dispersion can be designed near the minimum attenuation window at 1.55 μm . When the dispersion values are highly negative, these fibers can be utilized as DCFs [68]. By using different shapes in fiber geometry, one can design fibers with flat dispersion for a large band of frequencies which are called as dispersion flattened fibers (DFFs).

Depending on the sign of β_2 , nonlinear effects in fiber can produce different behavior. When $\beta_2 > 0$, the normal dispersion regime (NDR) in the fiber is enabled. In this region, blue shifted wave propagate slower than the red shifted wave. When $\beta_2 < 0$, anomalous dispersion regime (ADR) will be dominant in the fiber where red shifted wave will propagate slower than blue shifted wave.

Due to the mismatch in group velocities of pulses, different wavelength travels at different speeds within a fiber. This results in a walk-off mechanism which can be used to explain the nonlinear interaction inside optical fiber between traveling pulses. The interaction takes place when the fast traveling pulse walks through the slower traveling pulse. The walk-off parameter is denoted by d_{12} and is defined by

$$d_{12} = \beta_1(\lambda_1) - \beta_1(\lambda_2) = v_g^{-1}(\lambda_1) - v_g^{-1}(\lambda_2) \quad (2.39)$$

where λ_1 and λ_2 denotes the center wavelengths of two pulses [49].

Dispersion management is a very important feature for long haul optical fiber communication. By careful design, one can reduce the dependency of the wavelength on the group velocity dispersion (GVD) in PCFs at very low air-filling fractions. With multi-component glasses such as Schott SF6, SF57, Silicon, Chalcogenide, etc., the flexibility in GVD design can be increased. In a highly nonlinear PCF (HNPCF) with small-core size, whole dispersion window can be transferred at larger wavelengths than in a silica based PCF with the same geometrical parameters.

The material dispersion can be managed by selecting the material, which is used to design the fiber whereas the waveguide dispersion depends on the design

parameter of the waveguide. In this way, tailoring of the total dispersion can be done. Material dispersion and waveguide dispersion normally cancel out each other at ZDWs. ZDW mainly depends on the material and geometry of fiber. A zero-dispersion magnitude and small slope is desired for most telecommunication applications especially for SCG. ZDW is having an important role in estimating the nonlinear effects. In addition to that, the dispersion is having an important role in SCG as dispersion helps in spectrum broadening as in NDR. Mainly phase matched four wave mixing (FWM) or self phase modulation (SPM) helps in broadening of the pulse as in this process no additional frequency components are produced, just the phase shifting of pulse occurs due to the dispersion chirps [27].

Alternatively, in anomalous dispersion regime, nonlinearity plays an important role as nonlinear length is kept slightly higher than the dispersion length. In this regime, the nonlinear chirp and dispersion chirp cancel out each other, when the input power is high enough. This whole process helps in generating a stable pulse, which can travel over long haul distance without any distortion. This type of pulse is called soliton [69].

To sum up, the explanation and concepts stated above substantiate the purpose of the study, that is, the presence of high order dispersion in the fiber may distort the long distance transmission of the signal. However, the presence of dispersion with the nonlinear effects may prove to be a positive factor, as these processes with the combined effect induce the soliton pulses that are recognized as the stable waves that are very suitable for undistorted propagation in the long distance communication. In the next section, the concept of nonlinear effects has been explained that seems to be mainly used for nonlinear signal processing applications.

2.4.3 Nonlinearity

One of the peculiar characteristics of PCF is to achieve high nonlinearity within a very small length of the fiber. As nonlinear effects can be used in performing various optical applications like optical amplification, wavelength conversion, optical switching, optical signal regeneration and optical demultiplexing, etc. [70]. If the nonlinearity is enhanced, then these applications can be realized with a less pump power and shorter length as compared with the conventional fiber. Nonlinear optical fiber amplifiers especially Raman amplifier and Brillouin amplifiers have aroused

great concern in the field of optical communication systems as these nonlinear effects can move the gain regions of amplifiers arbitrarily as per the pump wavelength. These fields may require the generation of additional frequency elements while propagation, which let the spectral broadening of the pulse. In fact, the implementation of all-optical functionalities is relied on strong fiber nonlinearities [23].

The optical nonlinearities discussed here can be used to generate new wavelengths, conversion of wavelengths, parametric gain or amplification, switching and control the shape of the pulse. Nonlinearities can be divided into following two categories [49]:

A. Nonlinearities that originated from scattering phenomenon such as stimulated Raman scattering (SRS) and stimulated Brillouin scattering (SBS).

B. Nonlinearities that originate from a light induced change in refractive index that can result in a variation of phase (e.g., self-phase modulation (SPM) and cross phase modulation (XPM)) or generation of new wavelengths (e.g., four wave mixing (FWM)).

The static or dynamic material optical response is modified by the presence of a high electric field. This material response is expressed by expansion of polarization [71]

$$P = \chi^{(1)}E + \chi^{(2)}EE + \chi^{(3)}EEE + \dots \quad (2.40)$$

where $\chi^{(n)}$ is nth order susceptibility. As silica is a symmetrical molecule, the second order susceptibility of silica is zero. The nonlinear susceptibilities $\chi^{(n)}$, having real and imaginary parts, are responsible for various types of nonlinearities. The real part of nonlinear susceptibility corresponds to the refractive index whereas the imaginary part corresponds to the time or phase delay response of the material. SRS and SBS contribute to imaginary part of $\chi^{(3)}$ susceptibility, while FWM corresponds to the real part of $\chi^{(3)}$ susceptibility.

A. Nonlinearities originated from nonlinear refraction

The nonlinearity originates in the medium by modulation of refractive index of the material that depends on the input power intensity. This phenomenon is called Kerr Effect [49]. The beam intensities, like those generated by lasers that are of the order of 1 GW cm^{-2} , are necessary to bring about considerable variations in refractive index.

The optical Kerr effect is also called AC Kerr effect. The following expression governs the variation of refractive index with intensity

$$n(\omega, I) = n(\omega) + n_2 I = n + n_2 |E|^2 \quad (2.41)$$

where $n(\omega)$ denotes the linear refractive index in a low-intensity regime that is determined by Sellmeier's equation, n_2 denotes the nonlinear refractive index; I denote the optical intensity of electromagnetic wave that associates with the electric field of wave E [49].

The relation between n_2 and $\chi^{(3)}$ susceptibility is given by [72]

$$n_2 = \frac{3}{8n} RE(\chi^{(3)}) \quad (2.42)$$

The light intensity or the electric field variation results in modulation of refractive index. This varying refractive index generates the phase shift in the pulse and this phase shift results in a change of frequency spectrum of the pulse. In this way, extra frequency is generated and helps in enhancing nonlinearity. The nonlinear effects that originates are such as SPM, XPM, FWM, modulation instability and soliton dynamics.

SPM, XPM and FWM nonlinear processes originates from a common source, which can be expressed numerically by taking into consideration the interaction of two beams. The net electric field can be described as [73]

$$E(r, t) = \frac{1}{2} [E_1 \exp(-i\omega_1 t) + E_2 \exp(-i\omega_2 t)] + c. c. \quad (2.43)$$

Then, substituting in (2.40) produces a variety of P_{NL} terms:

1. $P_{NL}(\omega_1) \propto (|E_1|^2 + 2|E_2|^2)E_1$ and $P_{NL}(\omega_2) \propto (|E_2|^2 + 2|E_1|^2)E_2$ carry both SPM (first term in each) and XPM (second term in each);
2. $P_{NL}(2\omega_1 - \omega_2) \propto E_1^2 E_2^*$ and $P_{NL}(2\omega_2 - \omega_1) \propto E_2^2 E_1^*$ represents the FWM terms.

Following discussion explains the characteristics of these nonlinearities. Their effect on light propagating through the fiber, their examples, and applications in the field of optical communication is described.

A.1 SPM: This process works when the high-intensity pulse interacts with the medium, which leads to variation in refractive index which in turn generates a shift in the instantaneous phase of the pulse. This change is time-dependent, and it results in spectral broadening [74]

$$\Delta\omega(z, t) = -\frac{\partial\phi_{NL}}{\partial t} = -\frac{2\pi n_2}{\lambda A_{eff}} \frac{dp(t)}{dt} z = -n_2 \frac{dI(t)}{dt} kz \quad (2.44)$$

Where k , λ and I can be defined as the wave vector, wavelength, and optical intensity, respectively. Additionally, P and A_{eff} denote the optical power and the effective area of mode. It is observed from Fig. 2.5 that SPM is a pulse related concept since a time derivative term is present in (2.44) with the leading edge of the signal being red-shifted and the trailing edge being blue-shifted. Moreover, it is observed that the pulse transmission displays characteristics oscillation that are caused by involvement of components of a pulse having similar frequency but different phases. The benefit of nonlinear spectral broadening can be seen in neutralization or amplification of dispersion of the fiber. It is also noted that in case of the NDR (i.e. $\lambda < \lambda_{ZDW}$), red light transmits faster than blue light where the nonlinear dispersion dominates that leads to increased widening. On the other side, in case of ADR (i.e. $\lambda > \lambda_{ZDW}$), the nonlinear dispersion is neutralized which leads to pulse shrinking, and if both are equal, it results in solitons formation [75].

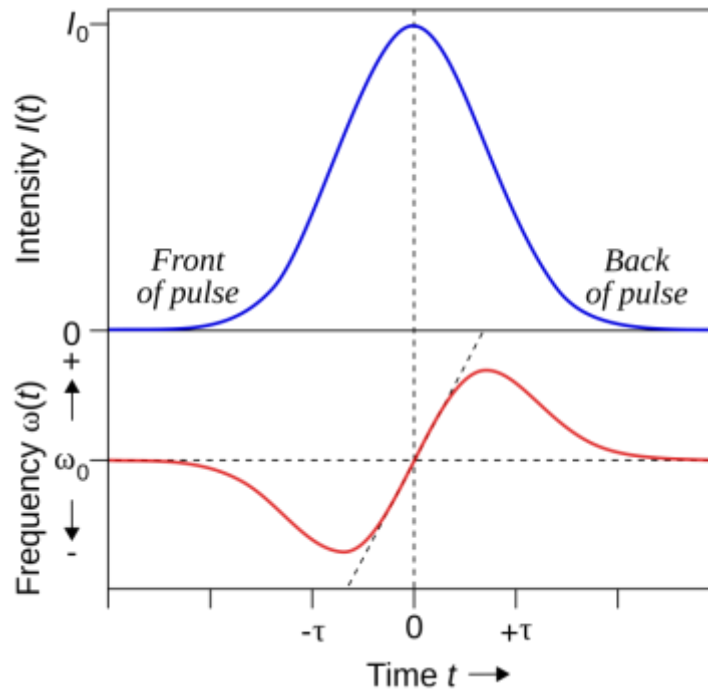


Fig. 2.5 Self Phase Modulation

A.2 XPM: Whenever there is a multi channel transmission in the optical fiber, XPM phenomena gets activated. When there is sufficient power in all the transmitted

channels, then there will be a change in a phase shift in each signal because of the presence of another signal. Due to the nonlinearity, all the signals in the fiber move with a more or less same group velocity. So the walk-off time would be much longer, and there would be strong interaction between the different signals. In this way effect of XPM would be much more. The broadening occurring in XPM is double as compared to SPM [76] since the total intensity is square of the sum of two amplitudes.

$$\begin{aligned} n &= n_0 + n_2 |E_1 + E_2|^2 \quad \Rightarrow \phi_{NL}^{\omega_1} \\ &= \frac{2\pi n_2}{\lambda A_{eff}} [|E_1|^2 + 2|E_2|^2] \end{aligned} \quad (2.45)$$

Second beam, $\phi_{NL}^{\omega_2}$ can be expressed similarly. If one of the two beams is much stronger than other beam, XPM will dominantly act from pump beam to signal beam,. It can be clearly pointed that the two beams should overlap in both time and space for XPM to occur. Overall, if dispersion is equal to zero over wide wavelength range, the different frequency or signals will travel with same group velocity. This increases the interaction that raise the XPM effect, eventually this increases the nonlinearity coefficient and this in relation increases the SCG.

If polarization is also considered, some novel nonlinear effects can be observed in fibers. It is clear that these effects depend strongly on birefringence properties and the SOP of beams. This birefringence can be either intrinsic or can also be induced by nonlinear effects. This contribution can be given by [49]

$$\begin{aligned} \Delta n_x &= n_2 \left(|E_x|^2 + \frac{2}{3} |E_y|^2 \right) \quad \text{and} \\ \Delta n_y &= n_2 \left(|E_y|^2 + \frac{2}{3} |E_x|^2 \right) \end{aligned} \quad (2.46)$$

here n_2 refers to the nonlinear parameter. Form (2.46), it can be easily realized that nonlinear birefringence and its effects must be related to optical intensities along the x and y direction. These parts of birefringence interfere in a similar way to that of XPM, which leads to the phase shift between these components [49]:

$$\Delta\phi_{NL} = \gamma L_{eff} (1 - B) (P_x - P_y) \quad (2.47)$$

Here P_x and P_y in the above equation denotes the power in x and y components, and B denotes the fiber ellipticity. L_{eff} is the length over which a signal would

propagate through the fiber if it had a constant amplitude over that length and zero amplitude beyond. This type of nonlinear phase shift can be launched by x -polarized sturdy pump signal along with a randomly polarized signal. $\Delta\phi_{NL}$ determines the polarization state as the beam travels that can lead to polarization rotation i.e. optical Kerr effect [77,78].

A.3 FWM: This phenomenon is similar to the inter-channel mixing. Suppose, if we input two frequencies, a third frequency is generated due to the nonlinearity. Due to this, these frequencies give a product of sum and difference frequency. All these frequencies lie in the same frequency band. This phenomenon is known as four-wave mixing [73], which is shown in Fig. 2.6.

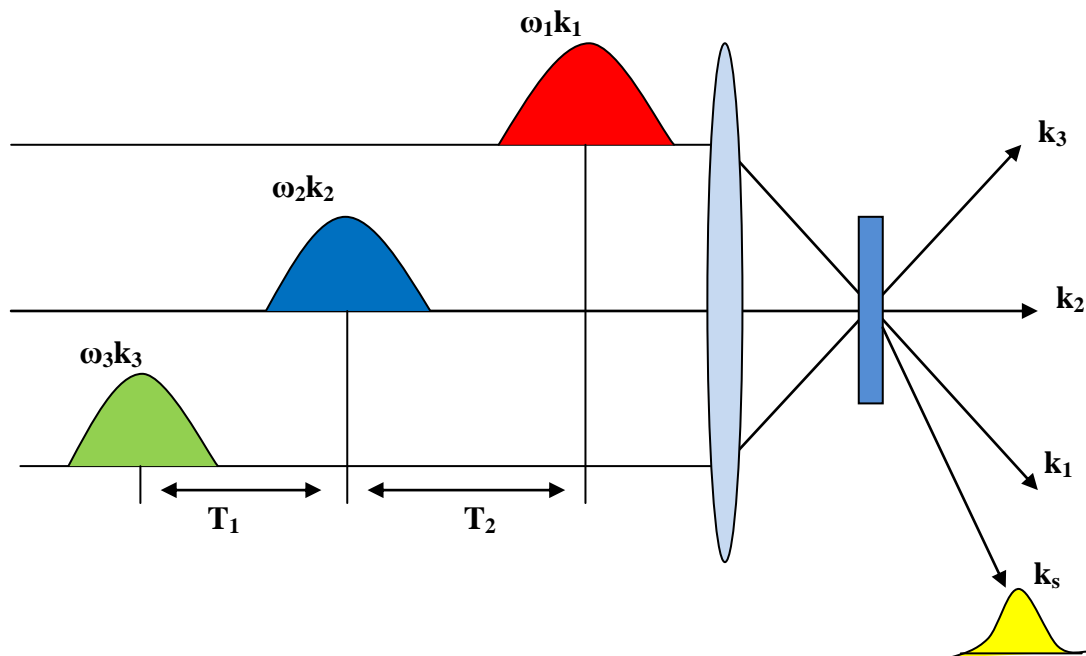


Fig.2.6 Four wave mixing

B. Nonlinearity originating from scattering

When light interacts with material, scattering phenomenon take place that can be linear or nonlinear in nature. Some of the important Scattering phenomenon in optical fiber is shown in Fig. 2.7. This type of nonlinearity is originated from stimulated inelastic scattering wherein some portion of the optical energy is shifted to the nonlinear medium.

B.1 SRS: When an incident photon strikes on a nonlinear medium, new wavelength components are generated due to the nonlinearity of the fiber or deformities in the fiber. If the scattered photon is less energetic than the incident photon, i.e., Stokes scattering and if the scattered photon has gained energy, i.e., anti-stokes scattering [79]. This phenomena is totally depended on the Raman effect, and this helps in soliton shifting that distributes the high order solitons. At Raman shift, the maximum gain is attained which is relative to the pump laser wavelength and not at a particular frequency [80].

B.2 SBS: In SBS, when the acoustic wave is co-propagating with an incident pump signal a Stokes wave is backscattered [81]. At the beginning of SBS, the reflected light enhanced sharply with incident optical power and the transmitted light gets finally saturated. The SBS occurs at very low threshold power compared to SRS, because the gain coefficient of SBS is relatively high in comparison to SRS.

The fundamental difference between SPB and SRS is that SBS phenomena can occur only in backward direction while SRS can occur in both forward and backward directions. Another difference is that optical phonon is generated in SRS whereas acoustic phonon is generated in SBS.

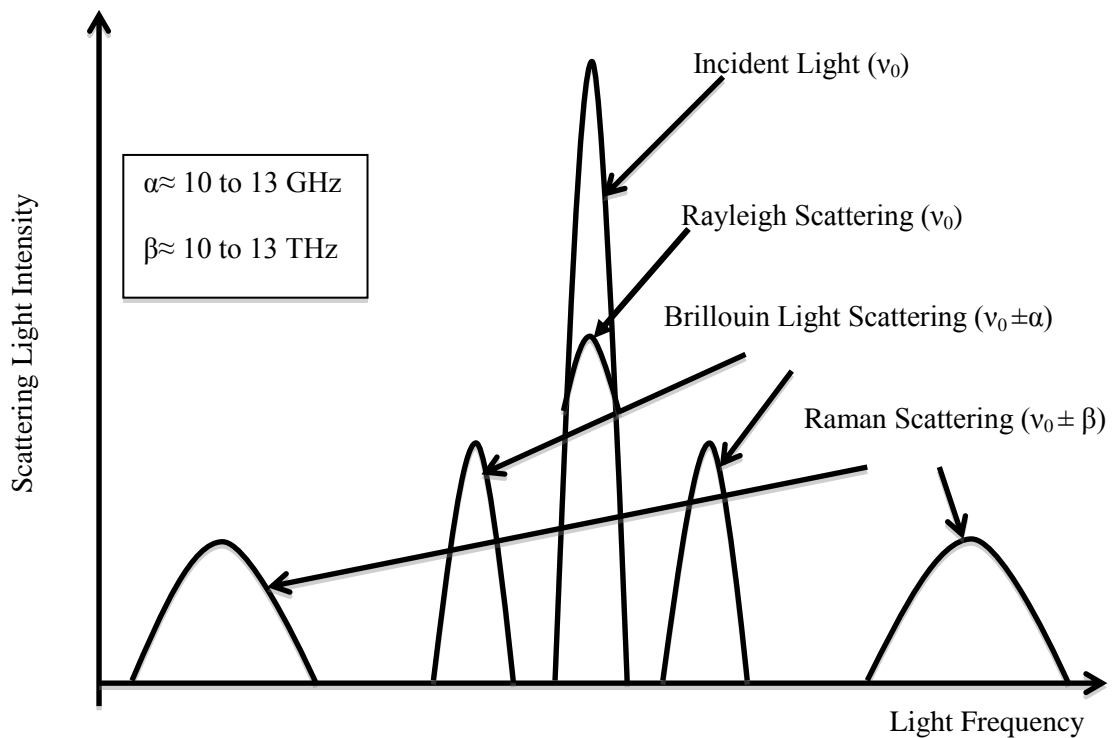


Fig. 2.7 Scattering phenomenon in optical fiber

Nonlinearity in PCFs is quantified regarding a nonlinear parameter known as γ , which is expressed in the following equation as follows [49]:

$$\text{Nonlinear coefficient } (\gamma) = \frac{2\pi n_2}{\lambda A_{eff}} \quad (2.48)$$

where A_{eff} represents the effective area of the guided mode. The nonlinear refractive index n_2 has the unit of m^2/W . Therefore, γ has units of $\text{W}^{-1}\text{m}^{-1}$. Effective area of PCF has a great significance. It is significant in context of numerical aperture, nonlinearity, confinement loss, bending loss, splicing loss etc.

The nonlinear coefficient (γ) varies directly in proportion to the refractive index (n_2) and is inversely proportional to the effective mode area (A_{eff}). This nonlinearity can be enhanced by using materials having a higher nonlinear refractive index and lower effective area of the core.

$$\text{Effective area } A_{eff} = \frac{(\iint |E|^2 dx dy)^2}{(\iint |E|^4 dx dy)} \quad (2.49)$$

The effective mode area of the fiber is defined as the area in which input light is confined in the optical fiber. This relation can be varied to generate various nonlinear and dispersion characteristics. As the effective mode area or core size increases, the nonlinearity will decrease [82]. For enabling the anomalous dispersion regime, the core size has to be smaller and controlled efficiently so that reduction of the size should not cross the limit as this may make the fiber distorted. Large index difference, which leads to tighter confinement, give PCF a higher γ , within a high air filling fraction.

One more pivotal parameter for nonlinearity is the effective length of fiber (L_{eff}) [83]. We can define effective nonlinear length as the characteristic length over which nonlinear effects become important.

$$L_{eff} = 1/\gamma P_0 \quad (2.50)$$

where P_0 denotes the peak power of the input pulse. It is clear from eq. 2.50 that a large γ (or long interaction lengths) is essential for efficient nonlinear observations. Thus during light propagation, different characteristics like dispersion, phase matching, polarization also have a dominant contribution to the development of nonlinearities.

From above discussion, we can conclude that optical characteristics of PCFs mainly depends on the index contrast between the core and the cladding that can be varied by altering size of the cladding air holes, which changes the effective refractive index of the cladding region. Control of the effective refractive index allows significant engineering of fiber characteristics like birefringence, dispersion, nonlinearity, confinement loss, etc. With a certain value of the ratio of hole diameter to pitch (A), PCFs can support the fundamental guided mode, regardless of wavelength. The periodic variation in the refractive index provides better interaction of the guided material and the light field, and can considerably affect the optical properties of the composite material.

2.5 Losses in PCFs

Solid-core fibers

Various types of losses occur during the propagation of input pulse. The inherent losses are a material loss. This kind of loss occurs due to the fiber material deformity that enhances the disruption in the propagation and decreases the propagation efficiency of the light pulse. Intrinsic absorption mainly due to free electrons and resonances associated with bound electrons and ions and impurities are the main cause of extrinsic absorption.

The optical loss α_{dB} that can be measured in dB/km, of PCFs with a adequately reduced confinement loss, which can be described as [44]

$$\alpha_{dB} = \frac{A}{\lambda^4} + B + \alpha_{OH} + \alpha_{IR} \quad (2.51)$$

here A , B , α_{OH} , and α_{IR} refer to the Rayleigh scattering coefficient, the imperfection loss, and OH and infrared absorption losses, respectively.

Presently, dominant losses in the fiber are *OH*-absorption loss and imperfection loss [84]. In PCF, the *OH*-absorption loss is induced more than 10 dB/km at 1380 nm and in turn, this results in an additional optical loss of 0.1 dB/km at around 1.55 μm . As this induced loss seems to be analogous to the intrinsic optical loss of pure silica glass at the same wavelength, the *OH*-absorption loss reduction becomes an significant and challenging problem. It has also been observed that *OH* impurities seem to pierce the PCF core during the fabrication process. For overcoming

this loss, a dehydration process can be utilized for reducing the OH-absorption loss [84].

Another major loss is the imperfection loss that induces mainly by surface roughness in the air hole. These surface roughness produced by small scratches and contamination. At a certain wavelength, this surface roughness may also cause scattering loss. Hence, it is important to make the polishing and etching process better to lessen the imperfection loss caused by the surface roughness. In addition to that, the fluctuation in the fiber structural parameters at the time of fiber drawing process may result in an additional imperfection loss [44,84].

Other losses are confinement loss and splicing loss. The confinement factor denotes the ability of light confinement in the core region. Since the numbers of air ring in the PCF are finite, some power always leaks out from the core to cladding, which is called as confinement loss [85]. The confinement loss can be numerically determined as

$$CL(dB/km) = \frac{8.686 \times 2\pi \times 10^3}{\lambda} \text{Im}(n_{eff}) \quad (2.52)$$

where, $\text{Im}(n_{eff})$ is the imaginary part of effective refractive index.

It is a kind of loss that occurs during propagation of light into the fiber core. There is always a slight confinement loss in the fiber, and it increases if the difference between the effective index of the core and cladding is less, also if the hole size is too much small. To reduce the confinement loss, the n_{eff} difference has to be large enough and also the hole size should be large till a certain limit. The confinement loss may induce the coupling loss too, and eventually, it may distort the whole propagation over long haul distances. The light will propagate out of PCF if the air-holes are providing improper confinement. This implies that it is essential to select such features of the PCF design, such as, pitch or air-hole diameter and hole-to-hole spacing, to obtain low-loss PCFs. Especially the ratio of the air-hole diameter and the pitch should be selected large enough to confine light into the PCF [87,88]. Recently, a lot of research has been done to find the methods to design both index-guiding PCFs and PBG-based fibers with minimum leakage losses [89]. Confinement losses depend on the number of air-hole rings, particularly for fibers with the high air-filling fraction. Increased ring numbers can reduce leakage losses by a significant amount.

The splicing loss is another loss, which occurs when the holes are collapsed due to the overheating of the fiber during the cascading process that is done by heating the two fibers to melt and joined to each other. Controlling the air hole collapsing can reduce this kind of loss [44].

If the fibers are bent more tightly than a certainly limited radius, then these fibers may face additional loss, called bending loss. In conventional fibers, beyond the certain limit of wavelength, the light guiding is distorted and this cut off wavelength is termed as, “long-wavelength bend loss edge”. In the case of PCF, besides the long-wavelength bend loss edge, the “short-wavelength bend loss edge” is also considered. This is originated by bend induced coupling from low to high order modes that escape the core. In fact, at short wavelengths the guided mode is mainly confined into the material, and when the pitch becomes much greater than wavelength, the field can escape into the space between the air-holes. Consequently, the fiber becomes susceptible to bending [44].

2.6 Fabrication Techniques of PCF

The fabrication of semiconductor core fiber is somewhat challenging, but various methods have been developed for this purpose, each having their advantages and disadvantages. Few fabrication methods are explained below:

2.6.1 Stack and Draw Technique

For any fiber fabrication, the basic step is to form a fiber preform that is a structure from which fiber is drawn. In case of multiple thinning method, various number of capillary rods and tubes made of silica are stacked and arranged in a particular way according to the type of lattice structure we require. This fabrication method allows us to have large variations in shape and size of air hole structure in the cladding, as well as this flexibility in design, let us have control over the index profile of the fiber. Once the required preform is developed, a fiber drawing tower is used to draw fibers with kilometres of length. The high temperature of the drawing tower enables easy fiber drawing. This drawn fiber is passed through a cooling chamber where the fiber is cool down to attain its required structure.

One of the major fabrication problems arrives when the air hole structures in

the fiber deform and do not maintain their required lattice structure. Careful observation is required at the time of fiber drawing process to avoid this problem. The last step includes adding a protective covering to the fiber to grant strength and robustness to the fiber structure. The produced fibers are better than standard fibers in physical strength as well as in working [90]. Thus, The stack-and-draw method includes horizontally stacking two rods of different glasses into a macrostructure called a multi-rod preform and then, using a fiber drawing tower, slowly pulling this preform through a high-temperature furnace to scale it down in size. The temperature can be varied, between 600°-800°C for glasses and 150°–250°C for polymers, of the furnace [44].

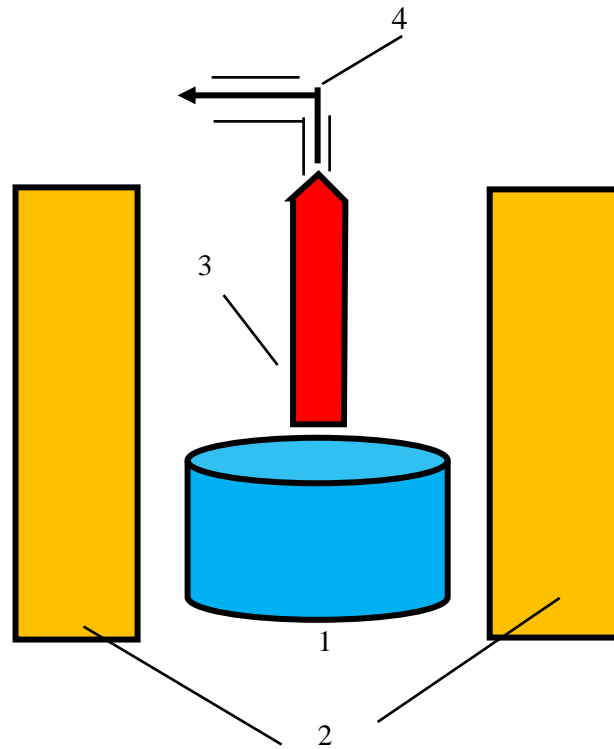
2.6.2 Extrusion Method

This fabrication method is primarily used for formation of soft glass PCF. In this process, the preform is formed by pouring the melted glass in a die, consisting of a predefined desired pattern of holes. After the fiber preform, the fiber is drawn from the preform in a conventional high-temperature drawing tower and extremely thin PCFs having kilometers of length are produced [44,91].

2.6.3 Die-cast Process

This fabrication process is performed into two parts as shown in Fig. 2.8 [92,93]. First, die is fabricated for preform of PCF. The PCF structure has glass as the background material and embedded air holes. To obtain die, the air holes can be changed with heat resisting alloy steel rods. Heat-resisting alloy steel can be used as the material for die because of the properties like resisting high temperature, oxidation, and glass etching. The die is kept in the vessel vertically with material to heat at melting temperature in the furnace. A vacuum pump is used for removing the air out of the die and glass is allowed to deposit in the die which is having negative internal pressure. The suitable filling rate is used to reduce mixing air bubble. When the die is fully filled with glass, the vacuum pump is removed and it is kept inside the furnace for annealing. When the die temperature approaches room temperature, the outer tube and two disks at the ends of the die are removed. To eliminate heat-resisting alloy steel rods, die is etched with an acidic solution. Further, in order to remove residual waste of metal, die is etched in a 20% hydrofluoric acid solution. Ultimately, the etched bundle is put in a furnace to dry so that it can be used as a PCF

perform. In order to achieve replica of hole shape and periodicity of the fiber, the outer diameter of the preform was thinned suitably in the drawn fiber tower at melting temperature.



1. Vessel, 2. Furnace, 3. Die, 4. Vacuum hose

Fig.2.8 Setup of PCF preform fabrication in Die-Cast Process.

2.6.4 Sol-gel Technique

Initially the sol-gel casting technique was expanded to generate large jacket tubes for optical waveguides . It was further evolved to fabricate MOFs [94,95]. A mold consisting of an array of mandrel elements is set-up and then supplied with colloidal silica distributed at strong pH having an appropriate mean size of the particle. The pH of the sol is reduced to the gel level. The mandrel elements are removed when the gel is still wet and leaving air columns inside the gel body. After that, impurities related to Water, organic and transition metals are reduced by considering the gel body thermochemically. The dried porous gel body is then moulded at 1600° C into a viscous glass and then drawn into the optical waveguide. For achieving required size and air-filling fraction, the air holes are pressurized during the draw. The mandrels are stretched separately and a digital camera observes their spacing and position to keep the consistency along the length of the preform. The sol-gel technique can be used to design any structure that can be transformed into a mould.

Comparing this method with stack and draw technique, stack and draw technique can only be used for compact structures such as hexagonal or triangular lattices and difficult to design circular structures. Drilling methods can be used to change the size of hole and spacing between the holes, but are restricted to a small number of holes and confined to circular shapes. Extrusion methods allow flexibility of design, but are normally limited for soft glasses which have large amount of material loss [96]. The sol-gel casting technique is having extra freedom of design that is necessary for fibers with small-bend loss, dispersion flattened waveguides or birefringent fibers because they need unconstrained structure. However, to implement the sol-gel technique, we need to deal with certain challenges. During the wet gel stage, elements of the mandrel are detached, while the gel body is weak. Removing of mandrels at this stage applies pressure on the gel that can lead to cracking of gel bodies and decreasing the overall yield. The low air-fill fraction glass preforms are etched with hydrofluoric acid solution uniformly along the length of the preform to obtain high air-fill fraction fibers. Thus, the sol-gel method is a cost effective and low-temperature process which provides the facility of controlling the chemical composition of the product [94].

While dealing with the fabrication problems, the major problem is deformity in the fiber structure and new air hole emerging in the fiber structure. When the fiber is drawn in a fiber drawing tower, often the air holes get deformed leaving their desired structure. This problem is vividly seen in case of a square lattice of circular air holes where the air holes tend to occupy the outer geometry structure, that is the air holes tend to be square in shape. This undesirable effect of deformity in air holes and new air holes emergence at the time of drawing of fiber can be avoided by precise control of the fabrication process. A way to avoid this effect is by adding more rings of capillaries around the fabricated structure. This will not only prevent deformities of air holes but will also provide robustness to the fiber structure. In addition to that, little other prevention can be taken to avoid such flaws in the fiber structure including having precise control over the temperature distribution of the fiber drawing process and the temperature in the oven. Moreover, control over the rate at which the fiber is fed and drawn from the fiber drawing tower allows us to avoid the flaws in the fiber structure [44,90].

2.7 Applications

In the preceding section 2.4, some basic properties of PCFs were described. Due to the inherited unique properties and better control over them generates numerous applications in the optical domain. Some of the latest applications attracting researchers are nonlinear properties of the PCF. Most attractive nonlinear phenomena in PCF is a SCG in PCFs which is having a number of applications as optical coherence tomography and spectroscopy. HNLF are a key element for all-optical signal processing at speed beyond the limits of electronics.

The following section reviews some devices that demonstrate the potential of PCF for practical applications.

2.7.1 Polarization Maintaining Fiber

PMF is a special type of fiber that has a built-in strong birefringence. This kind of fiber is a contrary solution to the effects caused by the stress and bendiness of the fiber [97]. High birefringence fibers are having well-known applications of intentionally introducing birefringence, which is introduced by fabrication process into the fiber. Due to this reason, these fibers have the property of maintaining the SOP of the input wave. The aim of introducing high birefringence is that when the light is incident on this fiber, the modes which are polarized orthogonally, they should be guided separately so that coupling between modes can be reduced up to great level [57]. If the light is properly guided and is coupled to only one of the polarized modes, then most of the light maintains its polarization. The polarization-holding capability of a birefringent fiber is known as beat length L_b , which is given by

$$L_b = \frac{2\pi}{\beta_x - \beta_y} = \frac{\lambda}{\Delta n_{eff}} \quad (2.53)$$

Where β_x and β_y denote the propagation constant and Δn_{eff} denotes the effective indices difference of two modes which are orthogonal at wavelength λ . L_b denotes the light propagation length after which the phase difference between two fundamental modes is 2π . So high birefringence leads to polarization holding capacity.

PMF can be realized by making the cladding in the elliptical shape around the core or by using an elliptical core. These techniques can help in introducing birefringence without any need of stress in the fiber. In this kind of fiber, the production is quite

complicated and expensive for long distance transmission and also the propagation losses may be high [98].

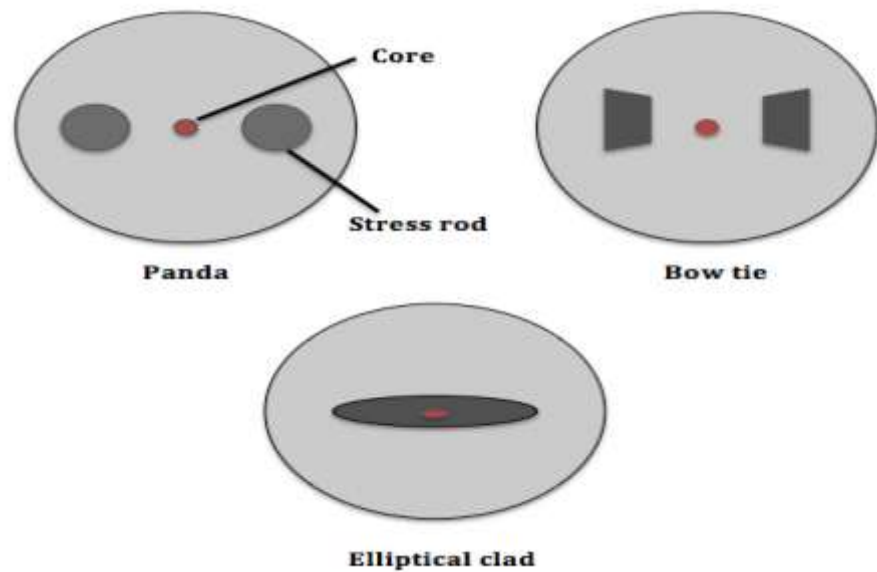


Fig. 2.9 Three types of conventional PMF

As shown in Fig. 2.9, PANDA or Bow-tie fibers [99], can achieve high birefringence up to 10^{-4} by applying stress to the core region of a standard fiber [100].

2.7.2 Dispersion Compensation Fiber

In long haul high data rate transmission systems, dispersion is one of the critical parameters in an optical link because it widens the pulse and restricts the available bandwidth of the system. To properly compensate the positive dispersion over a large distance, dispersion managing schemes should be applied. As we know, if the wavelength of the wave is centred around $1.55 \mu\text{m}$, then the higher wavelengths propagate with small velocity and the smaller wavelengths of wave propagate with larger velocity. This will help in broadening the pulse, and this happens in the ADR where the blue-shifted part will travel faster than the red-shifted part. This broadening of pulse creates problems when information is to be transmitted for long distance. This broadening of pulse signifies that this pulse has inter symbol interference with the second pulse and no identifiable data will be received at the output. Thus, broadening of pulse limits the rate at which pulse can be propagated through the fiber. This will indirectly affect the available bandwidth [101]. Therefore broadening of pulse lower the bandwidth of the fiber.

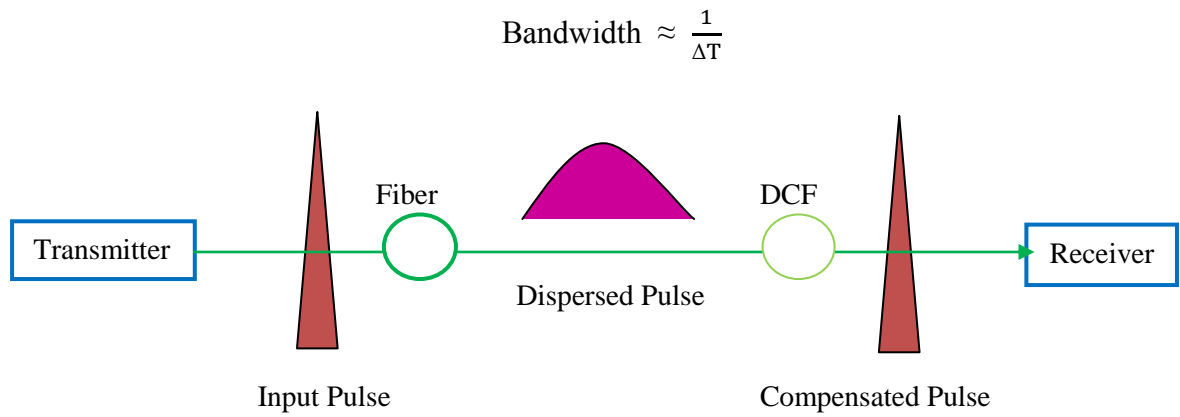


Fig. 2.10 Dispersion compensation fiber

To combat this limitation, an optical fiber with negative dispersion is required. After traveling certain length in such a fiber, where the group velocity varies. This will let the red shifted part travel faster than the blue shifted part and this occurs in the NDR. In this way, the wave tends to reshape itself into its normal form or in other words, get compressed. This is how the DCF phenomenon occurs. This phenomenon is shown in Fig. 2.10.

Since joining of the DCF to fiber optical system will increase the total loss of the system and so it would be problematic at detection end. By having very large negative dispersion coefficients, the required length of the DCF can be reduced [28]. Thus, it is significant to put research effort to get very large negative dispersion.

The DCF having large negative dispersion has various applications in tunable wavelength converter, RDCF and SCG [102]. Additionally, through properly generated large negative dispersion by accurately tailored fiber parameters, low positive dispersion, and long distance transmissions can be ensured.

2.7.3 Supercontinuum Generation

Supercontinuum is generated when multiple nonlinear processes and consideration of various parameters contribute together where input ultrashort pump pulse with high peak energy is transformed into light with very broad spectral bandwidth [44,103]. It is generally accomplished by transmitting optical pulses through a strongly nonlinear medium. This process needs various nonlinear processes such as SPM, XPM, FWM, Raman Scattering and Soliton dynamics [104]. It has various useful applications like gas sensing, molecular spectroscopy, cancer detection, optical coherence tomography,

food quality control, biomedicine, optical frequency metrology, an optical source for a WDM communication system, wideband tunable wavelength conversion, fluorescence microscopy and flow cytometer [103,105,106]. The priority for SCG is given to the PCF due to its capability of the variable parameter that can be altered as per the requirements. Also, the light beam can be strictly confined to the core area by adding a higher number of air holes to the cladding or increasing the size of the holes or increasing the effective index difference, which can help in reducing confinement loss in the pulse propagation over long haul distance. SCG is done in two regimes, those are, NDR and ADR [10]. Also, in two IR regions, SCG is gaining in attention such as mid-IR region and near IR region. The mid-IR region is considered as important for various applications because the fundamental molecular vibration absorption bands present in this region are found to be sturdy compared to the combinational absorption bands that exist in near IR region. It is based on the working wavelength range of applications that what IR region or regime we want to work on [107].

Furthermore, SCG can be held in both the ways where the pulse may just broaden in the outcome or new frequencies are generated in terms of solitons, is shown in Fig. 2.11 [108]. Mainly, in ADR, soliton dynamics, modulation instability and Raman scattering [109] is used as nonlinear processes as it helps in generating the stable wave through the whole distance. Additionally, higher order soliton pulses are very important in long distance optical fiber communication. Soliton pulses can be formed when the nonlinearity and dispersion in the fiber cancel each other. When propagating in the fiber, the soliton pulses are subjected to the Raman Scattering. Through Raman Scattering, the pulses with different frequencies are generated having different energy levels [108]. This causes an overall spectral shift of soliton towards longer wavelength, i.e., a soliton self-frequency shift [110]. The strength of this effect depends on the pulse duration since shorter pulse exhibits a higher peak power and a broader optical spectrum. Additionally, it is beneficial to have high order solitons as higher the order more will be the distribution of solitons and broader will be the output pulse[109]. The basic condition for this process is to first consider the pumping in the ADR and close to the fiber's ZDW or specifically pump wavelength greater than the ZDW for enabling ADR[10]. The ZDWs help in suppressing the distortion and so it is found beneficial to generate more of these. For generating high order solitons in order to broadening the spectra of stable pulses under SCG, the power of

the pump pulses has to be high enough. As higher the power of the pump, higher will be the soliton order. If the high order soliton pulse is achieved, it will break into N red-shifted solitons with varying group velocities.

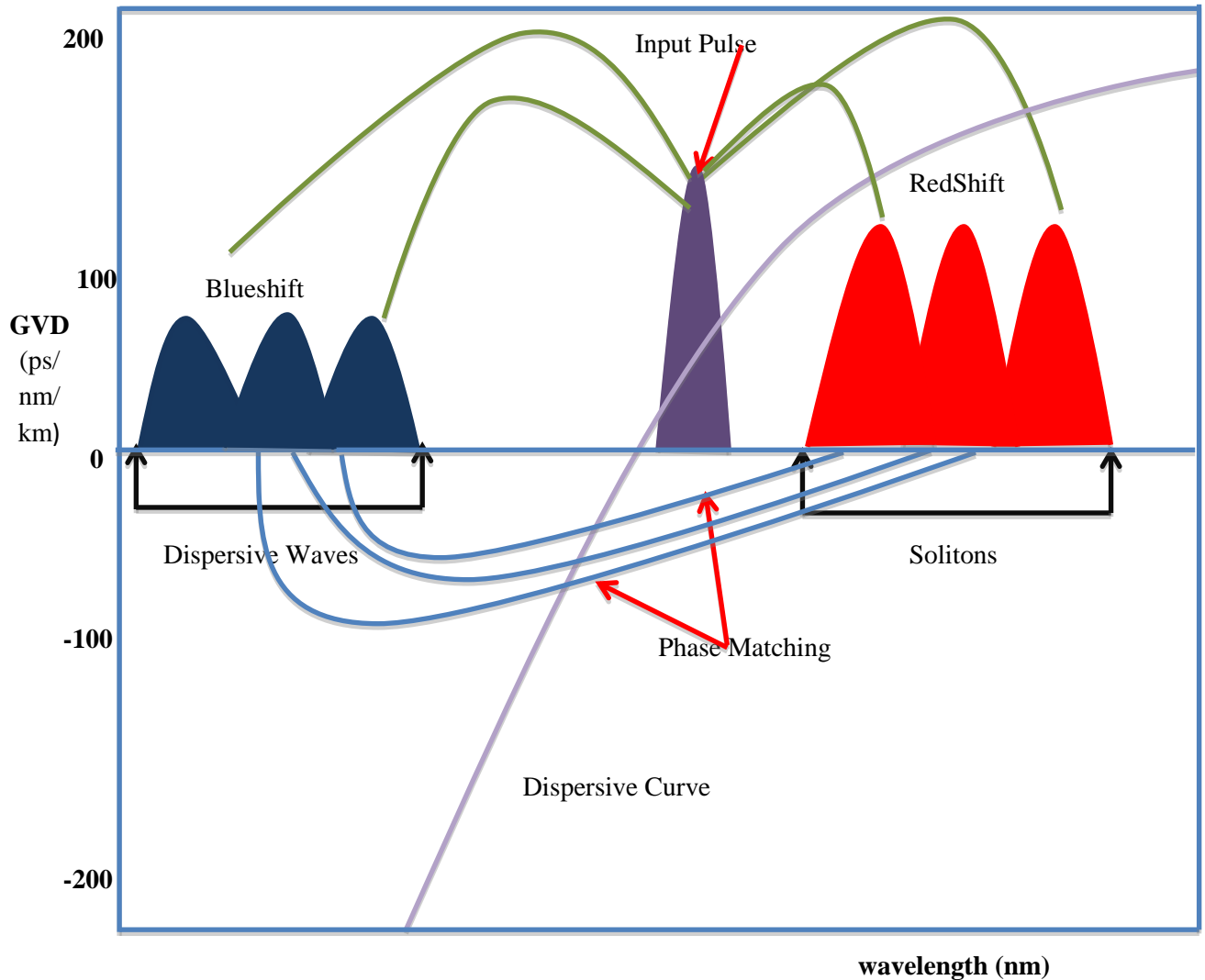


Fig: 2.11 Display of SCG by Soliton radiation and Non Soliton radiation

The distributed solitons pulses having leading edge of higher wavelength and the trailing edge of lower wavelength. In ADR, blue-shifted part (high frequency) will travel faster than the red-shifted part (low frequency). On the other hand, the higher wavelength part will travel faster than lower wavelength part of the pulse in the case of NDR. Additionally, when the dispersion is anomalous, and nonlinearity is present, the frequency chirps produced by dispersion and SPM or any nonlinear process is contradicted by each other[111].

In this way, there is a possibility that in ADR, the two chirps generated cancel each other and give chirp-free pulse when $L_D = L_{NL}$. In this state, neither the pulse contracts nor it broadens and remains stable over a long distance. This near to impeccable pulse is called soliton. The soliton dynamics is numerically based on the nonlinear Schrödinger equation that consists of the loss, dispersion, and nonlinear parameter. Also, this equation describes the low loss transmission of soliton in optical fiber[103]. It is given as

$$\frac{\partial A}{\partial z} - j \frac{\beta_2}{2} \frac{\partial^2 A}{\partial T^2} + \frac{\alpha}{2} A = -j\gamma |A|^2 A \quad (2.54)$$

Dispersion Loss Non-linearity

The SC is generated from dispersion characteristics also. When the input light is not much intense, the GVD parameter (β_2) has a big role in pulse broadening as it varies with the wavelength of the pulse. The chirp is added to the pulse due to the GVD, and this added chirp will be negative or positive that depends on dispersion regime of the fiber, i.e., ADR or NDR. Due to the high influence of GVD, the pulse only gets broaden; no new frequency components get generated [111]. The group velocity is given by

$$\beta_2 = -\frac{1}{v_g^2} \frac{\partial v_g}{\partial \omega} \quad (2.55)$$

Moreover, the input pulse is generated with two types of pulse width, i.e., femtosecond pulse and picosecond pulse. However, it has been examined that shorter the pulse, broader will be the output wave.

Self- Steepening Process: For intense optical pulse the refractive index and group velocity depend on the intensity of light[103]. So, when the intensity of light varies, the variation is introduced in the group velocity, and due to this, propagation speed of pulse peak becomes different from the leading and trailing edge speed. Consequently, if n_2 is positive then the pulse tries to form a shock at the trailing edge and for negative n_2 the pulse tries to form a shock on the leading edge. The Raman scattering has a big participation in leading to a self-steepening effect, which can lead further to the breakup of higher order solitons called soliton fission. This effect has a major contribution in the SCG. The influence of self-steepening on the propagation of higher order solitons is that it leads to the breakup of higher order solitons into N fundamental solitons [109].

Raman Effect: The proper and dominant nonlinear effect for SCG is the Raman effect as in the initial stage of SCG process it helps in generating additional spectral components. The principle of Raman scattering is that when a higher frequency pump-laser light propagates along the fiber length, it scatters off atoms in the fiber, this lets the signal to lose some energy to the scattered atoms. These scattered atoms act as the additional spectral components generated during the propagation that will help in broadening of spectra [103].

Hence, through the utilization of nonlinear effects, additional red-shifted spectral components are generated that contribute in broadening of the spectrum in the output. The output pulse eventually becomes highly stable through nonlinear processes and is eligible for propagating in long haul distance in the fiber. In this way, the SC is generated in PCF and studies are focusing on improving this phenomenon day by day, so that it can be applied in various applications more efficiently.

2.7.4 Coherent optical fiber communication

Although coherent detection is relatively new in optical communication. It has been around in Radio Communication for a long time. In the history of Lightwave technology development, a more important reason behind the coherent detection research work is its ability to amplify the received signal optically for better SNR [63,64]. Number of researchers have been explained various practical limitations in the development of coherent digital optical fiber communication systems. These limitations are mainly associated with the components of coherent digital optical fiber system. Development in component technology associated with coherent optical fiber communication (COFC) has resolved the difficulties up to a certain extent, still it needs more investigation. So it becomes important to study major limitations and their effect on the choice of system component. The components of coherent optical communication system which need specific requirement to achieve desired performance of the system are transmitter, receiver and transmission medium. Our research work is emphasized on the properties of transmission medium to achieve desired performance of COFC. As for COFC system, polarization, phase and frequency of transmitted optical signal and locally generated carrier signal must be matched to recover the message signal efficiently at receiving end. To achieve these

matching requirement of COFC, the properties of transmission medium such as attenuation, dispersion, birefringence play a important role.

For coherent optical communication detection the primary condition at receiver side is that the SOP of transmitted signal and locally generated carrier should be matched. To achieve this condition SOP of transmitted signal through optical medium must be maintained. Proposed structures of PCF have very large value of birefringence so beat length of fiber will be small and polarization will be maintained throughout the transmission fiber. So, at the receiving end, matching of polarization can be achieved easily.

Secondly, to provide coherent optical detection, dispersion of transmission medium can be reduced by using low-loss, DSF, with a zero dispersion in the 1.550 μm wavelength window. This solution is only partially satisfying in that there is a great base of installed conventional fiber. Additionally, the low-dispersion region in any fiber is narrow when compared to the range over which the fiber supports optical transmission. This limitation may become important in future multi gigabit wavelength-multiplexed systems. Alternative approach to overcome this limitation is that Chromatic dispersion can be compensated, in principle, by using an optical component with the opposite dispersion of that in the fiber [63,63]. Proposed PCF structures are able to provide chromatic dispersion that is opposite to dispersion of fiber, and achieved value of chromatic dispersion is $-1251 \text{ ps}/(\text{nm.km})$. Hence, by using these designs certain constraint of transmission line associated with COFC system can be resolved and system performance can be improved.

2.8 Summary

Through this study, it is understood that PCFs have more design flexibility that provides better control over fiber characteristics. The extraordinary features of PCF are proven to be beneficial for numerous applications. Proper fabrication techniques can reduce losses incurred during propagation. This study of PCF will be helpful in understanding the rest of the thesis.

Chapter 3: Research at a Glance

3.1 Introduction

This historical review of the fiber optics marks a huge importance as it covers the milestones achieved by various researchers from 2000 to 2017. Till now, significant researches have been done on this field and improvements in the characteristics of PCF has been achieved. Moreover, the possibility of a wide area of applications this concept provides, have been increasing day by day and in fact have been proven to be an impactful and beneficial for the present innovative generation.

3.2 Research contribution in past

In **2000**, the progress of advancement in PCF was observed. As with the introduction of ESM fiber in 1997, the PCF has been gone through many changes, and in this whole duration, many applications have been explored such as SCG, sensing applications, high sensitivity spectroscopy and ultra short-pulse lasers and amplifiers. Major applications require un-distorted pulses guiding through PCF, and this needs low dispersion and high birefringence [112]. The birefringence concept in PCF was first introduced in the year 2000, and from then it has been widening its area of applications. It can be utilized in polarisers, helps in making PCF insensitive to the temperature and is also being used in medical field [113]. The desired dispersion can be generated in PCF by its proper fabrication and variation of structural parameters. It is required to have flattened negative dispersion due to the need of better optical signal transmission systems over a long distance, as it provides an undistorted pulse. Additionally, as PCF provides us a facility of tailoring its structural parameters, high nonlinearity in PCF can be attained through this as it proves to be a promising characteristic for optical parametric amplification, Raman amplification, FWM, SCG for metrology and optical coherence tomography (OCT). A. Ortigosa-Blanch et al., have designed a silica PCF with hexagonal structure explaining the concept of birefringence, it has the immense applications in optical telecom components and in controlling light in long transmissions systems. In this study, the birefringence achieved is 3.7×10^{-3} because of high refractive index contrast in the fiber [22]. W.J. Wadsworth et al., have unanimously designed a pure silica triangular lattice PCF and

achieved solitons at 850nm with GVD of large $50 \text{ ps nm}^{-1} \text{ km}^{-1}$ and small $<10 \text{ ps nm}^{-1} \text{ km}^{-1}$ and low loss [114].

In **2001**, the progress continued in the direction of exploring more applications with the required results through PCF. N. Nishizawa et al., designed a silica PMF with the small size core having large nonlinear coefficient $21 \text{ W}^{-1} \text{ km}^{-1}$ and achieved birefringence is 3×10^{-4} [115]. Albert Ferrando et al., have designed a UFD silica core PCF with a hexagonal structure having a dispersion of $\pm 43 \text{ ps nm}^{-1} \text{ km}^{-1}$, else birefringence and confinement loss are not calculated in this study. The magnification M and air filling fraction f have been analyzed for dispersion characteristics [116]. Kazunori Suzuki et al., proposed a silica PMF with decagonal structure inducing birefringence of 1.4×10^{-3} . The high birefringence is achieved by enlarging the two center holes [57].

The study is continued to achieve better results through optimized PCF and in **2002**, K.P. Hansen et al., designed a silica PCF with triangular lattice including 6 rings of air holes having high nonlinear coefficient $20 \text{ W}^{-1} \text{ km}^{-1}$ and birefringence of 1.1×10^{-4} [117]. In addition to this, P. St. J. Russell proposed a silica containing two MOFs with a very small core and a hexagonal structure having a dispersion of $0 \pm 0.6 \text{ ps/nm.km}$ within $1.24 \text{ }\mu\text{m}$ - $1.44 \text{ }\mu\text{m}$ wavelength range and $0 \pm 1.2 \text{ ps/nm.km}$ dispersion within $1 \text{ }\mu\text{m}$ - $1.6 \text{ }\mu\text{m}$ wavelength range. Average dispersion slope is found to be $9.98 \times 10^{-4} \text{ ps/nm}^2 \cdot \text{km}$ and confinement loss is 0.56 dB/m at 1500 nm [118]. Bishnu P. Pal optimized a silica dual core DCF with triangular structure core having a negative dispersion of $-190 \text{ ps}/(\text{nm km})$ in the S- and C-bands and residual dispersion of $\pm 0.4 \text{ ps}/(\text{nm km})$ within the C-band [119].

The need of high nonlinearity, low dispersion, and high birefringence increased to meet the necessity of the growing applications in the optical domain. In **2003**, K. P. Hansen proposed a silica hybrid-core nonlinear PCF has a triangular lattice that induced a flattened dispersion of $0.001 \text{ ps}/(\text{km} \cdot \text{nm}^2)$. Also the nonlinearity coefficient greater than $11 \text{ W}^{-1} \text{ km}^{-1}$ and loss below 7.9 dB/km at $1.55 \text{ }\mu\text{m}$ was attained. The proposed fibers consist of a three-fold symmetric hybrid core region having a germanium-doped center element ($n=1.487$) covered by three fluorine-doped regions ($n=1.440$) embedded in a standard triangular air/silica cladding structure [120]. L. P. Shen et al. have attained a large negative dispersion of -474.5 ps/nm/km in silica core DCF with circular air holes and five rings that can compensate SMF

within ± 0.05 ps/nm/km over a 236-nm wavelength range [121]. A. Peyrilloux et al., have designed a silica hexagonal PCF that induces the birefringence below 10^{-4} [122].

Furthermore, various experiments have been done by introducing deformities in the fiber to achieve the required results. So in **2004**, F. Poli proposed a large hole silica hexagonal PCF where the size of the holes of the first, second, and third ring are varied for increasing the nonlinearity, inducing large negative dispersion of -1430 ps/(km.nm) and high nonlinear coefficient of $76 \text{ W}^{-1} \text{ km}^{-1}$ is achieved [123]. F. Gérôme proposed a silica dual-concentric-core PCF is achieving negative flattened dispersion of -2200 ps/(nm.km) at $1.55 \mu\text{m}$. The outer diameter of fiber has been varied and the winding of fiber is done to control the dispersion [124]. In the same year, P.R. Chaudhuri et al., designed near elliptical core PMF with an octagonal structure having 10^{-3} high birefringence. Having hole size 0.7 provides the maximum birefringence in this study [125]. The study continues with the purpose of achieving more suitable results by varying the fiber structure parameters.

In **2005**, F. Poletti et al. designed a pure silica ultra-flattened dispersion holey fibers with hexagonal structure achieving the flattened dispersion of 0 ± 0.1 ps/(nm.km) and high nonlinearity coefficient of $44 \text{ W}^{-1} \cdot \text{km}^{-1}$ at $1.55 \mu\text{m}$. Λ has been changed to small values, i.e., $0.5\text{--}2.5 \mu\text{m}$, to ensure having large nonlinear coefficient [126]. On the other side, T. Wu demonstrated the dispersion of 0 ± 0.25 ps/(nm.km) over 1295 to $1795 \mu\text{m}$ in silica PCF having four rings triangular lattice with two different air-hole sizes [127]. Kunimasa Saitoh et al. proposed a silica fiber with six fold rotational hexagonal symmetry and numerically analyzed. The dispersion of $0.1 - 0.3$ ps/(km.nm) over 1.41 to $1.68 \mu\text{m}$, confinement loss less than 0.1 dB/km at a wavelength shorter than $1.7 \mu\text{m}$ and birefringence of 3.7×10^{-3} is obtained [128].

Moreover, efforts have been made to achieve results applicable to broad wavelength range. In **2006**, Aleksandr V. Mitrofanov et al. designed a silicate glass PCF with hexagonal lattice having nonlinearity coefficient $25 \text{ W}^{-1} \text{ km}^{-1}$ and inducing high birefringence of 1.2×10^{-3} at $1.24 \mu\text{m}$. This design is suitable for high-spatial resolution and high-spectral-contrast nonlinear Raman micro spectroscopy [129]. Nikolaos Florouset et al proposed a new silica PCF with the hexagonal symmetry having flattened dispersion of 6.3 ± 0.5 ps/km/nm in the S+C+L wavelength band. Artificially created irregular air-hole ring in the cladding of the PCF for increasing the effective mode area and modulation of the core's effective index helps in controlling

of dispersion in this PCF [130]. In the same year, Krishna Mohan Gundu proposed a silica glass hexagonal structured PCF with the liquid hole filling technique that induces the dispersion of $0 \pm 0.5 \text{ ps}/(\text{nm}\cdot\text{km})$ over 430-510nm [131].

In addition to achieving low dispersion, efforts to achieve low loss and highly nonlinear materials are also made in further studies as in **2007**, Songbae Moon et al., designed an optical fiber doped with silicon nanoparticles that achieved a large nonlinear refractive index of $1.5 \times 10^{-15} \text{ m}^2/\text{W}$ at 1565 nm [132]. S.M. Abdur Razzak et al., designed a four ring octagonal PCF having a defected ring that is obtaining a dispersion of $\pm 0.50 \text{ ps}/(\text{nm}\cdot\text{km})$ over 1.31 to 1.70 nm, also confinement loss less than 0.001dB/km is obtained over 1.31 to 1.65 mm band. The fiber with these parameters is suitable for ultra flattened dispersion applications [133]. D. Chen et al. designed a high birefringence PCF with hexagonal lattice consisting of elliptical air holes having a large birefringence of 10^{-2} [60]. The benefits of slot structure waveguide realized in further years as it provides better nonlinear characteristics and good confinement.

In **2008**, Arismar Cerqueira S. Jr et al. proposed a fiber for generation of FWM products having a nonlinear coefficient of $215 \text{ W}^{-1}\cdot\text{km}^{-1}$ and low dispersion of $0.3 \text{ ps}/\text{nm}\cdot\text{km}$. Comb-like dispersion profiled fibers have been used to obtain the efficient generation of FWM products [134]. Zheng Zheng proposed a SOI-based slot structure has dispersion curve in NDR at 1500 nm [135]. In the same year, Chen Ming et al., designed a new type of PCF having four big elliptical air holes in the center having a birefringence of 2.263771×10^{-3} [136]. As to generate more stable pulses for undistorted transmission, more studies have been done for eliminating the trade off effects. In **2009**, flattened dispersion of $0 \pm 0.65 \text{ ps}/(\text{nm}\cdot\text{km})$ over 1.36– 1.62 μm was achieved by Feroza Begum et al., and nonlinear coefficient greater than $45 \text{ W}^{-1} \text{ km}^{-1}$ and low dispersion slope of $0.009 \text{ ps}/(\text{nm}^2\cdot\text{km})$ at 1.55 μm wavelength is also obtained. The silica PCF is considered with two types of air holes chosen to have hexagon structure for obtaining near zero dispersion [137]. On the other hand, F. Begum et al., have achieved a large negative dispersion coefficient in the range of -260 $\text{ps}/(\text{nm}\cdot\text{km})$ to -525 $\text{ps}/(\text{nm}\cdot\text{km})$ over 1.46 ~ 1.63 μm that apply to 40 Gb/s transmission systems and RDS value is 0.0039 nm^{-1} at 1.55 μm . The PCF with hexagonal structure is used with nine rings and three different sizes of air holes [138]. L. An et al., proposed a PCF is having a rectangular distribution of four air-holes and the elliptical shape of the holes induces high birefringence of 10^{-2} [139]. A similar

order of birefringence was achieved by H. Ademgil et al., who have introduced a silica–glass core PCF with a decagonal structure having three different sizes of air holes while maintaining the strong confinement. In this structure, high nonlinearity coefficient of $49 \text{ W}^{-1} \cdot \text{km}^{-1}$ at $1.55 \mu\text{m}$ and low confinement losses is also attained as it has minimal bending effects because of low effective mode area. The designed PCF with achieved results can be used in controlling of optical sensors and telecommunication systems [140]. Lin An et al., proposed a fused silica SPSM PCF has a hexagonal lattice with four identical elliptical air holes in the core region through which small mode area and near-zero dispersion is realized. Also, the high nonlinearity of $116 \text{ W}^{-1} \text{ km}^{-1}$ and GVD around $0\text{--}10 \text{ ps}/(\text{nm} \cdot \text{km})$ near to 820 nm wavelength is attained. Having these results, this PCF can be utilized in applications like parametric amplification, SCG and wavelength multicasting [141].

Research with slot waveguides continued with selecting different materials to achieve better results. In **2010**, Ya-Ni Zhang et al., designed a silica core PCF having squeezed hexagonal lattice structure with elliptical air hole that is showing nonlinearity coefficient as $150 \text{ W}^{-1} \text{ km}^{-1}$, low dispersion of $\pm 2.5 \text{ ps nm}^{-1} \text{ km}^{-1}$ over 1.43 to $1.8 \mu\text{m}$ and birefringence of 2.5×10^{-3} at $1.55 \mu\text{m}$ [142]. Lin Zhang et al. proposed highly nonlinear silicon slot waveguide having a dispersion of $0 \pm 0.16 \text{ ps}/(\text{nm} \cdot \text{km})$ over 244 nm bandwidth and As_2S_3 slot waveguide having a dispersion of $0 \pm 0.17 \text{ ps}/(\text{nm} \cdot \text{km})$ over a 249 nm bandwidth. The silicon waveguide is considered as better than As_2S_3 waveguide regarding inducing high nonlinearity due to large refractive index contrast [143]. Further, Lin Zhang et al. proposed a silicon strip/slot hybrid waveguide is having flattened dispersion of $0 \pm 16 \text{ ps}/(\text{nm} \cdot \text{km})$, over a 553-nm wavelength range. Three ZDWs have been generated for the first time with this waveguide and also this waveguide has been considered as highly suitable for propagating more confined light with high nonlinearity [144]. Additionally, Yongmin Jung et al., have worked on a silica microfiber with elliptic holes and the large contrast in refractive index provides high group birefringence, $B=5.3 \times 10^{-3}$ at $1.55 \mu\text{m}$. This microfiber offers control within high-resolution optical sensors, fiber lasers and resonators [145].

Furthermore, in **2011**, Yoshinori Namihira et al., proposed a pure silica doped with germanium PCF having an octagonal lattice that is suitable for achieving high nonlinearity. The large nonlinear coefficient of $56.3 \text{ W}^{-1} \text{ km}^{-1}$ and flattened dispersion

of around $-1 \text{ ps}/(\text{nm}\cdot\text{km})$ is obtained in this PCF [146]. Efforts have been made for more flattening of dispersion or compensation of dispersion as Feifei Shi proposed a silica ultra flattened fiber with the defected core and hexagonal structure to obtain high birefringence and two-mode propagation, having dispersion $-0.8 - 0.2 \text{ ps}/(\text{km}\cdot\text{nm})$ within 1.5 to $1.65 \text{ }\mu\text{m}$ wavelength range. High birefringence of 0.0014 and confinement loss less than 10^{-3} dB/m is also proposed [56]. In the same year, Ali Rostami proposed a dispersion profile of $2.9\pm 0.5 \text{ ps}/(\text{km}\cdot\text{nm})$ in the S+C+L band with the variation of the effective mode is greater than $80 \text{ }\mu\text{m}^2$. The PCF used having silica core with four air holes in a square structure within it and cladding has a hexagonal lattice. This structure has significantly brought effective variation in dispersion profile and effective mode area [147]. Furthermore, DCF has been playing a major role in compensating the dispersion through large negative dispersion and researchers have been a penchant for achieving large negative dispersion.

In **2012**, Huizhen Xu et al. has achieved a high nonlinearity coefficient of $31.5 \text{ W}^{-1} \text{ km}^{-1}$ having low dispersion slope of $5.12\times 10^{-4} \text{ ps}/(\text{km}\cdot\text{nm}^2)$ in the fluorine-doped trench-assisted structure [148]. Md. Selim Habib proposed a silica triangular lattice Dispersion Compensating PCF with nine rings and three different sizes of air holes having diameter d_1 , d_2 and d , also third and fourth air hole ring is reduced that attained a negative dispersion of $-360 \text{ ps}/(\text{nm}\cdot\text{km})$ at $1.55 \text{ }\mu\text{m}$ over $1460\text{-}1640 \text{ nm}$. This proposed fiber is capable of compensating in 10 Gb/s DWDM optical communication systems [149]. Then, So Eun Kim et, al, proposed an elliptical defected core fiber is having the hexagonal structure of elliptical holes with a high birefringence of the order of 10^{-2} [150]. Cheng Cheng Gui et al., have shown a study on soft-glass Elliptical–Spiral PCF, which has achieved nonlinear coefficient of up to $3089/3079 \text{ W}^{-1} \text{ km}^{-1}$, low dispersion of -95.45 to $-372.6, 153.2) \text{ ps}/ \text{ nm/km}$ and high birefringence of 0.05554 over $1000\text{--}1800 \text{ nm}$ [151]. Ming Zhu et al. came up with a design of silicon dual slot waveguide generating four ZDWs that is inducing high nonlinearity of $93.6 \text{ W}^{-1} \text{ m}^{-1}$ and flat dispersion in the range of -24 to $+22 \text{ ps}/(\text{nm}\cdot\text{km})$ at 1098 nm . This structure with the achieved parameters is beneficial for surface sensing devices and mid-infrared applications [152]. With the increasing work on PCF, Md. Asiful Islam, et al., designed silica Equiangular Spiral PCF that induces higher negative dispersion of $-393 \text{ ps}/\text{nm km}$ and high birefringence of 0.0278 at $1.55 \text{ }\mu\text{m}$. This ES-PCF is suitable for WDM optical fiber transmission system for RDCF

[153]. Sejin Lee et al., have proposed a silica hexagonal PCF using hollow ring defect that shows a flattened dispersion of 0 ± 0.51 ps/nm km at 1.44–1.61 μm with the maximum slope of -2.7×10^{-2} ps/nm² km. Also, confinement loss is found to be less than 5.75×10^{-8} dB/m. This PCF with such results have managed to eliminate the trade off, and so control on dispersion and losses is increased [154].

Also, to achieve large negative dispersion, it is necessary to regulate DCF over a long distance, and so further studies have been done in this direction. In **2013**, Mariusz Klimczak et al. contributed a hexagonal lattice tellurite PCF inducing high nonlinear coefficient of $238.6 \text{ W}^{-1} \text{ km}^{-1}$, birefringence below 10^{-6} and tellurite glass is seems to be very much suitable for SCG in this study [155]. M. M. Haque et al., proposed a silica core circular PCF with five air hole rings having a large negative flattened dispersion of -248.65 to -1069 ps/(nm.km) compensating in the range of 1360-1625 nm. Residual dispersion after compensating 40 km long SMF is within ± 62 ps/nm [156]. In another study proposed by M. Samiul Habib et al., dispersion of 0 ± 0.8 ps/nm/km over 1.33 to 1.71 μm is achieved with splice loss 3.82 dB at 1.55 μm . The hexagonal lattice PCF was designed for this purpose with the silica material, and large size outer diameter is chosen to increase the confinement [157]. Additionally, M. Samiul Habib et al., introduced a polarization maintaining spiral PCF having material SF57 with defects that offer high birefringence of 0.09 at 1.55 μm and Nonlinear coefficient of $7326 \text{ W}^{-1} \text{ km}^{-1}$ and $3919 \text{ W}^{-1} \text{ km}^{-1}$ at 700 nm and 1050 nm. This kind of fiber majorly contributes to SCG [158]. Xu et al. proposed a silica square lattice PCF is having two different size of air holes, which realizes the dispersion low as ± 12.6 ps $\text{km}^{-1} \text{ nm}^{-1}$, the birefringence of the order of 2.1×10^{-3} and the nonlinearity coefficient is about $28 \text{ W}^{-1} \text{ km}^{-1}$. This proposed PCF can have wide applications in Raman amplifier, wavelength converter and SCG [159].

Furthermore, the multifarious researches were done in **2014** by varying fiber parameters as to make the all-optical signal systems more efficient. Jianfei Liao et al., have proposed a silica slot core with square lattice of circular air holes and due to the small mode area, high nonlinear coefficient of $3.5739 \times 10^4 \text{ W}^{-1} \text{ km}^{-1}$ and birefringence of 0.5015 is achieved in this slot waveguide [160]. Xuyou Li achieved the higher nonlinear coefficient in the same year, that is, $33.2 \text{ W}^{-1} \cdot \text{km}^{-1}$ at 1.55 μm in the silica hexagonal PCF. Additionally, nearly zero ultra-flattened dispersion of 2.3 ps/nm \cdot km with a dispersion variation of 0.2 ps/nm \cdot km over the C+L+U wavelength bands and

dispersion slope of 2.2×10^{-3} ps/nm² was also achieved [161]. Jianfei Liao et al., have worked on a highly nonlinear fused silicon PCF with 6 spiral arms inducing high nonlinear coefficients greater than $224 \text{ W}^{-1}\text{m}^{-1}$ in quasi-TE mode and $226 \text{ W}^{-1}\text{m}^{-1}$ in quasi-TM mode at $1.55 \mu\text{m}$. Also ultra flattened dispersion of $0.91 \text{ ps}/(\text{nm}\cdot\text{km})$ in quasi-TE mode and $1.33 \text{ ps}/(\text{nm}\cdot\text{km})$ in quasi-TM mode is achieved over 150-nm , and two near-zero dispersion slopes of $-1.25 \times 10^{-3} \text{ ps}/(\text{nm}^2\cdot\text{km})$ in quasi-TE mode and $-4.82 \times 10^{-3} \text{ ps}/(\text{nm}^2\cdot\text{km})$ in quasi-TM mode at $1.55 \mu\text{m}$ is also attained. Achieving these parameters make the PCF very beneficial for all-optical signal processing applications [14]. Jin Hou et al. proposed a silica hexagonal PCF with still air holes by rotations of inner air-hole rings around the fiber core. This is inducing normal UFD PCF, and its corresponding dispersion $-21.1 \pm 0.7 \text{ ps}/\text{km}\cdot\text{nm}$ over $1.5\text{--}2.0 \mu\text{m}$ and anomalous corresponding dispersion variations are $-11.1 \pm 0.8 \text{ ps}/\text{km}\cdot\text{nm}$ over $1.25\text{--}1.65 \mu\text{m}$ [162]. A. Sonne et al., proposed a rectangular lattice PCF with small elliptical air holes in the core, obtaining high birefringence of 5.16×10^{-2} with low confinement loss $0.003 \text{ dB}/\text{km}$ over $1\text{--}1.76 \mu\text{m}$ [163]. The study on PCF characteristics continued with Fei Yu, et al., who proposed a silicon PCF with ellipse–rhombus air core achieving birefringence of the order of 10^{-3} and nonlinear coefficient of $0.018 \text{ W}^{-1}\text{m}^{-1}$. This PCF has mode area less than $8 \mu\text{m}^2$ due to which the fiber has low loss [164]. M. Samiul Habib et al., have proposed a silica hexagonal lattice SPSM DCF obtaining negative dispersion coefficient of $-712 \text{ ps}/(\text{nm km})$ and RDS of about 0.0036 nm^{-1} at $1.55 \mu\text{m}$. Also, the high birefringence of the order 2.11×10^{-2} with nonlinear coefficient about $57.57 \text{ W}^{-1} \text{ km}^{-1}$ at $1.55 \mu\text{m}$ is achieved. The defects in the center core region by omitting two air-holes were brought to increase birefringence. Such PCF structures are promising to compensate dispersion in high-bit-rate transmission network and for implement photonic sensors [165]. Md. Selim Habib et. al, have designed a silica octagonal-lattice PCF having five rings where air holes in first and second rings are kept greater than the other air holes to attain better dispersion showing negative dispersion over -134 to $-385 \text{ ps}/(\text{nm}\cdot\text{km})$ at E and U bands and a birefringence in the order of 2.13×10^{-2} at $1.55 \mu\text{m}$ [166]. Rui Hao et al., have proposed a silica Squeezed ortho-hexagonal PCF having four rings with the birefringence of 1.362×10^{-2} at $1.55 \mu\text{m}$ and is observed to be suitable for all optical signals systems [167].

Additionally, in **2015**, nonlinear coefficient of $65 \text{ W}^{-1}\text{km}^{-1}$ was achieved by G. Dhanu Krishna, et al.,. In addition to that, with air hole sizes of $d/\Lambda=0.5, 0.6$ and $0.7 \mu\text{m}$, the confinement losses of $1.2022 \times 10^{-2} \text{ dB/km}$, $7.7043 \times 10^{-6} \text{ dB/km}$ and $6.90186 \times 10^{-7} \text{ dB/km}$ are achieved. Also, the flattened dispersion of $55.27 \text{ ps}/(\text{nm}\cdot\text{km})$ over $1.3 \mu\text{m} - 1.7 \mu\text{m}$ is achieved in a silica PCF having octagonal lattice [168]. Xuyou Li designed a pentagonal PCF achieving a high birefringence of 1.67×10^{-2} and 1.75×10^{-2} at $1.55 \mu\text{m}$ and large negative dispersion of $-611.9 \text{ ps}/(\text{nm}\cdot\text{km})$ over $1460\text{--}1625 \text{ nm}$ and $-474 \text{ ps}/(\text{nm}\cdot\text{km})$ over $1425\text{--}1675 \text{ nm}$ by variation in the fiber parameters [102]. Moreover, in this year, Tianyu Yang et al., proposed a triangular silica PCF that is having the eccentric shape of the core. PCF design can realize high birefringence up to 10^{-2} , the high nonlinearity of $50 \text{ W}^{-1}\cdot\text{km}^{-1}$ and $68 \text{ W}^{-1}\cdot\text{km}^{-1}$ in X and Y polarizations mode and low confinement loss are less than 10^{-3}dB/km at a $1.55 \mu\text{m}$ wavelength. This triangular PCF has wide applications in polarization maintaining transmission systems, SCG for frequency metrology and optical fiber sensing [53]. S. REVATHI et al. proposed a Soft glass spiral PCF has five circular air holes in each spiral arm and an elliptical air hole in the center attaining high birefringence in the order of 10^{-2} , the high nonlinearity of $5828 \text{ W}^{-1}\cdot\text{km}^{-1}$ and high negative dispersion of $-1546.6 \text{ ps}/(\text{nm}\cdot\text{km})$ at $0.850 \mu\text{m}$. Due to the optimized results of this fiber, it plays a big role in nonlinear device applications [169]. Jianfei Liao et al., proposed slot silicon micro fiber having high birefringence of up to the order of 10^{-1} at 1.4 to $1.7 \mu\text{m}$, nonlinear coefficients of quasi-TE mode and quasi-TM mode at $1.55 \mu\text{m}$ are as high as $969.58 \text{ W}^{-1}\cdot\text{m}^{-1}$ and $156.74 \text{ W}^{-1}\cdot\text{m}^{-1}$ and by modifying the slot size, dispersion slope value can be reduced from $1.2358 \times 10^3 \text{ ps}/(\text{nm} \cdot \text{km})$ to $0 \text{ ps}/(\text{nm} \cdot \text{km})$. The excellent results of this fiber can be utilized in nonlinear signal processing applications of polarization maintaining systems [15]. Guangyu Jiang et al., designed a silica core rectangular-hole PCF having birefringence reaching the order of 10^{-3} that helps in bringing high precision in the optical system applications [170]. Jianfei Liao et al., proposed a nanoscale slot core with a high birefringence of 0.5015 and nonlinear coefficient of $3.5739 \times 10^4 \text{ W}^{-1}\cdot\text{km}^{-1}$ for the quasi-TM mode where nonlinear values increase when the slot width increases from 300 nm to 350 nm . This PCF is a good candidate for all-optical signal processing [160]. The studies have been in continuation and PCF have been a priority for achieving various characteristics as to make the transmission system soft and efficient over a long distance.

In **2016**, Md Asaduzzaman Shobug et al., proposed a silica Hexagonal PCF with five air hole rings achieving a nonlinearity of $12.15 \text{ W}^{-1}\text{km}^{-1}$, flattened dispersion of $0\pm 1 \text{ ps}/(\text{nm}\cdot\text{km})$, and confinement loss less than 10^{-2} dB/km at $1.55 \mu\text{m}$. The diameter of the first and second ring is kept low for obtaining a proper dispersion, and the size of the outer two rings are kept large for better confinement [172]. Russel Reza Mahmud et. al, proposed a SiO_2 (Silica) PCF with rectangular lattice having the structural parameters variation up to $+0.02 \mu\text{m}$ for inducing negative dispersion of $-650 \text{ ps}/(\text{nm}\cdot\text{km})$ within wavelength range of $1.46\text{-}1.63 \mu\text{m}$ and another silicate soft glass (SF57) having $-693 \text{ ps}/(\text{nm}\cdot\text{km})$ dispersion within wavelength range of $1.45\text{-}1.68 \mu\text{m}$ [173]. Furthermore, Md. Imran Hasan et al., designed a soft glass equiangular spiral PCF inducing a negative dispersion of $-526.99 \text{ ps}/\text{nm}/\text{km}$, having low dispersion variation of $3.70 \text{ ps}/\text{nm}/\text{km}$ over 1.05 to $1.70 \mu\text{m}$. Also, the high birefringence of 2.26×10^{-2} at $1.55 \mu\text{m}$ is achieved. The size of air holes from inner to outermost is increased step by step in this fiber for ensuring good confinement [174]. Moreover, Jui-Ming Hsu designed a hexagonal DCF that indicates an effective dispersion within $\pm 0.64 \text{ ps}/\text{nm}/\text{km}$ over a 226 nm band with the broad range of 1338 to 1564 nm and so can compensate for 40 Gbps signal [175]. Hao Rui has proposed an SF6 PCF with a squeezed core showing high birefringence of 1.544×10^{-2} and is suitable for optical parametric amplification and all-optical signal processing. The hole spacing has been varied for achieving high birefringence [176]. High Birefringence make the fiber insensitive to temperature, also due to the high need of low dispersion, the variations have been made in the PCFs to achieve it.

In **2017**, Shabbir Chowdhury et al. proposed a high nonlinear hexagonal fused silica PCF has high nonlinear coefficient $47.801 \text{ W}^{-1}\text{km}^{-1}$ for the S+C+L+U band. This study has also induced high birefringence of 0.0310 and large negative dispersion of $-529.18 \text{ ps}/\text{nm}\cdot\text{km}$ at $1.55 \mu\text{m}$. Achieving these parameters will be helpful in medical, nonlinear and sensing application. Two elliptical air holes in the center are included that help to increase the birefringence and also to increase the nonlinearity that reduces bending loss [177]. Furthermore, Jiayuan Li et al. designed an Aluminum Nitride Slot Waveguides that is used for investigating phase matching conditions in FWM process and induces dispersion within -13 and $+11 \text{ ps}/(\text{nm}\cdot\text{km})$ over 2000-nm band [178]. Moutusi De et al., have proposed a decagonal PCF achieving birefringence of the order of 10^{-2} and low confinement loss of the order of 10^{-2} dB/m

at 1.55 μm . They used couple of decagonal shaped circular air holes in the outer cladding region with two large circular and four elliptically shaped air holes in the inner cladding region to achieve targeted high birefringence. This D-PCF can be efficiently utilized in nonlinear applications, laser and sensors technology [179]. Chandru Selva Kumar et al. studied a circular and octagonal core PCF that realizes the characteristics such as dispersion of +77.55 ps/(nm km) and +77.34 ps/(nm km) and nonlinearity of the order of 4506 $\text{W}^{-1} \text{ km}^{-1}$ and 4498 $\text{W}^{-1} \text{ km}^{-1}$. The effective indices have been varied to control the dispersion. This PCF can hugely contribute to speed and capacity of optical communications [180].

3.3 Summary

Through over all analysis of the researchers, which has been done in between the year 2000 to 2017, on the generation of characteristics like Ultra flattened dispersion, birefringence, and nonlinearity through PCF or slotted PCF. It can be said that slotted PCF is being a better option than PCF in the enhancement of such characteristics, as it provides better confinement of signal in the core, low losses, and higher nonlinearity. The better and undistorted transmission of a signal over long distances can be ensured through slotted PCF. Though the studies on slotted PCF have been able to achieve the highest nonlinearity of 969.58 $\text{W}^{-1} \cdot \text{m}^{-1}$ and dispersion slope of $1.2358 \times 10^3 \text{ps}/(\text{nm} \cdot \text{km})$ to 0 ps/(nm · km), by varying the slotted PCF parameters, better results can be achieved. Also, by attaining the large negative dispersion and higher nonlinearity, length of the fiber can be reduced that will be profitable for short distance optical devices and in the cost effective deployment of fibers. Hence, it can be concluded from the yet achieved results that evolution of slotted PCF has been proved to be beneficial for the optical signal transmission systems and applications related to it.

Chapter 4: Numerical Investigation of High Index Elliptical Spiral Photonic Crystal Fiber

In the preceding chapters, some fundamental properties of MOFs and the past research in the field of PCFs were described. It was discussed that properties of fibers could be controlled by varying the fiber parameters. Through the facility of design flexibility feature, fiber properties can be mold according to the desired applications. In this chapter, an elliptical spiral structure is designed to obtain large nonlinearity, high birefringence with flat negative dispersion in telecom wavelength band to address numerous applications in the optical domain.

4.1 Introduction

Presently, index guiding PCFs have been comprehensively investigated because of its effective optical fiber characteristics in different fields of optical systems that seem to be inconceivable in conventional SMF. Index-guiding PCFs, also known as holey fibers or MOFs, consist of a high index solid core region enclosed by array of air holes in the low index cladding region. By tailoring the hole pitch Λ , the relative hole diameter ratio d/Λ in different rings and the refractive index of the core, the dispersion, birefringence, and nonlinear properties can be controlled.

In long haul high bit-rate optical communication systems, the dispersion is a critical aspect that has a great impact on bandwidth. Conventional optical fibers have non zero dispersion values that limit high bit-rate transmission. So dispersion controlling strategy should be present to neutralize the dispersion effect over long haul communications systems [153]. In recent years, PCFs has emerged as a dominant method for information transmission because of flexibility in design. The dispersion of PCFs can be regulated by optimizing the fiber parameters like air hole diameters, pitch size, etc. [162].

In order to attain a stable undistorted pulse, Ultra flattened dispersion is required. Additionally, for applications like WDM [181], compensation of dispersion over wide wavelength bands, propagation of ultrashort solitons, controlling of birefringence and SCG, the ultra flattened dispersion is required [182].

The invention of HNPCF has gained a huge attention of the world because of its ultrahigh nonlinearity and compatibility with the standard SMFs. Its various applications have also been realized keeping in consideration of its ability to guide a strongly confined light through a fiber. The applications are slow/fast light, pulse compression, wavelength conversion, SCG and all optical amplification[15,183]. The high fiber nonlinearity, long interaction length, and low loss are the basic characteristics that are needed for realizing nonlinear effects in the fiber. Utilization of HNPCF can be considered as beneficial due to the reason that it needs less power and less length [73]. Moreover, dispersion property needs to be controlled as to improve the nonlinear optical processes.

High birefringence is another important parameter of PCFs, which can be achieved by introducing asymmetry in PCF design such as, using elliptical air hole inside the fiber core [184] and using elliptical air holes instead of circular air hole in the cladding [185]. High birefringent PCFs maintain the SOP which proves useful in PMD compensation. Furthermore, birefringent PCFs have a variety of possible applications in optical sensor design, electro-optical modulation, and signal processing systems [186].

SCG [187] is most demanding and challenging field of nonlinear photonics. The emerging applications of broadband continuum light sources often entail coherence property of distributed radiation. SCG in NDR with high nonlinearity is an applicable solution to that necessity [188]. Thus we require a material that can provide large nonlinearity with negative flattened dispersion. In recent researches, it is found that non-silica soft glasses have this capability. One of the important reason for research in non-silica glasses is that they exhibit large nonlinearity with low fabrication temperature [189]. Lead silicate glass SF57 has a high concentration of lead that results in high refractive index value 1.80 at 1.55 μm wavelength. Sellmeier equation of SF57 is given by

$$n_{SF57}^2 = A_0 + A_1\lambda^2 + \frac{A_2}{\lambda^2} + \frac{A_3}{\lambda^4} + \frac{A_4}{\lambda^6} + \frac{A_5}{\lambda^8} \quad (4.1)$$

where, $A_0=3.24748$, $A_1=-0.00954782 \mu\text{m}^{-2}$, $A_2=0.0493686 \mu\text{m}^2$, $A_3=0.00294294 \mu\text{m}^4$, $A_4=-1.48144 \times 10^{-4} \mu\text{m}^6$, $A_5=2.78427 \times 10^{-5} \mu\text{m}^8$ [190].

Moreover, SF57 has a high nonlinear refractive value of $4.1 \times 10^{-19} \text{ m}^2/\text{w}$ [191], which is larger than silica. Due to the low softening temperature 519°C for SF57, extrusion of MOF preform from bulk SF57 glass is feasible.

A lot of researches has been done over dispersion, nonlinear coefficient, and birefringence. Franco *et al.* in [192] proposed micro structure optical fiber having a dispersion of $-179 \text{ ps}/(\text{nm.km})$ but only for the wavelength range of $1.48 - 1.675 \mu\text{m}$ band, nonlinear coefficient and birefringence is not discussed here. The proposed fiber in [193] by Silva *et al.* have a Ge-doped core PCF which obtained $-212 \text{ ps}/(\text{nm.km})$ dispersion with large deviation of $12 \text{ ps}/\text{nm.km}$ between $1.35 \mu\text{m}$ to $1.70 \mu\text{m}$ wavelength range, but there is no mention of birefringence and nonlinearity. PCF discussed in [194] has an equiangular spiral structure with a negative dispersion of $-227 \text{ ps}/(\text{nm.km})$, but has a large variation of $11 \text{ ps}/\text{nm.km}$ over E+S+C+L+U wavelength bands and nonlinearity is not discussed in that structure. Habib proposed a PCF structure [101], which has a flat dispersion of $-138 \text{ ps}/\text{nm.km}$ with a deviation of $12 \text{ ps}/\text{nm.km}$ in S to L wavelength band and nonlinearity of only $33.6 \text{ W}^{-1}\text{km}^{-1}$. PCF proposed by Hasan *et al.* in [195] has a dispersion of $-562.52 \text{ ps}/\text{nm.km}$ but only for the wavelength range from $1.46 \mu\text{m}$ to $1.70 \mu\text{m}$ and has achieved nonlinearity of $48.70 \text{ W}^{-1}\text{km}^{-1}$ that is quite low. Although, the PCF proposed in [196] has dispersion values of $-608.93 \text{ ps}/(\text{nm.km})$ over $1.46 \mu\text{m}$ to $1.625 \mu\text{m}$ wavelength range, but the negative dispersion is achieved for short wavelength band, and nonlinearity of PCF is not discussed in PCF design. In the PCF designs mentioned above, the dispersion, birefringence, and nonlinearity were not achieved simultaneously.

In this chapter, the proposed design is simultaneously achieving a negative flat dispersion with high nonlinearity and large birefringence. Due to negative flattened dispersion with very little deviation in dispersion, this PCF can be used in RDCF. Other applications are polarization maintaining and nonlinear signal processing. The effect of parametric variation in design on optical properties is also investigated and found that the design has an extremely low variation. For accurate analysis of various parameters, full vector FEM is applied.

4.2 Structure and Design of Elliptical Spiral PCF

The schematic view of a cross-section of elliptical spiral PCF is presented in the Fig.4.1. The host material is SF57 with spiral lattice in cladding that has ten arms and

each having five air holes. The air hole arranged in an arm is at an angular increment of θ than previous one. The diameter of air holes is enlarged step by step for good confinement of modes [174]. Elliptical spiral PCF structure has minor semi-axis as A and major semi-axis as B . Air holes in the innermost ring are elliptical with major semi-axis a and minor semi-axis b . Other rings have circular air holes which are having a diameter of D_1, D_2, D_3, D_4 as we move from 2nd to 5th ring.

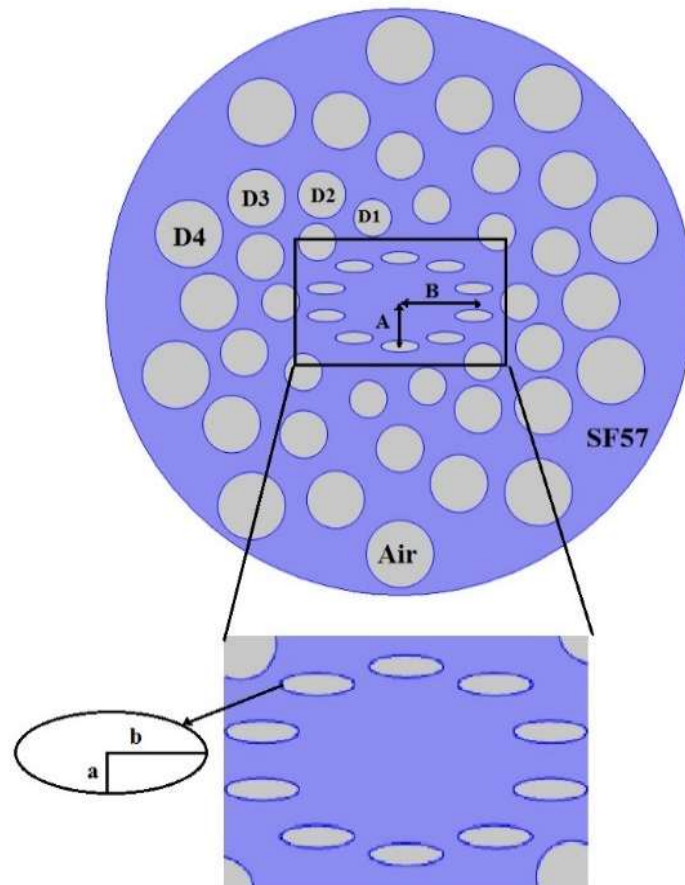


Fig. 4.1 Cross sectional view of elliptical spiral PCF

In comparison to conventional fiber, the elliptical spiral PCF have great flexibility in modifying birefringence, nonlinearity and dispersion and other characteristics. This elliptical spiral structure with elliptical air holes in innermost ring introduces more asymmetry between the two axes and hence large birefringence is achieved. Chromatic dispersion is also get flattened for large negative value. Because of spiral structure design, light is strongly confined to the low effective mode area that results in high nonlinearity.

Modal field distribution for each arrangement of fiber parameters relies on the constructive interference of the wave after multiple scattering from air holes. Variation in the phase of light at any point depends on the component of the wave vector by an alteration in hole positions. So even slight variations in holes position generate large phase deviations.

The modal distribution of fundamental modes of fiber at 1.55 μm is shown in fig. 4.2 with optimum fiber parameters as presented in table 4.1.

Table 4.1: Designing parameters of PCF

Material	Ellipticity of Structure		Angle between two arm	First ring elliptical air holes		Diameter of Air Holes (Second, Third, Fourth and Fifth Rings)			
	Semi Minor Axis 'A'	Semi Major Axis 'B'		Semi Minor Axis 'a'	Semi Major Axis 'b'	D ₁	D ₂	D ₃	D ₄
SF57	800 nm	1400 nm	36°	108.8 nm	340 nm	680 nm	860 nm	1040 nm	1220 nm

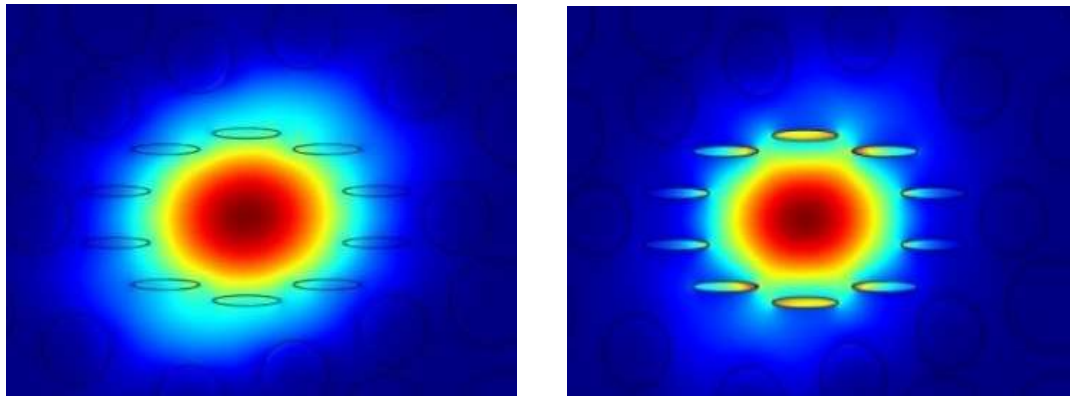


Fig.4.2 Fundamental modal field distribution for X and Y polarization

It can be observed from the structure that the effective refractive index of x-polarized mode is larger than the effective refractive index of y-polarized mode. This is because the air holes are dispersed more sparsely along x direction than along y direction. Effective refractive indices of fundamental modes are found to be 1.719 and

1.702. Hence, the light travelling speed along the x -axis mode is slower compared to the y -axis mode because of the higher effective refractive index of the x -axis mode. In this way, the x - polarized mode and the y -polarized mode act as slow axis mode and fast axis mode, respectively [195].

The role of the spiral structure with an elliptical air hole in the first ring of the proposed PCF is to flatten the chromatic dispersion and to enhance the value of birefringence in the order of 10^{-2} . As we increase ellipticity ratio, more flattened negative dispersion with large nonlinearity is achieved. But for the same structure, slightly low birefringence is attained. Hence, it can be seen that trade-off is occurring between flattened dispersion, large nonlinearity, and birefringence. So a optimum point is chosen where all the parameters have significant values with large flat negative dispersion for broad wavelength range.

4.3 Research Outcomes and Discussion

The numerical method, which is used to analyze the proposed elliptical spiral PCF, is full vector FEM that is more reliable and flexible than other known techniques. The fundamental equation for the FEM analysis, through Maxwell's equations, is expressed as,

$$\nabla \times ([\mu_r]^{-1} \nabla \times E) - k_0^2 [\epsilon_r] E = 0 \quad (4.2)$$

Here, $[\epsilon_r]$ and $[\mu_r]$ denotes the relative dielectric permittivity and magnetic permeability, E is the electric field, and k_0 is the free-space wave number, respectively.

The chromatic dispersion, birefringence, and nonlinearity coefficient can be obtained after the attainment of the modal effective index n_{eff} through solving an eigenvalue problem drawn from the Maxwell equations utilizing the FEM.

The PCFs have many important properties that allow them to be used as a fine transmission medium for small and long distances. In the long-haul optical communication system, the traditional optical fiber has non zero dispersion. In WDM system, dispersion in SMFs broadens the optical pulse that results in severe limitations in the high bit-rate transmissions. So to compensate this induced positive dispersion, a DCF must be introduced in the communication system that is having a large negative dispersion [197].

Total chromatic dispersion of fiber consists of material dispersion and waveguide dispersion, i.e., $D(\lambda) = D_w(\lambda) + D_m(\lambda)$ can be calculated as [174]

$$D(\lambda) = -\frac{\lambda}{c} \frac{d^2 \text{Re}[n_{eff}]}{d\lambda^2} \quad (4.3)$$

where $\text{Re}[n_{eff}]$ denotes the real part of effective mode index of PCF. With the help of the Sellmeier equation, the material dispersion is included into the calculation. Hence, the $D(\lambda)$ in eqn. (4.3) corresponds to the total dispersion of the PCF. The FEM directly solve the wave equations to obtain optimum value of the effective mode index, n_{eff} .

Effect of ellipticity ratio on dispersion flatness with $D_1 = 680$ nm, $D_2 = 860$ nm, $D_3 = 1040$ nm, $D_4 = 1220$ nm is shown in fig.4.3. It can be observed that the dispersion becomes more flattened as the ellipticity ratio of inner ring holes increases from $a/b = 0.10$ to 0.32 . At $a/b = 0.32$ ratio of elliptical air holes, the flat negative dispersion is achieved. But, as a/b ratio is further increased, the dispersion values are decreasing with increasing wavelength and also dispersion flattening curve starts fluctuating.

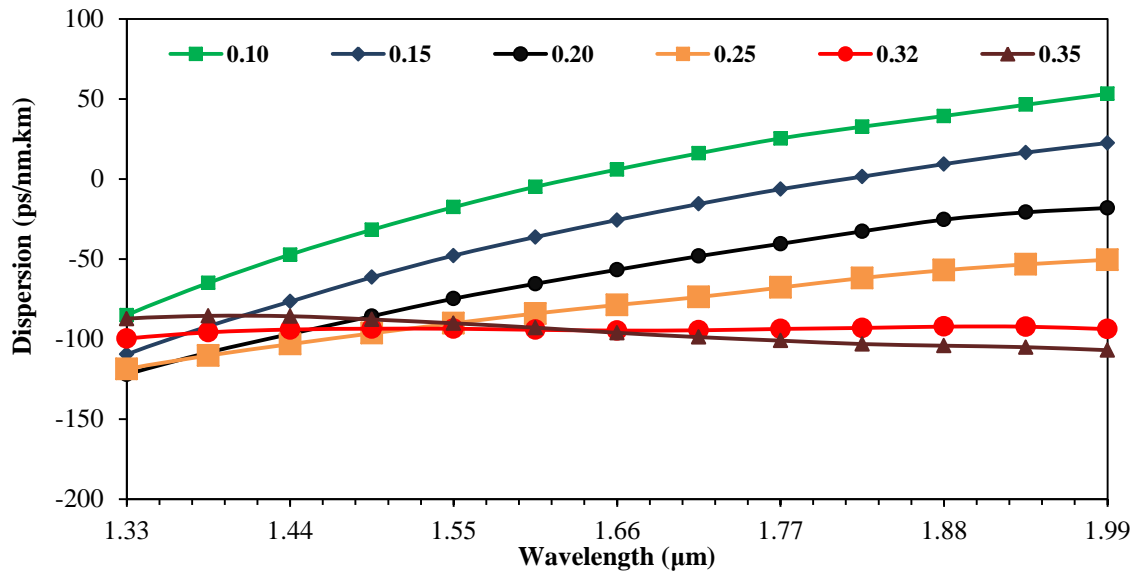


Fig. 4.3 Dispersion Vs. wavelength curve for different ellipticity ratio for wavelength range 1.33 μm -1.99 μm

The flattened part of a dispersion curve for 0.32 ellipticity ratio is shown in fig.4.4. It is observed that the proposed design has flat negative dispersion in a vast range of wavelength from 1.385 μm to 1.99 μm . The average dispersion is 93.80 ps/nm/km with a deviation of only ± 1.5 ps/nm/km.

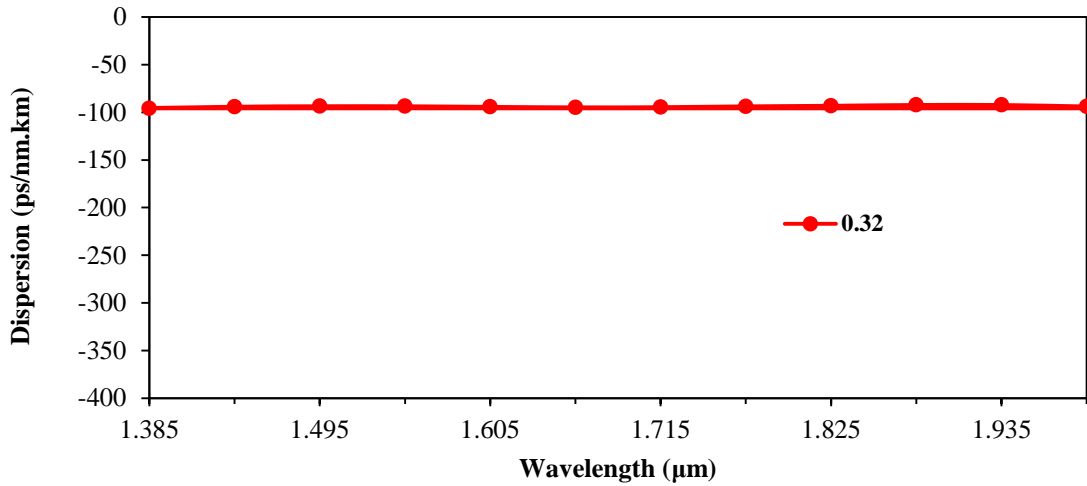


Fig.4.4 Flat dispersion curve for wavelength range of 1.385 μm-1.99 μm

The dispersion accuracy with global parameter variation of the designed PCF is carefully investigated. The variation of 1% in global fiber parameter of elliptical air holes has to be considered as it occurs unavoidably and so rough estimate of 2% accuracy is considered to ensure dispersion flatness [126,198,199]. The elliptical air hole size has a great effect on the flatness of dispersion curve.

As seen in Fig. 4.5, the ellipticity ratio is varied to $\pm 1\%$ and $\pm 2\%$ around the optimum value. It is evident from the figure that the global parameter variation for the proposed structure does not affect the average dispersion and dispersion variation much. But from the investigated results, it is found that the dispersion values and flatness is not varying significantly.

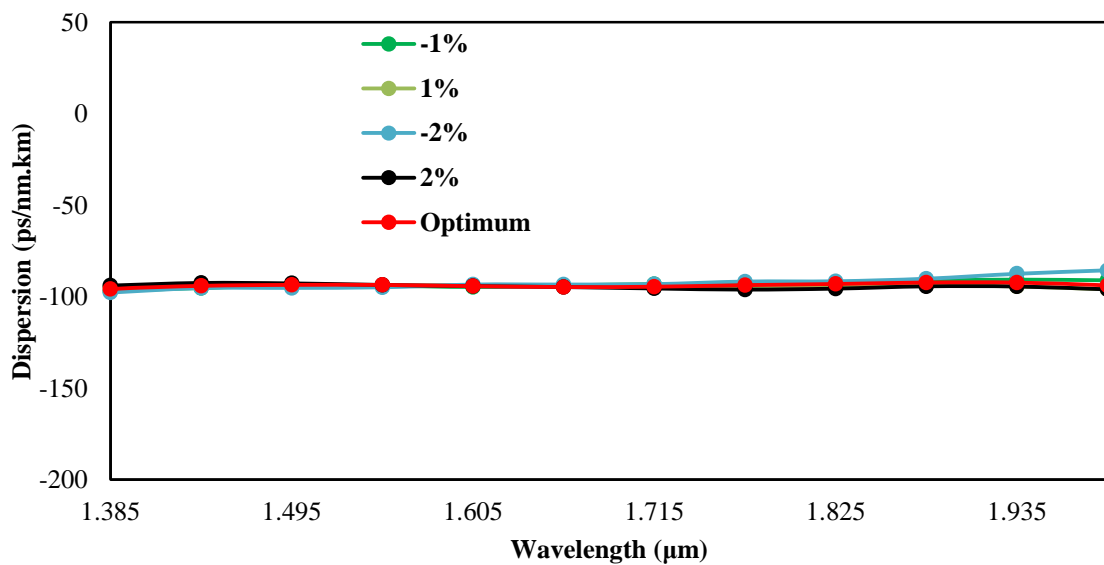


Fig.4.5 Dispersion variation for $\pm 1\%$ and $\pm 2\%$ variation of ellipticity ratio around optimum value.

Nonlinearity is another crucial characteristic of PCFs. Spiral shape structure, due to its compactness, can achieve strong light confinement with small effective mode area that is beneficial in attaining large nonlinearity. Nonlinear coefficient γ of designed fiber can be determined by the following equation

$$\gamma = \frac{2\pi n_2}{\lambda A_{eff}} \quad (4.4)$$

where, n_2 is nonlinear refractive index of material used, λ is wavelength of operation. Here, the nonlinear refractive index of SF57 used is $4.1 \times 10^{-19} \text{ m}^2/\text{W}$ [186].

The fiber mode efficiently covers the effective mode area, which is a numerical measure, in transverse dimensions. The effective area is a very important parameter as it is related to the nonlinearity and is crucial for studying optical nonlinearities in the PCF. Nonlinearity mainly depends on the power density inside the device and so higher the effective area; lower will be the nonlinearities for a fixed power. The effective mode area (A_{eff}) is given by

$$A_{eff} = \frac{(\int_{-\infty}^{\infty} \int_{-\infty}^{\infty} |E(x,y)|^2 dx dy)^2}{(\int_{-\infty}^{\infty} \int_{-\infty}^{\infty} |E(x,y)|^4 dx dy)} \quad (4.5)$$

here, E is the electric field confined in the core of the PCF. The effective area of PCF depends on the confinement of electric field inside the core of the PCF. A small value of effective area leads to large nonlinearity that would have many applications.

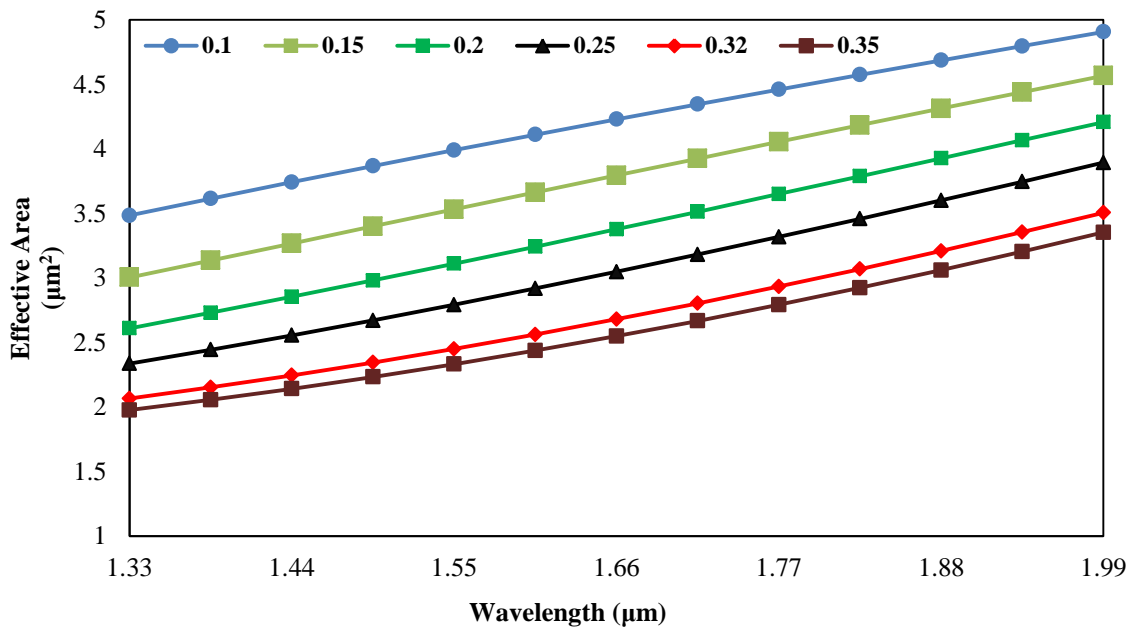


Fig.4.6 Effective area Vs. wavelength curves for various ellipticity ratios

The effect of the wavelength of operation on the effective area of PCF can be seen from Fig. 4.6. It can be observed that effective mode area is increasing with wavelength. This is because, at short wavelength, mode fields are strongly confined in the core region that results in the smaller effective area. Hence the nonlinear coefficient will correspondingly decrease with increase in wavelength. For optimized PCF parameters, at 1.55 μm wavelength, an effective area of $2.45 \mu\text{m}^2$ is obtained.

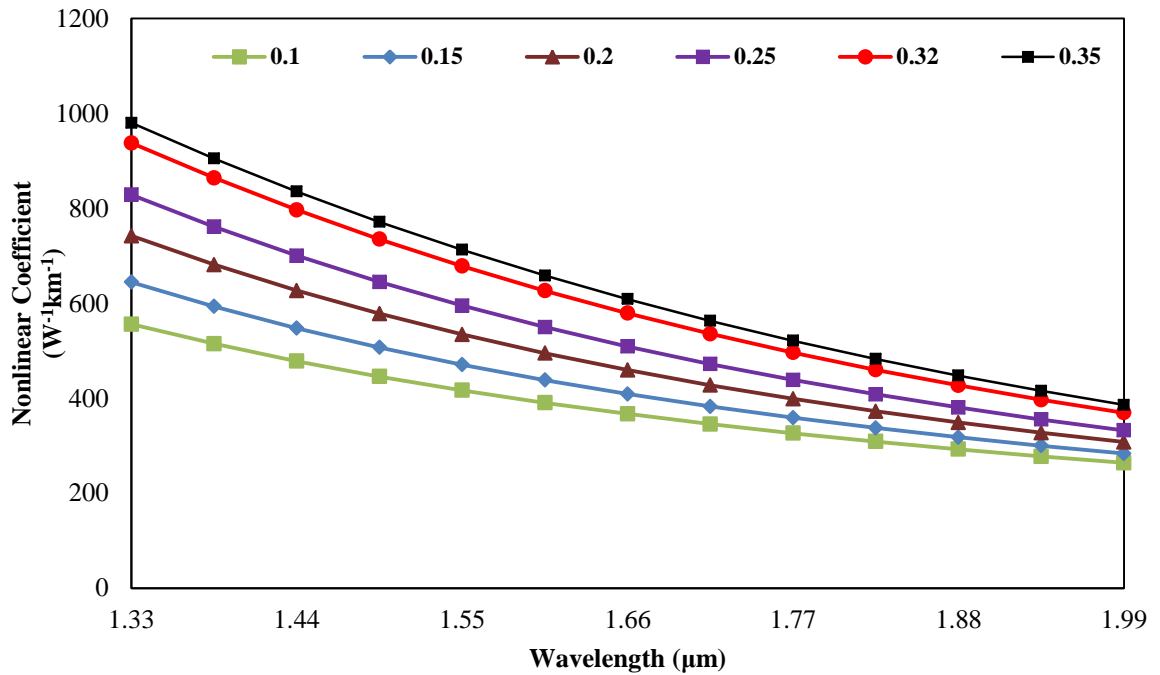


Fig.4.7 Nonlinearity of PCF for wavelength range 1.33 μm -1.99 μm

Effect of ellipticity ratio of elliptical air holes on nonlinearity can be observed from fig.4.7. As ellipticity ratio increases the size of elliptical air holes increase, which leads to better confinement of electric field in the core of the PCF, this, in turn, reduces the effective area of the core. Due to decrease in effective area of the core, the value of nonlinearity coefficient increases. Smaller effective area makes the fiber remain insensitive to the high bending loss [200]. At 1.55 μm wavelength, for optimized parameters nonlinear coefficient value of $763.485 \text{ W}^{-1}\text{km}^{-1}$ is achieved.

HNLF with flattened dispersion over a broad wavelength range has bragged significant interest in current years and would be potential candidates for application in the high-capacity all-optical signal processing and development of devices such as wavelength converters, parametric amplifiers, supercontinuum sources, and optical switches.

Birefringence B is one of the significant characteristics of PCFs that can be determined by taking the difference of effective mode index of two fundamental modes and the following expression measures it

$$B = \frac{|\beta_x - \beta_y|}{k_0} = |n_x - n_y| \quad (4.6)$$

where k_0 refers to the wave number and $k_0 = 2\pi/\lambda$, β_x and β_y are propagation constant of two orthogonally polarized modes. n_x and n_y indicates the refractive index of x and y polarised modes, respectively.

The elliptical air hole around the fiber core generates more asymmetry that would lead to high index difference between the two orthogonal modes. Due to which very high birefringence is obtained.

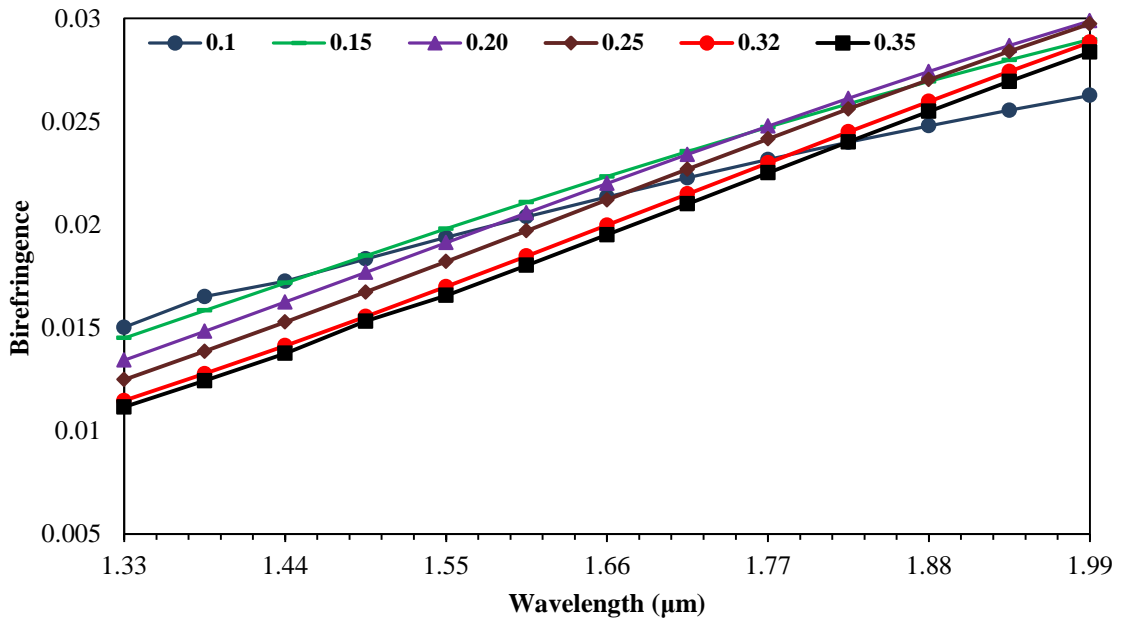


Fig.4.8 Birefringence Vs wavelength for different ellipticity ratios

Fig.4.8 depicts that as the wavelength of operation increases, the birefringence of PCF also increases. The birefringence value of designed PCF for 0.32 ellipticity ratio is 0.017 at 1.55 μm wavelength. This large birefringence is achieved due to the elliptical spiral structure with elliptical air holes in the first ring, as this generates more asymmetry in the structure. Beat length of the proposed design at 1.55 μm is 91.2 μm which is much lesser compared to conventional fiber. As seen in fig.4.8, by decreasing the ellipticity ratio, higher birefringence can be achieved in the proposed

structure. But, for lower values of ellipticity ratio, the flattened dispersion curve cannot be achieved and also nonlinearity coefficient of PCF decreases.

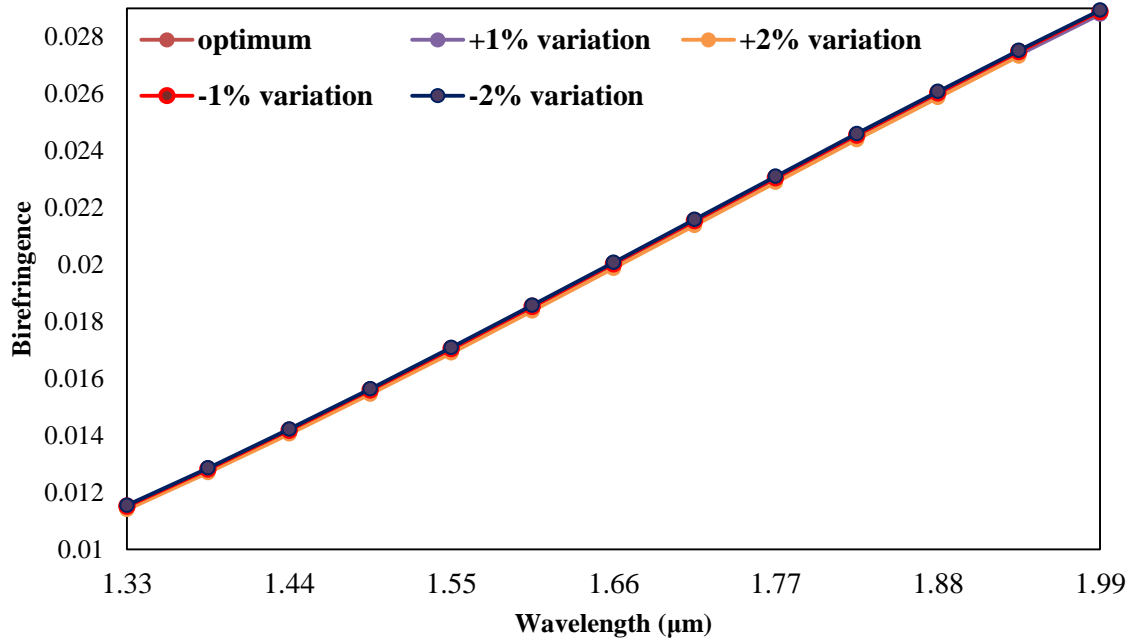


Fig.4.9 Birefringence variation for $\pm 1\%$ and $\pm 2\%$ variation of ellipticity ratio around optimum value.

To ensure the robustness of the design, birefringence sensitivity up to $\pm 2\%$ variation in optimum parameter is observed. In fig. 4.9, it is observed that there is no significant variation in birefringence for different parametric variation around optimum value. Insignificant variations in birefringence, validates negligible variation in beat length. Thus the proposed fiber with large birefringence has many applications in transmission systems like minimizing the PMD, in loop mirrors for sensing applications, etc. [201].

The fabrication process is one of the most crucial process of the PCF designing. Although, the proposed fiber design is looking to be quite difficult for fabrication, but it is possible to fabricate the proposed design without any problem because of the swift progress of fabrication technologies. During the fabrication process, the elliptical air holes are susceptible to losing their ellipticity and may acquire circular shape due to surface tension. But advancement in fabrication process made it possible to design elliptically shaped air holes in PCF [150]. Die cast method [93] given by Guiyao *et al.* is quite useful in the fabrication of asymmetric core PCFs and asymmetric air holes.

Additionally, silicon is embedded as a background material in the PCF design, instead of SF57. The fiber geometrical design parameters are kept same as the previous design as only the material is changed. In this case, nonlinearity is drastically enhanced and has the value of $14027 \text{ W}^{-1}\text{km}^{-1}$ at $1.55 \mu\text{m}$ wavelength, and flat positive dispersion is achieved. But, less birefringence of the order of 10^{-3} is achieved than the previous result. In the next chapter, new PCF design is discussed, using the silicon material, that has provided better results as compared to results of this chapter.

4.4 Elliptical Spiral PCF as Residual Dispersion Compensation Fiber

In the long haul transmission data systems, it is requisite to have a flattened dispersion or near to zero dispersion. The reason behind this is that intrinsic chromatic dispersion may induce nonlinear interactions, which leads to cross talks, information loss and disruptive transmission data rates. The standard mode fiber generates a dispersion of 10 to 22 ps/(nm.km) in the transmission [192]. This intrinsic dispersion can be compensated by adopting a dispersion compensating technique that generates a large negative dispersion, which has a capability of canceling out the intrinsic positive dispersion generated by the SMF. Additionally, after linking the SMF and DCF, dispersion compensation process can be carried out. However, even after compensating the dispersion to a certain limit, there is some non-zero dispersion always left, due to the presence of long transmission system and deformities present in it, which is called the residual dispersion. Compensation of this remaining dispersion would be called RDCF, which will need extra efforts towards compensating [202].

In addition to that, the RDCF would need very large negative dispersion that can be achieved by introducing a defect in the PCF core geometry or by bringing variation in the fiber cladding parameters [174]. As it is very well known that variation in cladding parameters or deformity in the fiber may increase losses in the transmission. To overcome this issue, the RDCF has to be as short as possible and to limit the length of the fiber; it is necessary to have a very large negative dispersion. For better values of RDCF, most of the focus has been given on hexagonal, orthogonal PCF, Equiangular spiral PCF as they provide better dispersion accuracy, good design flexibility, strong confinement and low losses [197]. Furthermore, the RDCF plays a big role in providing applications like long data transmissions, the design of sensors, SCG and fiber loop mirror [10].

4.5 Conclusion

In this study, an elliptical spiral soft-glass PCF design is proposed, and its optical characteristics are analyzed for a broad range of wavelength. It is found that elliptical spiral lattice PCF with an elliptical air hole in innermost ring has high negative flat dispersion, high nonlinearity and large birefringence in the communication band. By varying the ellipticity ratios, we have obtained optimum results that have -93.80 ps/nm/km average dispersion with a deviation of ± 1.5 ps/nm/km and nonlinearity coefficient of $763.485 \text{ W}^{-1}\text{km}^{-1}$. Birefringence of the order of 10^{-2} is also achieved in the proposed design. Due to negative flattened dispersion over a wide wavelength range, this PCF can be used in RDCF. This proposed design can also be used in PMF, parametric amplification, SCG, fiber sensor design, fiber loop mirror, etc.

4.6 Summary

In this chapter, high index guiding elliptical spiral PCF structure is studied. By optimizing the different geometrical parameters, proposed design has provided a large flattened negative dispersion with high nonlinearity and large birefringence. These attained results make the proposed design to be useful for many applications in the optical domain. Although the results obtained from this design are excellent but can be further improved by using different designs. In the coming chapter, a new design is discussed that will provide better results than the design described in this chapter.

Chapter 5 : Numerical Investigation of Low Index Slotted Spiral Silicon Photonic Crystal Fibers

In the last chapter, high index guiding PCF designs has been discussed that having high asymmetry, but it is found that this PCF designs are not able to achieve ultrahigh nonlinearity and large birefringence. For obtaining high nonlinearity, high birefringence and high negative dispersion in the fiber, a low index solid core PCF is introduced and discussed in this chapter. The work presented in this chapter shows how embedding a low index slot in the core of the fiber can be used to enhance optical characteristics at very large extent.

5.1 Introduction

In the past years, light propagation in the low index materials has become highly significant for various applications such as optical sensing, interaction with low index materials, nonlinear optics, optical modulators and switches, near-field optical microscopy and achieving high nonlinearity by having strong light confinement inside the core of the fiber[17].

The propagation of light in low index materials is prohibited in the conventional fiber structures based on TIR. Instead, external reflections from multiple dielectric layers or PCs [12] are mainly utilized. However, in these fiber structures, large dimensions are necessary for high reflections, but these structures are more sensitive to wavelength. One of the efficient fiber structure is the slot embedded PCF structure that has low index slot embedded in a high index material medium [16]. In comparison to the lossy modes in PBG fibers, the guided mode in low index solid core PCF structure is eigenmode, which does not depend on the resonance principles and so the fundamental mode is loss less and having very low sensitivity with wavelength. Moreover, this low index solid core PCF is well-suited with highly integrated photonics devices at nanometer size dimensions[17].

This low index slotted PCF structure works on the principle of operation that is based on the discontinuity of the electric field at the high index contrast interface[16,18]. One of the components of the electric field of the quasi-TE mode is perpendicular to the walls of the vertically aligned slot, showing high amplitude at the

low index slot due to the strong discontinuity at the walls. Additionally, the ratio of the electric field of both sides of the walls is equal to the square of the ratio of the refractive indices of both sides of the wall. The electric field within the slot is high when the slot dimensions are smaller than the field decay length from the interface. On the other hand, the magnetic field is incessant at the walls of the slot, and due to this the optical intensity in the slot is much higher than the high index region. In the case of quasi-TM mode, the major component of the electric field is parallel to the walls, and due to this, the effect of the presence of the slot is negligible[16,18]. The effective index of slot mode can be determined from the optical field decay rate in the cladding far away from the center of the slot fiber structure. With the assumption that power of the optical field decays exponentially from the center of the core[16].

Thus, propagation of light in the slotted PCF is not only confined to a low index material but it also has a much higher power intensity than that conceivable using conventional PC structures.

5.2 Material properties

Along with fiber structures, the properties of PCF are also dependent on the material. We choose the materials that are not only compatible with existing fiber structures, which are easily available and cost effective but also having a high nonlinear refractive index. [203] e.g., Silicon, Silica, Silicon nanocrystals. There are many applications of nonlinear photonic materials in the telecom industry that are used in various devices like switches, routers, wavelength converters, etc. Also, one more application is the optical logic gates that are designed using nonlinear Mach-Zehnder interferometers (MZI), which provide features such as scalability and flexibility [204].

5.2.1 Silicon

Silicon is one of the best-studied materials known to humanity and the most widely used in the semiconductor industry. Our knowledge of the properties of silicon has paved the way to the information technology revolution. The advances in the broad field of nanotechnology have shown that size reduction can overcome the limitations of bulk materials. Certain nonlinear properties of material Silicon are to be noted for its wide ranging applications in nonlinear photonics. The application of Silicon photonics near mid-infrared region draws the attention of most of the researchers.

Silicon photonics field is growing day-by-day and is becoming one of the most active areas of research with many useful applications like optical interconnects, nonlinear signal processing [205], biosensors[206]. The highly developed silicon-on-insulator (SOI) platform is the backbone of the progress in this area because of their strong mode confinement due to the large refractive index difference between the cladding and core of guide.

CMOS technology can be used to reduce the size of structures up to 10 nm at low cost [203,204]. Currently, with the progress in fabrication techniques, Silicon fibers which furnish a material compatibility with the traditional fiber structures, have gained a substantial attention. Silicon crystals, having band gap around 1.12 eV, become transparent in the wavelength region beyond 1.1 μm and exhibits optical properties that are required for a number of applications. The large refractive index of silicon provides better confinement of optical pulse to a submicron region using the SOI technology. Moreover, silicon has large third-order nonlinearity, as compared to silica, it provides 100 times higher Kerr coefficient and 1000 times higher Raman gain coefficient in the telecommunication band. The large non linearity index coupled with high optical confinement within SOI waveguides permits better nonlinear light matter interaction at the relatively small strength of signal inside a short SOI waveguide (<5cm long)[207]. Silicon is the basic material for the SOI platform. SOI is a manufacturing technique in which a thin layer of silicon on top of an insulating layer (generally made of SiO_2) resides on a silicon substrate. The functional optical elements are positioned in the thin top-silicon layer [208]. The better light confinement capability of silicon admits for ultra compact devices with a bent radius of the order of few micrometers, and functional waveguide elements of ten to a few hundred micrometers. Therefore, large-scale integration of many functional elements on a single chip is achievable [209].

Silicon is having a variety of nonlinearities [71,210,211], and they all are generated when the optical field interacts with electrons and phonons. In fact, it is the electric field of the optical wave that resonates with the electrons in the outer shells of the silicon atoms which causes polarization. Although a number of nonlinear effects are present in silicon that is not the reason why researchers are so much interested, instead of low cost and compatibility with VLSI technology, make it the material of more importance, and by having it we can have combined electronic as well as optical

integrated circuits (ICs) [208]. Suppose, in the conventional optical fiber if the material or refractive index of the core and cladding is same then the advanced application may not be able to be utilized. Also, the confinement loss is larger as pulse starts leaking out of the core because there is no confinement of pulse in the core due to the same refractive index. Hence, there has to be much difference in the refractive index of core and cladding, so the proper benefits of altered cladding can be used for applications like SCG and in understanding dispersion characteristics. The confinement loss can be controlled by varying the number of air holes on the cladding or increasing the size of air-holes.

5.2.2 Silicon nanocrystals

The limitations faced by the bulk of materials can be overcome by using nanocrystal materials. Silicon-based nanostructures hold a special place in the broad field of nanotechnology. Nanocrystal silicon has been proven a key material for silicon photonic applications in last few decades. As it provides low manufacturing cost and well-developed VLSI technology can provide integrated optical ICs [212]. The optical applications designed with bulk silicon can also be completed using low size silicon in the form of Nanocrystals embedded in a SiO_2 matrix [213]. The refractive index of Nanocrystals embedded in a SiO_2 can be controlled between 1.45 and 2.2 depending on the amount of silicon, through this, the light can be guided with better confinement than pure silica do [214-216]. More importantly, Silicon Nanocrystal/ SiO_2 composite is having large nonlinear coefficient than bulk silicon [217]. Recently measured Kerr coefficient and Raman gain of silicon Nanocrystal/ SiO_2 composite is 100 and 1000 times larger than silicon, respectively, even when the volume fraction of the Nanocrystals is less than 10%. Also, the most important advantage of using Si-nc is the compatibility with existing technology [218-220].

5.3 Research Background

Recently incredible growth in technology is driven by increasing demand of high bandwidth application, mainly video and data transmission. For satisfying this requirement, new resources such as power sources and raw materials are required. Ability to feed the technology advancement may someday become a hurdle due to the

heavy cost of operation[221]. So to negate this trend, researchers are working to find the ways through which efficiency of these networks can be improved[222].

By utilizing the tremendous large bandwidth and ultra fast response time of photonic materials, green photonics has emerged as a promising technology that can provide the data rate more than 100 Gb/s for a single channel [223,224]. Silicon based HNLFs have not only met the requirement of operation, but also Silicon has the potential for direct chip level integration. So by taking the benefit of HNLFs that require less number of pump lasers for performing the signal processing function, it is possible to exhibit the large potential of green photonics.

Additionally, HNLFs are having extensive applications such as SCG [25,225], optical parametric amplification and all optical wavelength conversion [226], distributed in-fiber amplification, pulse regeneration, optical monitoring, multiplexing and demultiplexing and switching[73]. Another main reason to enhance nonlinearity is that power requirement of the optical device can be reduced [227]. In most of the designs, the large nonlinear coefficient in PCF can be realized either by reducing the effective area of the core of PCF or using a material with high nonlinear refractive index value [14,15,53,180,189,228]. Here the slot effect is utilized to enhance the nonlinearity. Due to the slot effect, the electric field intensity gets further enhanced by a large factor. The problem lies in the field confinement within the core in nanometer size slot at the wavelength of operation. For effective utilization of nonlinearity in PCF, dispersion management is one more pivotal concern. Dispersion restricts the information carrying capacity of fiber, so it is necessary to design DCF to mitigate this effect.

Another important property of PCF is birefringence. PCF having high birefringence can be used as single-polarization mode fibers or PMF. PCFs maintain the SOP which proves usefulness of PCFs in PMD compensation. Furthermore, birefringent PCFs have very long list of important applications in optical sensor design, electro-optical modulation and signal processing systems [229,230]. Recent works show that high birefringence in PCFs can be attained by introducing a defect in the core or generating asymmetry in fiber structure [13,15,53,176,180,189]. Large birefringence is also required in addition to high nonlinearity and negative dispersion in all optical signal processing applications. In all optical signal processing applications along with high nonlinearity and negative dispersion, large birefringence

is also required. As various nonlinear effects are dependent on polarization, therefore sustaining the SOP is necessary for excellent performance.

To design an optical fiber having high nonlinearity, negative dispersion and large birefringence simultaneously is a continual challenge. Therefore, researchers are working on different geometries like hexagonal, octagonal, decagonal, spiral, etc. Our recent research study asserts that by using a slot spiral fiber design, negative dispersion, ultra-high nonlinearity and high birefringence can be achieved. The table 5.1 shows the recent research work of the different geometries of PCFs that is used to improve the optical properties.

Table 5.1: Proposed PCF structures reported in recent

<i>Design</i>	<i>Nonlinearity</i>	<i>Birefringence</i>	<i>Dispersion</i>
Silica–glass core decagonal PCF [140]	$49 \text{ W}^{-1} \cdot \text{km}^{-1}$	10^{-2}	-----
Silica core decagonal PCF [231]	-----	-----	$0 \pm 0.6 \text{ ps}/(\text{nm} \cdot \text{km})$ over 1300 nm to 1600 nm
Tellurite hexagonal lattice PCF [155]	$238.6 \text{ W}^{-1} \text{ km}^{-1}$	10^{-6}	-----
Silica octagonal-lattice PCF [166]	-----	2.13×10^{-2}	-134 to -385 ps/(nm km) at E and U bands
Fused silicon hexagonal slotted spiral PCF [14]	$224 \text{ W}^{-1} \text{ m}^{-1}$ in quasi-TE mode and $226 \text{ W}^{-1} \text{ m}^{-1}$ in quasi-TM mode	----- -	$0.91 \text{ ps}/(\text{nm} \cdot \text{km})$ in quasi-TE mode and $1.33 \text{ ps}/(\text{nm} \cdot \text{km})$ in quasi-TM mode over 150-nm
Silicon hexagonal slotted spiral PCF [13]	$1068 \text{ W}^{-1} \text{ m}^{-1}$	0.24886	-----
Silicon slotted PCF [15]	$969.58 \text{ W}^{-1} \cdot \text{m}^{-1}$ at quasi-TE mode and $156.74 \text{ W}^{-1} \cdot \text{m}^{-1}$ at quasi-TM mode	0.2006	$1.2358 \times 10^3 \text{ ps}/(\text{nm} \cdot \text{km})$
Silica octagonal lattice PCF [168]	-----	-----	$55.27 \text{ ps}/(\text{nm} \cdot \text{km})$ over 1300 nm - 1700 nm

Unique circular silica PCF [232]	56.42 W ⁻¹ km ⁻¹	0.0108	-220.9032 to -792.7265 (ps/nm.km) for E to U band
SF57 rectangular lattice PCF [173]	-----	-----	-693 ps/(nm.km) over 1450-1680 nm
Chalcogenide octagonal and circular PCF[180]	4506 W ⁻¹ km ⁻¹ and 4498 W ⁻¹ km ⁻¹	-----	+77.55ps/(nm.km) and +77.34ps/(nm.km)
As ₂ Se ₃ glass PCF [233]	2079 W ⁻¹ km ⁻¹	10 ⁻²	-----

From the above table, it is found that low index guiding slotted PCF structure are providing more improved optical properties as compared to regular high index guiding PCF structures.

Currently, with the progress in fabrication techniques, silicon fibers which furnish a material compatibility with the traditional fiber structures, have gained a substantial attention. Due to its wide availability and compatibility with established CMOS technology, silicon offers reduction in structure sizes up to 10 nm at very low cost [234,235]. In this chapter slot spiral PCF structures are designed to achieve ultra-high nonlinearity, high birefringence and large negative dispersion. Nano dimension slot in the core with low index material is defined to get the strong light confinement, which ultimately leads to enhanced nonlinearity. Due to these properties, fiber will have numerous applications in the optical field. For accurate analysis of optical characteristics of PCF, FEM is applied.

5.4 Highly Nonlinear Polarization Maintaining Dispersion Compensation Slotted Spiral PCF

5.4.1 Structure and Design of Slotted Spiral PCF

The proposed slotted silicon PCF structure is as shown in the Fig. 5.1. All the circular air holes of the varying radius in the cladding are arranged in a spiral lattice. To obtain the good mode confinement in the core region, diameters of air holes in cladding region are in increasing order $d_1 < d_2 < d_3 < d_4$ [174]. The spiral lattice structure is having six arms and each arm having four air holes. The distance from center to each

air hole of the first ring is r . The air hole arranged in an arm is at an angular increment of θ than the previous one. The benefit of using spiral lattice structure is that number of air holes gets reduced compared to regular hexagonal or triangular lattice. This results in small effective mode area.

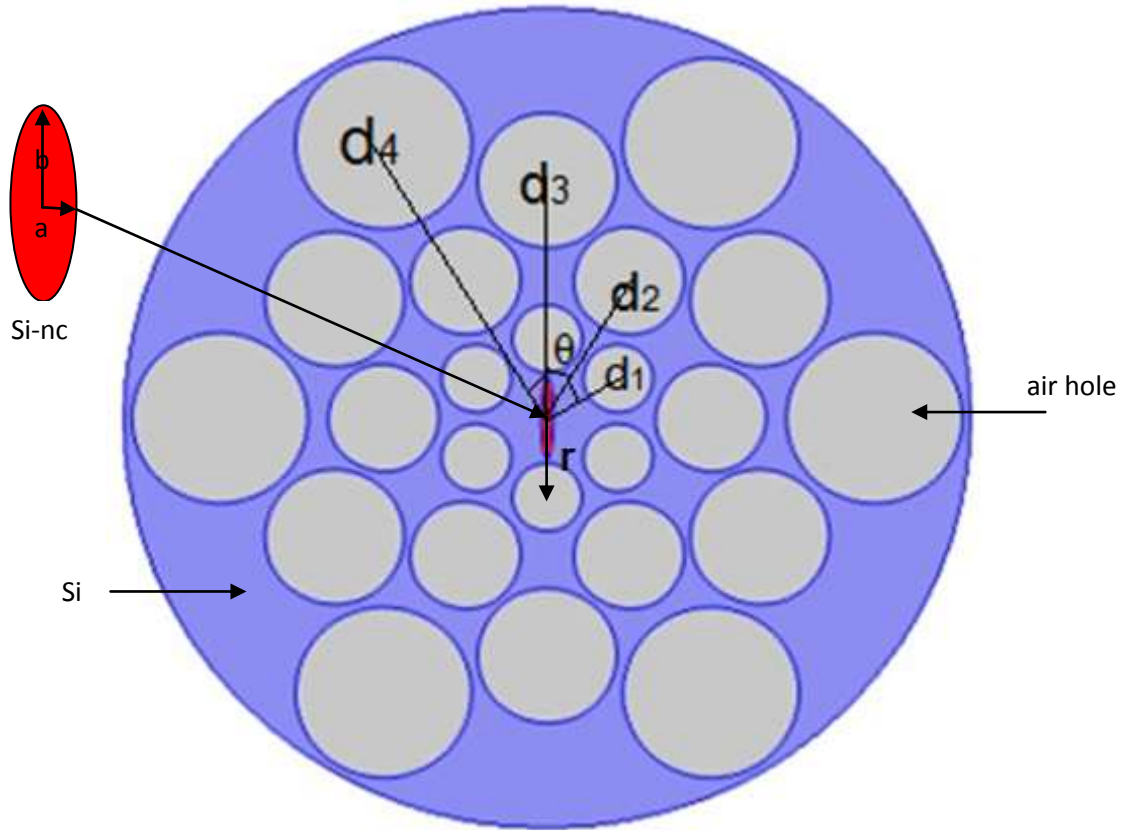


Fig.5.1 Cross sectional view of Ellipse slotted spiral PCF (design 1)

To get the benefit of slot effect, an elliptical hole consisting of a material having a low index silicon nanocrystals (Si-nc) is embedded in the center of the core. In slot region, air can also be used as low index materials but air has very low nonlinear refractive index ($5 \times 10^{-23} \text{ m}^2/\text{W}$). The basic principle of light confinement in nanometer size low index material is electric field discontinuity at the high index contrast interface. Since the normal component of electric displacement ($D = \epsilon E$) should be continuous across the interface [16]. The electric field inside the slot region is enhanced by the ratio of the refractive index of silicon to that of the slot material Si-nc. So to boost the field enhancement in low index slot region, material with high refractive index is preferable. The background of PCF is made of silicon which has refractive index of 3.48 at $1.55\mu\text{m}$ [207]. An elliptical slot is inserted in the core

region having semi minor axis of 'a' and semi major axis of 'b'. Refractive index of Si-nc can be calculated from the Sellmeier's equation [216]:

$$n^2(\lambda) = 1 + \frac{B_1\lambda^2}{\lambda^2 - C_1} + \frac{B_2\lambda^2}{\lambda^2 - C_2} + \frac{B_3\lambda^2}{\lambda^2 - C_3} \quad (5.1)$$

Where $B_1= 0.01$, $B_2= 1.96$, $B_3= 1.41$, $C_1=0.09 \mu\text{m}^2$, $C_2= 0.005 \mu\text{m}^2$, $C_3= 770.6 \mu\text{m}^2$ and λ is the wavelength of operation.

In comparison to conventional fiber, the elliptical slot spiral PCF offers enhanced freedom in engineering nonlinearity, dispersion and birefringence. Nanometer size slot introduces asymmetry between the two axes and hence large birefringence is obtained. The strong mode confinement and highly nonlinear material are proved to be beneficial for the proposed PCF in demonstrating ultrahigh nonlinear coefficient.

Due to the rapid advancements in fabrication techniques [236-239], it is possible to fabricate silicon PCF with less hassle. Firstly, a silica PCF with an elliptical shaped air hole in the core of the fiber is fabricated. Then silica PCF is converted to Silicon MOF by using magnesiothermic reduction technique. Finally, Si-nc layer is deposited in elliptical air hole by applying the Modified Chemical Vapour Deposition Method (MCVD) and then proposed structure could be fabricated. In the proposed , the losses originating from multiple mechanisms can be classified into three groups - confinement loss, scattering loss and absorption loss. Scattering loss occurs due to imperfections in fiber surface which can be reduced by using upgraded fabrication techniques. Although, the confinement loss of design is low because the imaginary part of quasi TE mode is on the order of 10^{-7} . Confinement losses can be further reduced by employing more layers of air holes. It should be noted that silicon fiber having losses nearby 5dB/cm is feasible [240]. On that account, it is concluded that the proposed design can be used to realize all-optical signal processing.

5.4.2 Characterization and Optical Properties of Slot Spiral PCF

In recent years, various theoretical models for analysis of PCFs have been developed, such as FEM, Plane Wave Method, Effective Index Method, Beam Propagation Method, and FDTD. At present, the FEM has become the most popular model to analyze the PCF characteristics, as flexibly and accurately; it can deal with

complicated structures on cross section. The basic equation for the FEM analysis, from Maxwell's equations, is given as,

$$\nabla \times ([\mu_r]^{-1} \nabla \times E) - k_0^2 [\epsilon_r] E = 0 \quad (5.2)$$

Here, ϵ_r and μ_r denotes the relative dielectric permittivity and magnetic permeability tensors, E denotes the electric field; k_0 is the free-space wave number, respectively. When a full-vector FEM is applied to PCFs, the fiber cross section is divided into a number of curvilinear hybrid elements these allow us a better approximation of the PCF structure. Guided fundamental mode is the symmetric quasi-TE mode which has high power confinement factor in the slot structure [135], the modal properties of other guided mode, quasi-TM mode is also studied. The modal effective index n can be found by analyzing the modal propagation constant. With the optimum fiber parameters that are mentioned in table 5.2, the field distribution of fundamental modes of fiber is achieved at $1.55\mu\text{m}$ that is shown in Fig. 5.2(a) and (b)

Table 5.2: Ellipse slotted PCF (design 1) parameters values for vertically aligned Slot

Radius (distance between center of slot to center of air hole)	Slot Semi minor axis	Slot Semi major axis	Diameter of air holes of first ring d_1	Diameter of air holes of second ring d_2	Diameter of air holes of third ring d_3	Diameter of air holes of fourth ring d_4
450 nm	32 nm	220 nm	400 nm	600 nm	800 nm	1000 nm

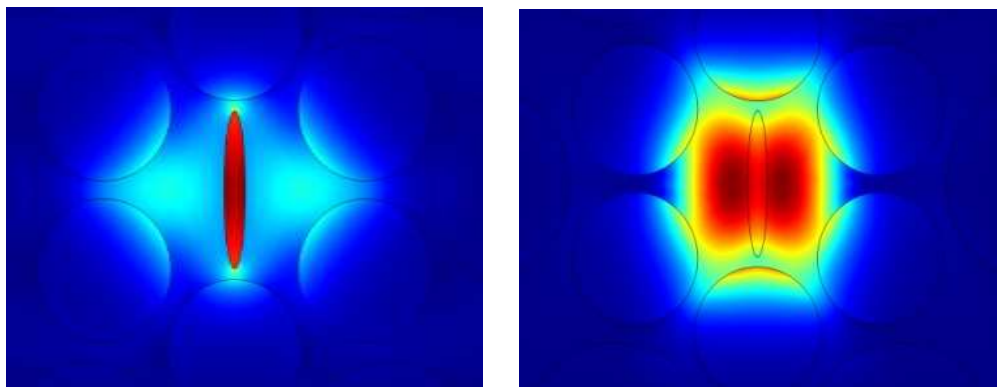


Fig.5.2 Field distribution of fundamental modes (a) Quasi TE-mode and(b) Quasi TM-mode at $1.55\mu\text{m}$ for vertically aligned Si-NC slot

Effective refractive index of fundamental quasi modes at 1.55 μm wavelength is 2.478 and 2.725. Cut off wavelength of this proposed fiber is 1.495 μm at above mentioned parameter values. From Fig.5.2(a) we can see that power confinement outside the slot region is very low for Quasi TE mode. Here the term vertical slot signifies that electric field discontinuity that provides a strong electric field confinement inside the slot take place at vertical interface so quasi TE polarization is supported in this design. On the other hand, when the slot is rotated in a horizontal direction, the quasi TM mode will become the polarized mode.

5.4.3 Research Outcomes and Discussion

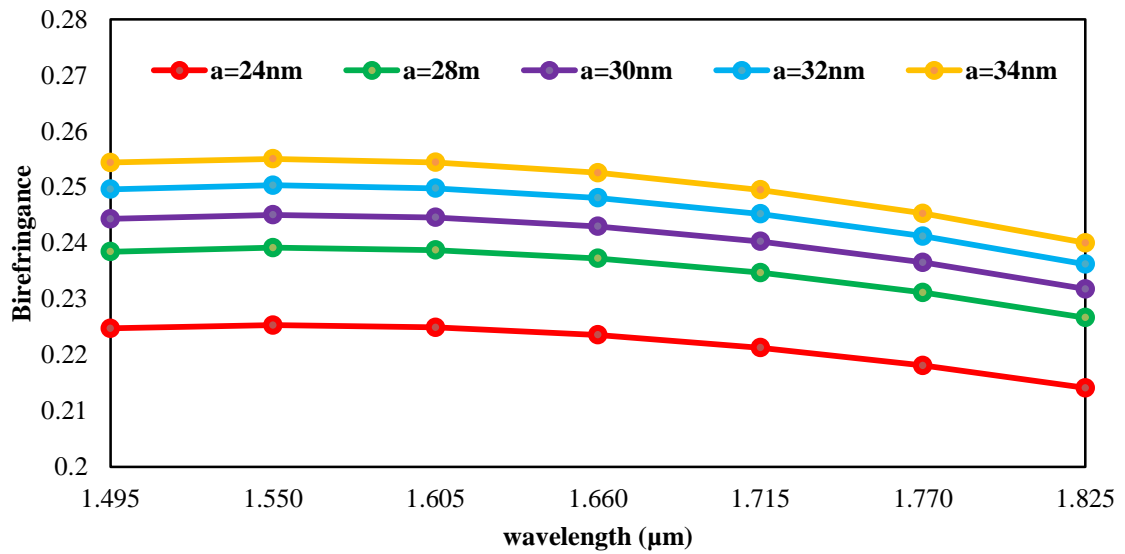
For analyzing the impact of slot geometry parameters on modal birefringence, the effects of width and height of slot on the fiber birefringence are studied within the wavelength range from 1.495 μm to 1.825 μm . The fiber design is numerically simulated using FEM. The cross section of PCF is divided into small discrete elements; these allow us a better approximation of the PCF structure. The optimum value of the effective refractive index, n_{eff} , can be obtained by solving the Maxwell equation by FEM. Once we obtained the value of n_{eff} , birefringence (B) can be obtained by calculating the difference of effective indices of two fundamental modes as given by the following expression

$$B = |n_{eff}^x - n_{eff}^y| \quad (5.3)$$

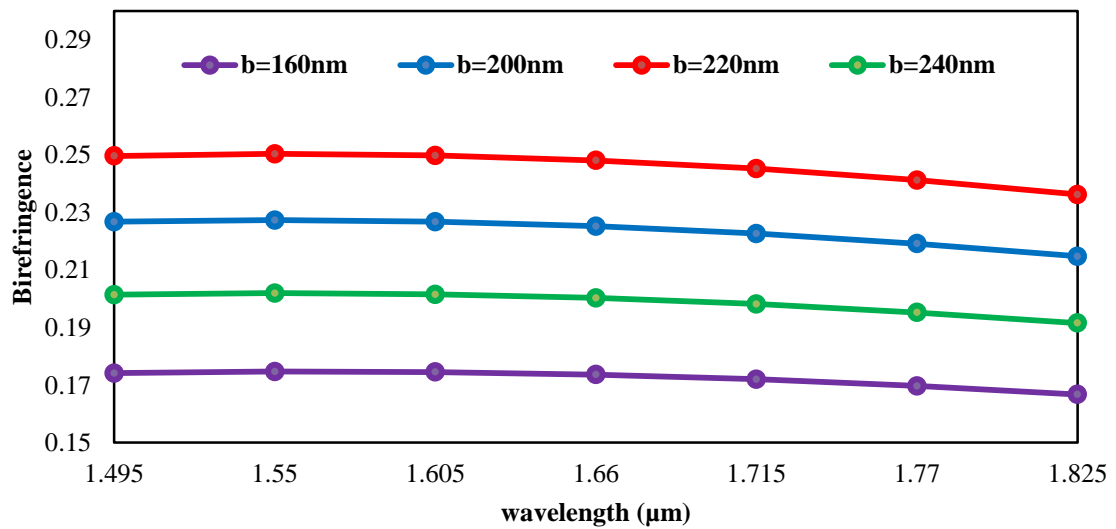
In equation (5.3), n_{eff}^x and n_{eff}^y denote the refractive index of x polarization mode and y polarization mode, respectively. The elliptical slot significantly breaks the symmetry of PCF leading to a large difference in effective index between the two fundamental modes. Progressively increasing the diameter of air holes in cladding region not only provide a good mode confinement but it also disturbs the symmetry of the structure, due to which very high birefringence is achieved.

In Fig.5.3(a), birefringence increases as ' a ' increases. Increase in minor dimension ' a ' of elliptical slot leads to generate more geometrical deformity that will result in a large difference between fundamental modes. But this characteristic shows different behavior for ' b ' values that are shown in Fig.5.3(b). Initially, birefringence values are increasing as the fiber parameter ' b ' increases for constant ' a ' = 32 nm, but

after ' b ' = 220 nm value, birefringence decreases. As for small values of ' b ' maximum field is confined in slot region but for higher values of ' b ' field enhancement weakens.



(a)



(b)

Fig.5.3 Birefringence Vs wavelength for vertical aligned slot in core with variation in (a) Semi Minor axis ' a ' for ' b ' = 220 nm and (b) Semi Major axis ' b ' for ' a ' = 32 nm.

Consequently, the difference of effective refractive indices of two fundamental quasi modes reduces. For optimum values of design parameters, the value of birefringence is obtained as 0.2503 at 1.550 μm wavelength. Beat length of proposed design at 1.55 μm is 6.19 μm. Beyond 34 nm, two fundamental modes are not achieved. If the value of ' b ' is increased beyond 220 nm, the value of birefringence is decreasing. So it is not

possible to calculate birefringence beyond this value. At 'a'= 34 nm and 'b' = 220 nm, birefringence is 0.25508 found at 1.55 μm .

Now, if the slot is arranged in a horizontal direction, properties of the PCF design are changed slightly. At the following fiber parameters presented in table 5.3.

Table 5.3: Ellipse Slotted PCF (design 1) parameters values for horizontally aligned slot

Radius (distance between center of slot to center of air hole)	Slot Semi minor axis	Slot Semi major axis	Diameter of air holes of first ring d_1	Diameter of air holes of second ring d_2	Diameter of air holes of third ring d_3	Diameter of air holes of fourth ring d_4
450 nm	32 nm	220 nm	400 nm	600 nm	800 nm	1000 nm

The electric field intensity distribution of fundamental quasi modes are shown in Fig.5.4. The effective index of quasi TM mode and quasi TE mode is 2.4926 and 2.7179 respectively.

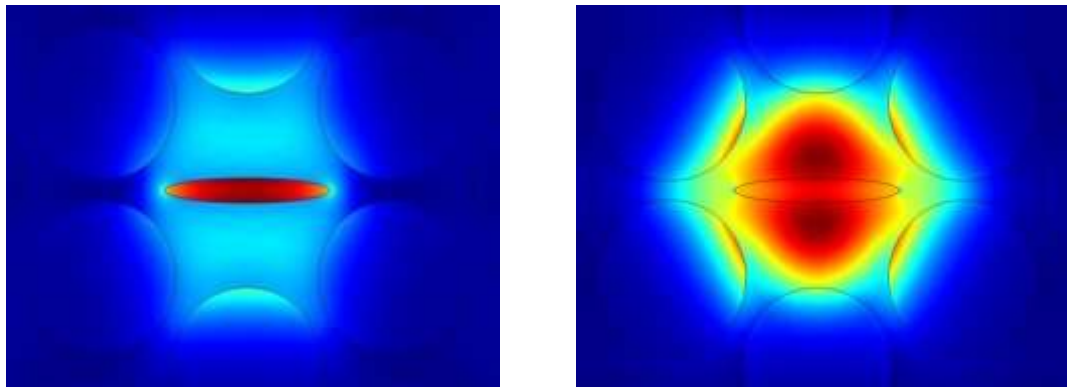
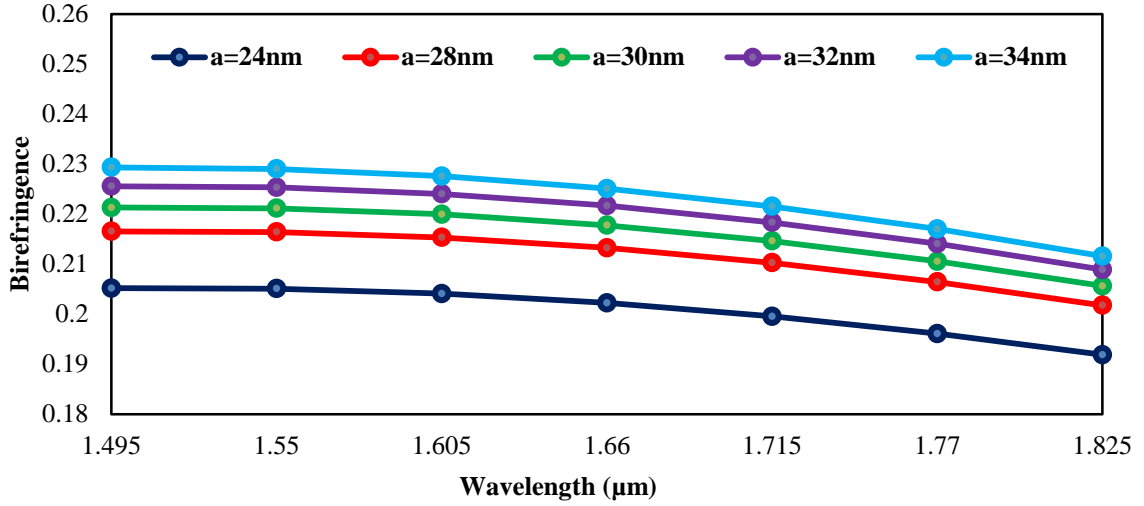


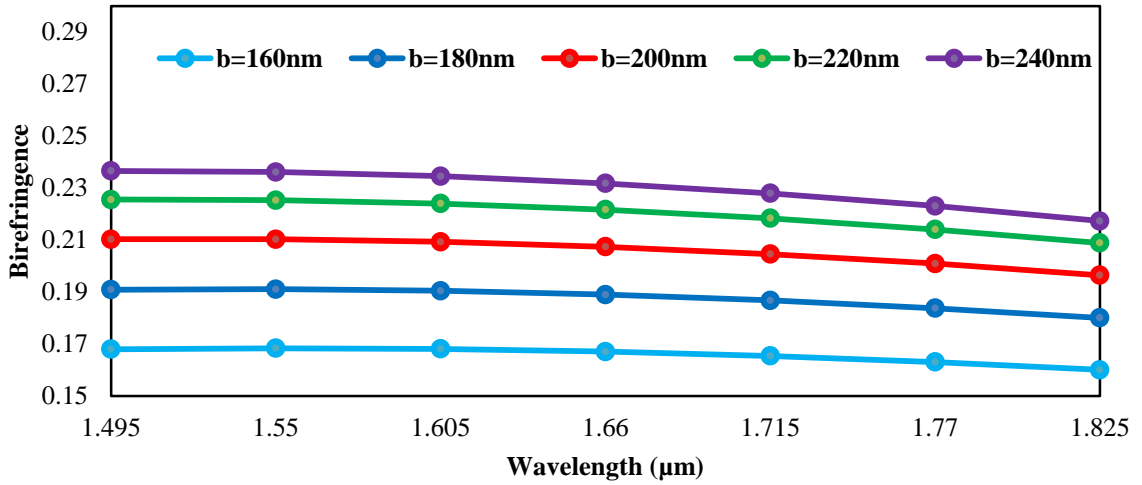
Fig.5.4 Electric Field intensity distribution of fundamental modes for (a) Quasi-TM Mode and (b) Quasi-TE Mode at 1.55 μm for horizontally aligned slot

In the case of horizontally aligned slot region, we have more flexibility to increase the dimensions of the slot. In this structure, due to the more gap between two air holes along the vertical direction, major semi axis 'b' can be varied for long length as compared to previous one. Fig.5.5(a) depicts that as the values of 'a' are increasing, more asymmetry is generated within the structure that will lead to more birefringence.

Similarly, for increasing values of 'b' increased birefringence is also obtained as shown in Fig.5.5(b). For optimum values of design parameters, the value of birefringence is found to be 0.2253 at 1.55 μm wavelength. Beat length of proposed design at 1.55 μm is 6.88 μm .



(a)



(b)

Fig.5.5 Birefringence Vs wavelength for horizontally aligned slot in core with variation in (a) Semi Minor axis 'a' for $b = 220 \text{ nm}$ and (b) Semi Major axis 'b' for $a = 32 \text{ nm}$.

Nonlinearity is another crucial property of PCFs. Nonlinear coefficient γ of proposed PCF can be obtained by using the following numerical equation (5.4)

$$\gamma = \frac{2\pi n_2}{\lambda A_{eff}} \quad (5.4)$$

where, A_{eff} denotes the effective area of PCF, n_2 denotes the nonlinear refractive index of the material, λ is the wavelength of operation. Here the nonlinear

refractive indices of Si-nc and Si are $0.47 \times 10^{-16} \text{ m}^2/\text{W}$ and $5 \times 10^{-18} \text{ m}^2/\text{W}$, respectively [218,241]. The effective area has a great importance in the context of nonlinearity, and it also affects the confinement loss, bending loss, splicing loss, etc. Thus an understanding of effective area is important for analyzing the nonlinear phenomenon. A_{eff} is an effective area of PCF which is calculated by using the following equation (5.5):

$$A_{eff} = \frac{(\iint_{-\infty}^{\infty} E^2 dx dy)^2}{\iint_{-\infty}^{\infty} E^4 dx dy} \quad (5.5)$$

The effective area of PCF depends on the electric field confinement in the core of the fiber. Small effective mode area results in large nonlinearity which would have many applications like parametric amplification, SCG, soliton pulse transmission, FWM and many nonlinear applications [140].

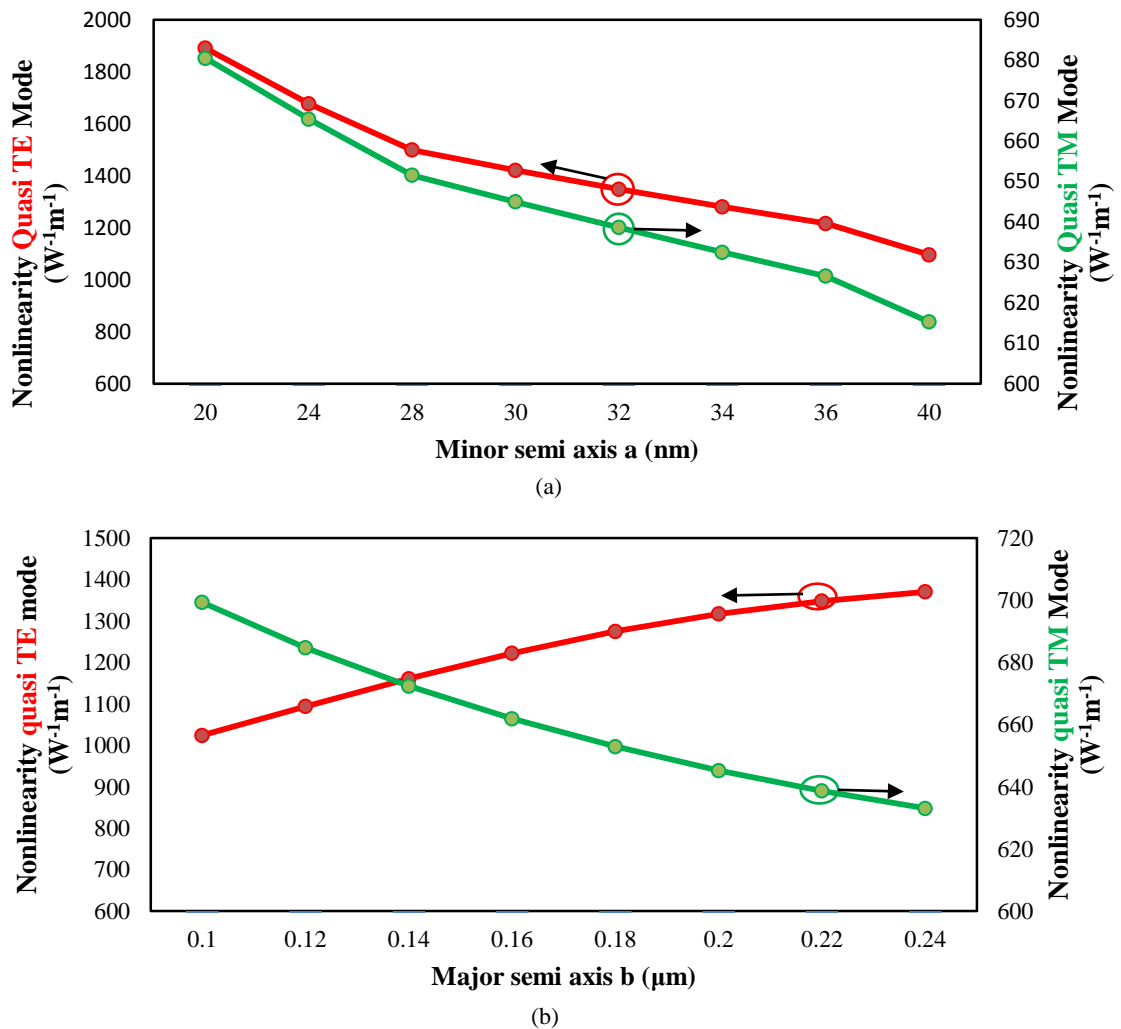


Fig.5.6 Nonlinearity variation of fundamental mode of vertical slot at $1.55 \mu\text{m}$ wavelength with variation in (a) Semi Minor axis 'a' and (b) Semi Major axis 'b'

In Fig.5.6 nonlinear coefficient γ of PCF for both fundamental quasi modes is shown with varying semi minor axis ' a ' and semi major axis ' b '. It is evident from Fig.5.6 (a) that as we increase the value of ' a ', the value of nonlinear coefficient decreases. The reason is that as we are increasing ' a ', the effective mode area is increasing, and hence the light confinement ability or confinement factor decreased. In Fig. 5.6(b), depicts the effect of ' b ' on nonlinearity. As we increase ' b ', nonlinearity increases as light become more confined. For vertically aligned slot structure, at 1.55 μm , the nonlinear coefficient γ , 1348 $\text{W}^{-1}\text{m}^{-1}$ and 638 $\text{W}^{-1}\text{m}^{-1}$ for quasi-TE and quasi-TM modes is achieved. As per the figures stated above, it is observed that nonlinearity or electric field strength is more sensitive to the variation of minor semi axis ' a ' as compared to the major semi axis ' b '. It is also found in this structure, that after varying the parameters, 1890 $\text{W}^{-1}\text{m}^{-1}$ is the highest achievable nonlinearity. For horizontal slot structure, the nonlinear coefficient γ for quasi-TM and quasi-TE modes are 1290 $\text{W}^{-1}\text{m}^{-1}$ and 634 $\text{W}^{-1}\text{m}^{-1}$, respectively.

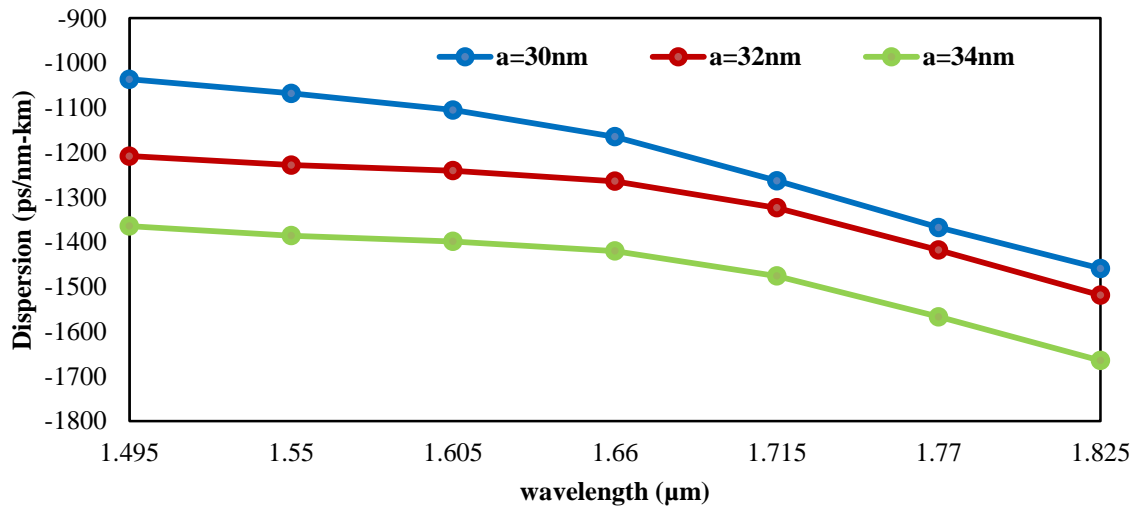
It is important to have long distance communication without any distortion but as it is known that dispersion limits the transmission distance and speed and so it is necessary to compensate it for long haul transmission. For this purpose, we need to have a negative dispersion for compensating the broadening of the pulse that occurs due to the inherited dispersion. Having large negative dispersion can also nullify the need of long fibers and help in reducing the cost. The total chromatic dispersion is defined as the summation of material dispersion and geometric dispersion. The material dispersion cannot be changed once the material is embedded in the fiber and is determined by the wavelength dependence of the fiber material. On the other hand, the geometrical dispersion can be controlled by altering the parameters of the fiber like pitch and hole size. The total chromatic dispersion of the PCFs is calculated using following expression [242]:

$$D(\lambda) = -\frac{\lambda}{c} \frac{\partial^2 \text{Re}(n_{eff})}{\partial \lambda^2} \quad (5.6)$$

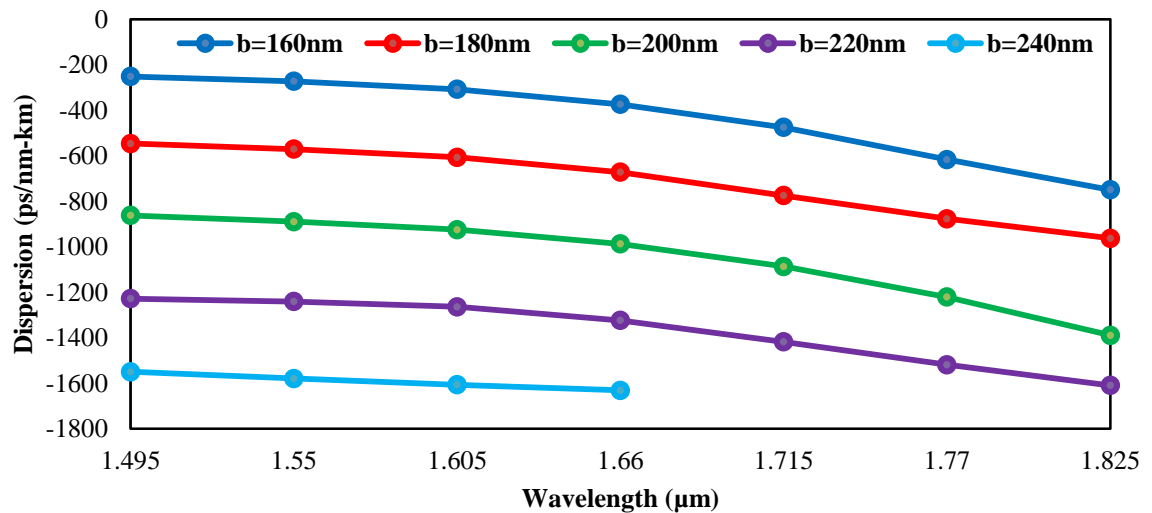
In equation (5.6), c is the speed of light in vacuum and λ denotes the operating wavelength.

The large index contrast between Si-nc and Silicon leads to strong light confinement in slot region. In this structure, dimensions of slot region are at the nanometer scale. A small variation in any dimension of slot region leads to large

variation in the total chromatic dispersion. So the overall dispersion is dominated by waveguide dispersion. This corroborates that the total dispersion is governed by the slot dimensions in this particular structure.



(a)



(b)

Fig.5.7 Dispersion Vs wavelength for vertically aligned slot with variation in (a) Semi Minor axis 'a' and (b) Semi Major axis b.

Fig.5.7 depicts the variation effect of semi minor axis 'a' and semi major axis 'b' on the chromatic dispersion of proposed PCF design. We can notice from Fig.7 that as values of 'a' are increasing, dispersion decreases rapidly. If 'a' is further increased, confinement is not obtained. So we cannot calculate dispersion beyond this value. Similarly, for increasing values of 'b', dispersion decreases rapidly. The value of 'b' cannot be increased beyond 240 nm because the slot will touch or merge with the air

holes of first ring. The large negative dispersion value makes this PCF design as a good DCF element. At optimum parameters, for vertically aligned slot structure, values at 1.55 μm wavelength, large negative dispersion value -1228 ps/nm/km is achieved. Whereas, in horizontally aligned slot structure for optimum design parameters the dispersion at 1.55 μm wavelength is -1005 ps/nm/km obtained.

It is worth noting that peak values of above mentioned fiber characteristics cannot be achieved simultaneously, as there is a trade off that occurs between the characteristics and so the optimum value point has to be considered, according to the need for specific applications.

We can conclude that ultra high nonlinearity, high birefringence with large negative dispersion can be attained by introducing a highly nonlinear elliptical slot in the core region. It has been shown through numerical results that by optimizing the fiber parameters, nonlinear coefficient of the fundamental quasi-TE mode, birefringence, and dispersion at the wavelength of 1.55 μm can be 1348 $\text{W}^{-1}\text{m}^{-1}$, 0.2503 and -1228 ps/nm/km respectively. The proposed design can be used for nonlinear signal processing applications. This high birefringence can also be used to reduce the PMD effect and many other applications such as sensing applications.

5.5 Ultrahigh Nonlinear Polarization Maintaining PCF with Flat Negative Dispersion

Further enhancement of optical characteristics can be done in this section by varying the design parameters. This will help in gaining better results for different characteristics like nonlinearity, birefringence, and dispersion. Due to the improvement of the optical characteristics, the proposed PCF can realize the benefits of various applications at very low length. The size reduction of the fiber will also make it compatible with the photonic integrated circuits (PICs).

In continuation of the previous research work that has been already discussed in the literature review and in section 5.4, it can be understood that for the purpose of achieving high nonlinearity, large birefringence and large negative dispersion, the refractive index contrast between the slot and the background material has to be very high. For this purpose, the slot should have low refractive index as well as high

nonlinear refractive index [243], and background material should have high refractive index[244].

5.5.1 Design of Elliptical Slot Spiral PCF

The cross-sectional view of this slotted spiral PCF design is similar to the previous structure and is shown in the fig. 5.1. The circular air holes in the cladding are arranged in the spiral lattice with air holes having diameter of d_1, d_2, d_3, d_4 , that are having different dimensions from the previous structure. Spiral lattice has 6 arms, each having 4 air holes and the distance from center to air holes of the first ring is r . The air hole arranged in an arm is at an angular increment of θ than the previous one. Diameter of air holes is enlarged step by step for good mode confinement [174]. The background material in PCF is chosen as silicon, in addition to this an elliptical slot of silicon nano-crystal is embedded in the core of the PCF with semi minor axis of ' a ' and semi major axis of ' b '. This slot introduces asymmetry between the two axes and hence induces birefringence. The presence of elliptical slot in core region offers better mode confinement, which in turn provide ultrahigh nonlinearity.

Light confinement mechanism inside the slot will remain the same for both the designs but this design offers more enhanced light intensity inside the slot region as compared to previous results. As it is discussed previously that enhancement results from the continuity of the normal component D_x of the dielectric displacement that is oriented parallel to the substrate plane [16]:

$$D_{x,Si} = D_{x,slot} \quad (5.7)$$

$$\epsilon_{Si} E_{x,Si} = \epsilon_{slot} E_{x,slot} \quad (5.8)$$

$$\epsilon = \sqrt{n} \quad (5.9)$$

So to maintain the boundary conditions at core-cladding interface, the electric field in the slot must be enhanced by

$$\frac{\epsilon_{Si}}{\epsilon_{slot}} = \left(\frac{n_{Si}}{n_{slot}} \right)^2 \quad (5.10)$$

Here background material is silicon which have a high refractive index $n_{Si} = 3.48$ at $1.55 \mu\text{m}$ and slot is embedded with silicon nanocrystals having refractive index $n_{slot} = 1.5$. Therefore, electric field is more confined in slot region and enhanced by a factor of 5.38 over the electric field in the silicon, which is a significant increase [16,208].

In comparison to conventional fiber, the elliptical slot spiral PCF offers increased freedom in tailoring birefringence and nonlinearity. The mode is well confined in elliptical slot region. The term vertical defines that electric field discontinuity, which provides strong field confinement inside the low index slot region occurs at the vertical interface [13-18]. For this purpose, quasi TE polarization must be used. The modal distribution of fundamental quasi modes of fiber at $1.55 \mu\text{m}$ is shown in fig. 5.8(a) and (b) with fiber parameters as mentioned in table 5.4.

Table 5.4: Ellipse Slotted PCF (design 2) parameters values for vertically aligned slot

Radius (distance between center of slot to center of air hole)	Slot Semi minor axis	Slot Semi major axis	Diameter of air holes of first ring d_1	Diameter of air holes of second ring d_2	Diameter of air holes of third ring d_3	Diameter of air holes of fourth ring d_4
400 nm	30 nm	200 nm	340 nm	540 nm	680 nm	860 nm

The effective index of quasi-TE and quasi-TM mode are 2.3505 and 2.6427, respectively. Cut off wavelength of design is $1.495 \mu\text{m}$ for above fiber parameters.

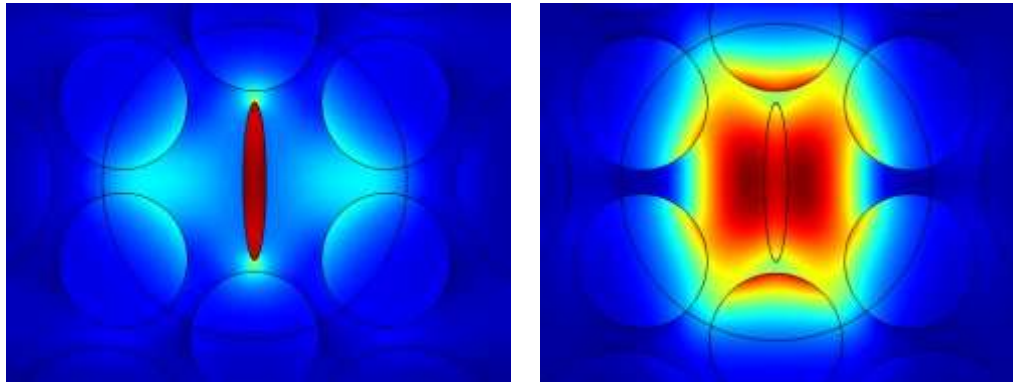


Fig.5.8 Field distribution of fundamental modes for (a) quasi TE mode and(b) quasi TM mode at $1.55 \mu\text{m}$ for vertically aligned Si-nc slot

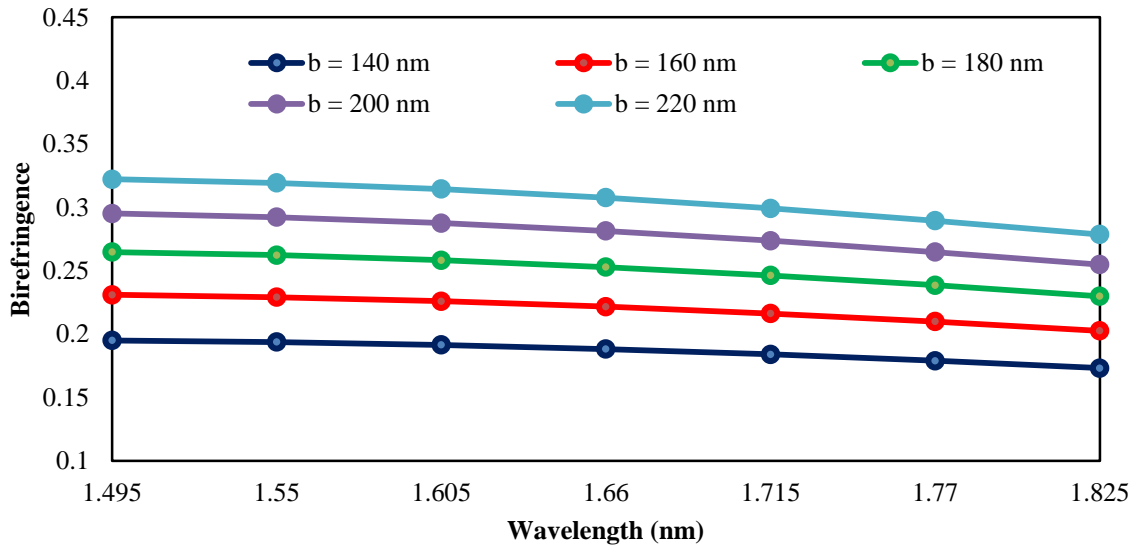
5.5.2 Research Outcomes and Discussion

In this work, to analyze the slotted spiral PCF, a full vector FEM is used. The FEM directly solve the Maxwell equations to obtain an optimum value of the effective refractive index, n_{eff} . Once we get the value of n_{eff} , birefringence B can be calculated

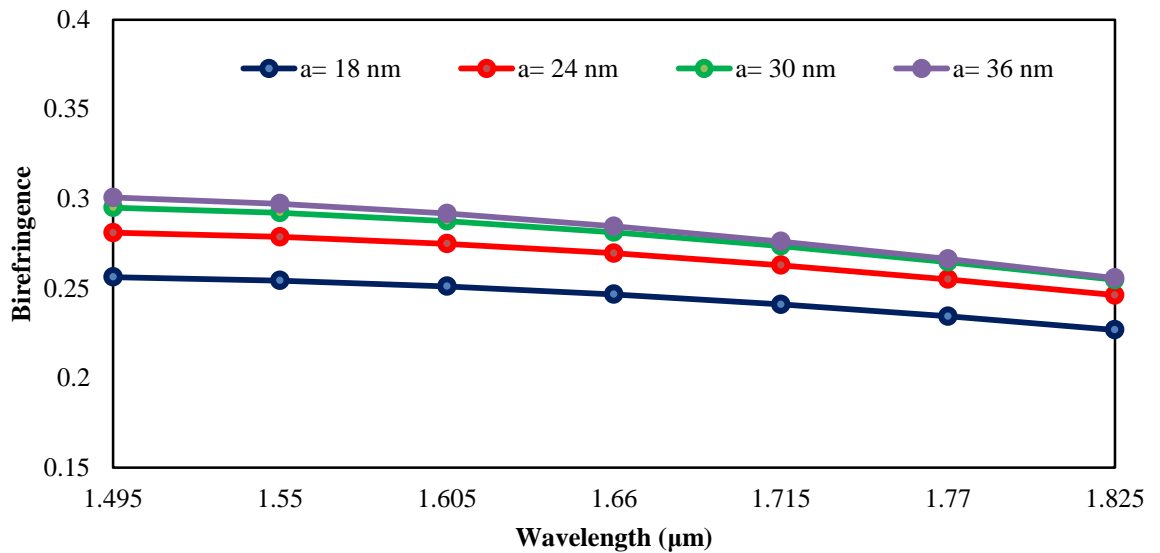
by taking the difference of effective indices of fundamental quasi modes, and it is given by following formula

$$B = \Delta n = |n_{eff}^x - n_{eff}^y| \quad (5.11)$$

where n_{eff}^x and n_{eff}^y indicates the refractive index of x polarization mode and y polarization mode, respectively. The elliptical slot significantly breaks the symmetry of PCF leading to large effective index difference between the two fundamental mode. Due to which very high birefringence can be achieved.



(a)



(b)

Fig.5.9 Birefringence Vs wavelength for vertical aligned slot in core with variation in (a) Semi Major axis 'b' for 'a' = 30 nm and (b) Semi Minor axis 'a' for 'b' = 200 nm.

As shown in Fig.5.9(a), birefringence values are increasing as the fiber parameter 'b' increases for constant 'a' = 30 nm, because of the higher values of semi major axis 'b' large asymmetry is induced in the fiber. But in the case of semi minor axis 'a', behavior of variation in birefringence is different. As it is depicted in Fig.5.9(b), birefringence first increases as 'a' increases but after 'a' = 36 nm, as we increase 'a', birefringence decreases. Because for small values of 'a', maximum field is confined in slot region but for higher values of 'a' field enhancement weakens. For optimum values of design parameters, the value of birefringence is found to be 0.292219 at 1.55 μm wavelength. Beat length of proposed design at 1.55 μm is 5.3 μm .

Now, if the slot is arranged in a horizontal direction, properties of the PCF design are changed slightly. At the following fiber parameters given in table 5.5.

Table 5.5: Ellipse Slotted PCF (design 2) parameters values for horizontally aligned slot

Radius (distance between center of slot to center of air hole	Slot Semi minor axis	Slot Semi major axis	Diameter of air holes of first ring d_1	Diameter of air holes of second ring d_2	Diameter of air holes of third ring d_3	Diameter of air holes of fourth ring d_4
400 nm	30 nm	200 nm	340 nm	540 nm	680 nm	860 nm

The electric field intensity distribution of fundamental quasi modes are shown in Fig.5.10. The effective index of quasi TM mode and quasi TE mode is 2.371 and 2.634 respectively.

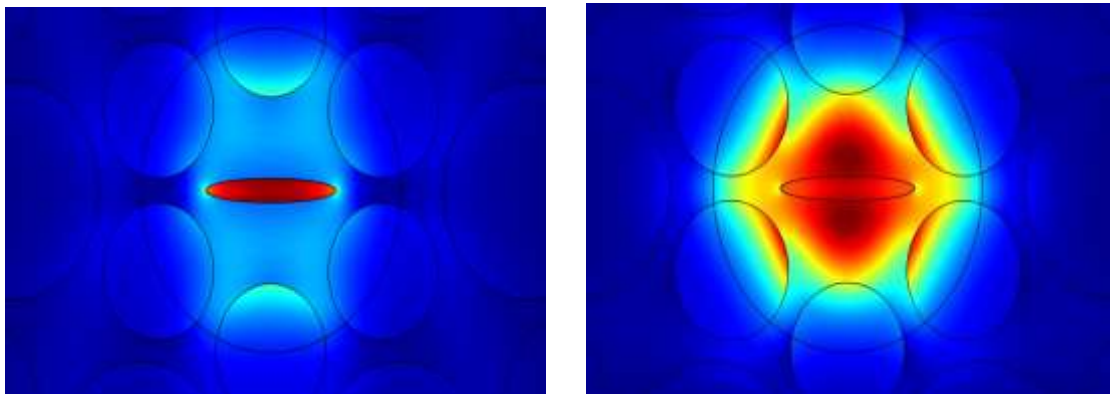


Fig.5.10 Field distribution of fundamental modes for (a) quasi-TM mode and (b) quasi-TE mode at 1.55 μm for horizontally aligned Si-nc slot

Due to the large gap between the air holes along the horizontal direction, the major semi axis length can be longer than the previous fiber structure. Birefringence values are observed within the range of semi major axis 'b' from 200 nm to 300 nm, similarly for semi minor axis 'a' from 24 nm to 42 nm.

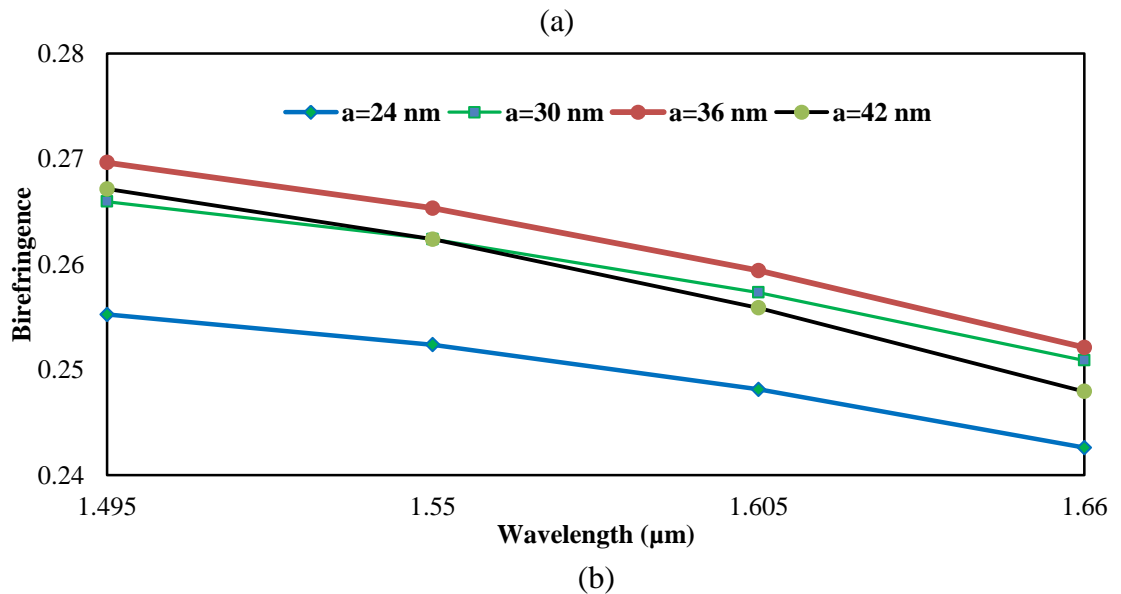
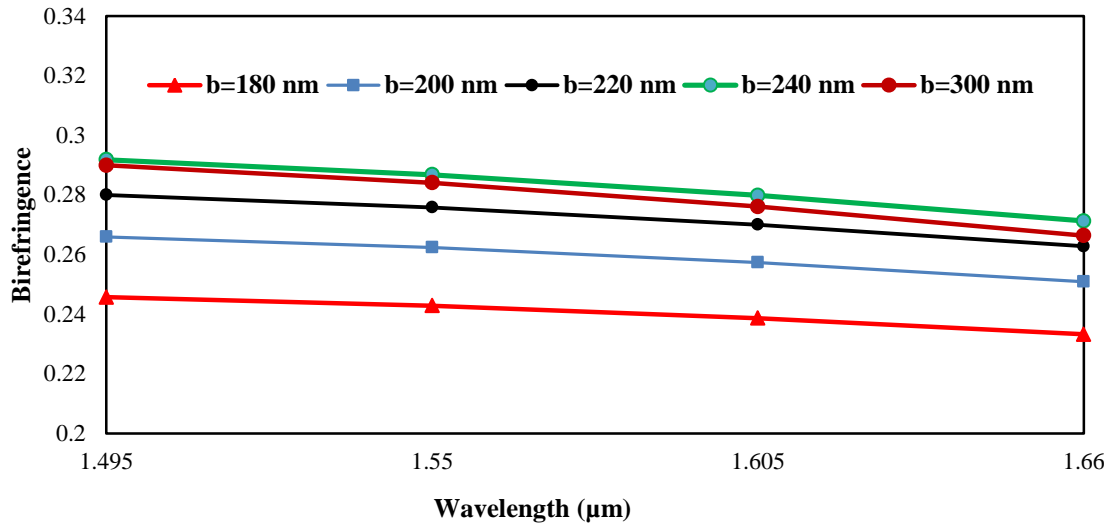


Fig.5.11 Birefringence Vs wavelength for horizontally aligned slot in core with variation in (a) Semi Major axis 'b' for 'a' = 30 nm and (b) Semi Minor axis 'a' for 'b' = 200 nm.

As shown in fig.5.11(a), birefringence increases as we increase 'b', but if we further increase 'b' value, then birefringence is decreased. As an example, for 'b' = 300 nm after 1.55 μm, birefringence values are lower than for 'b' = 240 nm. Similarly, birefringence increases as we increase 'a' but after 36 nm birefringence values start decreasing, as shown in fig.5.11(b). For optimum values of design parameters, the

value of birefringence is found to be 0.26239 at 1.55 μm wavelength. Beat length of proposed design at 1.55 μm is 5.91 μm .

Another important feature of PCFs is nonlinearity that can be calculated by the following equation

$$\gamma = \frac{2\pi n_2}{\lambda A_{eff}} \quad (5.12)$$

where, A_{eff} refers to effective area of PCF, n_2 is the nonlinear refractive index of the material used, and λ is wavelength of operation. Here the nonlinear refractive indices of Si and Si-nc are $5 \times 10^{-18} \text{ m}^2/\text{W}$ and $1 \times 10^{-16} \text{ m}^2/\text{W}$, respectively [15,243]. A_{eff} is effective area of PCF which is given by

$$A_{eff} = \frac{(\iint_{-\infty}^{\infty} E(x,y)^2 dx dy)^2}{\iint_{-\infty}^{\infty} E(x,y)^4 dx dy} \quad (5.13)$$

The effective area of PCF depends on the confinement of electric field in the core of the fiber. Small effective mode area leads to large nonlinearity that would have many applications such as SCG, HNLFF, soliton pulse generation and various nonlinear applications.

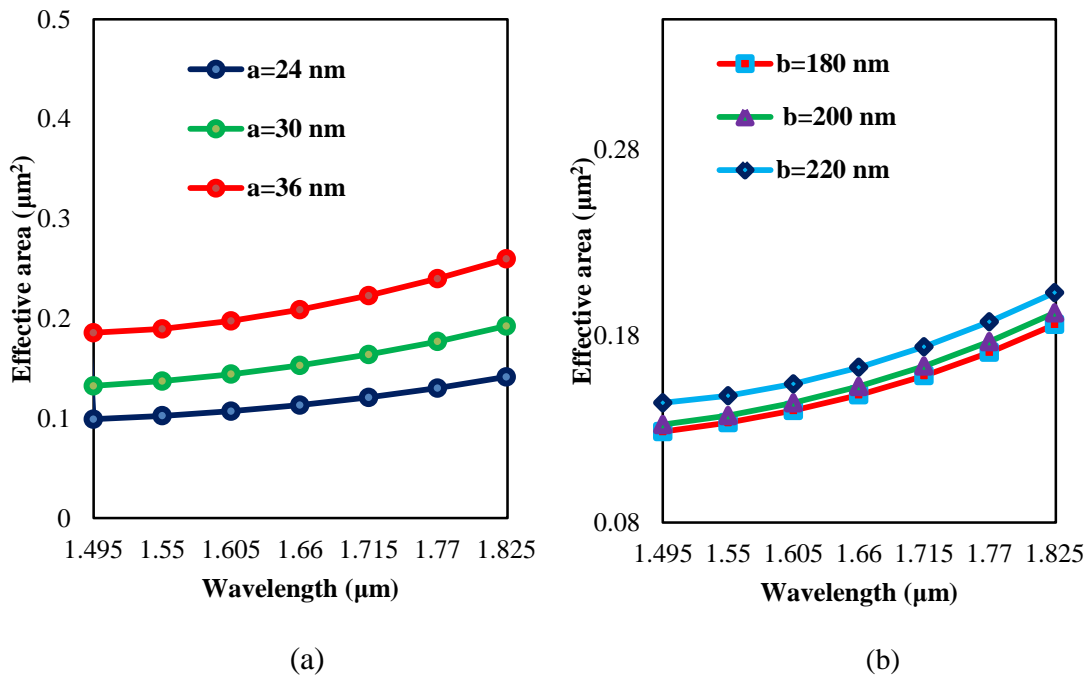


Fig. 5.12 Effective area vs. wavelength for variation in (a) semi minor axis 'a' and (b) semi major axis 'b'

It is observed from Fig. 5.12 that as the value of semi minor axis ' a ' increases, effective area get enlarged. Similarly, as the semi major axis ' b ' increases, the effective area is increasing. So it is concluded that as the wavelength increases, the effective mode area increases that means light confinement area increases with wavelength. Large effective area has adverse effects on nonlinearity and so nonlinearity also decreases for higher wavelengths. Variation of nonlinearity for different slot dimensions is described below.

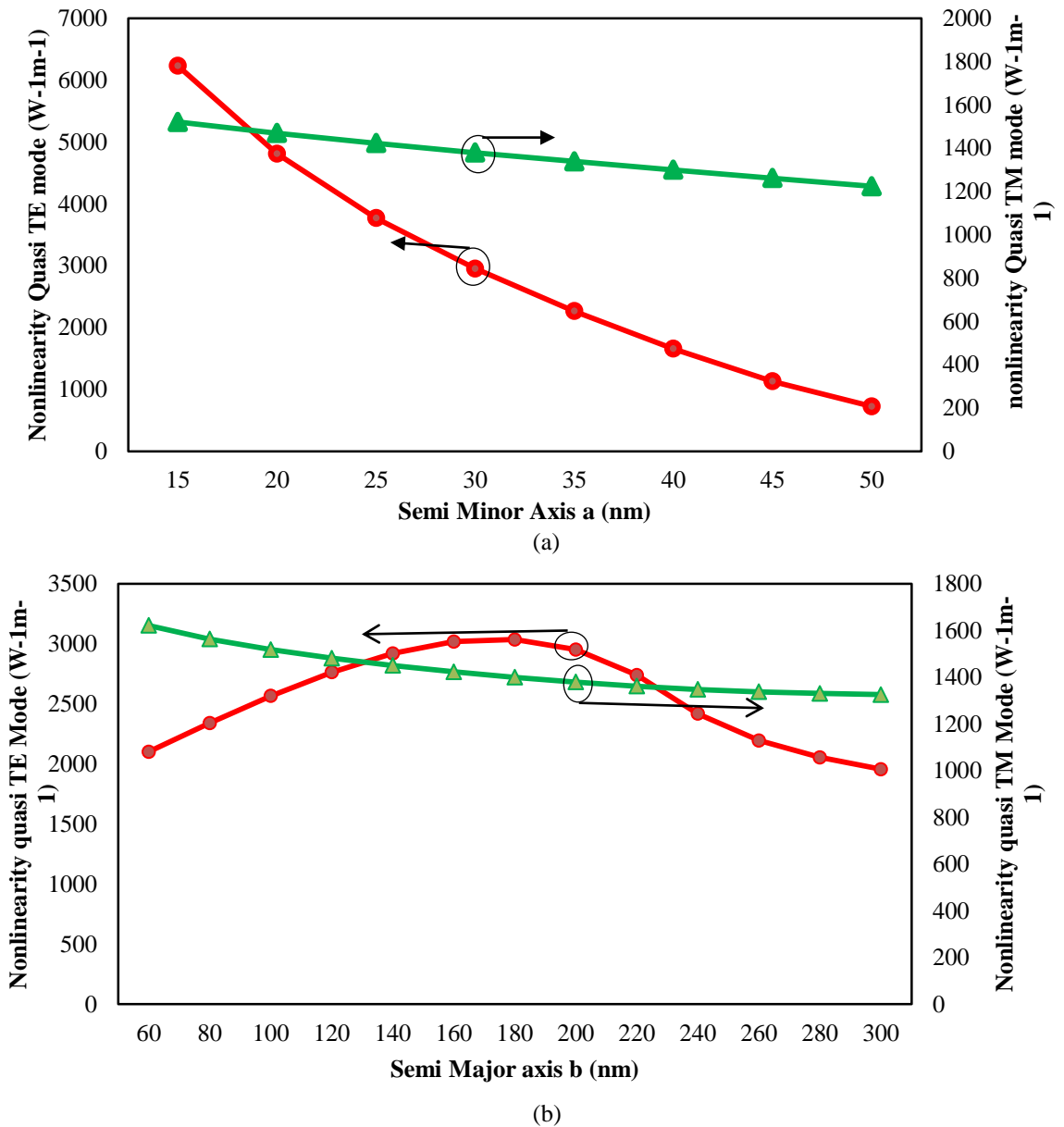


Fig.5.13 Nonlinearity variation of fundamental mode at $1.55 \mu\text{m}$ wavelength with variation in (a) Semi Minor axis ' a ' and (b) Semi Major axis ' b '

In Fig.5.13 nonlinear coefficient γ of PCF for both fundamental modes is shown with varying semi minor axis 'a' and semi major axis 'b'. It is apparent from Fig.5.13 (a) that the nonlinear coefficient value decreases as we increase 'a'. The reason is that as we are increasing 'a', the effective mode area is increasing and so the light confinement ability, or confinement factor decreases.

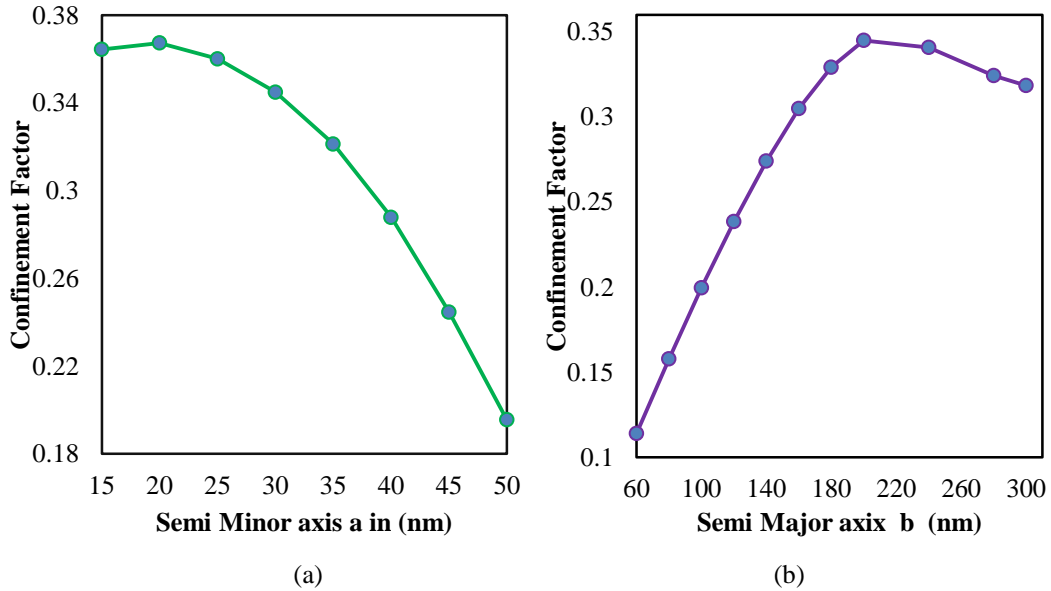


Fig.5.14 Confinement factor variation at 1.55 μm wavelength with variation in (a) Semi Minor axis 'a' and (b) Semi Major axis 'b'

Fig.5.14 (a) shows the variation of Confinement factor with semi minor axis 'a' that is supporting the last statement. In fig. 5.13(b) and 5.14(b), the effect of semi major axis 'b' on nonlinearity and confinement factor is presented. As we increase 'b', nonlinearity and confinement factor increases but when 'b' is greater than 200 nm both the values start decreasing. At 1.55 μm we have found that the nonlinear coefficient γ is 2951 $\text{W}^{-1}\text{m}^{-1}$ and 1379 $\text{W}^{-1}\text{m}^{-1}$ for quasi-TE and quasi-TM mode respectively and nonlinearity decreases with increase in wavelength.

Due to the increased traffic over transmission lines, the higher bit transmissions of more than 40 Gbps have been implemented in WDM technique. Distortion in the transmission caused by dispersion in a SMF severely restrict the high data rate transmission. Dispersion can be suppressed through a DCF. Large negative dispersion is required to compensate the dispersion incurred during the propagation of light through the fiber. Also, if the fiber is providing very high negative dispersion

values then the required fiber length to compensate the dispersion is reduced. The dispersion value can be measured through the relation [242],

$$D = D_m + D_w = -\frac{\lambda}{c} \frac{d^2 n(\lambda)}{d\lambda^2} \quad (5.14)$$

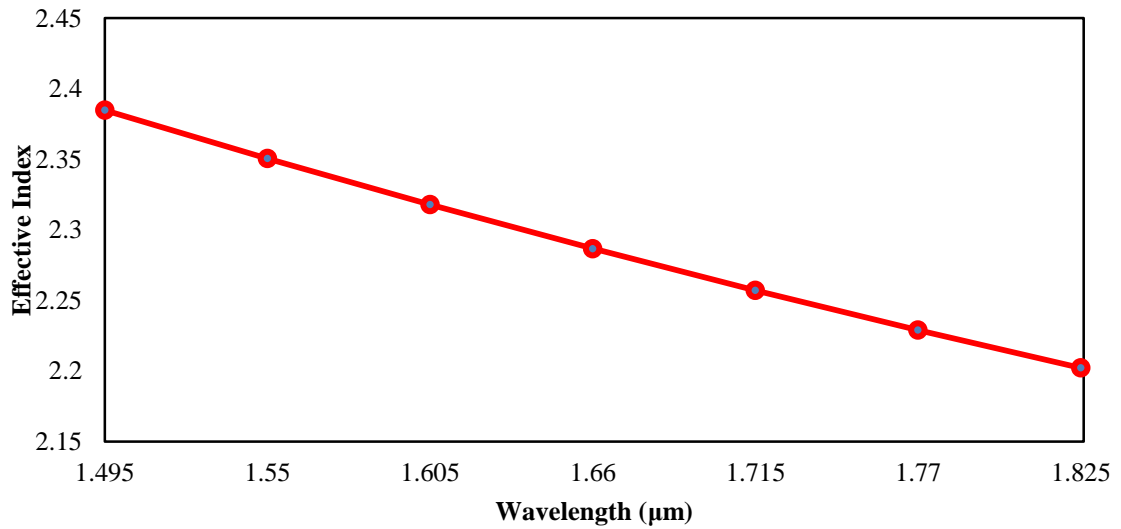


Fig.5.15 Effective index variation with wavelength for quasi TE mode at semi minor axis 'a' = 30 nm and semi major axis 'b' = 200 nm

Fig. 5.15 shows the variation of effective refractive index variation with wavelength that can be used to determine the chromatic dispersion. As dispersion is the second derivative of effective index with variation in wavelength.

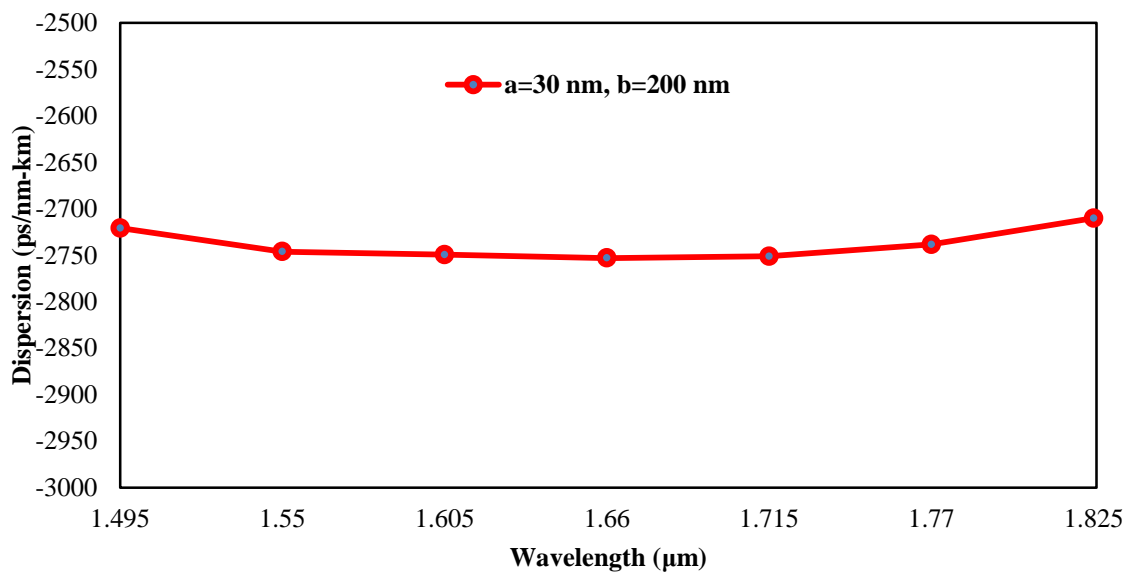


Fig.5.16 Dispersion for quasi TE mode at semi minor axis 'a' = 30 nm and semi major axis 'b' = 200 nm

From Fig. 5.16, it is found that in this design, large negative dispersion is achieved as compared to the previous design. Also this design offers flat negative dispersion as compared previous design. Comparison of first design and second design at 1.55 μm wavelength is presented in table 5.6.

Table 5.6: Comparison of design 1 and design 2 at 1.55 μm wavelength

	Birefringence	Nonlinearity	Dispersion
Design 1	0.2503	1348 $\text{W}^{-1}\text{m}^{-1}$	-1288 ps/nm/km
Design 2	0.2922	2951 $\text{W}^{-1}\text{m}^{-1}$	-2746 ps/nm/km

As it is evident from table 5.6, that the nonlinearity and birefringence are much higher in the second design than the first design because the fundamental quasi modes are more tightly bounded in the slot of the core region due to the high index contrast between the slot and the cladding. The large negative dispersion is also achieved that reduce the required DCF length.

Due to superior optical properties, the proposed fiber can be an excellent candidate for either all optical nonlinear signal processing or maintain single polarization, or in nonlinear optics applications. It can be concluded that ultra high nonlinearity and high birefringence can be attained by introducing a highly nonlinear elliptical slot in the core region. It has been shown through numerical results that by optimizing the fiber parameters, nonlinear coefficient of the fundamental quasi-TE mode and birefringence at the wavelength of 1.55 μm can be as high as 2951 $\text{W}^{-1}\text{m}^{-1}$ and 0.292219, respectively. This high birefringence can be used to reduce the PMD effect and many other applications such as sensing applications.

5.6 Ultrahigh Nonlinear Polarization Maintaining Rectangle Slotted PCF with Negative Dispersion

Optical properties such as a birefringence, chromatic dispersion, confinement loss, and nonlinear effects are highly important for any communication. PCF are the most promising candidate to achieve desired properties. By tailoring physical parameters including the diameter of the air holes, the shape of the holes, the defect at the center

of the fiber, the number of air hole rings in the area surrounding the core and the spacing between the adjacent air holes, it can be possible to achieve desired properties through the PCF.

5.6.1 Rectangle Slotted PCF Structure

In this section, the rectangular slot is embedded in the center of the core instead of elliptical slot in low index guiding PCF structure. The area of rectangle slot region in this design is kept same as elliptical slot region of first design (explained in section 5.4). The material used in rectangle slot region is silicon nanocrystal and the background material is silicon. Employing the Si-nc rod has many advantages that are as follows. Firstly, tight mode confinement can be achieved with the low index elliptical Si-nc rod with high nonlinear refractive index (n_2), which can ultimately provide ultrahigh nonlinearity. Additionally, the presence of the central rectangle Si-nc slot gives more flexibility to control the chromatic dispersion properties of the fiber and also introduce the asymmetry in the proposed fiber leading to an ultrahigh birefringence. FEM is utilized to examine the transmission properties of the proposed design, such as, the birefringence, chromatic dispersion, effective mode area and the nonlinearity.

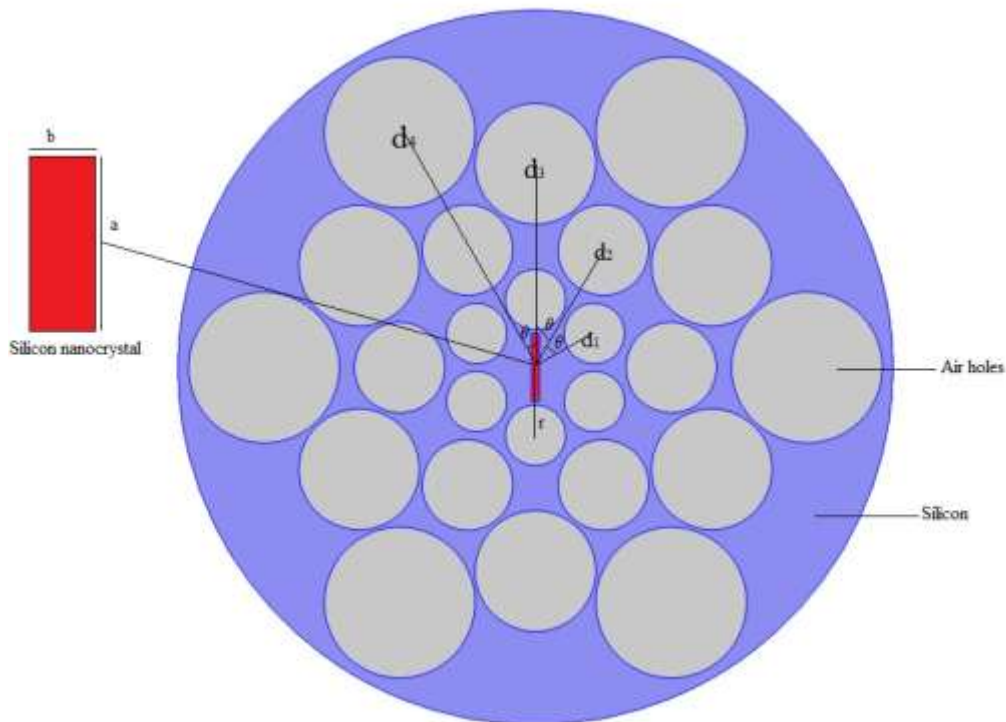


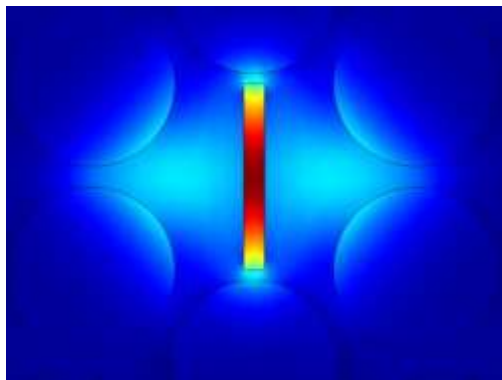
Fig.5.17 Cross sectional view of rectangle slotted PCF (third design)

The proposed rectangle slotted silicon PCF structure is shown in the Fig. 5.17. All the circular air holes of the varying radius in the cladding are arranged in a spiral lattice. To obtain the good mode confinement in the core region, diameters of air holes in cladding region are in increasing order $d_1 < d_2 < d_3 < d_4$ [174]. The spiral lattice structure is having six arms and each arm having four air holes. The distance from center to each air hole of the first ring is r . The air hole in an arm are placed at an angular increment of θ than the previous one. The benefit of using spiral lattice structure is that number of air holes gets reduced compared to the normal triangular lattice, which in turn results in small effective mode area. The background of PCF is silicon which has the high refractive index of 3.48 at $1.55\mu\text{m}$ and nonlinear refractive index of $5 \times 10^{-18} \text{ m}^2/\text{W}$ [13]. Rectangle slot in core region is having height of ' a ' and width of ' b '. Refractive index of Si-nc can be calculated from the Sellemier's equation[216] and nonlinear refractive index is $4.8 \times 10^{-17} \text{ m}^2/\text{W}$ [13].

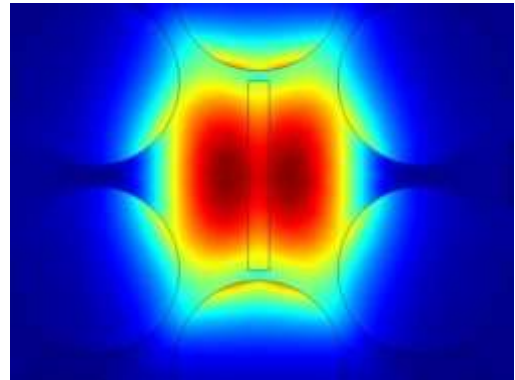
In fig. 5.18(a) and (b), fundamental quasi modes field distribution of fiber at $1.55 \mu\text{m}$ is shown with fiber parameters as presented in table 5.7.

Table 5.7: Rectangle Slotted PCF (design 3) parameter values for vertically aligned slot

Radius (distance between center of slot to center of air hole)	Slot Height	Slot Width	Diameter of air holes of first ring d_1	Diameter of air holes of second ring d_2	Diameter of air holes of third ring d_3	Diameter of air holes of fourth ring d_4
400 nm	450 nm	50 nm	400 nm	600 nm	800 nm	1000 nm



(a)



(b)

Fig. 5.18 Electric field distribution of fundamental quasi modes at $1.55 \mu\text{m}$ wavelength (a) quasi-TE mode (b) quasi-TM mode

The effective index of slow and fast axis modes are 2.7382 and 2.4793, respectively.

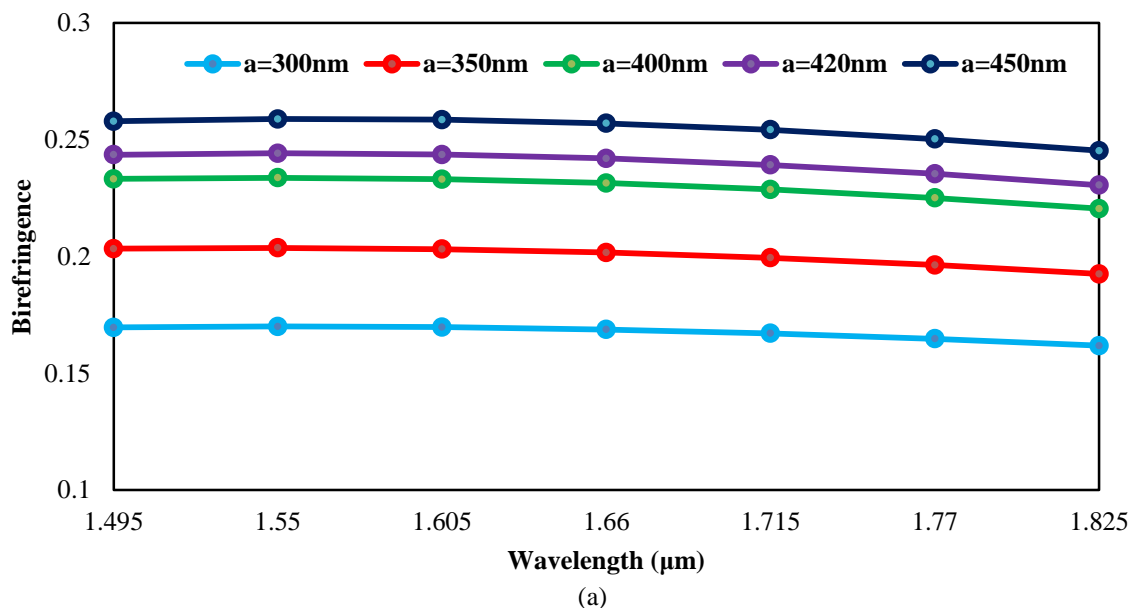
5.6.2 Research Outcomes and Discussion

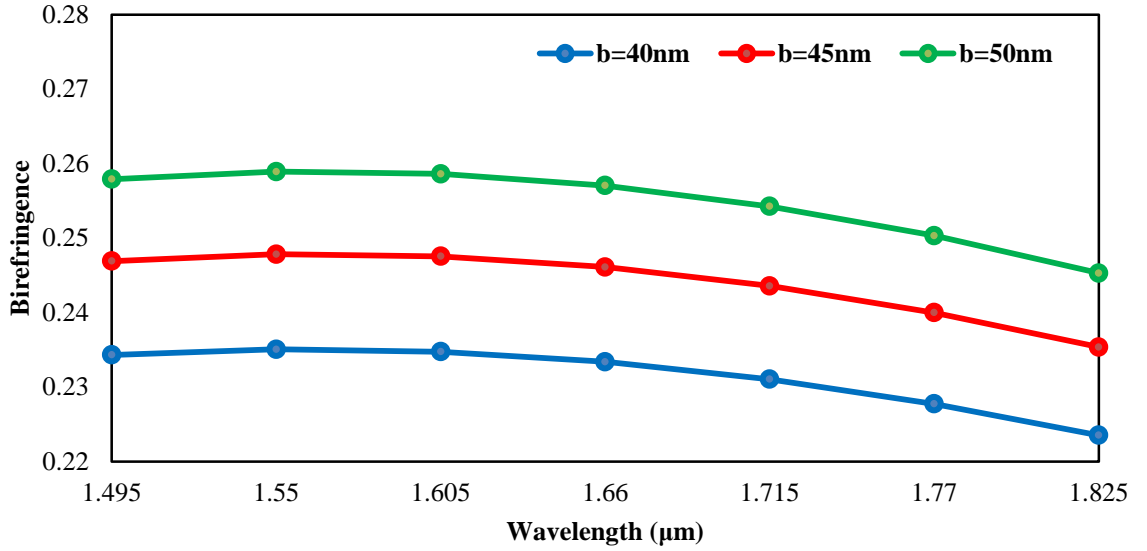
In comparison to the traditional fiber technology, in which the light is propagated having different refractive indices using solid glasses, through PCF technology various new characteristics can be realized. These unique characteristics can define the various applications.

FEM, is utilized to calculate the effective indices of both fundamental polarized modes through solving Maxwell's equation, which is suitable for examining our fiber structure. Through determination of the effective indices, birefringence, the chromatic dispersion, effective mode area and the nonlinear coefficient can be realized.

For the applications such as, coherent optical communication system, fiber optical sensors and interconnection of polarization sensitive devices, maintaining a SOP for large distance is an essential requirement [244]. The polarization state can be maintained by (i) increasing the birefringence deliberately to reduce the power coupling between the linearly polarized modes and (ii) by twisting the fiber, which is having low birefringence, to reduce the coupling between modes [245].

By varying the geometrical parameters of the fiber or by exerting the stress to the core, the high birefringence can be achieved. This high birefringence can be beneficial to reduce the coupling between the modes of degeneration.





(b)

Fig.5.19 Birefringence as a function of wavelength when slot height 'a' and slot width 'b' are varied

From fig.5.19, it is clear that highest birefringence is achieved in this design at $a = 450$ nm and $b = 50$ nm. Maximum birefringence for this design is 0.2589 at 1.55 μm . So the beat length of proposed design at 1.55 μm is 5.99 μm whereas the conventional fiber has beat length in meters. . This small value of beat length makes the fiber useful as a polarization maintaining fiber. If slot height 'a' and slot width 'b' is reduced from optimum value then birefringence decreases. Here, slot height 'a' cannot be increased beyond 450 nm, otherwise it will touch the air holes of first ring. The design is also analyzed for higher values of slot width 'b' but at those values we are not getting birefringence for whole wavelength range from 1.495 μm to 1.825 μm .

The effective area of the fiber core A_{eff} is defined as,

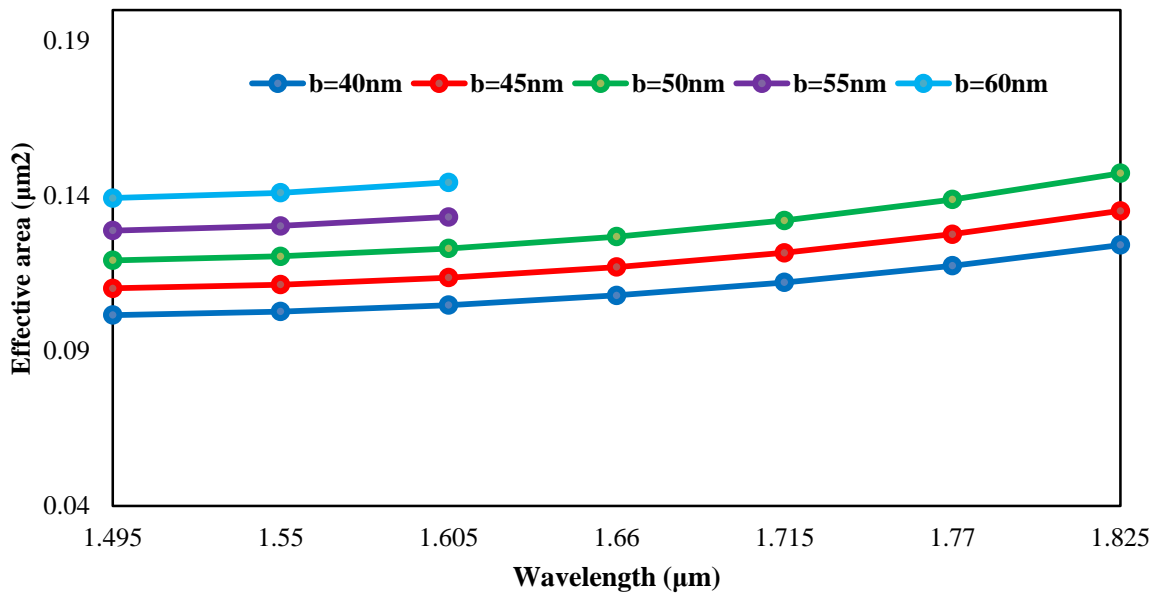
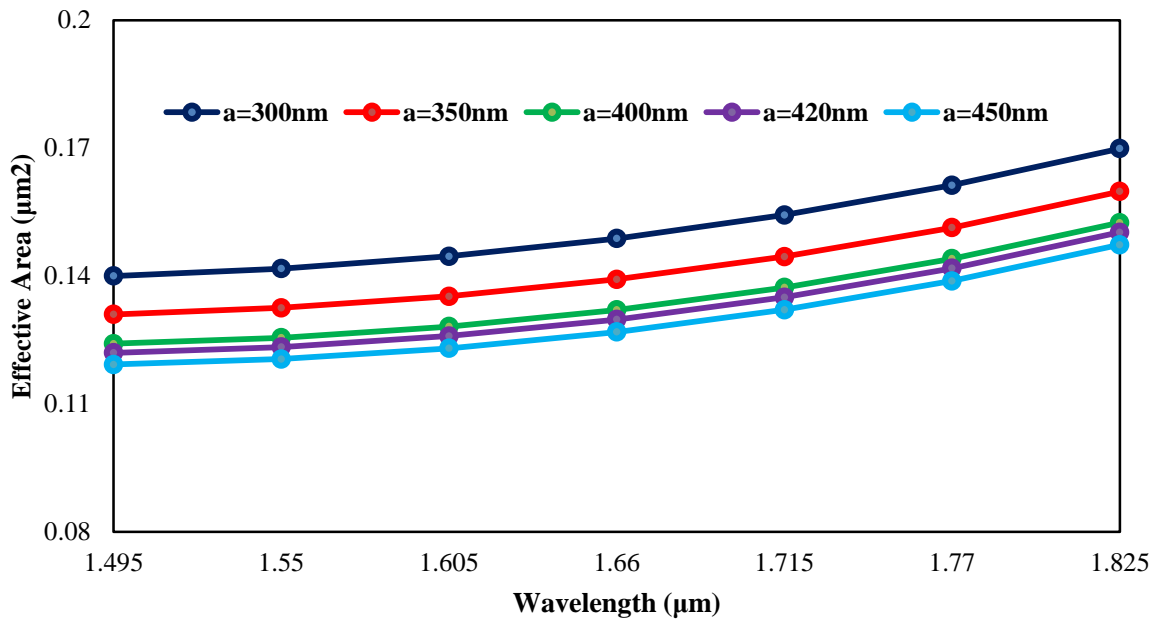
$$A_{eff} = \frac{(\iint_S |E_t|^2 dx dy)^2}{\iint_S |E_t|^4 dx dy} \quad (5.15)$$

Here, E_t denotes the transverse electric field vector and S denotes the whole fiber cross section [128]. When the air-hole size is increased, the mode becomes more confined, and in turn, the effective area and the confinement loss are both reduced. In addition to that, by increasing the number of air-holes rings, the confinement loss can be decreased significantly. On the other hand, the effective mode area is found to be independent of the number of air-holes rings.

The crucial parameter nonlinearity is related to the effective mode area and its parameter is given by:

$$\gamma = \frac{2\pi n_2}{\lambda A_{eff}} \quad (5.16)$$

Here, $n_2 = 5 \times 10^{-18} \text{ m}^2/\text{w}$ is the nonlinear refractive index of silicon material [15]. Stimulation of high nonlinearity can be expected from the PCFs, since they have the capability to confine light with high intensity. Effective mode area is related to the nonlinearity as higher the mode area, the lower will be the effect of nonlinearities.



(a)

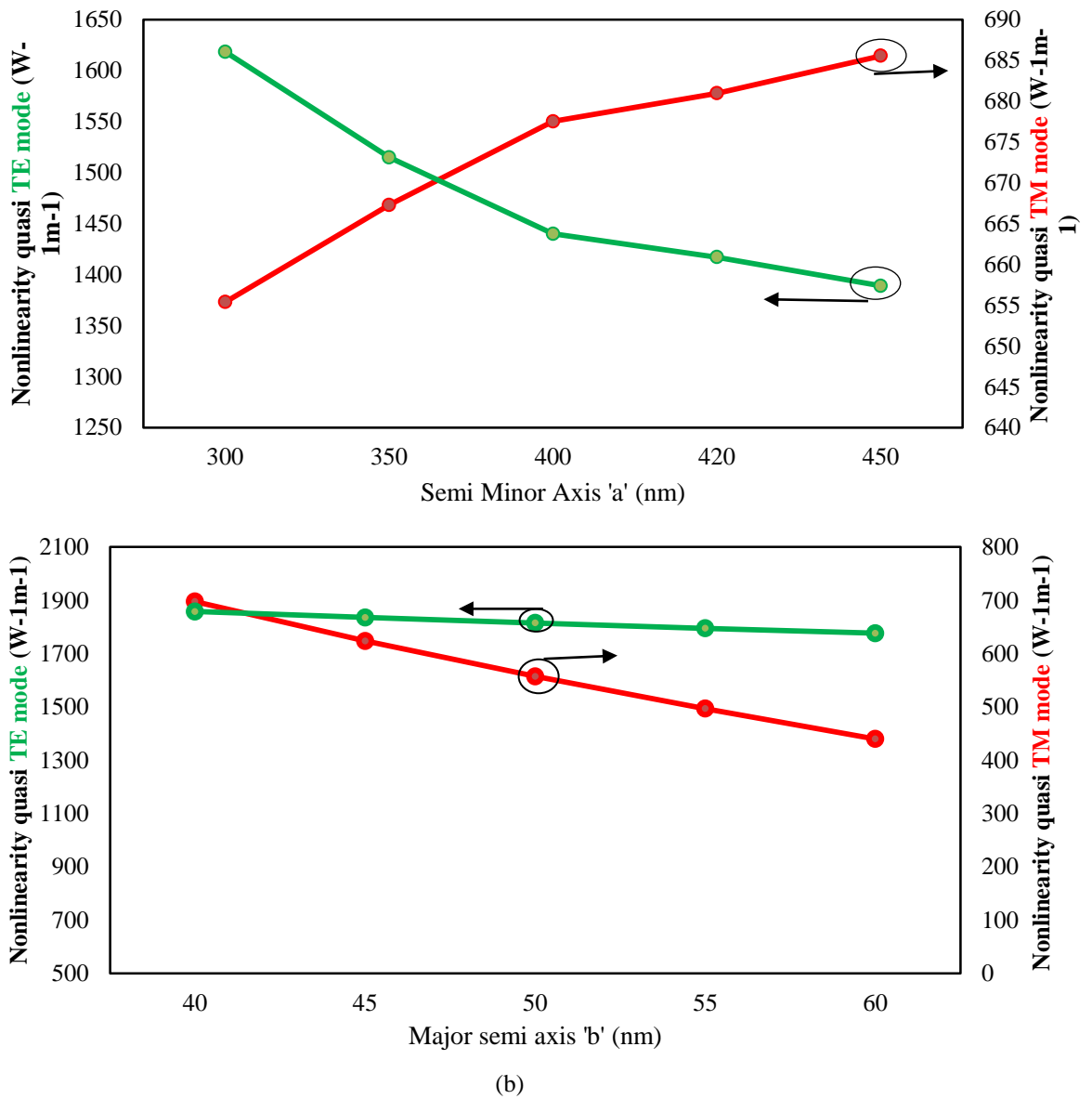


Fig. 5.20 (a) Effective area and Nonlinearity variation with variation in slot height (b) Effective area and Nonlinearity variation with variation in slot width

The variation of effective mode area and nonlinear coefficient with wavelength is shown in Fig. 5.20. Effective area defines the area in which the electric field is confined. The wavelength is related to the effective area and the nonlinearity. As the effective mode area increases with wavelength correspondingly nonlinearity decreases with wavelength. With the low effective mode area and higher index difference, higher nonlinear coefficient can be achieved. The mode area is $0.12 \mu\text{m}^2$ at $1.55 \mu\text{m}$. Fig. 5.20 shows that as the slot height 'a' is increasing, the effective area is decreasing that results in higher nonlinearity. But, if slot width 'b' is increasing the effective area is decreasing, therefore the nonlinearity reduces. For $b = 55 \text{ \& } 60 \text{ nm}$, the light is not

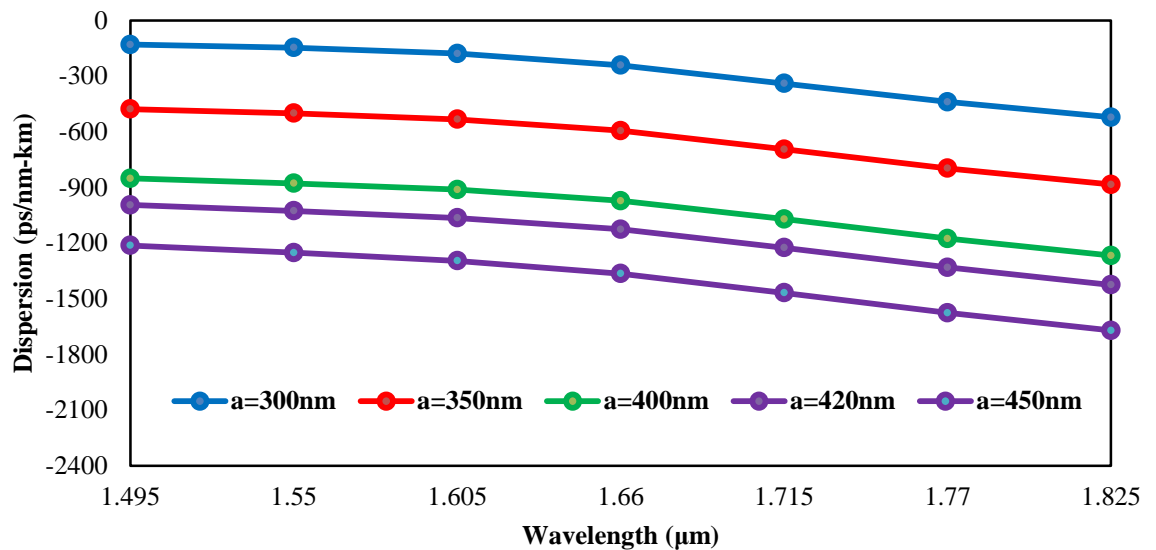
confined beyond 1.605 μm within the core region so we are not getting effective area and nonlinearity for these two values. As the electric field has Gaussian distribution so for large values of 'a', peak value of electric field are well confined within the slot which leads to more nonlinearity. Thus, nonlinearity is more sensitive to the variation in slot height 'a', therefore effective nonlinearity is high. For the slot dimension at which the slotted area of this design and first design are same, nonlinearity up to $1614 \text{ W}^{-1}\text{m}^{-1}$ is obtained.

In optical communication system, information carrying capacity of the PCF is significantly affected by chromatic dispersion of the fiber. Hence, it becomes essential to study the chromatic dispersion behavior in the PCF. Control of chromatic dispersion in PCF generates numerous applications in optical domain such as DCF, nonlinear optics, etc. [86] as PCFs has the property of design flexibility. By varying the air-holes diameter and the air-holes pitch, the chromatic dispersion can be easily controlled. Till now, PCFs with noteworthy dispersion properties have been observed.

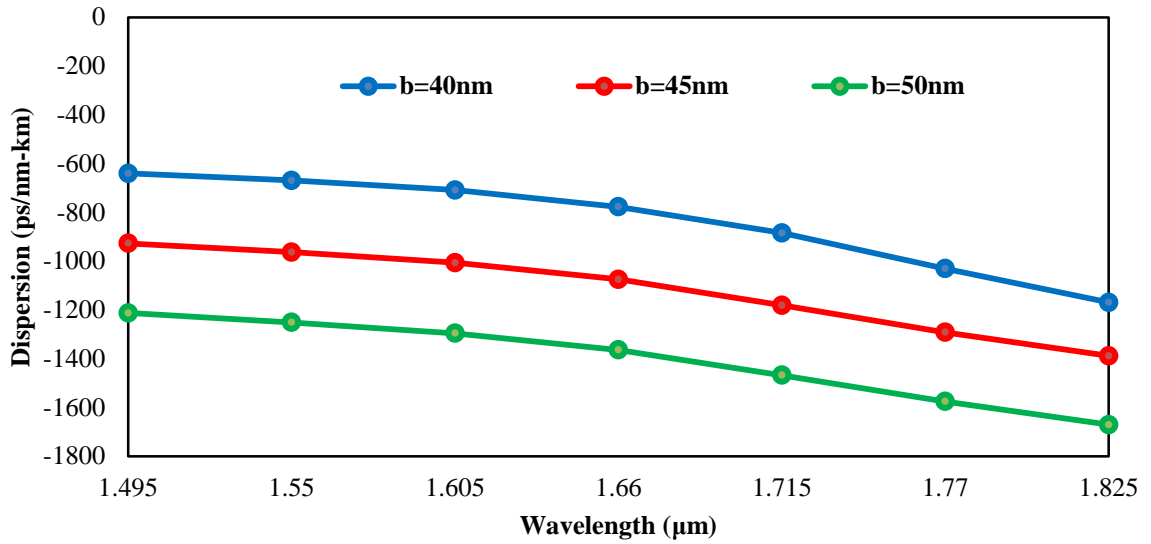
The chromatic dispersion D can be calculated from the effective refractive index of the fundamental mode n_{eff} and it is a second order derivative of refractive index with variation in the wavelength.

$$D = D_m + D_w = -\frac{\lambda}{c} \frac{\partial^2 \text{Re}(n_{eff})}{\partial \lambda^2} \quad (5.17)$$

where c is the velocity of light in a vacuum. The material dispersion using Sellmeier equation is already considered in formulations.



(a)



(b)

Fig.5.21 Dispersion characteristics as a function of wavelength for the PCF with variation in (a) slot height 'a' (b) slot width 'b'

It has been carefully investigated the dispersion behaviour with the variation in slot dimensions that is shown in fig 5.21. If slot height 'a' is increased then more negative dispersion is achieved. Similarly for larger values of slot width 'b', high negative dispersion is achieved. This shows that in slotted PCF structures, the dispersion is mainly determined or depended on waveguide dispersion.

Table 5.8 given below, consists of the comparison of different optical characteristics of the design 1 and design 3.

Table 5.8: Comparison between different designs (design 1 and design 3)

	Birefringence	Nonlinearity	Dispersion
Design 1	0.2503	1348 $W^{-1}m^{-1}$ (Quasi-TE mode)	-1288 ps/nm/km
Design 3	0.2589	1614 $W^{-1}m^{-1}$ (Quasi-TE mode)	-1251 ps/nm/km

Design 3 is not only providing better properties as compared to design 1, but fabrication of rectangle slot is much easier as compared to elliptical slot. It can be observed that the birefringence and nonlinearity achieved in third design is higher compared to the first design. Nevertheless, first design has attained slightly large negative dispersion than the third design. The enhancement of effective nonlinearity realizes the compact nonlinear devices with low power, which offers new possibilities

in the domain of all-optical signal processing. Due to the large birefringence, design also has extensive applications in PMFs, optical fiber sensors, coherent optical communications systems, etc.

5.7 Slot Spiral PCF Application: Nonlinear Optical Signal Processing

With the growing researches in the direction of achieving efficient optical signal processing, ‘green photonics’ is an alternative that has been adopted to gain improved performance with lower costs and energy. The aggrandizing high bandwidth requirement and fast signal transmission have greatly affected the energy consumption and cost factor. Due to the increasing number of Internet users, data and video sharing, data collection systems, cloud computing and data storing have been increased. This huge Internet traffic is likely to grow with the higher-capacity network infrastructures. This issue has raised the concern about power consumption and efficiency of the devices used in the optical network. For tackling this issue, the ‘Green Photonics’ term is coined to induce a wave of advanced technologies and strategies that can ensure the energy efficiency of the devices, lower power consumption, and cost effectiveness. The ‘Green’ term here represents the better optical output at lower power consumption that can help in preventing the loss of environment and resources [221].

Additionally, through having benefits of the unlimited bandwidth of optics and femtosecond response of the materials, the green photonics can improve the transmission of signals by providing fast responses and efficient use of network resources. HNLF in the optical signaling field plays a major role in supporting green photonics solutions [104]. Utilizing the third order or second order nonlinearity with the HNLFs can be crucial for implementing the green photonic solutions [246]. Additionally, to provide green operation through optical signal processing, materials such as Silica, Silicon, periodically poled lithium niobate (PPLN), Bismuth oxide, Chalcogenide, and Tellurite are used to create nonlinear fibers suitable for signal processing. Out of these, silica based HNLFs is one of the most common choices for applications like wavelength conversion, format conversion, and regeneration [247-249].

Optical systems have always been compared to the electronics as both the systems have its pros and cons. Optics is known for performing functions very fast,

and electronics is known to be best for performing complex computations with full accuracy including buffers and memory. In other words, optics provide high speed to the signal and the electronics provide accuracy. In addition to that, as optical signals are spectrally efficient, one can process many bits of information optically at a time. On the other hand, through electronics, memory can be easily accessible, and it is capable of mass integration for signal processing with high accuracy [250]. Another parameters, through which optics and electronics can be compared, have the ability to process a signal at the line rate of optics, quality of the signal (e.g., degradation of signal-to-noise ratio) and power consumption. For power consumption analysis, optical pump powers, nonlinear efficiencies and electronic power consumption have to be undertaken. However, it has to be noted that optical signal processing provides high-speed transmission to the systems with limited functions and applications that need more processing or efforts [251].

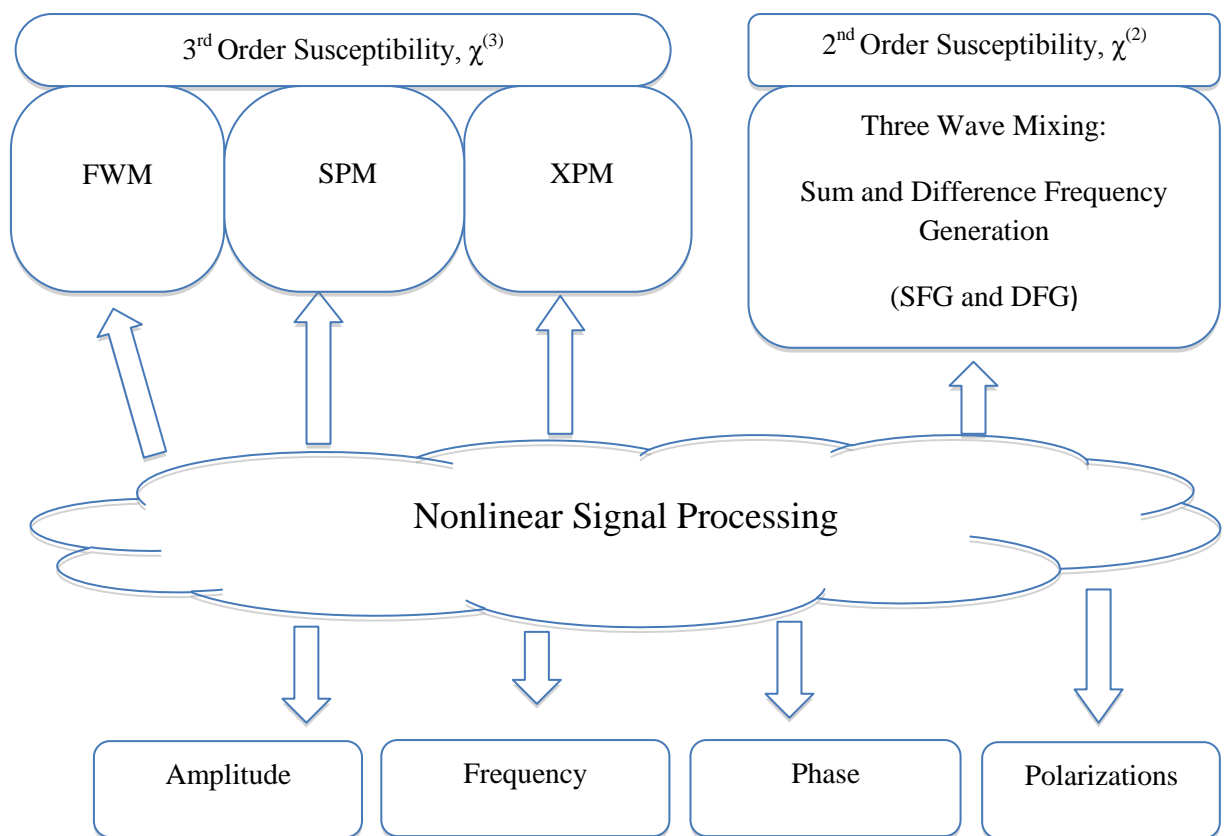


Fig.5.22 Nonlinearities and optical wave parameters used for data encoding and signal processing

Optical signal processing utilizes many physical phenomena and devices. Nonlinear optical phenomena comprise a large part of optical signal processing.

Various useful new effects are originated due to optical nonlinearities in fiber. FWM, SPM, XPM are originated due to third order susceptibility χ^3 (see fig. 5.22). Second order susceptibility χ^2 originated nonlinearities can mix the waves in different forms such as sum frequency generation (SFG), difference frequency generation (DFG) and second harmonic generation (SHG) and cascading of such mixing [252]. Next, various photonic materials and devices can be utilized to process the optical signal. HNLF [253], silicon waveguides [208,254], PCs [255] are some of the material and devices. Third, photonics utilize amplitude, phase, frequency, and polarization of an optical wave for data encoding and signal processing. Fourth are the operations that can be performed by using these phenomena and devices such as regeneration, equalization, multicasting, correlation, FIR filtering, optical FFT and DFT, multiplexing and demultiplexing, optical logic gates, wavelength conversion, tunable delays, etc.

With the use of nonlinear processes, the large potential of green photonics can be ensured as these processes use less number of high power pump lasers [10]. The total energy consumption in the optical network is estimated by the utilization of a number of high-power optical lasers that is required to perform the signal processing. The first high power device is the coupler; it is a device that transfers desirable or undesirable energy from one medium to another medium, for example from one optical fiber to another, from one electronic circuit to another [256]. Another device is filter; it is a circuit capable of selectively filtering a frequency or range of frequencies from a mix of different frequencies in a device. On the other side, amplifier is a device that is used to increase the current, voltage or power and are mainly used in audio equipment's, broadcasting and wireless communication [35]. Use of couplers, filters and high-power amplifiers significantly increase the consumption of power. In this case, the 'green photonics' can be dominant by utilization of nonlinear processes that require a minimum number of high power lasers. In this way, the high power devices can be eliminated from the power source setups. For example, there is a need for N probe lasers for N -fold multicasting, but with highly nonlinear medium and low-dispersion, the parametric gain can be obtained with higher pump powers. This makes the pump quantity $N/2$ for the N fold multicasting. The nonlinear processes suitable for such process are degenerate FWM and XPM. Additionally, for WDM-to-TDM conversion, XPM process is observed to be beneficial for energy compensation as it has the advantage of high efficiency regarding optical bandwidth and needs less

number of pumps. Overall, it is analyzed that wave mixing, or Kerr-effect-based multicasting approaches require less number of laser pumps and have proved to be beneficial for power consumption [222].

Moreover, The HNLFF has to have very high nonlinearity (γ) and low attenuation to attain long effective interaction length. The reason behind increasing nonlinearity is to obtain the applications like SCG, multicasting [257], wavelength conversion, food quality control, in military field [258], de-multiplexing, multiplexing [10], in cancer detection and tunable optical delays [252]. These fields may require the generation of additional frequency elements while propagation, in other words, it can be said as spectrum broadening of the pulse. Additionally, HNLFFs can be classified as by tapered fiber, micro-structured fiber and PCF. With the variation of materials and structural parameters, nonlinearity can be controlled [259]. There are some of the operations that contribute to optical signal processing. These operations are such as wavelength multicasting, multiplexing, and de-multiplexing and tunable optical delays.

Wavelength Multicasting: It is a process that takes use of nonlinearities to make multiple copies of the input signal at different wavelength [260]. For this operation, different nonlinear processes can be adopted such as degenerate FWM, non-degenerate FWM, SCG, etc. These processes can help in generating new signals with the help of HNLFF [261].

Multiplexing and de-multiplexing: The multiplexing process combines multiple signals of different amplitudes, wavelengths, and phase and time slots into one channel [262]. On the other hand, de-multiplexing disjoint data signals from one channel into its original form. The utilization of nonlinear processes such as XPM, FWM in HNLFFs can be done to enable this process. For example, through XPM process in HNLFF, 16 input data channels at 40 Gb/s can be multiplexed to a 640 Gb/s channel and then for de-multiplexing 640 Gb/s channel can be de-multiplexed to 10 Gb/s channels through the same process [263].

Tunable Optical Delays: This is a process, which helps in delaying the optical signal. Tapped-delay line or a finite impulse response filter to process digital applications like discrete Fourier transform, modulation format conversion, etc. and other applications like D/A and A/D conversions, microwave delays, etc. utilizes this concept [34]. This

process is beneficial in providing efficient data traffic for future networks and better filter designs. Also, digital applications include modulation format conversion, equalization, correlation and discrete Fourier transform [264]. Analog applications include microwave photonic applications, D/A and A/D conversions and FIR filtering [265]. This concept works as by sending an input signal at particular wavelength into the HNLF to create a wavelength shifted signal and then this signal is sent to the DCF, through which broadening of signal occurs due to inter-channeling. Due to this, the signal will cause a delay, and it can be as low as 100 fs and as high as 3.6 μ s [266].

Chronically, with the ballooning technological advances, integrated photonics has grabbed a huge attention with its advanced features. It has a cost effective production and easier packaging. Also as it consists of a smaller chip size, it enables faster electro-optic interaction and provides photonic devices that consume less energy [267]. Moreover, integrated photonics provide a better optical signal processing by cascading multiple components on a single chip and so, in turn, it acquires less power density. Integrated photonics also require nonlinearity for signal processing as characteristics like optical power; nonlinear coefficient and nonlinear interaction length are prior things for integrated photonics. In addition to that, due to the short length of integrated devices, nonlinear coefficient has to very high so as to keep the energy consumption very low. The nonlinear coefficient can be kept high as it relies on a nonlinear refractive index of materials and effective mode area [243].

Furthermore, with the growing years, researchers have been in the process to develop new advanced nonlinear material and fiber structures that provide strong light confinement [219]. The materials like silicon, Si nanocrystals (Si-nc or Si-rich oxide) are mainly used for highly nonlinear integrated optical fiber structure [218], [268-270]. The nonlinear refractive index for Silicon and Si-nc is of the order of 10^{-18} and 10^{-16} m^2/W , respectively. The electric field discontinuity at material interfaces and low index highly nonlinear materials have been utilized for providing strong confinement by slotted PCF structure. This provides the opportunity of reducing the effective area more to $0.01 \mu\text{m}^2$. Additionally, slotted PCF have a capability of achieving low dispersion over a wide wavelength band, strong confinement and desirable ZDWs due to the presence of high index contrast and high controlling of chromatic dispersion. Hence, it can be ensured that fiber structure will contribute to the high of its ability to the green photonics as it has proved its potential in the present

market of optical field on the basis of its better confinement and high nonlinear characteristics. More researches have been in underway to improve its cost effectiveness and efficiency in order to make it more penchants towards green photonics.

5.8 Conclusion

The study is concluded that by introducing a low index elliptical or rectangle slot in the core region, ultra high nonlinearity, high birefringence with large negative dispersion can be attained. It is found that by optimizing the fiber parameters, maximum value of nonlinear coefficient of the fundamental quasi-TE mode, birefringence, and dispersion at the wavelength of 1.55 μm can be 2951 $\text{W}^{-1}\text{m}^{-1}$, 0.2922 and 2746 $\text{ps}/(\text{nm}\cdot\text{km})$ is obtained in second design (elliptical slot). Third PCF (rectangle slot) design is providing 1614 $\text{W}^{-1}\text{m}^{-1}$ nonlinearity and 0.2589 birefringence whereas first design (elliptical slot) is providing 1348 $\text{W}^{-1}\text{m}^{-1}$ nonlinearity and 0.2503 birefringence. Also the fabrication of rectangle slot is easier as compared to elliptical slot. Proposed designs have the potential to realize optical signal processing at short length. Also designs can be utilized as PMF, fiber sensor, parametric amplification, DCF etc.

5.9 Summary

In summary, it is observed that low index material PCF structures are providing better results as compared to high index PCF structures. Silicon and silicon nanocrystals are seen to be the better choice as compared to other materials. Here, three designs of slotted spiral PCF have been presented and its optical characteristics are investigated over a wide wavelength range. FEM is used to analyze the performance of the designs. By optimizing the fiber parameters, high nonlinearity, large birefringence and negative dispersion is simultaneously obtained. Although all the designs are providing birefringence of the order of 10^{-1} but second design provides large birefringence as compared to first and third design. In addition to this, large nonlinearity and negative dispersion is provided by all three designs. Finally, all optical signal processing that is related to the proposed research work is explained.

Chapter 6: Conclusion and Future Scope

6.1 Conclusion

In this thesis, theoretical and numerical analysis of optical properties of PCFs are investigated. The increased interest of PCFs has been observed in the optical fiber communications because of its unique properties. As flexible engineering of fiber design is allowed in the PCF, which is an advancement as compared to the traditional SMF. This flexibility in design provides better control over different optical properties such as birefringence, dispersion, and nonlinearity which generates numerous applications.

Recently, index guiding PCFs have emerged as a promising candidate for realization of different applications in the optical domain. It is comprehensively studied because of their effective optical characteristics in different areas of optical systems that are seems to be inconceivable in conventional SMFs. Our research work is divided into two major sections. Firstly, in this thesis, high index guiding PCF structures, which works on the principle of TIR phenomena, were optimized for different optical properties. Next, low index solid core PC structures, which works on the principle of electric field discontinuity, were optimized to further improve the optical properties. The FEM was utilized for solving Maxwell's equations because of its verified reliability and high precision for analyzing the optical properties of PCF. The applications of different PCF geometries are also described, such as HNLF, PMF, and DCF.

Initially, researchers designed the PCF structure in hexagonal shape and optimized the design parameters to obtain the desired optical properties for different applications. In order to further enhance the optical properties and to reduce the confinement loss, octagonal and decagonal structures are found to be beneficial. To further enhance the optical characteristics, researchers started using spiral fiber structure. This structure provides more freedom in tailoring the fiber parameters that results in better light confinement in the core, large negative or positive flattened dispersion with high birefringence. Because of these improved optical characteristics, it became possible to realize different applications at very low fiber length. Along with fiber structures, the material of the fiber also plays a crucial role in realizing the

properties of PCFs. The selection of materials should be such that it is not only compatible with existing fiber structures, but also has to be easily available and cost effective and having a high nonlinear refractive index.

Deformities in the core cladding interface induce random birefringence, in the standard fiber transmission systems, that leads to randomly polarized light. For overcoming such kind of problem, larger uniform birefringence has to be introduced in the fiber. The invention of HNPCF has gained a huge attention of the world because of its ultrahigh nonlinearity and compatibility with the standard SMFs. Its various applications have also been realized keeping in consideration of its ability to guide a strongly confined light through a fiber. The applications are slow/fast light, pulse compression, wavelength conversion, SCG and all optical amplification. It is important to have long distance communication without any distortion but as it is known that dispersion limits the transmission distance and speed and so it is necessary to compensate it for long haul transmission. For this purpose, we need to have a negative dispersion for compensating the broadening of the pulse. In optical transmission the loss depends on the wavelength. So, there is a specific band of wavelength where the signal attenuation is minimum which is known as optical or operating window. The wavelength of operation from the optical window is selected as they offer minimum attenuation.

The attenuation decreases at $1.55 \mu\text{m}$ i.e 0.2 dB/km which is very very low attenuation and repeater spacing and amplifier spacing will be increased and which reduces the cost of the long haul network(like under sea network) and more over all the components like fiber ,amplifier are designed to work at this wavelength.

In the initial phase of our research work, an elliptical spiral high index guiding PCF structure was designed to obtain high birefringence, large nonlinearity with flat negative dispersion. A number of simulations were carried out to attain the optimized outcomes. For achieving the optimized fiber parameters, the air hole diameter and pitch were precisely tailored. The simulation results of the design are found to be quite satisfactory, which further motivated and directed our research work. In the first elliptical spiral PCF design, soft glass SF57 was used as a background material and in this structure first inner ring is having elliptical air holes. To obtain better light confinement in core, diameter of air holes was monotonically increased. By bringing variation in the ellipticity ratio, the optimum results are obtained, such as, average

dispersion of -93.80 ps/nm/km with a deviation of ± 1.5 ps/nm/km and nonlinearity coefficient of 763.485 $W^{-1}km^{-1}$. Also, Birefringence of the order of 10^{-2} is achieved in the proposed design. The achieved negative flattened dispersion over a broad wavelength range in this PCF can be utilized in RDCF. This designed PCF is a potential candidate that can also be utilized in PMF, parametric amplification, SCG, fiber sensor design, fiber loop mirror, etc. Alternatively, By keeping the geometrical design parameters of elliptical spiral PCF, silicon is set in as a background material instead of SF57. In this case, nonlinearity is drastically enhanced and has the value of 14027 $W^{-1}km^{-1}$ at 1.55 μm wavelength, and flat positive dispersion is achieved. But, less birefringence of the order of 10^{-3} is achieved than the previous result.

For obtaining high nonlinearity, large birefringence and large negative dispersion in the fiber, a low index solid core PCF is introduced. Low index guiding PCF structures are gaining much attention from past few years, as these structures can provide better light confinement with high birefringence. The first design of low index PCF has a spiral lattice structure with slot region embedded in the center of the core. Slot region is in an elliptical shape that consists of a low index material such as silicon nanocrystal. It is demonstrated through numerical results that by optimizing the fiber parameters, nonlinearity coefficient of the fundamental modes, birefringence, and dispersion at the wavelength of 1.55 μm can be 1348 $W^{-1}m^{-1}$, 0.2503 and -1228 ps/nm/km respectively. Further enhancement of optical characteristics can be brought in by varying the design parameters. Due to enhanced optical properties, the designed fiber can be an outstanding candidate for all optical nonlinear signal processing with maintaining single polarization, and in nonlinear optics applications. Numerical results of the second design show that nonlinear coefficient of the fundamental mode and birefringence at the wavelength of 1.55 μm can be as high as 2951 $W^{-1}m^{-1}$ and 0.292219 , respectively. This high birefringence can be used to reduce the PMD effect and many other applications such as sensing applications. Due to the improvement of the optical characteristics, the proposed PCF can realize the benefits of various applications at very low length. The size reduction of the fiber will also make it compatible with the PICs. In last design of low index guiding PCF, a rectangular slot is embedded in the center of the core instead of an elliptical slot in spiral PCF design. The area of rectangle slot region in this design is kept same as elliptical slot region of the first design. by optimizing the fiber geometrical parameters, nonlinear coefficient

of the fundamental quasi-TE mode and birefringence at the wavelength of $1.55 \mu\text{m}$ as high as $1614 \text{ W}^{-1}\text{m}^{-1}$ and 0.2589 is achieved, respectively. Beat length of proposed design at $1.55 \mu\text{m}$ is $5.99 \mu\text{m}$ whereas the conventional fiber has beat length in meters. This small value of beat length makes the fiber useful as a polarization maintaining fiber. Thus, from the obtained results, it can be concluded that low index guiding PCF structures can provide tight light confinement as compared to high index guiding PCF structures. Due to tremendous results, proposed designs can realize different applications at very short length.

6.2 Future Scope

Through utilization of the metamaterial in slotted structure, optical intensity can be more than 25 times stronger than a traditional silicon slotted structure. A higher refractive index material is desirable to further improve the optical field intensity inside the low index slot region. The metamaterials have the capability to provide high refractive index at an optical wavelength that is not viable to achieve with ordinary materials.

High propagation loss is induced in the slot structures when the light is strongly confined in the slot. The major reason behind the induction of propagation loss is the imperfections in the structure, such as the introduction of surface roughness during the fabrication process. These randomly generated imperfections produce the scattering loss that makes it difficult for light to travel over long haul distance. To overcome the propagation loss due to imperfections in the structure, dry or wet etching techniques using chemicals can be utilized to smoothen the surfaces.

References:

1. P. St.J. Russell, "Photonic crystal fibers", *Science*, Vol. 299, no. 5605, pp. 358–362, Jan. 2003.
2. C. M. Bowden, J. P. Dowling, H. O. Everitt, Eds., Special issue of *J. Opt. Soc. Am.* Vol. 10, pp. 279, 1993.
3. Pochi Yeh, Amnon Yariv, and Emanuel Marom, "Theory of Bragg fiber", *J. Opt. Soc. Am.* Vol. 68, pp. 1196-1201, 1978.
4. Eli Yablonovitch, "Inhibited Spontaneous Emission in Solid-State Physics and Electronics", *Physical Review Letters*, Vol. 58, no. 20, 18 MAY 1987.
5. Sanjeev John, "Strong localization of photons in certain disordered dielectric super lattices", *Phys. Rev. Letters*, Vol. 58, no. 23, pp. 2486-2489, June 1987.
6. C. M. Bowden, J. P. Dowling, and H. O. Everitt, "Development and applications of materials exhibiting photonic band gaps: Introduction", *J. Opt. Soc. Amer. B, Opt. Phys.*, Vol. 10, no. 2, pp. 280–413, Feb. 1993.
7. P. St. J. Russell, "Photonic crystal fibers", *Journal of Lightwave technology*, Vol. 24, No. 12, Dec. 2006.
8. Russell, Philip S., "Photonic band gaps", *Physics World*, Vol. 5, pp. 37-42, 1992.
9. T. A. Birks, J. C. Knight, and P. St.J. Russell, "Endlessly single mode photonic crystal fiber", *Opt. Lett.*, Vol. 22, no. 13, pp. 961–963, Jul. 1997.
10. J. C. Knight, T. A. Birks, P. St. J. Russell, and J.-P. de Sandro, "Properties of photonic crystal fiber and the effective index model", *J. Opt. Soc. Amer. A, Opt. Image Sci.*, Vol. 15, no. 3, pp. 748–752, Mar. 1998.
11. J. C. Knight, J. Broeng, T. A. Birks, and P. St. J. Russell, "Photonic band gap guidance in optical fibers", *Science*, Vol. 282, no. 5393, pp. 1476–1478, Nov. 1998.
12. R. F. Cregan, B. J. Mangan, J. C. Knight, T. A. Birks, P. St. J. Russell, P. J. Roberts, and D. C. Allan, "Single-mode photonic band gap guidance of light in air", *Science*, Vol. 285, no. 5433, pp. 1537–1539, Sep. 1999.
13. T. Huang, J. Liao, S. Fu, M. Tang, P. Shum and D. Liu, "Slot Spiral Silicon Photonic Crystal Fiber With Property of Both High Birefringence and High Nonlinearity", in *IEEE Photonics Journal*, Vol. 6, no. 3, pp. 1-7, June 2014.
14. Jianfei Liao, Junqiang Sun, Mingdi Du, and Yi Qin, "Highly nonlinear dispersion-flattened slotted spiral photonic crystal fibers", *IEEE Photonics Technology Letters*, Vol. 26, pp. 380-383, 2014.
15. Jianfei Liao, Fan Yang, Yingmao Xie, Xinghua Wang, Tianye Huang, Zuzhou Xiong, Fanguang Kuang, "Ultrahigh birefringent nonlinear slot silicon microfiber with low dispersion", *IEEE Photon. Technol. Lett.*, Vol. 27, pp. 1868-1871, 2015.

16. Vilson R. Almeida, Qianfan Xu, Carlos A. Barrios, and Michal Lipson, "Guiding and confining light in void nanostructure", *Opt. Lett.* Vol. 29, pp. 1209-1211, 2004.
17. Vilson R. Almeida, Qianfan Xu, Roberto R. Panepucci, Carlos A. Barrios, and Michal Lipson, "Light Guiding in Low Index Materials using High-Index-Contrast Waveguides", *Mat. Res. Soc. Symp. Proc.* Vol. 797, pp. 1801-1803, 2004.
18. Qianfan Xu, Vilson R. Almeida, Roberto R. Panepucci, and Michal Lipson, "Experimental demonstration of guiding and confining light in nanometer-size low-refractive-index material", *Opt. Lett.* Vol. 29, pp. 1626-1628, 2004.
19. J. C. Knight, T. A. Birks, R. F. Cregan, P. St.J. Russell, and J.-P. de Sandro, "Large mode area photonic crystal fiber", *Electron. Lett.*, Vol. 34, no. 13, pp. 1347-1348, Jun. 1998.
20. D. Mogilevtsev, T. A. Birks, and P. St.J. Russell, "Group-velocity dispersion in photonic crystal fibers", *Opt. Lett.*, Vol. 23, no. 21, pp. 1662-1664, Nov. 1998.
21. J. C. Knight, J. Arriaga, T. A. Birks, A. Ortigosa-Blanch, W. J. Wadsworth, and P. St. J. Russell, "Anomalous dispersion in photonic crystal fibers", *IEEE Photon. Technol. Lett.*, Vol. 12, no. 7, pp. 807-809, Jul. 2000.
22. A. Ortigosa-Blanch, J. C. Knight, W. J. Wadsworth, J. Arriaga, B. J. Mangan, T. A. Birks, and P. St. J. Russell, "Highly birefringent photonic crystal fibers", *Opt. Lett.*, Vol. 25, no. 18, pp. 1325-1327, Sep. 2000.
23. E.-H. Lee, K. H. Kim, and H. K. Lee, "Nonlinear effects in optical fiber: Advantages and disadvantages for high capacity all-optical communication application", *Opt. Quantum Electron.*, Vol. 34, no. 12, pp. 1167-1174, Dec. 2002.
24. J. Hansryd, P. A. Andrekson, M. Westlund, J. Li, and P.-O. Hedekvist, "Fiber-based optical parametric amplifiers and their applications", *IEEE J. Sel. Topics Quantum Electron.*, Vol. 8, no. 3, pp. 506-520, May/Jun. 2002.
25. A. Baili, Rim Cherif, M. Zghal, Maximizing the bandwidth of coherent, "mid-IR supercontinuum using highly nonlinear a periodic nano fibers", *Journal of Modern Optics*, Vol. 61, iss. 8, pp. 650-661, 2014.
26. V. E. Perlin and H. G. Winful, "All-fiber wavelength conversion using cross-phase modulation and Bragg gratings", *IEEE Photon. Technol. Lett.*, Vol. 14, no. 2, pp. 176-178, Feb. 2002.
27. W. J. Wadsworth, A. Ortigosa-Blanch, J. C. Knight, T. A. Birks, T.-P. M. Man, and P. S. J. Russell, "Supercontinuum generation in photonic crystal fibers and optical fiber tapers: A novel light source", *J. Opt. Soc. Amer., B, Opt. Phys.*, Vol. 19, no. 9, pp. 2148-2155, Sep. 2002.

28. M.A.R. Franco, V.A. Serrão, F. Sircilli, “Microstructured optical fiber for residual dispersion compensation over S + C + L + U wavelength bands”, *IEEE Photon. Technol. Lett.*, Vol. 20, pp. 751–753, 2008.
29. S.F. Kaijage, Y. Namihira, N.H. Hai, F. Begum, S.M.A. Razzak, T. Kinjo, K. Miyagi, N. Zou, “Broadband dispersion compensating octagonal photonic crystal fiber for optical communication applications”, *Jpn. J. Appl. Phys.*, Vol. 48, pp. 052401–052408, 2009.
30. Lou Shu-Qin, Wang Zhi, Ren Guo-Bin and Jian Shui-Sheng, "Polarization-maintaining photonic crystal fiber", *Chinese Physics*, Vol. 13, Number 7, 2004.
31. R. Boufenar, M. Bouamar, A. Hocini, "Numerical analysis of highly birefringent photonic crystal fiber for temperature sensing application", *Photonics and Nanostructures - Fundamentals and Applications*, Vol. 24, Pages 47-52, 2017.
32. M. T. Hill, H. J. Dorren, T. De Vries, X. J. Leijtens, J. H. Den Besten, B. Smalbrugge, Y.-S. Oei, H. Binsma, G.-D. Khoe, and M. K. Smit, “A fast low-power optical memory based on coupled micro-ring lasers”, *Nature Photon*, Vol. 432, pp. 206–209, 2004.
33. K. Nozaki, A. Shinya, S. Matsuo, Y. Suzaki, T. Segawa, T. Sato, Y. Kawaguchi, R. Takahashi, and M. Notomi, “Ultralow-power all optical RAM based on nano cavities”, *Nature Photon.*, Vol. 6, pp. 248–252, 2012.
34. J. Capmany and D. Novak, “Microwave photonics combines two worlds”, *Nature Photon.*, Vol. 1, no. 6, pp. 319–330, Jun. 2007.
35. J. Yao, “Microwave Photonics”, *IEEE Journal of Lightwave Technology*, Vol. 27, no. 3, pp. 314–335, Feb. 2009.
36. Y. Fink, D. J. Ripin, S. Fan, C. Chen, J. D. Joannopoulos, and E. L. Thomas, “Guiding optical light in air using an all-dielectric structure”, *J. Lightwave Technology*, Vol. 17, pp. 2039-2041, 1999.
37. J. C. Knight, T. A. Birks, P. St. J. Russell, “in *Optics of Nanostructured Materials*”, V. A. Markel, T. F. George, Eds. Vol. 11, pp. 39 –71, 2001.
38. C. M. Soukoulis, “*Photonic Crystal and Light Localization in the 21st Century*”, 1st edition, Springer Publication, 2001.
39. J. C. Knight, T. A. Birks, P. St. J. Russell, and D. M. Atkin, “Pure silica single-mode fiber with hexagonal photonic crystal cladding”, presented at the Conf. Optical Fiber Commun. (OFC), San Jose, CA, Mar. 1996.
40. Jan Sporik, Miloslav Filka, Vladimír Tejkal, Pavel Reichert, “Principle of photonic crystal fibers”, Vol.2,No.2, 2011.
41. G. Vienne, Y. Xu, C. Jakobsen, H. J. Deyerl, T. P. Hansen, B. H. Larsen, J. B. Jensen, T. Sørensen, M. Terrel, Y. Huang, R. K. Lee, N. A. Mortensen, J. Broeng, H.

- Simonsen, A. Bjarklev, A. Yariv, "First demonstration of air-silica Bragg fiber", Proc. OFC, 2004.
42. S. D. Hart, G. R. Maskaly, B. Temelkuran, P. H. Prideaux, J. D. Joannopoulos, and Y. Fink, "External reflection from omnidirectional dielectric mirror fibers", Vol. 296, pp. 510-513, 2002.
 43. J. D. Joannopoulos, S. G. Johnson, J. N. Winn, and R. D. Meade, "Photonic Crystals: Molding the Flow of Light", Princeton University Press, second ed., February 2008.
 44. **Poli F., Cucinotta A., Selleri S.**, "Photonic crystal fibers: Properties and Applications", 1st edition, 2007.
 45. J. C. Knight, T. A. Birks, P. S. J. Russell, and D. M. Atkin, "All-silica single-mode optical fiber with photonic crystal cladding", Opt. Lett., Vol. 21, no. 19, pp. 1547–1549, Oct. 1996.
 46. T. A. Birks, J. C. Knight, and P. S. J. Russell, "Endlessly single-mode photonic crystal fiber", Opt. Lett., Vol. 22, no. 13, pp. 961–963, Jul. 1997.
 47. Agrawal, G. P, "Fiber-Optic communication systems", 3rd ed., 2012.
 48. Sadiku, Mathew N. O., "Elements of Electromagnetics", 3rd edition, 2001.
 49. Agrawal, G. P, "Nonlinear Fiber Optics", 5th ed., 2013.
 50. Martin Dybendal Nielsen and Niels Asger Mortensen, "Photonic crystal fiber design based on the V –parameter", Optical Society of America, Vol. 11, pp. 2762-2768, 2003.
 51. N. A. Mortensen, J. R. Folkenberg, M. D. Nielsen, and K. P. Hansen, "Modal cut-off and the V parameter in photonic crystal fibers", Opt. Lett. Vol. 28, pp. 1879-1881, 2003.
 52. M. N. Amin, M. Faisal and M. M. Rahman, "Ultrahigh birefringent index guiding photonic crystal fibers", 2016 IEEE Region 10 Conference (TENCON), Singapore, Vol. 26, pp. 2722-2725, 2016.
 53. Tianyu Yang, Erlei Wang, Haiming Jiang, Zhijia Hu, and Kang Xie, "High birefringence photonic crystal fiber with high nonlinearity and low confinement loss", Opt. Express 23, Vol. 24, pp.8329-8337, 2015.
 54. Sankaran, Vanitha, and Joseph T. Walsh, "Birefringence measurement of rapid structural changes during collagen denaturation", Photochemistry and Photobiology, Vol. 68(6), pp. 846-851, 1998.
 55. Rongfeng Guan, Fulong Zhu, Zhiyin Gan, Dexiu Huang, Sheng Liu, "Stress birefringence analysis of polarization maintaining optical fibers", In Optical Fiber Technology, Vol.11, Issue 3, pp. 240-254, 2005,.

56. F. Shi, Y. Wu, M. Li, Y. Zhao and L. Zhao, "Highly Birefringent Two-Mode Photonic Crystal Fibers With Near-Zero Flattened Dispersion", in *IEEE Photonics Journal*, Vol. 3, no. 6, pp. 1181-1188, Dec. 2011.
57. Kazunori Suzuki, Hirokazu Kubota, Satoki Kawanishi, Masatoshi Tanaka, and Moriyuki Fujita, "Optical properties of a low-loss polarization-maintaining photonic crystal fiber", *Opt. Express*, Vol. 9, pp. 676-680, 2001.
58. X. Chen, M.-J. Li, N. Venkataraman, M.T. Gallagher, W.A. Wood, A.M. Crowley, J.P. Carberry, L.A. Zenteno, K.W. Koch, "Highly birefringent hollow-core photonic bandgap fiber", *Opt. Express*, Vol. 12, pp. 3888–3893, 2004.
59. T. Ritari, H. Ludvigsen, "Experimental study of polarization properties of highly birefringent photonic crystal fibers", *Opt. Express*, Vol. 12, pp. 5931–5939, 2004.
60. D. Chen, L. Shen, "Ultrahigh birefringent photonic crystal fiber with ultralow confinement loss", *Photon. Technol. Lett.* Vol. 19, pp. 185–187, 2007.
61. T.P. Hansen, J. Broeng, S.E.B. Libori, E. Knudsen, A. Bjarklev, J.R. Jensen, H. Simonsen, "Highly birefringent index-guiding photonic crystal fibers", *Photon. Technology Lett.* Vol. 13, pp. 588–590, 2001.
62. D. Marcuse, *Light Transmission Optics* (Van Nostrand Reinhold, 1982), Chaps 8 and 12.
63. R. P. Khare, "Fiber optics and optoelectronics", 1st edition, Oxford press, 2004.
64. Gerd Keiser, "Optical fiber communication", 5th edition, Tata Mcgraw Hill Education Press, 2013.
65. Govind P. Agrawal and M. J. Potasek, "Nonlinear pulse distortion in single-mode optical fibers at the zero-dispersion wavelength", *Phys. Rev.* Vol. 33, 1765 – Published 1 March 1986.
66. A. W. Snyder and J. D. Love, "Optical Waveguide Theory", 1st edition, Springer Publication, 1983.
67. M. J. Adams, "An Introduction to Optical Waveguides", 1st edition, John Wiley & Sons, 1981.
68. B. J. Ainslie and C. R. Day, "Optoelectronic Technology and Lightwave Communications Systems", 1st edition, Springer Publication, 1986.
69. Y.S. Kivshar, G.P. Agrawal, "Optical solitons—from fibers to photonic crystals", Academic Press, SanDiego, 2003.
70. B. B. Tiwari, V. Prakash, V. Tripathi, and N. Malaviya, "Nonlinear effects in optical fiber transmission system", *IETE Tech. Rev.*, Vol. 16, no. 5–6, pp. 461–479, Sep.–Dec. 1999.
71. R. Boyd, *Non Linear Optics*. San Diego, CA: Academic, 1992.

72. H. A. Haus, *Waves and Fields in Optoelectronics*. Englewood Cliffs, NJ: Prentice-Hall, ch. 10, 1984.
73. J. Toulouse, "Optical Nonlinearities in Fibers: Review, Recent Examples, and Systems Applications", *Journal of Lightwave Technology*, Vol. 23, no. 11, pp. 1161-1165, November 2005.
74. R. H. Stolen and C. Lin, "Self-phase modulation in silica optical fibers", *Phys. Rev., A*, Vol. 17, no. 4, pp. 1448, 1978.
75. J. M. Dudley, A. C. Peacock, and G. Millot, "The cancellation of nonlinear and dispersive phase components on the fundamental optical fiber soliton: A pedagogical note", *Opt. Commun.*, Vol. 193, no. 1–6, pp. 253–259, Jun. 15, 2001.
76. M. N. Islam, L. F. Mollenauer, R. H. Stolen, J. R. Simpson, and H. T. Shang, "Cross-phase modulation in optical fibers", *Opt. Lett.*, Vol. 12, no. 8, p. 625, Aug. 1987.
77. R. H. Stolen and A. Ashkin, "Optical Kerr effect in glass waveguides", *Appl. Phys. Lett.*, Vol. 22, no. 6, p. 294, Mar. 1973.
78. Q. Lin and G. P. Agrawal, "Vector theory of cross-phase modulation: Role of nonlinear polarization rotation", *IEEE J. Quantum Electron.*, Vol. 40, no. 7, pp. 958–964, Jul. 2004.
79. K. Vilhelmsson, "Simultaneous forward and backward Raman scattering in low-attenuation single-mode fibers", *J. Lightwave Technol.*, Vol. LT-4, no. 4, pp. 400–404, Apr. 1986.
80. D. C. Johnson, K. O. Hill, B. S. Kawasaki, and D. Kato, "Tunable Raman fiber optic laser", *Electron. Lett.* Vol. 13, no. 2, p. 53, Jan. 1977.
81. E. P. Ippen and R. H. Stolen, "Stimulated Brillouin scattering in optical fibers", *Appl. Phys. Lett.*, Vol. 21, no. 11, p. 539, Dec. 1972.
82. Niels Asger Mortensen, "Effective area of photonic crystal fibers", *Opt. Express*, Vol. 10, pp. 341-348, 2002.
83. Govind P. Agrawal, "Nonlinear fiber optics: its history and recent progress [Invited]", *J. Opt. Soc. Am. B*, Vol. 28, pp. A1-A10, 2011.
84. K. Kurokawa, K. Tajima, K. Tsujikawa, and K. Nakajima, "Reducing the losses in photonic crystal fibres", in *Proc. European Conference on Optical Communication ECOC 2005*, Glasgow, Scotland, Sept. 25–29, 2005.
85. Md. Mahbub Hossain and Md. Maniruzzaman, "Analysis of dispersion and confinement loss in photonic crystal fiber", *ICEEICT*, 2014
86. Philip St.J. Russell, "Photonic-Crystal Fibers", *Journal of Lightwave Technology*, Vol. 24, no. 12, pp. 358-362, 2006.

87. Aihan-Yin, Lei Xiong, "Highly nonlinear with low confinement losses square photonic crystal fiber based on a four-hole unit", *Infrared Physics & Technology*, Vol. 66, pp. 29-33, 2014
88. Pranaw Kumar, Rohan, Vikash Kumar, Jibendu Sekhar Roy, "decagonal photonic crystal fibers with negative dispersion and low confinement loss", *Optik - International Journal for Light and Electron Optics*, Vol. 144, pp. 363-369, 2017.
89. P. J. Roberts, F. Couny, H. Sabert, B. J. Mangan, D. P. Williams, L. Farr, M. W. Mason, A. Tomlinson, T. A. Birks, J. C. Knight, and P. St.J. Russell, "Ultimate low loss of hollow-core photonic crystal fibers", *Opt. Express*, Vol. 13, no. 1, pp. 236–244, 2005.
90. Buczynski, R. Photonic Crystal Fibers, *Acta Physica Polonica A*, Vol. 106(2), pp. 141-167, 2004.
91. D. J. Richardson, F. Poletti, J. Y. Y. Leong, X. Feng, H. Ebendorff Heidepriem, V. Finazzi, K. E. Frampton, S. Asimakis, R. C. Moore, J. C. Baggett, J. R. Hayes, M. N. Petrovich, M. L. Tse, R. Amezcua, J. H. V. Price, N. G. R. Broderick, P. Petropoulos, and T. M. Monro, "Advances in microstructured fiber technology", in *Proc. IEEE/LEOS Workshop on Fibers and Optical Passive Components WFOPC 2005*, Palermo, Italy, June 22–24, 2005.
92. Z. Guiyao, H. Lantian, H. Zhiyun and L. Shuguang, "A Novel Method for the Fabrication of Photonic Crystal Fiber", 2006 International Conference on Communications, Circuits and Systems, Guilin, 2006, Vol. 28, pp. 1958-1960.
93. Zhou Guiyao, Hou Zhiyun, Li Shuguang, and Hou Lantian, "Fabrication of glass photonic crystal fibers with a die-cast process", *Appl. Opt.* Vol. 45, pp. 4433-4436, 2006.
94. R. T. Bise and D. J. Trevor, "Sol-gel derived microstructured fiber: fabrication and characterization", *OFC/NFOEC Technical Digest. Optical Fiber Communication Conference*, Vol. 3, pp. 3, 2005.
95. J.B. MacChesney, D. W. Johnson, S. Bhandarkar, M.P. Bohrer, J.W.F leming, E.M.M onberg, and D.J.T revor, "Optical fibers by a hybrid process using sol-gel silica over cladding tubes", *IN on-Cyst. Solids*, Vol. 226 (3), pp. 232-238, 1998.
96. T. Monro, "High nonlinearity extruded single-mode optical fiber", presented at the *Optical Fiber Communications conference*, Anaheim, 2002.
97. T. Schreiber, F. Röser, O. Schmidt, J. Limpert, R. Iliew, F. Lederer, A. Petersson, C. Jacobsen, K. P. Hansen, J. Broeng, and A. Tünnermann, "Stress-induced single-polarization single-transverse mode photonic crystal fiber with low nonlinearity", *Opt. Express* Vol. 13, pp. 7621-7630 (2005).

98. J. Noda, K. Okamoto and Y. Sasaki, "Polarization-maintaining fibers and their applications", in *Journal of Lightwave Technology*, Vol. 4, no. 8, pp. 1071-1089, Aug 1986.
99. K.-H. Tsai, K.-S. Kim, and T. F. Morse, "General solution for stress induced polarization in optical fibers", *J. Lightwave Technol.*, Vol. 9, pp. 7–17, Jan. 1991.
100. K. Tajima and Y. Sasaki, "Transmission loss of a 125 m diameter PANDA fiber with circular stress-applying parts", *J. Lightwave Technol.*, Vol. 7, pp. 674–679, Apr. 1989.
101. M. Samiul Habib , M. Selim Habib , M.I. Hasan , S.M.A. Razzak, "A single mode ultra-flat high negative residual dispersion compensating photonic crystal fiber", *Optical Fiber Technol.*, Vol. 20, pp. 328–332, 2014.
102. Xuyou Li, Pan Liu, Zhenlong Xu, and Zhiyong Zhang, "Design of a pentagonal photonic crystal fiber with high birefringence and large flattened negative dispersion", *Appl. Opt.* Vol. 54, pp. 7350-7357, 2015.
103. Dudley, J. M., Genty, G. & Coen, S., "Supercontinuum generation in photonic crystal fiber", *Rev. Mod. Phys.* Vol. 78, pp. 1135-1184, 2006.
104. A. E. Willner, S. Khaleghi, M. R. Chitgarha and O. F. Yilmaz, "All-Optical Signal Processing", *Journal of Lightwave Technology*, Vol. 32, no. 4, pp. 660-680, Feb.15, 2014.
105. M. R. Karim, B. M. A. Rahman, Y. O. Azabi, A. Agrawal, and Govind P. Agrawal, "Ultrabroadband mid-infrared supercontinuum generation through dispersion engineering of chalcogenide microstructured fibers", *J. Opt. Soc. Am. B* Vol. 32, pp. 2343-2351, 2015.
106. Wanjun Bi, Juanjuan Gao, Xia Li, Liangming Xiong, and Meisong Liao, "Mid-infrared supercontinuum generation in silica photonic crystal fibers", *Appl. Opt.* Vol. 55, pp. 6355-6362, 2016.
107. A. G. N. Chaitanya, Than Singh Saini, Ajeet Kumar and Ravindra Kumar Sinha, "Ultra broadband mid-IR super-continuum generation in Ge_{11.5}As₂₄Se_{64.5} based chalcogenide graded-index photonic crystal fiber: design and analysis", *OSA*, Vol. 55, No. 36, pp. 2011-2014, 2016.
108. D. V. Skryabin, F. Luan, J. C. Knight, P. St. J. Russell, "Soliton Self-Frequency Shift Cancellation in Photonic Crystal Fibers", Vol. 301, pp. 1705-1708 2003.
109. Do Thanh Thuy, Nguyen Thanh Vinh, Bui Dinh Thuan, Cao Long Van, "Influence of Self-steepening and Higher Dispersion Effects on the Propagation Characteristics of Solitons in Optical Fibers", Vol. 22, No. 4, pp. 239-243, 2016.
110. S. P. Singh, R. Gangwar, and N. Singh, "Nonlinear Scattering Effects In Optical Fibers", *Progress In Electromagnetics Research*, Vol. 74, pp. 379–405, 2007.
111. D. T. Reid, I. G. Cormack, W. J. Wadsworth, J. C. Knight and P. S. J. Russell,

- "Soliton self-frequency shift effects in photonic crystal fiber", *Lasers and Electro-Optics*, Vol.1, pp. 456, 2002.
112. P.St.J. Russell, J.C. Knight, T.A. Birks, B.J. Mangan and W.J. Wadsworth, "Recent Progress in Photonic Crystal Fibres", Optical Society of America, 2000.
 113. R. Scarmozzino, A. Gopinath, R. Pregla, S. Helfert, *IEEE J. Selected Topics in Quantum Electronics* Vol. 6, No. 150, pp. 1161-1162, 2000.
 114. W. J. Wadsworth; J. C. Knight; A. Ortigosa-Blanch; B. J. Mangan; P. St. J. Russell, "Soliton propagation at short wavelengths in photonic crystal fibres", Vol. 28, pp. 241 – 242, IEEE Conference Publications, 2000.
 115. N. Nishizawa and T. Goto, "Widely wavelength-tunable ultrashort pulse generation using polarization maintaining optical fibers", *IEEE Journal of Selected Topics in Quantum Electronics*, Vol. 7, No. 4, pp. 518-524, 2001.
 116. Albert Ferrando, Enrique Silvestre, and Pedro Andrés, "Designing the properties of dispersion-flattened photonic crystal fibers", Optical Society of America, Vol.9, pp. 687-697, 2001.
 117. K. P. Hansen, J. R. Jensen, C. Jacobsen, H. R. Simonsen, J. Broeng, P. M. W. Skovgaard, A. Petersson, and A. Bjarklev, "Highly Nonlinear Photonic Crystal Fiber with Zero-Dispersion at 1.55 μm ," in *Optical Fiber Communications Conference*, A. Sawchuk, ed., Vol. 70 of OSA Trends in Optics and Photonics (Optical Society of America, 2002), paper FA9..
 118. W.H. Reeves, J.C. Knight, and P.St.J. Russell, "Demonstration of ultra-flattened dispersion in photonic crystal fibers", Optical Society of America, Vol. 10, No. 14, pp. 791-795, 2002.
 119. B.P. Pal and K. Pande, "Optimization of a dual-core dispersion slope compensating fiber for DWDM transmission in the 1480-1610 nm band through G.652 single-mode fibers", *Opt. Commun.*, Vol. 201, pp. 335–344, 2002.
 120. K. P. Hansen, "Dispersion flattened hybrid-core nonlinear photonic crystal fiber", *Opt. Express*, Vol. 11, pp.1503–1509, 2003.
 121. L. P. Shen, W.-P. Huang, G. X. Chen, and S. S. Jian, "Design and Optimization of Photonic Crystal Fibers for Broad-Band Dispersion Compensation", *IEEE Photonics Technology Letters*, Vol. 15, No. 4, pp. 981-985, April 2003.
 122. A. Peyrilloux, T. Chartier, A. Hideur, L. Berthelot, G. Melin, S. Lempereur, D. Pagnoux, P. Roy, "Theoretical and experimental study of the birefringence of a photonic crystal fiber", *Journal of Lightwave Technology*, Vol. 21, pp. 536, 2003.
 123. F. Poli, A. Cucinotta, S. Selleri, and A. H. Bouk, "Tailoring of flattened dispersion in highly nonlinear photonic crystal fibers", *IEEE Photon. Technol. Lett.*, Vol. 16, pp. 1065–1067, 2004.

124. F. Gérôme, J.L. Auguste, S. Février, J. Maury, J.M. Blondy, L. Gasca, and L. Provost, "Dual concentric core dispersion compensating fiber optimized for WDM application", *Elec. Lett.* Vol. 41, pp. 116-117, 2005.
125. P. R. Chaudhuri, V. Paulose, Chunliu Zhao, Chao Lu, "Near-elliptic core polarization-maintaining photonic crystal fiber: modeling birefringence characteristics and realization", *IEEE Photonics Technology Letters*, Vol. 16, No. 5, pp. 1301-1303, 2004.
126. F. Poletti, V. Finazzi, T. M. Monro, and N. G. R. Broderick, "Inverse design and fabrication tolerances of ultra-flattened dispersion holey fibers", *Opt. Express*, Vol. 13, pp. 3728–3736, 2005.
127. T. Wu and C. Chao, "A novel ultra-flattened dispersion photonic crystal fiber", *IEEE Photon. Technol. Lett.* Vol. 17, pp. 67–69, 2005.
128. Kunimasa Saitoh and Masanori Koshiba, "Numerical Modeling of Photonic Crystal Fibers", *Journal of Lightwave Technology*, Vol. 23, No. 11, pp. 3580, 2005.
129. Aleksandr V. Mitrofanov, Yaroslav M. Linik, Ryszard Buczynski, Dariusz Pysz, Dusan Lorenc, Ignac Bugar, Anatoly A. Ivanov, Mikhail V. Alfimov, Andrei B. Fedotov, and Aleksei M. Zheltikov, "Highly birefringent silicate glass photonic-crystal fiber with polarization-controlled frequency-shifted output: A promising fiber light source for nonlinear Raman micro spectroscopy", *Optical Society of America*, Vol. 14, No. 22, pp. 10645-10651, 2006.
130. J. Florous, K. Saitoh, and M. Koshiba, "The role of artificial defects for engineering large effective mode area, flat chromatic dispersion and low leakage losses in photonic crystal fibers: Towards high-speed reconfigurable transmission platforms", *Opt. Express*, Vol. 14, pp. 901-913, 2006.
131. Gundu K M, Kolesik M, Moloney J V, "Ultra-flattened-dispersion selectively liquid-filled photonic crystal fibers", *Opt. Express*, Vol. 14, pp. 6870-6878, 2006.
132. Songbae Moon, Aoxiang Lin, Bok Hyeon Kim, Pramod R. Watekar, Won-Taek Han, "Linear and nonlinear optical properties of the optical fiber doped with silicon nanoparticles", *Journal of Non-Crystalline Solids*, Vol. 354, pp. 602-606, 2007.
133. S.M. Abdur Razzak, Y. Namihira and F. Begum, "Ultra-flattened dispersion photonic crystal fibre", *Institution of Engineering and Technology*, 2007 Vol. 43, No. 11, pp. 512-517, 2007.
134. Arismar Cerqueira S. Jr, J. M. Chavez Boggio, A. A. Rieznik, H. E. Hernandez-Figueroa, H. L. Fragnito, and J. C. Knight, "Highly efficient generation of broadband cascaded four-wave mixing products", *Optical Society of America*, Vol. 16, No. 4, pp. 2816-2828, 2008.
135. Zheng Zheng, Muddassir Iqbal, Jiansheng Liu, "Dispersion characteristics of SOI-

- based slot optical waveguides”, *Optics Communications*, Vol. 281, pp. 5151-5155, 2008.
136. Chen Ming, Yang Si-gang, Yin Fei-fe, Chen Hong-wei, and Xie Shi-zhong, “Design of a new type high birefringence photonic crystal fiber”, *Optoelectronics Letters*, Vol.4 No.1, pp. 661-665, 2008.
 137. Feroza Begum, Yoshinori Namihira, S.M. Abdur Razzak, Shubi Kaijage, Nguyen Hoang Hai, Tatsuya Kinjo, Kazuya Miyagi, Nianyu Zou, “Design and analysis of novel highly nonlinear photonic crystal fibers with ultra-flattened chromatic dispersion”, Vol. 282, pp. 1416–1421, 2009.
 138. F. Begum, Y. Namihira, S. F. Kaijage, S.M.A. Razzak, N. H. Hai, T. Kinjo, K. Miyagi, and N. Zou, “Design of Broadband Dispersion Compensating Photonic Crystal Fibers for High Speed Transmission Systems”, *Optical Society of America*, 2009.
 139. L. An, Z Zheng, Z. Li, T. Zhou, and J. Chen, “Ultrahigh birefringent photonic crystal fiber with ultralow confinement loss using four air holes in the core”, *J. Lightwave Technol.* Vol. 20 No.15, pp. 3175–3180, 2009.
 140. H. Ademgil, S. Haxha, “Highly nonlinear birefringent photonic crystal fiber”, *Optics Communications*, Vol. 282, No. 14, pp. 2831-2835, 2009.
 141. Lin An, Zheng Zheng, Zheng Li, Tao Zhou, Jiangtao Cheng, “Ultra-wideband single-polarization single-mode, high nonlinearity photonic crystal fiber”, Vol. 282, No. 16, pp. 3266-3269, 2009.
 142. Ya-Ni Zhang, Li-Yong Ren, Yong-Kang Gong, Xiao-Hui Li, Lei-Ran Wang, and Chuan-Dong Sun, “Design and optimization of highly nonlinear low-dispersion crystal fiber with high birefringence for four-wave mixing”, *Optical Society of America*, Vol. 49, No. 16, pp. 3208-3214, 2010.
 143. Lin Zhang, Yang Yue, Yinying Xiao-Li, Jian Wang, Raymond G. Beausoleil, and Alan E. Willner, “Flat and low dispersion in highly nonlinear slot waveguides”, *Optical Society of America*, Vol. 18, No. 12, pp. 13187-13193, 2010.
 144. Lin Zhang, Yang Yue, Raymond G. Beausoleil, and Alan E. Willner, “Flattened dispersion in silicon slot waveguides”, *Optical Society of America*, Vol. 18, No. 19, pp. 20529-20534, 2010.
 145. Yongmin Jung, Gilberto Brambilla, Kyunghwan Oh, and David J. Richardson, “Highly birefringent silica microfiber”, *Optics Letters*, Vol. 35, No. 3, pp. 378-380, 2010.
 146. Yoshinori Namihira, Jingjing Liu, Taito Koga, Feroza Begum, Md. Anwar Hossain, Nianyu Zou, Shubi F. Kaijage, Yuki Hirako, Hiroki Higa, Md. Asrafur Islam, “Design of highly nonlinear octagonal photonic crystal fiber with near-zero flattened

- dispersion at 1.31 μ m waveband”, Optical Society of America, Vol. 18, No. 6, pp. 436–440, 2011.
147. Ali Rostami and Hadi Soofi, “Correspondence between Effective Mode Area and Dispersion Variations in Defected Core Photonic Crystal Fibers” Journal of Lightwave Technology, Vol. 29, no. 2, pp. 467-470, 2011.
 148. Huizhen Xu, Jian Wu, Kun Xu, Yitang Dai, and Jintong Lin, “Highly nonlinear all-solid photonic crystal fibers with low dispersion slope”, Optical Society of America, Vol. 51, No. 8, pp. 1021-1027, 2012.
 149. Md. Selim Habib, Md. Samiul Habib, S.M.A. Razzak, M. A. G. Khan, “Design of Broadband Dispersion Compensating Photonic Crystal Fiber”, International Journal of Engineering and Technology, Vol. 4, pp. 384-394, 2012.
 150. So Eun Kim, Bok Hyeon Kim, Chung Ghiu Lee, Sejin Lee, Kyunghwan Oh, and Chul-Sik Kee, “Elliptical defected core photonic crystal fiber with high birefringence and negative flattened dispersion”, Optical Society of America, Vol. 20, No. 2, pp. 1385-1391, 2012.
 151. Chengcheng Gui and Jian Wang, “Elliptical–Spiral Photonic Crystal Fibers With Wideband High Birefringence, Large Nonlinearity, and Low Dispersion”, Vol. 4, No. 6, pp. 776-780, 2012.
 152. Ming Zhu, Hong, Jun Liu, Xuefeng Li, Nan Huang, Qibing Sun, Jin Wen, and Zhaolu Wang, “Ultra broadband flat dispersion tailoring of dual-slot silicon waveguides”, Optical Society of America, Vol. 20, No. 14, pp. 15899-15907, 2012.
 153. Md. Asiful Islam and M. Shah Alam, “Design Optimization of Equiangular Spiral Photonic Crystal Fiber for Large Negative Flat Dispersion and High Birefringence”, Journal Of Lightwave Technology, Vol. 30, No. 22, pp. 3545-3551, 2012.
 154. Sejin Lee, Woosung Ha, Iyoung Park, Soan Kim, Kyunghwan Oh, “A new design of low-loss and ultra-flat zero dispersion photonic crystal fiber using hollow ring defect”, Optics Communications, Vol. 285, No. 20, pp. 4082-4087, 2012.
 155. Mariusz Klimczak, Grzegorz Stepniewski, Henry Bookey, Agnieszka Szolno, Ryszard Stepien, Dariusz Pysz, Ajoy Kar, Andrew Waddie, Mohammad R. Taghizadehand Ryszard Buczynski, “Broadband infrared supercontinuum generation in hexagonal-lattice tellurite photonic crystal fiber with dispersion optimized for pumping near 1560 nm”, Optical Society of America, Vol. 38, No. 22, pp. 4679-4681, 2013.
 156. M. M. Haque, M. S. Rahman, M. Samiul Habib, M. Selim Habib, S. M. A. Razzak, “A new circular photonic crystal fiber for effective dispersion compensation over E to L wavelength bands”, Journal of Microwaves, Optoelectronics and Electromagnetic Applications, Vol. 12, No. 2, pp. 556-580, 2013.

157. M. S. Habib, M. A. Motin, M. I. Hasan, M. S. Habib, S. M. A. Razzak and M. A. G. Khan, "Modelling of dispersion flattened photonic crystal fibers for communication application," 2013 International Conference on Informatics, Electronics and Vision (ICIEV), Dhaka, 2013,
158. M. Samiul Habib, M. Selim Habib, M. Imran Hasan, S.M.A. Razzak, "Highly nonlinear polarization maintaining two zero dispersion spiral photonic crystal fiber using artificial defects", *Optical Fiber Technology*, Vol. 19, No. 6, pp. 539-542, 2013.
159. Qiang Xu, Runcai Miao and Yani Zhang, "High birefringence low-dispersion of nonlinear photonic crystal fiber", Vol. 124, No.15, pp. 2269-2272, 2013.
160. Jianfei Liao, Tianye Huang, "Highly nonlinear photonic crystal fiber with ultrahigh birefringence using a nano-scale slot core", *Optical Fiber Technology*, Vol. 22, pp.107–112, 2014.
161. Xuyou Li, Zhenlong Xu, Weiwei Ling, and Pan Liu, "Design of highly nonlinear photonic crystal fibers with flattened chromatic dispersion", *Optical Society of America*, Vol. 53, No. 29, pp. 6682-6687, 2014.
162. Jin Hou, Jiajia Zhao, Chunyong Yang, Zhiyou Zhong, Yihua Gao, and Shaoping Chen, "Engineering ultra-flattened-dispersion photonic crystal fibers with uniform holes by rotations of inner rings", *Optical Society of America*, Vol. 2, No. 2, pp. 59-63, 2014.
163. A. Sonne & A. Ouchar, "Improving of high birefringence photonic crystal fiber with low confinement loss using small elliptical air holes in the core region", *Journal of Modern Optics*, Vol. 62, No. 7, pp. 588–592, 2014.
164. Fei Yu, Zhenpeng Wang, Yonggang Zhang, Yukui Yu, Chongyang Lv, "Analysis of a highly birefringent photonic crystal fiber with ellipse–rhombus air core", Vol. 125, No. 20, pp. 6266-6269, 2014.
165. M. Samiul Habib, Redwan Ahmad, M. Selim Habib, S.M.A. Razzak, "Design of single polarization single mode dispersion compensating photonic crystal fiber", *International Journal for Light and Electron Optics*, Vol. 125, No. 16, pp. 4313-4318, 2014.
166. Md. Selim Habib, Md. Shohel Rana, Md. Moniruzzaman, Md. Sharafat Ali, N. Ahmed, "Highly birefringent broadband-dispersion-compensating photonic crystal fibre over the E + S + C + L + U wavelength bands", *Optical Fiber Technology*, Vol. 20, No. 5, pp. 527-532, 2014.
167. Rui Hao, Zhiquan Li, Huijing Du, Liyong Niu, "Squeezed hexagonal highly birefringent photonic crystal fiber with low effective modal area", *International Journal for Light and Electron Optics*, Vol. 125, No. 8, pp. 1971-1974, 2014.

168. G. Dhanu Krishna, G. Prasannan, S. K. Sudheer, V.P. Mahadevan Pillai, "Design of Ultra-Low Loss Highly Nonlinear Dispersion Flattened Octagonal Photonic Crystal Fibers", *Optics and Photonics Journal*, Vol. 5, pp. 335-343, 2015.
169. S. Revathi, Srinivasa Inabathini, Ram Sandeep, "Soft glass spiral photonic crystal fiber for large nonlinearity and high birefringence", *Optica Applicata*, Vol. XLV, No. 1, pp. 2015.
170. Guangyu Jiang, Yanjun Fu, Yan Huang, "High birefringence rectangular-hole photonic crystal fiber", *Optical Fiber Technology*, Vol. 26, pp. 163-171, 2015.
171. Yanmei Cao, Libin Zhang, Yonghao Fei, Xun Lei, Shaowu Chen, "Effect of frequency chirp on super-continuum generation in silicon waveguides with two zero-dispersion wavelengths", *Optics Communications*, Vol. 334, pp. 190-195, 2015.
172. Md Asaduzzaman Shobug and Rosni Sayed, "Characterization of Hexagonal Photonic Crystal Fiber for Zero Flattened Dispersion with Lower Confinement Loss and Residual Dispersion Compensation Over 500 nm Wavelength Bandwidth", *Journal of Electrical and Electronics Engineering*, Vol. 11, No. 4, 2016.
173. R. R. Mahmud, M. A. G. Khan and S. M. A. Razzak, "Design and Comparison of SF57 Over SiO₂ on Same Structured PCF for Residual Dispersion Compensation", *IEEE Photonics Journal*, Vol. 8, No. 6, pp. 1-10, 2016.
174. Md. Imran Hasan, R. R. Mahmud, Monir Morshed & Md. Rabiul Hasan, "Ultra-flattened negative dispersion for residual dispersion compensation using soft glass equiangular spiral photonic crystal fiber", *Journal of Modern Optics*, Vol. 63, pp. 1681-1687, 2016.
175. Jui-Ming Hsu & Bing-Liang Wang, "Tailoring of broadband dispersion-compensating photonic crystal fiber", *Journal of Modern Optics*, Vol. 64, no. 12, pp. 1134–1145, 2016.
176. Hao Rui, "Highly birefringent photonic crystal fiber with a squeezed core and small modal area", *International Journal for Light and Electron Optics*, Vol. 127, No. 13, pp. 5245-5248, 2016.
177. Shabbir Chowdhury and Jagodananda Mondal, "Ultra-high birefringent and high non-linear PCF for S+C+L+U wavebands", *Electrical, Computer and Communication Engineering Conference*, pp. 60-62, 2017.
178. Jiayuan Li, Ke Xu and Jiangbing Du, "Ultrabroadband and Flattened Dispersion in Aluminum Nitride Slot Waveguides", *IEEE Photonics Journal* Vol. 9, No. 4, pp. 1-8, 2017.
179. Moutusi De, Rahul Kumar Gangwar, Vinod Kumar Singh, "Designing of highly birefringence, dispersion shifted decagonal photonic crystal fiber with low

- confinement loss”, *Photonics and Nanostructures - Fundamentals and Applications* Vol. 26 pp. 15–23, 2017.
180. Chandru Selva Kumar, Rajesh Anbazhagan, “Investigation on chalcogenide and silica based photonic crystal fibers with circular and octagonal core”, Vol. 72, pp. 40-45, 2017.
 181. Saeed Olyae and Fahimeh Taghipour, “A new design of photonic crystal fiber with ultra-flattened dispersion to simultaneously minimize the dispersion and confinement loss”, *3rd International Photonics & Opto Electronics Meetings*, Vol. 276, no. 1, 2011.
 182. Partha Sona Maji, Partha Roy Chaudhuri, “A New Design of Ultra-Flattened Near-zero Dispersion PCF Using Selectively Liquid Infiltration”, *arxiv, physics optics*, pp. 1-5, 2014.
 183. Yashar E. Monfared, Sergey A. Ponomarenko, “Highly nonlinear liquid-filled photonic crystal fibers”, *2015 Photonics North*, pp. 1-1, 2015.
 184. Md. Rabiul Hasan, Md. Shamim Anower, Md. Imran Hasan, “A polarization maintaining single mode photonic crystal fiber for residual dispersion compensation”, DOI 10.1109/LPT.2016.2572141, *IEEE Photonics Technology Letters*, Vol. 28, No. 16, August 15, 2016.
 185. Rahul Kumar Gangwar, Vinod Kumar Singh, “Study of highly birefringence dispersion shifted photonic crystal fiber with asymmetrical cladding”, *Elsevier, Optik*, Vol. 127, pp. 11854-11859, 2016.
 186. M.R. Hasan, M.S. Anower and M.I. Hasan, “Polarization maintaining highly nonlinear photonic crystal fiber with closely lying two zero dispersion wavelengths”, *Optical Engineering*, Vol. 55, No. 5, pp.056107, May 2016.
 187. Li Shu-Guang, Zhu Xing-Ping, Xue Jian-Rong, "Supercontinuum generation in all-normal dispersion photonic crystal fiber", *Acta Phys. Sin*, Vol. 22, No. 7, 2013.
 188. Zheng Guo, Jinhui Yuan, Chongxiu Yu, Xinzhu Sang, Kuiru Wang, Binbin Yan, Lixiao Li, Shuai Kang, and Xue Kang, "Highly Coherent Supercontinuum Generation in the Normal Dispersion Liquid-Core Photonic Crystal Fiber", *Progress In Electromagnetics Research M*, Vol. 48, pp. 67–76, 2016.
 189. Mohamed Farhat Othman Hameed, Salah S. A. Obayya, and Hamdi A. El-Mikati, “Highly nonlinear birefringent soft glass photonic crystal fiber with liquid crystal core”, *IEEE Photonics Technology Letters*, Vol. 23, No. 20, October 15, 2011.
 190. Michele Bottacini, Federica Poli, Annamaria Cucinotta, and Stefano Selleri, “Modelling of photonic crystal fiber Raman amplifiers”, *Journal of Lightwave Technology*, Vol. 22, No. 7, pp. 1707, July 2004.

191. V.I. Kalashnikov, E. Sorokin, I.T. Sorokin, "Raman effects in the infrared supercontinuum generation in soft-glass PCFs", *Applied Physics B* Vol. 87, pp. 37-44, 2007.
192. Marcos A.R. Franco, Valdir A. serraio and Francisco Sircilli, "Microstructured optical fiber for residual dispersion compensation over S+C+L+U wavelength bands", *IEEE Photonics Technology Letters*, Vol. 20, No. 9, pp. 751-753, May 1,2008.
193. J. P. da Silva, D. S. Bezerra, V. F. Rodriguez-Esquerre, I. E. da Fonseca and H. E. Hernandez-Figueroa, "Ge-doped defect-core microstructured fiber design by genetic algorithm for residual dispersion compensation", *IEEE Photon. Technol. Lett.*, Vol. 22, No. 18, pp. 1337–1339, Sep. 2010.
194. M. A. Islam and M. Shah Alam, "Design of a polarization-maintaining equiangular spiral photonic crystal fiber for residual dispersion compensation over E+S+C+L+U wavelength bands", *IEEE Photon. Technol. Lett.*, Vol. 24, no. 11, pp. 930–932, Jun. 2012.
195. M. I. Hasan, S. M. Abdur Razzak and Md. Samiul Habib "Design and characterization of highly birefringent residual dispersion compensating photonic crystal fiber", *IEEE J. Lightwave Technol.*, Vol. 32, No. 23, pp. 3976–3982, 2014.
196. M. R. Hasan, M. S. Anower and M. I. Hasan, "A Polarization Maintaining Single-Mode Photonic Crystal Fiber for Residual Dispersion Compensation", in *IEEE Photonics Technology Letters*, Vol. 28, no. 16, pp. 1782-1785, Aug.15, 15 2016.
197. Md. Imran Hasan, M. Samiul Habib, and S. M. A. Razzak, "An Elliptical-shaped Core Residual Dispersion Compensating Octagonal Photonic Crystal Fiber", *IEEE Photonics Technology Letters*, Vol. 26, NO. 20, pp. 2047-2050, October 15, 2014.
198. Reeves, W.H.; Knight, J.C.; Russell, P.S.J. *Opt. Express*, Vol. 10, pp. 609–613, 2012.
199. S.M.A. Razzak and Y. Namihira, "Tailoring dispersion and confinement losses of photonic crystal fiber using hybrid cladding", *Journal of Lightwave Technology*, Vol.26, No. 13, pp. 1909-1914, July 2008.
200. H. Ademgil, S. Haxha and F. A. Malek, "Highly nonlinear bending insensitive birefringent photonic crystal fibers", *Engineering* Vol. 2(8), pp. 608-616, 2010.
201. S. Kim, C. S. Kee and C. G. Lee, "Modified rectangular lattice photonic crystal fibers with high birefringence and negative dispersion", *Opt. Exp.* Vol.17, no. 10, pp. 7952-7957, Apr. 2009.
202. D. C. Tee, M. H. A. Bakar, N. Tamchek, and F. R. M. Adikan, "Photonic crystal fiber in photonic crystal fiber for residual dispersion compensation over E + S + C + L + U wavelength bands", *IEEE Photon. J.*, Vol. 5, no. 3, pp. 262-264, June 2013.
203. D. Van Thourhout, J. V. Campenhout, P. Rojo-Romeo, P. Regreny, C. Seassal, P. Binetti, X. Leijtens, R. Nötzel, M. Smit, L. Di Cioccio, C. Lagahe, J.-M. Fedeli, and

- R. Baets, "PICMOS—A photonic interconnect layer on CMOS", in Proc. 33rd Eur. Conf. Opt. Commun. (ECOC '07), Berlin, Germany, pp. 1-2, Sep. 16–20, Paper 6.3.1, 2007.
204. L. Tsybeskov, D. J. Lockwood and M. Ichikawa, "Silicon Photonics: CMOS Going Optical [Scanning the Issue]," in Proceedings of the IEEE, vol. 97, no. 7, pp. 1161-1165, July 2009.
205. Alan E. Willner, Omer Faruk Yilmaz, Jian Wang, Xiaoxia Wu, Antonella Bogoni, Lin Zhang and Scott R. Nuccio, "Optical Efficient Nonlinear Signal Processing", IEEE Journal of Selected Topics in Quantum Electronics, VOL. 17, NO. 2, MARCH/APRIL 2011.
206. Densmore, D.-X. Xu, S. Janz, P. Waldron, T. Mischki, G. Lopinski, A. Del age, J. Lapointe, P. Cheben, B. Lamontagne, and J. H. Schmid, "Spiral-path high-sensitivity silicon photonic wire molecular sensor with temperature-independent response", Opt. Lett. Vol. 33, pp. 596–598, 2008.
207. C. J. Benton, "Solitons and nonlinear optics in silicon-on-insulator photonic wires", Ph.D. dissertation, Dept. Phys., Bath Univ., Bath, U.K., 2009.
208. J. Leuthold, C. Koos and W. Freude, "Nonlinear silicon photonics", Nature Photonics Vol. 4, pp. 535 -544, 2010.
209. T. Tsuchizawa, T. Watanabe, K. Yamada, T. Shoji, J. Takahashi and S. Itabashi, "Micro photonics devices based on silicon micro fabrication technology," The 16th Annual Meeting of the IEEE Lasers and Electro-Optics Society, 2003. LEOS 2003, pp. 585-586 vol.2, 2003.
210. Lin, Q., Painter, O. J. & Agrawal G. P. "Nonlinear optical phenomena in silicon waveguides: Modeling and applications". Opt. Express Vol. 15, pp. 16604–16644, 2007.
211. R. M. Osgood, N. C. Panoiu, J. I. Dadap, Xiaoping Liu, Xiaogang Chen, I-Wei Hsieh, E. Dulkeith, W. M.J. Green, and Y. A. Vlasov, "Engineering nonlinearities in nanoscale optical systems: physics and applications in dispersion-engineered silicon nanophotonic wires," Adv. Opt. Photon. Vol. 1, Issue no. 1, pp 162-235, 2009.
212. Alejandro Mart nez, Javier Blasco, Pablo Sanchis, Jose V. Gala n, Jaime Garc a-Rupe rez, Emmanuel Jordana, Pauline Gautier, Youcef Lebour, Sergi Hern andez, Romain Guider, Nicola Daldosso, Blas Garrido, Jean Marc Fedeli, Lorenzo Pavesi, and Javier Mart , "Ultrafast All-Optical Switching in a Silicon-Nanocrystal-Based Silicon Waveguide at Telecom Wavelengths", American Chemical Society, Nano Lett., Vol. 22, pp. 1506–1511, 2010.
213. Lorenzo Mangolini, "Synthesis, properties, and applications of silicon nanocrystals",

- Journal of Vacuum Science & Technology B, Nanotechnology and Microelectronics: Materials, Processing, Measurement, and Phenomena Vol. 31, pp. 020801, 2013.
214. L. Pavesi, L. Dal Negro, C. Mazzoleni, G. Franzò and F. Priolo, "Optical gain in silicon nanocrystals", *Nature* Vol. 408, pp. 440-444, 2000.
215. G. Vijaya Prakash, et al., "Linear and nonlinear optical properties of plasma-enhanced chemical-vapour deposition grown silicon nanocrystals", *J. Mod. Opt.*, Vol. 49, pp. 719-730, 2002.
216. R. Spano, J. V. Galan, P. Sanchis, A. Martinez, J. Marti and L. Pavesi, "Group velocity dispersion in horizontal slot waveguides filled by Si nanocrystals", 2008 5th IEEE International Conference on Group IV Photonics, Cardiff, pp. 314-316, 2008.
217. Rita Spano, Massimo Cazzanelli, Nicola Daldosso, Zeno Gaburro, Luigi Ferraioli, Luca Tartara, Jin Yu, Vittorio Degiorgio, Sergi Hernandez, Youcef Lebour, Paolo Pellegrino, Blas Garrido, Emmanuel Jordana, Jean Marc Fedeli and Lorenzo Pavesi, "Non-linear optical properties of Si nanocrystals", *MRS Proc.* Vol. 958, pp. L08-06, 2007.
218. R. Spano, N. Daldosso, M. Cazzanelli, L. Ferraioli, L. Tartara, J. Yu, V. Degiorgio, E. Jordana, J. M. Fedeli, and L. Pavesi, "Bound electronic and free carrier nonlinearities in Silicon nanocrystals at 1550nm", *Opt. Express* Vol. 17, pp. 3941-3950, 2009.
219. Q. Lin, Oskar J. Painter and Govind P. Agrawal, "Nonlinear optical phenomena in silicon waveguides: Modeling and applications", *Optics Express*, Vol. 44, pp. 1516604-16608, 2007.
220. K. Jiang, S. Fu, P. Shum, and C. Lin, BA "wavelength-switchable passively harmonically mode-locked fiber laser with low pumping threshold using single-walled carbon nanotubes", *IEEE Photon. Technol. Lett.*, Vol. 22, no. 11, pp. 754-756, Jun. 2010.
221. J. Marti and K. Williams, "Is all-optical processing green?" presented at Workshop OFC, San Diego, CA, 2010.
222. R. S. Tucker, "A green internet", in *Proc. IEEE Lasers Electro-Opt. Soc. Annu. Meeting*, pp. 4-5, 2008.
223. H. G. Weber, S. Ferber, M. Kroh, C. Schmidt-Langhorst, R. Ludwig, V. Marembert, C. Boerner, F. Futami, S. Watanabe, and C. Schubert, "Single channel 1.28 Tbit/s and 2.56 Tbit/s DQPSK transmission", *Electron. Lett.* Vol. 42, no. 3, pp. 178-179, 2006.
224. H. C. Hansen Mulvad, M. Galili, L. K. Oxenløwe, H. Hu, A. T. Clausen, J. B. Jensen, C. Peucheret, and P. Jeppesen, "Demonstration of 5.1 Tbit/s data capacity on a single-wavelength channel", *Opt. Exp.*, Vol. 18, no. 2, pp. 1438-1443, Jan. 2010.

225. M. Sharma, N. Borgohain, and S. Konar, "Supercontinuum generation in photonic crystal fibers possessing high birefringence and large optical nonlinearity", *Phys. Exp.*, Vol. 4, no. 26, pp. 1–9, Jan. 2014.
226. Y.P. Yatsenko, A.D. Pryamikov, "Parametric frequency conversion in photonic crystal fibers with germano silicate core", *J. Opt. A* Vol. 9, pp. 716–722, 2007.
227. Alan E. Willner, Omer Faruk Yilmaz, Jian Wang, Xiaoxia Wu, Antonella Bogoni, Lin Zhang and Scott R. Nuccio, "Optically Efficient Nonlinear Signal Processing", *IEEE Journal of Selected Topics In Quantum Electronics*, Vol. 17, No.2, pp 320-332, Mar/April 2011.
228. T. S. Saini, A. Baili, A. Kumar, Rim Cherif, M. Zghal, R. K. Sinha, "Design and analysis of equiangular spiral photonic crystal fiber for mid-IR supercontinuum generation", *Journal of Modern Optics* Vol.64:2, pages 143-149, 2015.
229. K. Saitoh and M. Koshiba, "Single-polarization single-mode photonic crystal fibers", *IEEE Photon. Technol. Lett.* Vol. 15(10), pp. 1384–1386, 2003.
230. S. L. Jiao, M. Todorović, G. Stoica, and L. V. Wang, "Fiber-based polarization-sensitive Mueller matrix optical coherence tomography with continuous source polarization modulation", *Appl. Opt.* Vol. 44(26), pp. 5463–5467, 2005.
231. M. S. Habib, M. A. Motin, M. I. Hasan, M. S. Habib, S. M. A. Razzak and M. A. G. Khan, "Dispersion and confinement loss control with decagonal photonic crystal fibers for wideband transmission systems", 2013 International Conference on Informatics, Electronics and Vision (ICIEV), Dhaka, pp. 1-4, 2013.
232. U. A. Siddika and M. S. Rahman, "Modelling of highly birefringent dispersion compensating circular Photonic Crystal Fiber", 2015 2nd International Conference on Electrical Information and Communication Technologies (EICT), Khulna, pp. 320-325, 2015.
233. Tongtong Zhao, Zhenggang Lian, Trevor Benson, Xin Wang, Wan Zhang, Shuqin Lou, "Highly-nonlinear polarization-maintaining AsSe-based photonic quasi-crystal fiber for super-continuum generation", *Optical Materials*, Vol. 73, pp. 343-349, 2017.
234. D. Van Thourhout J. Van Campenhout, P. Rojo-Romeo, P. Regren, c. Seassal, P. Binetti, X.J.M. Leijtens, R. Nbtzel, M.K.Smit, L. Oi Cioccio, c. Lagahe, J.-M. Fedeli, R. Baets, "Photonic interconnect layer on CMOS", *Proc. 33rd European Conf. Optical Communications*, pp. 16-20, 2007.
235. Tsybeskov, L., Lockwood, D. J. & Ichikawa, M., "Silicon photonics: CMOS going optical", *Proc. of the IEEE*, Vol. 97, issue 7, pp. 1161–1165, 2009.
236. Ademgil, H. and Haxha, S., "Bending Insensitive Large Mode Area Photonic Crystal Fiber". *Optik-International Journal for Light and Electron Optics*, Vol. 122, pp. 1950-1956, 2011.

237. N. Vukovic, N. Healy, and A. C. Peacock, "Guiding properties of large mode area silicon microstructured fibers: A route to effective single mode operation", *J. Opt. Soc. Amer. B, Opt. Phys.*, Vol. 28, no. 6, pp. 1529–1533, June 2011.
238. F. Yaman, H. Pang, X. B. Xie, P. Li Kam Wa, and G. F. Li, "Silicon photonic crystal fiber", in *Proc. of Conference on Lasers and Electro-Optics/International Quantum Electronics Conference, OSA Technical Digest (CD) (Optical Society of America)*, paper CTuDD7, Baltimore, Maryland United States, pp. 1–2, Jun. 2009.
239. W. Belardi, G. Bouwmans, L. Provino, and M. Douay, "Form-induced birefringence in elliptical hollow photonic crystal fiber with large mode area", *IEEE J. Quantum Electron.*, Vol. 41, no. 12, pp. 1558–1565, Dec. 2005.
240. C. Peacock, J. R. Sparks, and N. Healy, "Semiconductor optical fibers: Progress and opportunities", *Laser Photon. Rev.*, Vol. 8, no. 1, pp. 53–72, Jan. 2014.
241. K. Jiang, S. Fu, P. Shum, and C. Lin, "Wavelength-switchable passively harmonically mode-locked fiber laser with low pumping threshold using single-walled carbon nanotubes", *IEEE Photon. Technol. Lett.*, Vol. 22, no. 11, pp. 754–756, 2010,
242. K. Saitoh, M. Koshiba, T. Hasegawa, and E. Sasaoka, "Chromatic dispersion control in photonic crystal fibers: application to ultra-flattened dispersion", *Opt. Express* Vol. 11, pp.843-852, 2003.
243. C. Koos, L. Jacome, C. Poulton, J. Leuthold and W. Freude, "Nonlinear silicon-on-insulator waveguides for all-optical signal processing", *Opt. Express*, Vol. 15, pp. 5976-5990, 2007.
244. Y. Yamamoto and T. Kimura, "Coherent optical fiber transmission systems", *IEEE J. Quant. Electron.*, Vol. 17, pp. 919-935, 1981.
245. I. P. Kaminow, "Polarization in optical fibers", *IEEE J. Quant. Electron.*, Vol. 17, pp. 15-22, 1981.
246. Shigeki Watanabe, "All-optical Signal Processing Using Nonlinear Fibers", *Optical Society of America*, Vol. 5595, 2002.
247. M. D. Pelusi, F. Luan, E. Magi, M. R. Lamont, D. J. Moss, B. J. Eggleton, J. S. Sanghera, L. B. Shaw, and I. D. Aggarwal, "High bit rate all-optical signal processing in a fiber photonic wire", *Opt. Exp.*, Vol. 16, no. 15, pp. 11506–11512, Jul. 2008.
248. J. Fatome, C. Fortier, T. N. Nguyen, T. Chartier, F. Smektala, K. Messaad, B. Kibler, S. Pitois, G. Gadret, C. Finot, J. Troles, F. Desevedavy, P. Houizot, G. Renversez, L. Brilland, and N. Traynor, "Linear and nonlinear characterizations of chalcogenide photonic crystal fibers", *J. Lightw. Technol.*, Vol. 27, no. 11, pp. 1707–1715, Jun. 2009.

249. J. Hu, C. R. Menyuk, L. B. Shaw, J. S. Sanghera, and I. D. Aggarwal, "Maximizing the bandwidth of supercontinuum generation in As₂Se₃ chalcogenide fibers", *Opt. Exp.*, Vol. 18, pp. 6722–6739, Mar. 2010.
250. R. S. Tucker and K. Hinton, "Energy consumption and energy density in optical and electronic signal processing", *IEEE Photon. J.*, Vol. 3, pp. 821–833, 2011.
251. K. L. Lee, B. Sedighi, R. S. Tucker, H. K. Chow and P. Vetter, "Energy efficiency of optical transceivers in fiber access networks", *IEEE J. Opt. Commun. Network*, Vol. 4, no. 9, pp. A59–A68, 2012.
252. C. Langrock, S. Kumar, J. E. McGeehan, A. E. Willner, and M. M. Fejer, "All-optical signal processing using χ^2 nonlinearities in guided-wave devices", *J. Lightw. Technol.*, Vol. 24, no. 7, pp. 2579–2592, Jul. 2006.
253. S. Radic, "Parametric Signal Processing", *IEEE J. Sel. Topics Quantum Electron.*, Vol. 18, no. 2, pp. 670–680, Mar./Apr. 2012.
254. M. A. Foster, A. C. Turner, R. Salem, M. Lipson and A. L. Gaeta, "Broad-band continuous-wave parametric wavelength conversion in silicon nanowaveguides", *Opt. Exp.*, Vol. 15, no. 20, pp. 12949–12958, 2007.
255. J. C. Knight and D. V. Skryabin, "Nonlinear waveguide optics and photonic crystal fibers", *Opt. Exp.*, Vol. 15, pp. 15365–15376, 2007.
256. J. Leuthold, L. Moller, J. Jaques, S. Cabot, L. Zhang, P. Bernasconi, M. Cappuzzo, L. Gomez, E. Laskowski, E. Chen, A. Wong-Foy, and A. Griffin, "160 Gbit/s SOA all-optical wavelength converter and assessment of its regenerative properties", *IEEE Electron. Lett.*, Vol. 40, no. 9, pp. 554–555, Apr. 2004.
257. O. F. Yilmaz, J. Wang, S. Khaleghi, X. Wang, S. R. Nuccio, X. Wu, and A. E. Willner, "Pre conversion phase modulation of input differential phase-shift-keying signals for wavelength conversion and multicasting applications using phase-modulated pumps", *Opt. Lett.*, Vol. 36, pp. 731–733, 2011.
258. P. De Dobbelaere, K. Falta, S. Gloeckner, and S. Patra, "Digital MEMS for optical switching", *IEEE Commun. Mag.*, Vol. 40, no. 3, pp. 88–95, Mar. 2002.
259. Govind P. Agrawal, "Highly Nonlinear Fibers and Their Applications", Institute of Optics, 2007.
260. G. Contestabile, M. Presi, and E. Ciaramella, "Multiple wavelength conversion for WDM multicasting by FWM in an SOA", *IEEE Photon. Technol. Lett.* Vol. 16, no. 7, pp. 1775–1777, 2004.
261. L. Xu, N. Chi, K. Yvind, L. Christiansen, L. Oxenløwe, J. Mørk, P. Jeppesen, and J. Hanberg, "7×40 Gb/s base-rate RZ all-optical broadcasting utilizing an electro absorption modulator", *Opt. Exp.*, Vol. 12, pp. 416–420, 2004.

262. V. R. Supradeepa, C. M. Long, R. Wu, F. Ferdous, E. Hamidi, D. E. Leaird, and A. M. Weiner, “Comb-based radiofrequency photonic filters with rapid tunability and high selectivity”, *Nature Photon.*, Vol. 6, pp. 186–194, 2011.
263. Bogoni, X. Wu, S. R. Nuccio, J. Wang, Z. Bakhtiari, and A. E. Willner, “Photonic 640-Gb/s reconfigurable OTDM add-drop multiplexer based on pump depletion in a single PPLN waveguide”, *IEEE J. Sel. Topics Quantum Electron.*, Vol. 18, no. 2, pp. 709–716, 2012.
264. H. C. H. Mulvad, M. Galili, L. K. Oxenløwe, H. Hu, A. T. Clausen, J.B. Jensen, C. Peucheret, and P. Jeppesen, “Demonstration of 5.1 Tbit/s data capacity on a single-wavelength channel”, *Opt. Exp.*, Vol. 18, pp. 1438–1443, 2010.
265. S. R. Nuccio, O. F. Yilmaz, X. Wu, and A. E. Willner, “Fine tuning of conversion/dispersion based optical delays with a 1 pm tunable laser using cascaded acousto-optic mixing”, *Opt. Lett.*, Vol. 35, no. 4, pp. 523–525, 2010.
266. S. R. Nuccio, O. F. Yilmaz, X. Wang, H. Huang, J. Wang, X. Wu, and A. E. Willner, “Higher-order dispersion compensation to enable a 3.6 μ s wavelength-maintaining delay of a 100 Gb/s DQPSK signal”, *Opt. Lett.*, Vol. 35, pp. 2985–2987, 2010.
267. L. Zhang and A. E. Willner, “Micro-resonators for communication and signal processing applications”, in *Photonic Microresonator Research and Applications* (Springer Series in Optical Sciences). New York: Springer-Verlag, Vol. 156, 2010.
268. J. S. Levy, A. Gondarenko, A. C. Turner-Foster, M. A. Foster, A. L. Gaeta, and M. Lipson, “Four-wave mixing in integrated silicon nitride waveguide”, presented at the CLEO, 2009..
269. Z. Yuan, A. Anopchenko, N. Daldosso, R. Guider, D. Navarro-Urrios, A. Pitanti, R. Spano, and L. Pavesi, “Silicon nanocrystals as an enabling material for silicon photonics”, *Proc. IEEE*, Vol. 97, no. 7, pp. 1250–1268, 2009.
270. H. Q. Le and S. Di Cecca, “Ultrafast, room-temperature, resonance-enhanced third-order optical susceptibility tensor of an AlGaAs/GaAs quantum well”, *Opt. Lett.*, Vol. 16, pp. 901–903, 1991.

Appendix A

Numerical Method For Design Analysis

To develop the potential of PCFs, accurate modelling is necessary. A range of methods has been developed, such as plane wave expansion (PWE) method, effective index method, multipole method, FEM, finite difference time domain method (FDTD) etc.

Finite Element Method

Initially, the FEM started for structural analysis. Until 1968, this method was not applicable for EM problems [1]. This method is used to solve differential equations. The finite difference method cannot be applied to structure having irregularly shaped boundaries. In order to solve such problems, the FEM was developed [2-4].

The FEM of a problem requires four steps to be solved: (1) dividing the solution region into finite number of sub regions or elements, (2) finding control equations for a particular element, (3) collecting all elements in the solution region, and (4) solving the obtained system of equations.

1) Discretization

The complete solution region is divided into numbers of finite elements. We try to approximate potential V_e within an element e and relate the potential in various elements in a way that the potential remains continuous across inter-element boundaries. So approximately, the voltage is given as

$$V(x, y) = \sum_{e=1}^N V_e(x, y) \quad (1)$$

Where N is the number of triangular elements into which the region is divided.

The polynomial approximation was applied to approximate V_e , like

$$V_e(x, y) = a + bx + cy \quad (2)$$

For triangular element and

$$V_e(x, y) = a + bx + cy + dxy \quad (3)$$

For quadrilateral element. Generally. Potential V_e is nonzero within element e and zero outside e . Quadrilateral elements has some difficulty in approximating the boundary of the solution region since these elements can only be used where boundaries are acceptably uniform. Hence, triangular elements are preferred.

2) Element governing equations

For a triangular element, the potential V_{e1} , V_{e2} , and V_{e3} at nodes 1, 2, and 3, respectively, can be given by,

$$\begin{bmatrix} V_{e1} \\ V_{e2} \\ V_{e3} \end{bmatrix} = \begin{bmatrix} 1 & x_1 & y_1 \\ 1 & x_2 & y_2 \\ 1 & x_3 & y_3 \end{bmatrix} \begin{bmatrix} a \\ b \\ c \end{bmatrix} \quad (4)$$

The coefficient a, b, and c are evaluated from eqn. (4) as

$$\begin{bmatrix} a \\ b \\ c \end{bmatrix} = \begin{bmatrix} 1 & x_1 & y_1 \\ 1 & x_2 & y_2 \\ 1 & x_3 & y_3 \end{bmatrix}^{-1} \begin{bmatrix} V_{e1} \\ V_{e2} \\ V_{e3} \end{bmatrix} \quad (5)$$

Substituting in eqn. (2), we obtain

$$V_e = [1 \quad x \quad y] \frac{1}{2A} \begin{bmatrix} (x_2y_3 - x_3y_2) & (x_3y_1 - x_1y_3) & (x_1y_2 - x_2y_1) \\ (y_2 - y_3) & (y_3 - y_1) & (y_1 - y_2) \\ (x_3 - x_2) & (x_1 - x_3) & (x_2 - x_1) \end{bmatrix} \begin{bmatrix} V_{e1} \\ V_{e2} \\ V_{e3} \end{bmatrix} \quad (6)$$

$$V_e = \sum_{i=1}^3 \alpha_i(x, y) V_{ei} \quad (7)$$

Where

$$\alpha_1 = \frac{1}{2A} [(x_2y_3 - x_3y_2) + (y_2 - y_3)x + (x_3 - x_2)y] \quad (7a)$$

$$\alpha_2 = \frac{1}{2A} [(x_3y_1 - x_1y_3) + (y_3 - y_1)x + (x_1 - x_3)y] \quad (7b)$$

$$\alpha_3 = \frac{1}{2A} [(x_1y_2 - x_2y_1) + (y_1 - y_2)x + (x_2 - x_1)y] \quad (7c)$$

And A is the area of element e given by,

$$2A = \begin{vmatrix} 1 & x_1 & y_1 \\ 1 & x_2 & y_2 \\ 1 & x_3 & y_3 \end{vmatrix}$$

$$= (x_1y_2 - x_2y_1) + (x_3y_1 - x_1y_3) + (x_2y_3 - x_3y_2)$$

Or

$$A = 1/2 [(x_2 - x_1)(y_3 - y_1) - (x_3 - x_1)(y_2 - y_1)] \quad (8)$$

To keep the value of A positive, the nodes are numbered anticlockwise. From eqn. (7), potential at any point within the element can be obtained if potentials of vertices are known. Also α_i are linear interpolation functions. They are called the elemental shape functions and are characterized as:

$$\alpha_i(x_j, y_j) = \begin{cases} 1, & i = j \\ 0, & i \neq j \end{cases} \quad (9a)$$

$$\sum_{i=1}^3 \alpha_i(x, y) = 1 \quad (9b)$$

The energy per unit length related to the element e is given by

$$W_e = \frac{1}{2} \int \varepsilon |E|^2 dS = \frac{1}{2} \int \varepsilon |\nabla V_e|^2 dS \quad (10)$$

From eqn. (7),

$$\nabla V_e = \sum_{i=1}^3 V_{ei} \nabla \alpha_i \quad (11)$$

Substituting eqn. (11) in eqn. (10), we get

$$W_e = \frac{1}{2} \sum_{i=1}^3 \sum_{j=1}^3 \varepsilon V_{ei} \left[\int \nabla \alpha_i \cdot \nabla \alpha_j dS \right] V_{ej} \quad (12)$$

If the bracket terms are defined as

$$C_{ij}^{(e)} = \int \nabla \alpha_i \cdot \nabla \alpha_j dS \quad (13)$$

We can write eqn. (12) in matrix form as

$$W_e = \frac{1}{2} \varepsilon [V_e]^T [C^{(e)}] [V_e] \quad (14)$$

Where superscript T denotes the transpose of a matrix,

$$[V_e] = \begin{bmatrix} V_{e1} \\ V_{e2} \\ V_{e3} \end{bmatrix} \quad (15a)$$

And

$$[C^{(e)}] = \begin{bmatrix} C_{11}^{(e)} & C_{12}^{(e)} & C_{13}^{(e)} \\ C_{21}^{(e)} & C_{22}^{(e)} & C_{23}^{(e)} \\ C_{31}^{(e)} & C_{32}^{(e)} & C_{33}^{(e)} \end{bmatrix} \quad (15b)$$

The matrix $[C^{(e)}]$ is generally called as element coefficient matrix. The matrix element $C_{ij}^{(e)}$ defines the coupling between nodes i and j . its value is obtained from eqn. (7) and (13). For example,

$$\begin{aligned} C_{12}^{(e)} &= \int \nabla \alpha_1 \cdot \nabla \alpha_2 dS \\ &= \frac{1}{4A^2} [(y_2 - y_3)(y_3 - y_1) + (x_3 - x_2)(x_1 - x_3)] \int dS \\ &= \frac{1}{4A} [(y_2 - y_3)(y_3 - y_1) + (x_3 - x_2)(x_1 - x_3)] \end{aligned} \quad (16a)$$

Similarly:

$$C_{11}^{(e)} = \frac{1}{4A} [(y_2 - y_3)^2 + (x_3 - x_2)^2] \quad (16b)$$

$$C_{13}^{(e)} = \frac{1}{4A} [(y_2 - y_3)(y_1 - y_2) + (x_3 - x_2)(x_2 - x_1)] \quad (16c)$$

$$C_{22}^{(e)} = \frac{1}{4A} [(y_3 - y_1)^2 + (x_1 - x_3)^2] \quad (16d)$$

$$C_{23}^{(e)} = \frac{1}{4A} [(y_3 - y_1)(y_1 - y_2) + (x_1 - x_3)(x_2 - x_1)] \quad (16e)$$

$$C_{33}^{(e)} = \frac{1}{4A} [(y_1 - y_2)^2 + (x_2 - x_1)^2] \quad (16f)$$

Also

$$C_{21}^{(e)} = C_{12}^{(e)}, \quad C_{23}^{(e)} = C_{32}^{(e)}, \quad C_{13}^{(e)} = C_{31}^{(e)} \quad (16g)$$

For making calculations easy, we define

$$\begin{aligned} P_1 &= (y_2 - y_3), & P_2 &= (y_3 - y_1), & P_3 &= (y_1 - y_2) \\ Q_1 &= (x_3 - x_2), & Q_2 &= (x_1 - x_3), & Q_3 &= (x_2 - x_1) \end{aligned} \quad (17a)$$

Using these equations, each term of elemental coefficient matrix is given as

$$C_{ij}^{(e)} = \frac{1}{4} [P_i P_j + Q_i Q_j] \quad (17b)$$

Where

$$A = \frac{1}{2} (P_2 Q_3 - P_3 Q_2) \quad (17c)$$

Note that $P_1 + P_2 + P_3 = 0 = Q_1 + Q_2 + Q_3$ and hence $\sum_{i=1}^3 C_{ij}^{(e)} = 0 = \sum_{j=1}^3 C_{ij}^{(e)}$. This can be used to verify our calculations.

3) Assembling of all elements

After observing a particular element, now all the elements are assembled into the solution region. The energy related with the collection of all elements in the region can be given by

$$W = \sum_{e=1}^n W_e = \frac{1}{2} \varepsilon [V]^T [C] [V] \quad (18)$$

Where

$$[V] = \begin{bmatrix} V_1 \\ V_2 \\ \vdots \\ V_n \end{bmatrix} \quad (19)$$

N is the number of nodes, N is the number of elements and $[C]$ is the global coefficient matrix which is obtained by collection of individual elements. The major concern is to obtain $[C]$ from $[C^{(e)}]$.

The process of assembling of particular element coefficient matrices into the global coefficient matrix can be explained with the help of an example. We consider a mesh having three finite elements. There is two types of numbering, global numbering and local numbering. So there are 5 global nodes in the diagram. So a general form of the global coefficient matrix can be written as

$$[C] = \begin{bmatrix} C_{11} & C_{12} & C_{13} & C_{14} & C_{15} \\ C_{21} & C_{22} & C_{23} & C_{24} & C_{25} \\ C_{31} & C_{32} & C_{33} & C_{34} & C_{35} \\ C_{41} & C_{42} & C_{43} & C_{44} & C_{45} \\ C_{51} & C_{52} & C_{53} & C_{54} & C_{55} \end{bmatrix} \quad (20)$$

Since there are 5 nodes, matrix is having an order of 5×5 . It is already known that C_{ij} denotes the coupling between i and j nodes. We can calculate C_{ij} by using the fact that potential must be continuous across the boundaries. For example, if we want to find C_{11} , it is clear that global node 1 is common for both elements 1 and 2 and it is marked as local node 1 in both. So we can write,

$$C_{11} = C_{11}^{(1)} + C_{11}^{(2)} \quad (21a)$$

Similarly, by observing from figure, we can write

$$C_{22} = C_{33}^{(1)} \quad (21b)$$

$$C_{44} = C_{22}^{(1)} + C_{33}^{(2)} + C_{33}^{(3)} \quad (21c)$$

$$C_{14} = C_{12}^{(1)} + C_{13}^{(2)} \quad (21d)$$

As there is no direct link between nodes 2 and 3,

$$C_{23} = C_{32} = 0 \quad (21e)$$

By following this trend, we can obtain all the terms of global coefficient matrix as

$$[C] = \begin{bmatrix} C_{11}^{(1)} + C_{11}^{(2)} & C_{13}^{(1)} & C_{12}^{(2)} & C_{12}^{(1)} + C_{13}^{(2)} & 0 \\ C_{31}^{(1)} & C_{33}^{(1)} & 0 & C_{32}^{(1)} & 0 \\ C_{21}^{(2)} & 0 & C_{22}^{(2)} + C_{11}^{(3)} & C_{23}^{(2)} + C_{13}^{(3)} & C_{12}^{(3)} \\ C_{21}^{(1)} + C_{31}^{(2)} & C_{23}^{(1)} & C_{32}^{(2)} + C_{31}^{(3)} & C_{22}^{(1)} + C_{33}^{(2)} + C_{33}^{(3)} & C_{32}^{(3)} \\ 0 & 0 & C_{21}^{(3)} & C_{23}^{(3)} & C_{22}^{(3)} \end{bmatrix} \quad (22)$$

This matrix has following properties:

1. It is symmetric i.e. $C_{ij} = C_{ji}$.
2. If there is no coupling between two nodes then $C_{ij} = 0$, so it is concluded that for large number of elements matrix becomes compact.
3. It is singular. It might not be clear but it can be proved using eqn. (15b).

4) Solving the obtained equations

It is clear that Laplace's (or Poisson's) equation is true only when the net energy in the solution region is minimum. Hence it is concluded that the partial derivative of W with respect to each nodal potential should be zero; that is,

$$\frac{\partial W}{\partial V_1} = \frac{\partial W}{\partial V_2} = \dots = \frac{\partial W}{\partial V_n} = 0$$

Or

$$\frac{\partial W}{\partial V_k} = 0, \quad k = 1, 2, \dots, n \quad (23)$$

For example, to achieve $\partial W / \partial V_1 = 0$ for a mesh having finite element, we substitute eqn. (20) in eqn. (18) and calculate the partial derivative of W with respect to V_1 , we obtain

$$0 = \frac{\partial W}{\partial V_1} = 2V_1 C_{11} + V_2 C_{12} + V_3 C_{13} + V_4 C_{14} + V_5 C_{15} + V_2 C_{21} + V_3 C_{31} + V_4 C_{41} + V_5 C_{51}$$

Or

$$0 = V_1 C_{11} + V_2 C_{12} + V_3 C_{13} + V_4 C_{14} + V_5 C_{15} \quad (24)$$

Generally, for $\partial W / \partial V_k = 0$, we can write,

$$\sum_{i=1}^n V_i C_{ik} = 0 \quad (25)$$

Where n is the number of nodes in the mesh. If eqn. (25) is written for all nodes $k = 1, 2, \dots, n$ a system of equations is obtained by which the solution of $[V]^T = [V_1 \ V_2 \ \dots \ V_n]$ can be found. There are two methods to solve this.

Iteration method

The potential at node 1 can be obtained from eqn. (24) as

$$V_1 = -\frac{1}{C_{11}} \sum_{i=2}^5 V_i C_{1i} \quad (26)$$

Generally, the potential at any node k can be obtained from eqn. (25) as

$$V_k = -\frac{1}{C_{kk}} \sum_{i=1, i \neq k}^n V_i C_{ik} \quad (27)$$

This is used iteratively for all n nodes present in the mesh. If a direct link is not present between node I and node k then $C_{ki} = 0$ hence nodes that are directly connected to node k effects the V_k in eqn. (27).

Thus W_e potentials of nodes connected to node k are obtained, we can determine V_k using eqn. (27). We start the iteration process by assigning the potential at free nodes to be zero or average potential.

$$V_{avg} = 1/2 (V_{min} + V_{max}) \quad (28)$$

Where V_{min} and V_{max} are minimum and maximum values of node under investigation. If these initial values are known, by using eqn. (27) we can calculate potential at node k . By using these initial values the new values are calculated after the first iteration and these values become initial values for the second iteration. This process is repeated until the difference between consecutive iterations is negligible.

Band matrix method

If all free nodes are numbered first and the fixed nodes last, eqn. (18) can be written as

$$W = \frac{1}{2} \varepsilon [V_f \quad V_p] \begin{bmatrix} C_{ff} & C_{fp} \\ C_{pf} & C_{pp} \end{bmatrix} \begin{bmatrix} V_f \\ V_p \end{bmatrix} \quad (29)$$

Where subscripts f and p denote the nodes with free and prescribed potentials, respectively. As V_p has known and fixed values, we take differentiation with respect to only V_f so using eqn. (23) in eqn. (29), we get

$$C_{ff}V_f + C_{fp}V_p = 0$$

Or

$$[C_{ff}][V_f] = -[C_{fp}][V_p] \quad (30)$$

Simplifying this equation, it can be written as

$$[A][V] = [B] \quad (31a)$$

Or

$$[V] = [A]^{-1}[B] \quad (31b)$$

Where $[V] = [V_f]$, $[A] = [C_{ff}]$, and $[B] = -[C_{fp}][V_p]$. The potential at free nodes can be found by using eqn. (30). From eqn. (31a), $[V]$ can be solved by using Gaussian elimination technique. But if the matrix inversion can be performed easily then we can use eqn. (31b) to get $[V]$.

A main disadvantage associated with this method is that a relatively large amount of computer memory is required to save the matrix elements. However, numerous algorithms are prepared to reduce this problem to some extent.

The FEM has many benefits as compared to the finite difference method (FDM). First, the FEM can easily be applied for complex regions. Second, there is a generalized approach used in FEM, so it possible to develop a general-purpose program which can be used to solve many problems. Problems having different solution regions and different boundary conditions but are governed by same partial differential equations, can be solved using a single program by changing only the input data. However, the FEM is also having its own limits such that it is difficult to understand and program as

compared to FDM. The input data is also required to be prepared which can be monotonous. Here FEM is compared with other numerical methods [5-7].

FEM (Finite element method)	FDTD (Finite difference time domain)	BPM (Beam Propagation method)	PWE (Plane wave expansion method)
Application of nonlinearity effect four wave mixing like Wavelength conversion can be performed	Easily incorporates nonlinear behavior	Good for forward only and nonlinear optical devices.	Inefficient incorporation of nonlinearity
Scaling will improve in domain decomposition	FDTD simulations can be treated as generic simulations that can be scaled	Scaling supported	Scales poorly
Unstructured grid is highly efficient. It is good to represent curved structures	It has a structured grid which is less efficient so it difficult to resolve curved surface.	It is inaccurate for the modeling of structure in which light propagate in large range of angles	-----
Efficient and easy solution to complex geometry	Improved handling of geometry details in finite difference time domain method	Erroneous in case of 2D and 3D geometry	It is faster for 3D
Efficient error control	Error estimation methods are to be defined	Reduced error calculated by mode mismatch loss calculation	1D is erroneous while others display better results
Effective dispersion analysis	It's not good to incorporate dispersion.	Simple to implement and easily incorporate dispersion.	Cannot model scattering and incorporate dispersion
Automatic adaptive mesh refinement.	No meshing	No meshing	No meshing
Incorporates accurate results	Solve Maxwell's equations (less approximation)	Use paraxial approximation	Precise optical model is required for accurate results.

References: (Appendix A)

1. P. P. Silvester and R. L. Ferrari, *Finite Elements for Electrical Engineers*. Cambridge, England: Cambridge Univ. Press, 1983.
2. AGRAWAL, G. P, "Fiber-Optic communication systems", 3rd ed., 2012.
3. Sadiku, Mathew N. O., " Elements of Electromagnetics", 3rd edition, 2001.
4. AGRAWAL, G. P, "Nonlinear Fiber Optics", 5th ed., 2013.
5. K. F. Warnick, "An intuitive error analysis for FDTD and comparison to MoM," in *IEEE Antennas and Propagation Magazine*, vol. 47, no. 6, pp. 111-115, Dec. 2005.
6. Kai Xiao. "Part I: Improved handling of geometry details in finite difference time domain method; Part II: Method of circuit extraction using finite difference frequency domain matrix formulation with application to power bus modeling " Missouri University of Science and Technology, Rolla, 2005
7. J. Yamauchi, J. Shibayama and H. Nakano, "Modified finite-difference beam propagation method based on the generalized Douglas scheme for variable coefficients," in *IEEE Photonics Technology Letters*, vol. 7, no. 6, pp. 661-663, June 1995.

Appendix B

List of publications

(i) Published/Accepted:

1. Ashish Kumar Ghunawat, R. C. Suryavanshi, Ghanshyam Singh “Design of an Ultra-Flattened Negative Dispersion elliptical spiral Photonic Crystal Fiber with High Nonlinearity and High Birefringence” *IEEE International Conference ‘COMPTTELIX-2017’*, July 1-2, 2017, Jaipur, *IEEE Xplore Digital Library*, Page(s):623 – 627, DOI: 10.1109/COMPTTELIX.2017.8004001.
2. A. K. Ghunawat, R. Chandra, M. Tiwari, G. Singh, “Design Optimization of a highly birefringent and highly nonlinear Silicon Photonic Crystal Fiber” *International Conference on Optical and Wireless Technologies (March 18-19, 2017)*, To be published in Special Book Edition, Springer Publication, 2017.
3. A. K. Ghunawat, A. Jain, K. Nikita, M. Tiwari, G. Singh “Optical Properties of Photonic Crystal Fiber” *International Conference on Optical and Wireless Technologies (March 18-19, 2017)*, To be published in Special Book Edition, Springer Publication, 2017.
4. R. C. Suyavanshi, A. K. Ghunawat, S. Jain, Ghanshyam Singh “Optimization of Highly Nonlinear Soft Glass Photonic Crystal Fiber with High Birefringence” *IEEE International Conference ‘COMPTTELIX-2017’*, July 1-2, 2017, Jaipur, *IEEE Xplore Digital Library*, Page(s): 618 – 622, DOI: 10.1109/COMPTTELIX.2017.8004001.
5. A. K. Ghunawat, S. Bangarwa, G. Singh “Design and Analyses of a Highly Non-linear fiber based Raman Laser: A Review”, *In Proceed. of International conference on Recent Trends in Engineering and Material Sciences (ICEMS), JNU Jaipur, India, March 17-19,2016*.
6. A. K. Ghunawat, A. K. Sharma,” Maximal Signal Intensity Variation with input conditions in Silicon-Nano Crystal waveguide”, *In Proceed. of International Conference on Advance Research & Innovation in Engineering & Technology, Jaipur, March 3-4, 2015*.
http://www.academia.edu/12174095/Maximal_signal_intensity_variation_with_input_conditions_in_silicon-Nano_crystal_waveguide, 2015.

7. Ashish Kumar Ghunawat, H. Kohli, S. Pareek, G. Singh "Review paper on highly nonlinear fiber and applications" *In Proceed. of IETE National conference, MNIT Jaipur, ICTHC_156, pp. 20, March 5th, 2016.*

8. A. K. Ghunawat, K. Atal, L. Agrawal, G. Singh, "Photonic Crystal fiber: Review, Recent Examples and System Applications", *In Proceed. of IETE National conference, MNIT Jaipur, ICTHC_154, pp. 18, March 5th, 2016.*

(ii) Communicated/Under review (SCI Indexed Journals):

1. Ashish Kumar Ghunawat, Rim Cherif, Ghanshyam Singh, "Ultra High Nonlinear Polarization Maintaining Dispersion Compensating Photonic Crystal Fiber", *Under review (Revised version) with Optica Applicata, November 2017.*

2. Harshul balani, Ghanshyam Singh, Manish Tiwari, Vijay Janyani, Ashish Kumar Ghunawat, "Supercontinuum Generation at 1.55 μm in As_2S_3 Core Photonic Crystal Fiber", *Under review with Applied Optics, November 2017.*

Appendix C

Profile Summary:

Ashish Kumar Ghunawat has more than 11 years of teaching & research experience and is currently an Assistant Professor in the Department of Electronics & Communication Engineering at Malaviya National Institute of Technology Jaipur, India. He was born in Sawai Madhopur, Rajasthan, India on February 28th, 1983. He received Bachelor of Technology and Master of Technology degree(s) in Electronics and Communication Engineering from Malaviya National Institute of Technology Jaipur in 2004 and 2006 respectively. In mid of July 2008, he joined the academic staff of Malaviya National Institute of Technology Jaipur (an Institute of importance owned by Ministry of HRD, Government of India). He has worked as Research Engineer with Centre Development of Telematics (CDoT, New Delhi) during August 2006 – July 2008. He has extensive teaching experience (for various UG and PG level students) on various important subjects Optical Communication System, Optical Networking and Electronics Devices and Circuits. He is currently pursuing Ph.D. at Malaviya National Institute of Technology Jaipur, India, in the field of novel structuring of photonic crystal fibers. He has guided more than 12 Master's theses and several undergraduate projects. Mr. Ghunawat is a regular member of Optical Society of America, IEEE, SPIE, Nature Photonics and IETE. His current research interest includes Micro and Nano-structured photonic crystal fibers and their linear & non-linear characteristics. (For more details, please check: http://mnit.ac.in/dept_ece/preprofile.php).
